

Coláiste na Tríonóide, Baile Átha Cliath
Trinity College Dublin
Ollscoil Átha Cliath | The University of Dublin

ENHANCING VENTILATION IN URBAN STREET CANYON ENVIRONMENTS USING ADJUSTABLE WIND FLOW DEFLECTORS

MADHAVAN VASUDEVAN



A thesis submitted in partial fulfillment of the requirements for the degree of
Doctor Of Philosophy

in the

Department of Civil, Structural and Environmental Engineering
Trinity College Dublin
Ireland
May, 2025

Declaration

I declare that this thesis has not been submitted as an exercise for a degree at this or any other university and it is entirely my own work.

I agree to deposit this thesis in the University's open-access institutional repository or allow the Library to do so on my behalf, subject to Irish Copyright Legislation and Trinity College Library conditions of use and acknowledgment.

I consent/do not consent to the examiner retaining a copy of the thesis beyond the examining period, should they so wish (EU GDPR May 2018).

Signature Madhavan Vasudevan

Madhavan Vasudevan
Civil, Struct. & Env. Engg.
Trinity College Dublin

Date 27/09/2024

Summary

Near-road buildings in densely built environments experience poor air quality due to traffic emissions and passive mitigation strategies are widely considered to tackle the concern. Despite the dynamic nature of the urban environment, passive interventions have been largely introduced in a static setup in the past; the risk of them offering counter-productive results under conditions they are not designed for and the opportunity to adapt them to the local environment is a research area that deems further exploration. However, developing solutions on a case-to-case basis is a computationally impractical exercise, and the applicability of such solutions in a real-street environment would be far from being straightforward. Therefore, the current study has been conducted to offer a methodology to develop adaptive passive interventions, wind deflectors, from both quantitative and qualitative standpoints; quantitative through evaluation of personal exposure to pollutants and qualitative through assessment of pollution removal mechanisms respectively. The performance analysis of adjustable wind deflectors in this study corroborates their conceptualization, sensitivity to environmental variables and practicality for their deployment in a real-street environment.

Wind deflectors in 2D urban and 3D city-type environments maneuvered average street canyon concentrations ($\bar{C}_{canyon}$) by regulating the amount of pollution removed from the same through mean (PCH_{mean}) and turbulent fluctuations (PCH_{fluc}) induced fluxes. Results from both 2D and 3D simulations provided sufficient evidence for the hypothesis conceived in the work that if the ambient above-roof winds were deflected optimally into the street canyons to maximize PCH_{mean}, a lower $\bar{C}_{canyon}$ could be achieved by reducing the dependence on turbulence that facilitated relatively localized pollution removal. Apart from analyzing the removal mechanisms through mean and turbulence-induced fluxes, field synergy theory was applied to the performance assessment of wind deflectors for asymmetric city-type

environments. A higher field synergy (resulting in a high field synergy number, FS_n and Sherwood number, sh) meant enhanced synergy between velocity and concentration fields, and therefore an increased pollution removal by convective fluxes and reduced dependence on the diffusive fluxes for the same. The inverse correlation between Sh and $\bar{C}_{canyon}$ supported the notion that convective fluxes aided in facilitating a global clean-up of the street canyons and that it is beneficial to maximize the same. It also saliently demonstrated that the wind deflectors were effective in regulating pollution removal through convective and diffusive fluxes as they were PCH_{mean} and PCH_{fluc}.

As with the conceptualization of the adjustable wind deflectors, their sensitivity was firstly evaluated under 2D settings by evaluating the ventilation performance of the deflectors when placed at different positions at the roof level between the leeward and windward facades. In a specific configuration when the deflector was 2m away from the leeward facade, $\bar{C}_{canyon}$ was reduced by 2.84 folds. Furthermore, in another specific configuration where the deflector was positioned 0.25m from the leeward facade, counterbalancing vortices were generated within the street canyons which facilitated washdown along both the leeward and windward facade resulting in an 86.5 and 8.45% exposure reduction along the same. The performance sensitivity was extended to ideal and asymmetric city-type (step-up, step-down and steep) street canyon environments for differing pollution source configurations, Cross Road Pollution (CRP) and Side Road Pollution (SRP) source models. These models were considered to represent the diurnal changes in traffic flow directions. For an ideal city-type environment, the wind deflectors performed modestly for the CRP source model by reducing 7%, 11% and 13% of CO exposure on the leeward wall, upwind side wall and downwind side wall without affecting the windward wall of the target street canyon. Whereas for the SRP source model, it reduced 91%, 32% and 34% on the same with a 17% reduction on the windward wall of the target street canyon. Furthermore, the concept of an adjustable deflector system was demonstrated to mitigate prolonged high exposure for building occupants exposed to changing traffic emission sources via all the surrounding building facades and at the ground by considering 4 linearly interpolated cases from the CRP and SRP source models including 0, 8, 16 and 24 hours of CRP in day and rest SRP. Mixed results were obtained for asymmetric city-type street canyons. For the step-down canyon, the deflectors promoted pollution reduction in building facades by 73.55% and 34.79% from leeward and windward walls under a Cross Road Pollution (CRP) source. A 16.57% pollution exposure was reduced on side walls under a Side Road Pollution

(SRP) source. However, apart from the 13.87% CO reduction across windward walls under the CRP source, the wind deflectors predominantly resulted in detrimental results for step-up canyons.

Another layer of complexity was added to the steep street canyons by considering changes in wind direction in tandem with traffic flow changes. To handle the changes in wind direction, the "tilted" configuration of wind deflectors was tested where they were tilted about their optimal locations to deflect the ambient winds perpendicularly. A combined multi-parameter sensitivity was conducted to evaluate the risk of using no deflectors as opposed to using deflectors that could only be positioned at the optimal location based on the traffic emission source and deflectors that could be both positioned at the optimal location based on the traffic source and be tilted according to the wind direction. These scenarios were evaluated for their impact on the leeward, windward and side facades under 16 linearly interpolated scenarios from 0, 8, 16 and 24 hours of CRP in day and rest SRP and 0, 8, 16 and 24 hours of orthogonal winds and rest obliquely respectively. The results indicated that although the "tilted" configuration of the deflectors only imparted a modest influence on the windward and the side facades, they reduced exposure across the leeward in the target street canyon by 47.3% and 62.2% under CRP and SRP source models respectively.

Finally, considering the dynamism of the street canyon environment, and the challenges associated with implementing a dynamic adjustable wind flow deflector that is sufficiently responsive to the rapidity of changes in the environment, a multi-directional wind deflector design was introduced. They were evaluated for efficacy in diverting ambient winds that are parallel, perpendicular and oblique at 45° to the street canyon under study, with a common multi directional wind deflector design. The design was efficient in enhancing ground level ventilation for parallel ambient winds while under orthogonal and oblique winds, the leeward and windward walls experienced generally positive and negative impacts respectively based on their relative location in the street canyon. Further, based on Weibull distribution for wind flow in Dublin city centre and meteorological wind data recorded for six months at the Dublin Airport, the efficacy of multi-directional wind deflector was evaluated for predominant flow conditions in Pearse Street neighborhood in Dublin, Ireland. The multi directional wind deflectors modestly reduced about 15% CO exposure across the target leeward facades while it developed mixed implications with a modest detriment to improvement between -20% and 16% on various target windward facades. Finally, the major outcomes from the work were utilized to conclude the

scope of potential, inherent limitations of the analyses conducted, implications under usage and further opportunities for improved understanding of the functionality of the wind deflectors and deployment of the same in future.

Acknowledgements

First of all, I am immensely grateful to my supervisor, Prof. Aonghus McNabola, for providing me with the opportunity to pursue a PhD under his guidance. He generously offered his time, knowledge, and ideas, which were instrumental in the successful completion of this PhD work. His advice in formulating the structure of the PhD work and help in suggesting relevant resources at various stages is deeply appreciated. I would like to acknowledge Prof. Francesco Pilla for his valuable suggestions, especially in disseminating the findings from my PhD work. I also extend my thanks to Prof. Ratnakishore V for his valuable technical inputs and for organizing computational resources. I am thankful to the Environmental Protection Agency (EPA), Ireland, for funding this research and the Irish Centre for High-End Computing (ICHEC) for sponsoring access to their High-Performance Computing facility.

I am grateful to my parents, Mr. Vasudevan and Mrs. Sudhavalli Tatachari Vijayaraghavan, for providing me with the right opportunities and unwavering support throughout my life. My mother has been a pure source of inspiration throughout my life in maintaining a positive intent and staying true to the purpose one has. I can proudly say that I have taken a few leaves out of her book on more than one occasion during this PhD. I would like to thank my brother, Dr. Sudharsan Vasudevan, and my friends, Dr. Madhu Krishna Murali and Mr. Calvin Stephen, for their moral support. Last but not least, I am extremely thankful to my wife, Mrs. Sahana Raghavan, for her love and support. Your trust in my PhD journey is second to none and for that, I will forever be indebted to you.

Contents

List of Figures **v**

List of Tables **xv**

1 Introduction **1**

1.1 Background 1
1.2 Problem Description 3
1.3 Aims and Objectives 4
1.4 Outline of the thesis 6

2 Literature review **7**

2.1 Structure of Literature Review 7
2.2 Overview of Air pollution 8
2.2.1 History 8
2.2.2 Types of Air Pollution 9
2.2.3 Insight into pollutants 10
2.2.4 Health impacts of Air Pollution 11
2.2.5 Air Pollution & Climate Change Nexus 12
2.2.6 Policies to Mitigate Air Pollution 13
2.3 Urban Environments and Passive Interventions 15
2.3.1 Air pollution in street canyons & General terminologies . . . 15
2.3.2 Using passive interventions to engineer street canyon air quality 15
2.3.3 Effect of Asymmetry, Roof Shapes and Other Urban Features 16
2.3.4 Effect of wind directions 18
2.3.5 Other Passive Interventions 20
2.3.6 Low Boundary Walls & Parked Cars 21
2.3.7 Noise Barriers 23

2.3.8 Wind Catchers 26
2.4 Urban Ventilation Indices and Applications 27
2.5 Gaps in literature 37

3 CFD Methodology **39**
3.1 Research Overview 39
3.2 Computational Fluid Dynamics 41
3.2.1 Governing Equations and Closure Problem 41
3.2.2 Turbulence Modelling 41
3.2.3 Species Transport Model 45
3.2.4 Other Aspects of CFD Solving 46
3.3 Validation studies 46
3.3.1 Validation of Flow Measurements 47
3.3.2 Validation of Concentration Measurements- 2D 51
3.3.3 Validation of Concentration Measurements- 3D 53

4 2D and 3D Analyses of Wind Flow Deflectors **61**
4.1 Introduction 61
4.2 Adjustable Wind Deflectors 63
4.3 Problem Description 63
4.4 Computation Domain and Boundary Conditions 67
4.4.1 2D Environment 67
4.4.2 3D City-Type Environment 67
4.5 Case Description 68
4.6 Mesh convergence 69
4.6.1 2D simulations 69
4.6.2 3D simulations 69
4.7 Key Assessment Indicators 70
4.8 Target regions of study 72
4.9 Results 72
4.9.1 2D simulations 72
4.9.2 City-Scale 3D simulations 78
4.10 Discussions 85
4.10.1 θ Vs $\overline{C}_{canyon}$ relationship 85
4.10.2 Indoor and near-vehicle pollution exposure 88
4.11 Conclusions 95

5 Wind Flow Deflectors for Asymmetric City-Type Environments 97
5.1 Introduction . . . 97
5.2 Problem Description . . . 98
5.3 Theory . . . 99
5.3.1 Field Synergy Theory . . . 99
5.3.2 Pollution removal by mean and fluctuations induced fluxes . 100
5.3.3 Performance of θ v/s Sh . . . 100
5.4 Computational Domain & Boundary Conditions . . . 101
5.5 Case Descriptions . . . 102
5.6 Mesh Convergence . . . 102
5.7 Key assessment parameters & target regions of study . . . 102
5.8 Results . . . 107
5.8.1 Step Down Canyons . . . 107
5.8.2 Step Up Canyons . . . 118
5.9 Conclusions . . . 126

6 Multi-environmental parameter response of wind deflectors 129
6.1 Introduction . . . 129
6.2 Problem Description . . . 130
6.3 Computational Domain and Boundary conditions . . . 132
6.3.1 Orthogonal winds . . . 132
6.4 Case Descriptions . . . 137
6.5 Mesh Convergence . . . 138
6.6 Key assessing parameter & target regions of study . . . 139
6.7 Results . . . 139
6.7.1 Orthogonal Winds . . . 139
6.7.2 Oblique Winds . . . 146
6.8 Discussion . . . 152
6.9 Conclusions . . . 158

7 Adjustable Wind Flow Deflectors in Dublin City- A Real World Analyses 161
7.1 Introduction . . . 161
7.2 Problem Description . . . 162
7.3 Computational Domain and Boundary Conditions . . . 164
7.3.1 Theoretical cases . . . 164

7.3.2 Pearse Street Environment 164
7.4 Case Description 167
7.5 Mesh Convergence 168
7.6 Key Assessing Parameters 168
7.7 Target regions of study 168
7.8 Results & Discussions 172
7.8.1 Theoretical cases 172
7.8.2 Pearse Street environment 185
7.8.3 Conclusions 189

8 Conclusions and future work **191**
8.1 General summary 191
8.2 Major findings 192
8.3 Future work 194

Bibliography **197**

List of Figures

1.1 Outline of thesis. 6

2.1 Bimodal Particle Number Distribution (PND) for the variation of particulate size (Vallero, 2014). 9

2.2 Figure showing interference, skimming and isolated roughness flows within street canyons of varying ARs; modified from Oke (1988). . . 16

2.3 Schematic representation of a) single primary recirculation in street canyons with AR<4 and b) formation of multi-vortex recirculation pattern when the AR increases from 4 to 5 (He et al., 2017). 17

2.4 Figure showing crosswinds across highways with upstream barrier (Ahangar et al., 2017). 25

2.5 Figure showing asymmetric street canyons considered in Li et al., 2020 and inclusion of wind catchers. 26

2.6 a) Schematic figure representing ACH^{+} and ACH^{-} at the roof level in a 2D street canyon (Cheng et al., 2008). 30

3.1 Flowchart highlighting the research overview adopted in this study . 40

3.2 The energy cascade; spectral variation of energy of eddies with eddy wave-number, κ ($\kappa \propto L^{-1}$) (Davidson et al., 2011) 42

3.3 Near wall regions of fluid flow v/s y^{+} (Davidson et al., 2011) 43

3.4 a) Schematic arrangement of 77 city-like buildings in the wind tunnel experiment conducted by Brown et al. (top); b) Computational domain and measurement probe locations considered for numerical validation of velocity fields Lien and Yee, 2004 (bottom). 48

3.5 Validation of CFD model against flow measurements from Lien and Yee (2004) 50

3.6 Figure from Meroney et al. (1996) showing the ethane gas concentration measurement probe locations and isolated street canyon model under orthogonal ambient wind 52

3.7 Validation of CFD model against concentration measurements obtained by Meroney et al. (1996); *dotted lines (-.), dashed lines (–) and solid lines (-) indicate the coarse, medium and fine meshes respectively.* 53

3.8 a) Schematic of long isolated street canyon in the wind tunnel experiment (CODASC)- computational domain and boundary conditions; b) Top-view showing the line pollution source regions; c) Leeward and windward facades with measurement probe locations (where considered for validation). 55

3.9 Validation of CFD model against concentration measurements from CODASC database pertaining to isolated street canyon under parallel ambient winds 56

3.10 Validation of CFD model against concentration measurements from CODASC database pertaining to isolated street canyon under orthogonal ambient winds 57

3.11 Validation of CFD model against concentration measurements from CODASC database for isolated street canyon under oblique ambient winds at 45°. The dashed lines (–) and dash-dotted lines (-.) indicate the coarse and fine meshes respectively. 58

4.1 a) Conventional flow pattern inside the target street canyon with **no wind deflectors** (left); b) Modified flow pattern with **deflector** washing down both leeward and windward facades with clean rooftop air (right). *Results obtained from 2D CFD simulations.* 63

4.2 a) Computational domain considered for 2D street canyons b) Deflector position and orientation analyses 64

4.3 isometric view of 3D city-type model with canyons and planes marked for CRP and SRP model analyses (b) CRP model (c) SRP model. . 66

4.4 a) Mesh convergence study for 2D urban environment comparing the streamwise velocity profile against wall normal distance at the center of the target street canyon (x_{mid} shown in Figure 4.2) 69

4.5 a) Mesh convergence study for 3D city-type environment comparing the streamwise velocity profile against wall normal distance at the center of the target street canyon (at x_2, as shown in Figure 3.4, in Chapter 2) in the range $0 \leq$ z/H ≤ 7 (on the left). b). Zoomed-in plot of the left in the range $0.8 \leq$ z/H ≤ 1 (on the right) 70

4.6 (a) Reference floors and windows for indoor IF_p calculations for all the building facades (b) Region of evaluation for near-vehicle outdoor IF_p on crossroads (c) Region of evaluation for near-vehicle outdoor IF_p on the side-roads. 73

4.7 a) Sensitivity to turbulence models (2D street canyons), comparing the non-dimensional mean canyon concentration for different deflector positions (on the left); b) Sensitivity to reference wind velocity(2D street canyons), comparing the non-dimensional mean canyon concentration for different deflector positions (on the right). 74

4.8 Overlayed images of contour plots of the concentration of CO gas and vector plot of velocity magnitude in all 11 deflector configurations studied with AR 1. 76

4.9 (a) Comparison of Windward and Leeward facade concentration, overall street canyon concentrations and θ (top); (b) Comparison of normalized Air Exchange Rates for varying deflector positions (bottom). *Solid lines (-) indicate the cases with the deflectors and the dashed lines (–) indicate the reference case without the deflector* . . 77

4.10 Streamlines showing the airflow pattern in the target street canyon and the influence of wind deflectors when placed 2, 4, 6, 8 and 10m away from the leeward walls. 79

4.11 Overlayed images of contour plots of the concentration of CO gas and vector plot of velocity magnitude for the CRP source model with deflectors in the third central canyon. 80

4.12 Correlation of PCH_{mean}/PCH_{tot} (θ) and average concentration of the entire street canyon for CRP model $\bar{C}_{canyon}$. 83

4.13 streamwise flow for no deflectors and deflectors at 2, 6 and 10m away from the leeward walls. 86

4.14 Correlation of PCH_{mean}/PCH_{tot} (θ) and average concentration of the entire street canyon for SRP model $\bar{C}_{canyon}$. 87

4.15 Performance of wind deflectors when placed at 2 and 4m from the leeward against the no-deflector case in affecting the indoor air quality in canyon 3 *(Central canyons: solid lines indicate the leeward wall and dashed lines indicate the windward walls. Side canyons: solid lines indicate the side-1 facade and the dashed lines indicate the side-2 facade).* 91

4.16 Performance of wind deflectors when placed at 4, 6, 8 and 10m the leeward wall in affecting the indoor air quality in canyon 3 *(Central canyons: solid lines indicate the leeward wall and dashed lines indicate the windward walls. Side canyons: solid lines indicate the side-1 facade and the dashed lines indicate the side-2 facade).* 92

4.17 Cumulative (for all floors) daily average IF_p of facades due to diurnal changes in traffic flow, comparing no-deflector case with deflectors at 2 and 4m from the leeward wall. 93

4.18 Daily average IF_p of the near-vehicle outdoor population due to diurnal changes in traffic flow, comparing no-deflector case with deflectors at 2, 4, 6, 8 and 10m from the leeward wall. 94

5.1 a) Computational domain considered for step-up and step-down canyons with CRP source model; b) Computational domain considered for step-up and step-down canyons with SRP source model; c) Window arrangement on all the walls surrounding the target street canyon for estimating the indoor IF_p. 104

5.2 a) Schematic figure showing the target central and side street canyons for step-down canyon arrangement; b) Schematic figure showing the target central and side street canyons for step-up canyon arrangement 105

5.3 a.1) Enclosing planes for the central street canyon in step-down configuration; a.2) Enclosing planes for the side street canyon in step-down configuration; b.1) Enclosing planes for the central street canyon in step-up configuration; b.2) Enclosing planes for the side street canyon in step-up configuration. 106

5.4 Streamlines of the airflow in the target step-down street canyon for the reference no-deflector case and when deflectors were placed 2.5, 5, 7.5, 10 and 12.5m away from the leeward wall. 108

5.5 Contour plot of IF_p on the leeward facade for reference no-deflector case and when the deflectors were placed 2.5, 5, 7.5, 10 and 12.5m respectively from the leeward wall in step-down street canyons. . . . 109
5.6 Contour plot of IF_p on the windward facade for reference no-deflector case and when the deflectors were placed 2.5, 5, 7.5, 10 and 12.5m respectively from the leeward wall in step-down street canyon. . . . 110
5.7 Step-down target street canyon- a) IF_p along leeward facade (floors 1-10) under CRP source model; b) IF_p along windward facade (floors 1-5) under CRP source model; c) IF_p along windward facade (floors 1-5) under SRP source model. 112
5.8 Vector plots of velocity magnitude at y = 14.5m plane for no deflector reference case and when deflectors were placed at 2.5, 5 and 12.5m away from the leeward wall in step-down street canyons. 115
5.9 Step-down target street canyon- Comparison of $\overline{C}_{canyon}$ against θ under - a) CRP conditions in central street canyon, b) SRP conditions in side street canyon; Comparison of $\overline{C}_{canyon}$ against FS_n under - c) CRP conditions in central street canyon, d) SRP conditions in side street canyon; Comparison of $\overline{C}_{canyon}$ against Sh under - e) CRP conditions in central street canyon, f) SRP conditions in side street canyon. 117
5.10 Streamlines of the airflow in the target street step-up canyon for the reference no-deflector case and when deflectors were placed 2.5, 5, 7.5, 10 and 12.5m away from the leeward wall. 118
5.11 Contour plot of IF_p on the leeward facade for reference no-deflector case and when the deflectors were placed 2.5, 5, 7.5, 10 and 12.5m respectively from the leeward wall in step-up street canyons. 119
5.12 Contour plot of IF_p on the leeward facade for reference no-deflector case and when the deflectors were placed 2.5, 5, 7.5, 10 and 12.5m respectively from the leeward wall in step-up street canyons. 120
5.13 Step-up target street canyon- a) IF_p along leeward facade (floors 1-10) under CRP source model; b) IF_p along windward facade (floors 1-5) under CRP source model; c) IF_p along windward facade (floors 1-5) under SRP source model. 122
5.14 Vector plots of velocity magnitude at y = 14.5m plane for no deflector reference case and when deflectors were placed at 2.5, 5 and 12.5m away from the leeward wall in step-up street canyons. 124

5.15 Step-up target street canyons- Comparison of $\overline{C}_{canyon}$ against θ under - a)CRP conditions in central street canyon, b) SRP conditions in side street canyon; Comparison of $\overline{C}_{canyon}$ against FS_n under - c)CRP conditions in central street canyon, d) SRP conditions in side street canyon; Comparison of $\overline{C}_{canyon}$ against Sh under - e)CRP conditions in central street canyon, f) SRP conditions in side street canyon. . 126

6.1 A Matrix illustrating the 16 possible combinations of scenarios from two variations in traffic flow (CRP and SRP) and wind flow directions (orthogonal and oblique). 131

6.2 Schematic representation including top and side views of the computational domain considered for steep-asymmetric canyons with a.1) CRP source model; a.2) SRP source model; b) regions where exposure of pollutants are evaluated for each building facade (windows). 133

6.3 Top view of the computational domain of the city-type environment considered for the oblique wind conditions. 135

6.4 a) Schematic representation with top and side views of standard deflector orientation under oblique wind conditions for CRP and SRP source models (top); b) Schematic representation with top and side views of standard deflector orientation under oblique wind conditions for CRP and SRP source models (bottom). 136

6.5 Flow chart representing the two-step strategy adopted in the current work to optimize the wind deflector performance for simultaneous changes in traffic and wind flow directions. 138

6.6 Streamlines of the airflow in the target steep street canyon for the reference no-deflector case and when deflectors were placed 2.5, 5, 7.5, 10 and 12.5m from the leeward wall under orthogonal wind conditions. 140

6.7 Steep target street canyon- a) IF_p along leeward facade (floors 1-10) under CRP source model; b) IF_p along windward facade (floors 1-10) under CRP source model; c) IF_p along downwind side facade (floors 1-10) under SRP source model and orthogonal winds. 142

6.8 Vector plots of velocity magnitude at y = 14.5m plane for no deflector reference case and when deflectors were placed at 2.5, 5, 7.5, 10 and 12.5m away from the leeward wall in the target steep street canyons. 145

6.9 Steep target street canyon under oblique wind conditions with no-deflector, standard deflector and tilted deflector configurations for CRP and SRP source models. 146
6.10 Steep target street canyon- IF_p along the leeward facade, windward and downwind side facade for no-deflector case (left), and scenarios including standard (center) and tilted deflector configurations (right) under oblique winds with CRP source model. 148
6.11 Steep target street canyon under oblique winds- a) IF_p along leeward facade (floors 1-10) under CRP and SRP source model; b) IF_p along windward facade (floors 1-10) under CRP and SRP source model; c) IF_p along downwind side facade (floors 1-10) under CRP and SRP source model. 149
6.12 Steep target street canyon- IF_p along the leeward facade, windward and downwind side facade for no-deflector case (left), and scenarios including standard (center) and tilted deflector configurations (right) under oblique winds with SRP source model. 150
6.13 Combined sensitivity chart for the performance of wind deflector across the leeward facade for combined changes in traffic and wind flow directions. 155
6.14 Combined sensitivity chart for the performance of wind deflector across the windward facade for combined changes in traffic and wind flow directions. 156
6.15 Combined sensitivity chart for the performance of wind deflector across the side facade for combined changes in traffic and wind flow directions. 157

7.1 Schematic of a hexagonal multi-directional wind deflector to orthogonally deflect incoming ambient winds at 0°, 45° and 90° respectively. 163
7.2 Methodological sequence of developing a CFD model for flow in Pearse Street environment from 2D plan layout and 3D information from lidar data of the neighborhood; a) Plan view of Pearse Street neighborhood from Google Earth; b) 2D plan view layout of Pearse Street neighborhood mapped in AutoCAD; c) 3D Lidar data of buildings in Pearse Street neighborhood in ArcGIS; d) 3D solid models of buildings in SpaceClaim; e) Polyhexacore mesh of Pearse Street neighborhood in Ansys Fluent. 166

7.3 Wind rose diagram representing the statistical distribution of speeds and directions of ambient wind flows in Dublin. 167

7.4 Schematic of case studies considered for the performance assessment of multi-directional wind deflector under ambient winds at a) 0°, b) 45° and c) 90° respectively in ideal street canyon environment. . . . 169

7.5 a) Schematic representing the different regions of the isolated street canyon under different ambient wind directions; b) Schematic representing the arrangement of windows considered in the study for the evaluation of near-road building CO IF_p. 170

7.6 a) Isometric view of the Pearse Street environment and direction of the ambient wind; b) Front view of target leeward facades ;c) Front view of target windward facades 171

7.7 Streamlines of the flow (plotted $0 \leq y/H \leq 10$) under parallel ambient winds with no deflectors and one, two and three deflectors respectively. 172

7.8 Contour of CO IF_p across the windward/ leeward facade (plotted $0 \leq y/H \leq 10$) under parallel ambient winds with no deflectors and one, two and three deflectors respectively. 173

7.9 Localized variation of CO IF_p across the height of the leeward and windward facades under parallel ambient winds with no deflectors and one, two and three deflectors respectively. 174

7.10 Streamlines of the flow (plotted $0 \leq y/H \leq 5$, as symmetry about y/H= 0) under perpendicular ambient winds with no deflectors and one, two and three deflectors respectively. 175

7.11 Contour of CO IF_p across the windward and leeward facade (plotted $0 \leq y/H \leq 5$, as symmetry about y/H= 0) under perpendicular ambient winds with no deflectors and one, two and three deflectors respectively. 177

7.12 Localized variation of CO IF_p across the height of the leeward and windward facades under perpendicular ambient winds with no deflectors and one, two and three deflectors respectively. 178

7.13 Streamlines of the flow (plotted $0 \leq y/H \leq 5$, as symmetry about y/H= 0) under oblique ambient winds at 45° with no deflectors and one, two and three deflectors respectively. 179

7.14 Contour of CO IF_p across the leeward facade (plotted $-5 \leq y/H \leq 5$) under oblique ambient winds at 45° with no deflectors and one, two and three deflectors respectively. 181
7.15 Contour of CO IF_p across the windward facade (plotted $-5 \leq y/H \leq 5$) under oblique ambient winds at 45° with no deflectors and one, two and three deflectors respectively. 182
7.16 Localized variation of CO IF_p across the height of the leeward under oblique ambient winds at 45° with no deflectors and one, two and three deflectors respectively. 183
7.17 Localized variation of CO IF_p across the height of the windward under oblique ambient winds at 45° with no deflectors and one, two and three deflectors respectively. 184
7.18 Comparison of flow streamlines in the Pearse Street environment with and without the inclusion of multi-directional wind flow deflectors. . 185
7.19 Contour plots of CO IF_p and velocity magnitude in the Pearse Street environment with and without the inclusion of multi-directional wind flow deflectors. 187
7.20 Comparison of average CO IF_p across the target windward and leeward facades in the Pearse Street environment with and without the inclusion of multi-directional wind flow deflectors. 188

List of Tables

3.1 Statistical measure of CFD validation of flow measurements conducted by Brown et al. (from Lien and Yee (2004)). 50

3.2 Statistical measure of CFD validation of flow measurements conducted by Meroney et al. (1996). 53

3.3 Statistical measure of CFD validation of concentration measurements conducted from CODASC database for isolated street canyon under parallel ambient winds. 59

3.4 Statistical measure of CFD validation of concentration measurements conducted from CODASC database for isolated street canyon under orthogonal ambient winds. 59

3.5 Statistical measure of CFD validation of concentration measurements conducted from CODASC database for isolated street canyon under oblique ambient winds at 45°. 59

4.1 Summary of case studies for conceptualization of wind deflectors . 68

5.1 Summary of case studies 102

5.2 Percentage reduction of average CO exposure along the leeward facade in step-down street canyons in step-down street canyons. . . . 111

5.3 Percentage reduction of average CO exposure along the windward facade in step-down street canyons. 111

5.4 Percentage reduction of average CO exposure along downwind building side facade in step-down street canyons. 114

5.5 Percentage reduction of average CO exposure along the leeward facade in step-up street canyons. 121

5.6 Percentage reduction of average CO exposure along the windward facade in step-up street canyons. 121

5.7 Percentage reduction of average CO exposure along the downwind-side facade in step-up street canyons. 124

6.1 Summary of case studies 137
6.2 Percentage reduction of average CO exposure along the leeward facade in the steep street canyons under orthogonal wind conditions with CRP source model. 142
6.3 Percentage reduction of average CO exposure along the windward facade in the steep street canyons under orthogonal wind conditions with CRP source model. 143
6.4 Percentage reduction of average CO exposure along the side facade in the steep street canyons under orthogonal wind conditions with SRP source model. 144

7.1 Summary of case studies for performance analyses of multi-directional wind deflectors 168

Chapter 1

Introduction

1.1 Background

Air pollution is a potential concern for human morbidity and mortality worldwide by being responsible for and capable of claiming 6.4 million premature deaths in 2015 and 9 million deaths in 2060 upon failure to implement aggressive control measures (Landrigan, 2017). However, studies suggest that complying with World Health Organization's (WHO's) air quality standards could prevent 51213 deaths per year from $PM_{2.5}$ exposure, and 900 deaths per year from NO_2 exposure (Khomenko et al., 2021). Khomenko et al. (2021) also showed that 124729 and 79435 deaths could be prevented if $PM_{2.5}$ and NO_2 levels could reduced to the lowest measured concentrations. The economic and social development opportunities in cities have resulted in an increasing trend of population influx from rural to urban settlements. By 2030, more than 60% of the global population is estimated to live in cities and as much as 80% in high-income countries (Rydin et al., 2012). With the increased developmental status of cities, less intense sources of air pollution in rural areas are replaced by rising population, traffic, industrialization and energy use in cities (Mage et al., 1996; Mayer, 1999). It is estimated that nine out of every ten urban dwellers are exposed to higher fine Particulate Matter $PM_{2.5}$ concentrations than annual World Health Organization (WHO) guideline mean concentrations (WHO et al., 2019). Ambient air pollution which accounts for two-thirds of the deaths associated with air pollution, finds its sources in vehicle exhausts, power stations, crustal dust and domestic wood combustion (Hime et al.,

2018). On the other hand, indoor air pollution has continued to be a serious concern with about 3 billion people still relying on a combination of unclean fuel and heating technologies for household requirements (WHO et al., 2019). However, in urban environments, there is a clear relationship between indoor Air Quality (AQ) and outside pollution levels, thereby impacting building occupants who are exposed indirectly via ventilation and infiltration (Challoner and Gill, 2014). Exposure assessments in Dublin have shown that people spend $> 90\%$ of their time indoors or in an enclosed transport mode (McCreddin et al., 2013). On the other hand, the challenge of mitigating air pollution hot spots including traffic signals and junctions for the benefit of near-road buildings, pedestrians and vehicle commuters remains imminent. Traffic signals were shown to contribute to 25% of overall air pollution exposure while only accounting for 2% of the overall journey time and peak hour exposures in traffic intersections could be as high as 29 folds higher than free-flowing traffic (Goel and Kumar, 2015).

Although significant efforts in research and policy have been made to control air pollution by addressing the quantity and intensity of emissions, they are largely focused on tackling the problem at the source including low emissions zones, congestion charging, eco-driving initiatives, changes in road infrastructure, speed limit controls, improvements in public transport, and behavioral change initiatives to mention a few. Low emissions zones for example were shown to reduce air pollution within an affected area in London by 2-3%, and by just 1% outside it (Ellison et al., 2013). License plate restrictions on traffic within a restriction zone in Hangzhou China decreased air pollution by 6.9% (Pu et al., 2015). The implementation of Eco-driving has also been shown to reduce emissions rates of individual vehicles by typically 5-15% in a variety of road conditions and vehicle types (Alam and McNabola, 2014). However, the improvements in air quality brought about by the changes in emissions from many interventions and policies of these types are relatively moderate or negligible in some cases (Tang et al., 2019). Investigations have shown that emissions restriction zones resulted in significant detouring of traffic within a city, resulting in slightly lower emissions within the zone but air pollution increases in the city as a whole (Tang et al., 2017). Indeed the level of investment and enforcement required in low emissions zones or speed limit changes for example is significant relative to the moderate reductions in air pollution associated with these approaches. Furthermore, the health impact arising from low to moderate improvements in emissions from the transport sector has facilitated lower changes in AQ as background concentrations and other sources of pollution remain unaf-

fected. This failure to reduce air pollution concentrations by significant amounts in the urban environment is part of the reason why it has remained a significant environmental issue for the past several decades. As such alternative and complementary approaches require equal attention to those interventions considering source control. Passive air pollution control aims to engineer the natural airflow patterns to facilitate enhanced dispersion and dilution in targeted regions within a street canyon, a key feature of urban environments (Gallagher, 2013). Roof-level interventions offer multiple advantages including the promotion of mixing between the polluted air contained within the street canyon and relatively fresher air above it. However previous investigations have mostly focused on, changes to localized dispersion within the street canyons using street-level interventions, including changes in surface and subsurface infrastructure and diurnal and seasonal variability as in the case of parked cars and vegetation respectively (Buccolieri et al., 2022). Moreover, because roof-level interventions can maneuver the airflow within the street canyons in its entirety, it can bring a global change to the dispersion mechanism within a street canyon which otherwise would have necessitated a major change in the built environment including Aspect Rations (ARs) and roof shapes or inclusion of a major infrastructure such as a viaduct for example. The current research aims to evaluate the merits and demerits of using roof-level interventions in a dynamic setup as that remains an unexplored theme in the context of air pollution control.

1.2 Problem Description

Although passive air pollution control interventions offer effective mechanisms to tackle the air pollution crisis in urban environments, they are inherently coupled with scientific and practical limitations. Firstly, the wind flow and pollution dispersion patterns within street canyons are complex and therefore require extensive modeling and analyses to realize the impact of passive interventions in street canyon environments. Apart from computational resources which are also crucial, there is a substantial lead time in determining the optimal configuration of a passive intervention in a particular environment. However, interventions in general are either designed for extreme or predominant scenarios. On the other hand, designing passive interventions for all plausible scenarios is neither practical nor useful given the dynamic nature of outdoor environments. The risk of passive intervention deteriorating the street canyon environment ventilation more under other scenarios remains significant. For instance, in a modeling study relating to Pearse Street,

Dublin, a combination of parked cars and low boundary walls reduced 21-22% pollution exposure across a specific pedestrian region along the leeward side when the ambient winds were in the predominant direction. However, the same combination of low boundary walls and parked cars increased pollution exposure in the same region for similar traffic flow by 34-40% when the winds were perpendicular to the street canyon. Therefore, a trade-off is necessary between the two approaches. It is worth noting that the changes in air flow dynamics within the street canyons due wind pattern, temperature and humidity are only some of the several factors that affect the static passive barriers (Oke, 1988; Vardoulakis et al., 2003). As cities and urban environments evolve, structural changes including new buildings, traffic flow adjustments and changes in land use strategies, short and long-term fluctuations in the emissions along with climate change including rising temperatures, shifting weather patterns and frequently occurring extreme events largely leave the static barriers under the threat of being counter-productive (Buccolieri et al., 2010.) Lastly, adding to the complexity, vegetation which are included in street canyon as potential passive mitigation intervention undergo natural changes due to seasonality and ambient conditions (Abhijith et al., 2017). Therefore, the first approach involves designing passive interventions based on extreme or predominant conditions carries the risk of negatively impacting the street canyon under other environmental conditions. The second approach involves creating a comprehensive solution database. This database would detail how to optimally operate different passive air control interventions for various environmental factors. However, this comes at the cost of increased computational resources, time, and uncertainty regarding practical implementation.

Although roof-level interventions can holistically improve the overall ventilation and positively impact all the stakeholders of the street canyon environments including the near-road building occupants, pedestrians and vehicle commuters, their rigid installation framework corroborates the same limitation as any other passive intervention. Therefore, the problem pursued in this research includes the demonstration of the risks and benefits of deploying a static and adjustable wind deflector system to respond to realistic environmental changes in an urban environment.

1.3 Aims and Objectives

This research aimed to evaluate and demonstrate the benefit of deploying an adjustable wind deflector system, responsive to changes in micro-environmental

conditions. Two different analysis approaches were undertaken to explore this concept. First, the impact of the position and orientation of roof-level wind deflectors, adjustably controlled for the changing traffic and wind conditions, on street canyon air quality was explored (objectives 1-3). Second, a common multi-directional wind deflector was developed and its impacts were assessed for changing wind conditions (objective 4). The following objectives were incorporated to realize a quantitative (objectives 1-4) and qualitative (objective 5, integrated with objectives 1 and 2 in the study) influence of adjustable wind deflector systems on air quality in a street canyon environment under diverse conditions.

1. Conceptualize and illustrate the potential of adjustable wind deflectors on air quality in a simple 2D environment and a complex 3D city-type environment with daily traffic flow direction changes respectively.
2. Illustrate the versatility of adjustable wind deflectors for varying street canyon ARs.
3. Investigate the performance of the wind deflector system in terms of its response to multiple simultaneously changing conditions of the environment including traffic and wind flow direction changes.
4. Evaluate the efficacy of the multi-directional wind deflector system and ascertain its region of influence for changing wind directions.
5. Assess the fundamental impacts of roof-level deflectors on street canyon ventilation using appropriate ventilation indices.

1.4 Outline of the thesis

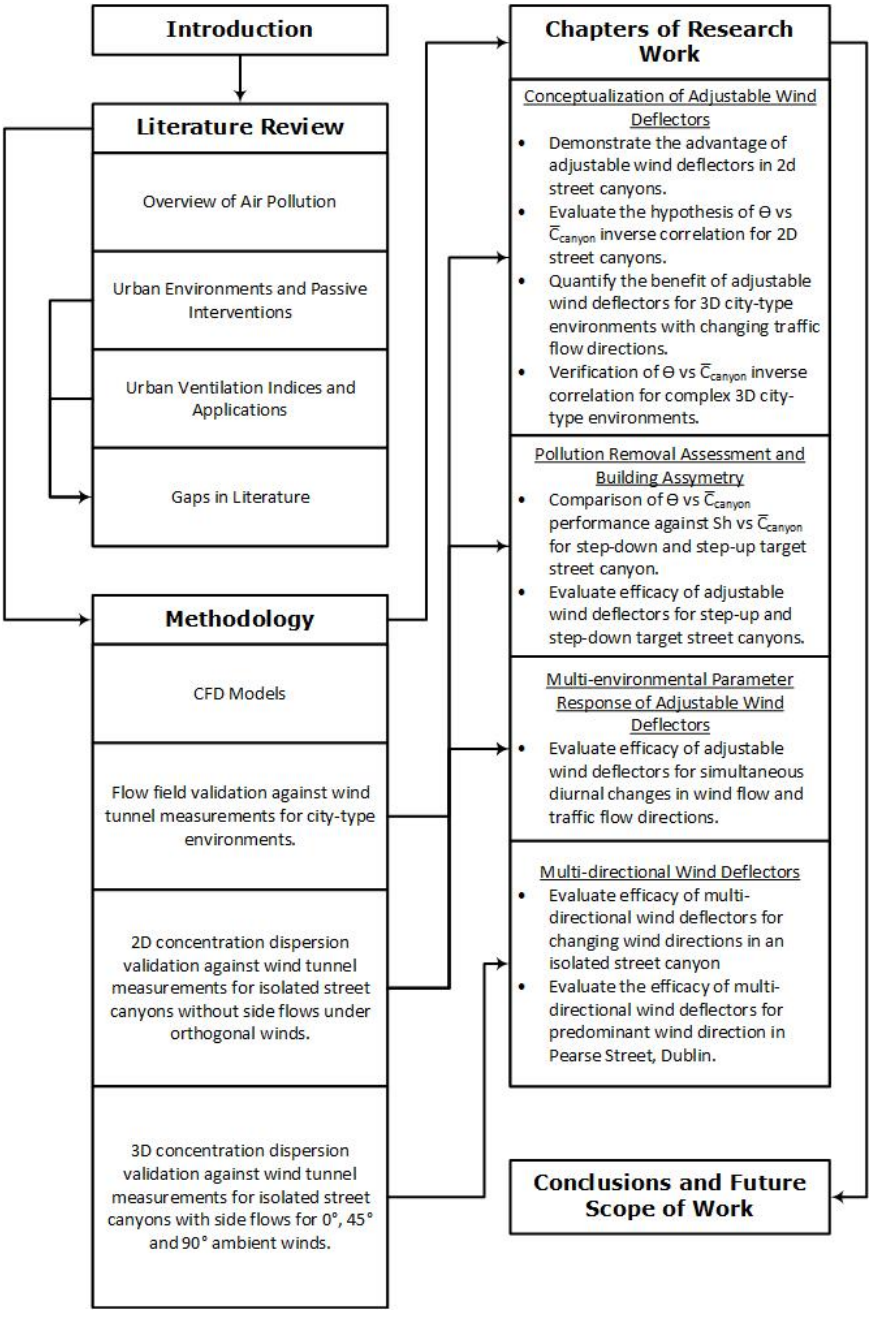

Figure 1.1: Outline of thesis. [1]

[1] Ventilation indices including $\bar{C}_{canyon}$, θ and Sh are detailed in Chapter 2.

Chapter 2

Literature review

2.1 Structure of Literature Review

The literature review is divided into four sections including an overview of air pollution, a summary of various passive barriers and urban environmental configurations studied apriori, ventilation indices developed and applied to urban street ventilation, and identified gaps in the literature. The overview of air pollution examines the evidence and the evolution of human efforts to tackle the concern. It includes information on different types of pollutants present in the atmosphere and their characteristics based on their physical and chemical properties, and longevity of presence in and influence on the environment, their impact on human health, the nexus this forms with climate change and policy-based measures undertaken thus far to mitigate the problem. With a brief outline of the necessity for modeling-based studies and passive interventions, the second section covers aspects relating to the effect of changing wind directions, building shapes and Aspect Ratios (ARs) of the street canyons, passive interventions including boundary walls, vegetation, wind catchers to mention a few, and active interventions including Pedestrian Ventilation Systems (PVS) and surface heating. The last section details the definition of traditional ventilation indices used thus far in the study of fundamental mechanisms of pollution removal in street canyons. The sensitivity of these indices under differing conditions as applied by previous studies for various situations is also explored.

2.2 Overview of Air pollution

2.2.1 History

Air pollution has affected human livelihood through both natural and anthropogenic sources. Incidents including volcanic eruptions emitting Particulate Matter (PM), pollutant gases such as SO_2 and H_2S and greenhouse gases including methane and forest fires releasing smoke, unburned hydrocarbons, CO, CO_2, NO_x and ash have been a part of the earth's evolution (Vallero, 2014). However, the scale and context of air pollution substantially changed after the advent of the Industrial Revolution in the eighteenth century. This period witnessed extensive exhaust from the combustion of coal and oils in the second half of the century. As of the 1780s, the coal imports in London had increased by a factor of 2.5 compared to the previous century (Brimblecombe, 1978). Concerns including soot-fall and continuous smoke from the forges prevailed amongst the inhabitants of London during the time. Meanwhile, several severe air pollution incidents in other parts of the world and the infamous London smog episode in 1952 (Polivka, 2018) highlighted the seriousness of the crisis. Finally, both national and international commitments have been pursued by different governments in their efforts to protect the air and contain climate change. Starting with the formation of the United Nations Framework Convention on Climate Change (UNFCCC, 1992), the aim was to regulate greenhouse gas concentrations in the atmosphere to avoid the dangerous interference of anthropogenic pollutants with the climate system (Bodansky, 1993). This was followed by the iconic Kyoto Protocol (1997) when developed nations agreed to reduce emissions of six greenhouse gases (CO_2, CH_4, N_2O (Iwata and Okada, 2014), Hydro-fluorocarbons HFCs, Perfluorocarbons PFCs and SF_6) to prevent global warming. Later, the Paris Agreement (2015) was adopted to limit the global temperature increase to be well below 2° C as in the pre-industrial times and drive countries toward becoming low greenhouse gas emitting and climate-change resilient economies (Delbeke et al., 2019). Lastly, in the twentieth century, the extent of automobiles used redefined the pollution exposure trends in major cities (Mayer, 1999) and hence the focus of regulation has turned towards the same.

2.2.2 Types of Air Pollution

In the overall context of the longevity of presence in, and influence on, the environment, air pollutants could broadly be classified to belong to the global scale (Carbon cycle), regional scale (Sulphur and Nitrogen cycle) and local scale (Fluoride cycle) pollutants (Vallero, 2014). The CAFE directive highlights eight critical pollutants including Particulate Matter (PM), CO, PAHs, NO_x, O_3, SO_2, VOCs and Heavy Metals (UNION et al., 2008) from both, the direct or indirect sources in the three scales. Global scale pollutants are characterized by the combustion process of fossil fuels resulting in the emission of CO, CO_2 and organic compounds including PAHs and VOCs. Concentrations of these pollutants are steadily increasing as they primarily depend on naturally slow photosynthesis for their decay in the atmosphere and cause global impacts including global warming. SO_x and NO_x acidify in water to cause acid rain and their reduction by bacterial action followed by hydrogenation of SO_x and photochemical activity of NO_x leading to H_2S and O_3 respectively, with regionally (Vallero, 2014). Some PM falls under this category, for example in the case of sandstorms (Haerens, 2011). Heavy metals and PM not supported by buoyancy for longer carriage and relatively chemically inert pollutants usually comprise the local scale pollutants.

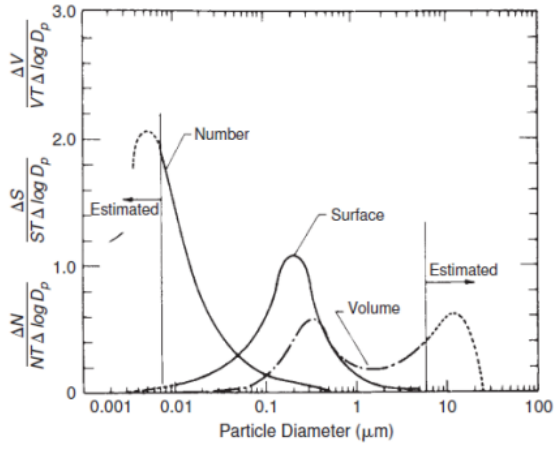

Figure 2.1: Bimodal Particle Number Distribution (PND) for the variation of particulate size (Vallero, 2014).

2.2.3 Insight into pollutants

1. **Particulate Matter:** A natural bimodal distribution on a mass/ volume basis is observed for PM as shown in Figure 2.1 and are usually spherical due to the liquid surface tension drawing its organic and inorganic constituents so (Vallero, 2014). Peak at smaller sizes reflects on condensation and coagulation of aerosol particles and at larger sizes, it shows earth and sea particles and agglomeration (Vallero, 2014). Vehicular traffic, coal combustion and industries, agricultural stubble burning (Beig et al., 2020) and domestic solid fuel combustion contribute to the addition of PMs. The annual and daily mean PM_{10} exposure are $20\mu g/m^3$ and $50\mu g/m^3$ respectively (WHO, 2006). However, the WHO-guided limits for annual and daily mean $PM_{2.5}$ exposure are as low as $10\mu g/m^3$ and $25\mu g/m^3$ respectively (WHO, 2006).
2. **Gaseous pollutants:** CO, PAHs, NO_x, O_3, SO_2 and $VOCs$ fall under this category. Despite other sources of CO gas including Methylene Chloride and other solvent removers used in paints, tobacco smoking, propane-operated forklifts and poorly functioning heating systems, CO from motor vehicle exhaust fumes accounted for the maximum proportion of CO poisoning deaths in the US (Ernst and Zibrak, 1998). It is easily ignitable and lighter than air making it dangerous to handle in higher quantities (Reyes et al., 1923). The WHO-guided limits for eight and 24-hour mean CO exposure include $10.5\mu g/m^3$ and $7\mu g/m^3$ respectively (WHO et al., 2010). Incomplete combustion and pyrolysis of materials containing carbon and hydrogen, such as coal, oil, wood and petroleum products account for the addition of atmospheric PAHs. Roofing tar, plastics and pesticides also include PAHs (Ravindra et al., 2008). The release of PAHs largely depends upon the atmospheric humidity and the ignition temperature (Dat and Chang, 2017). NO_x which is responsible for increasing ground-level ozone, formation of acid rain, acidification of aquatic systems, forest damage, degradation of visibility, and formation of fine particles, is generally formed by the combustion of Nitrogen in the air (thermal NO_x) or through oxidation of fuel Nitrogen (fuel NO_x) (Srivastava et al., 2005). The WHO-guided limits for hourly and annual mean NO_2 exposure include $40\mu g/m^3$ and $200\mu g/m^3$ respectively (WHO et al., 2010). O_3 is considered a transboundary pollutant as it peaks several kilometers downwind of major sources of its precursors including NO_x and VOCs after wind carries away after their peaks near their major sources. WHO guided limit for O_3 con-

centration is $100\mu g/m3$ for 8 and 24-hours mean (Krzyzanowski and Cohen, 2008). The 15 monitoring pollution monitoring sites in Ireland recorded O3 concentrations to be within EU guidelines throughout the year 2018, but 13 of the sites recorded values exceeding the WHO guidelines. Despite its short lifetime in the atmosphere, the contribution of SO_2 to the Sulphur cycle and thereby influence on human health and the environment makes it a criteria pollutant (Kharol et al., 2017). WHO guided limit for SO_2 concentration is 500 $\mu g/m3$ and 20 $\mu g/m3$ for 10-minute and 24-hour averages (Krzyzanowski and Cohen, 2008). Finally, coal combustion, biomass burning, gasoline and diesel vehicles and painting account for the addition of atmospheric VOCs.

2.2.4 Health impacts of Air Pollution

Heart diseases (38% & 27%), stroke (20% & 18%) and pulmonary diseases (43% & 54%), including Chronic Pulmonary Obstructive Diseases (COPD), pneumonia and lung cancer, account for total deaths related to ambient and household air pollution (WHO et al., 2019). Findings on acute PM exposure indicate an increase in cardiovascular deaths by 1% for every increase of 10 $\mu g/m^3$ of daily $PM_{2.5}$ concentration, a two- hours long exposure to PM_{10} concentration of 25 $\mu g/m^3$ increases the risk of myocardial infractions by 48%, and an increased potential for heart attack incidents by a factor of 2.73 following a 1-hour of traffic jam (Zhang et al., 2016). Days following high PM concentrations have also been associated with decreased lung function, increased incidents of respiratory symptoms, increased school absenteeism, and increased respiratory hospital admissions (Park et al., 2002, Zhang et al., 2021), particularly in children (Roy et al., 2011). Besides, chronic PM exposure is studied to induce neuro-toxicity (Fu et al., 2019; Kim et al., 2020) and increased exposure to the same has been linked to the development of neurodegenerative diseases including Alzheimer's disease, Parkinson's disease and neurodevelopmental disorders, including autism spectrum disorder (Costa et al., 2020). Prolonged O_3 exposure results in cellular and structural changes in the lungs. Although minimal exposures as low as five minutes are recognized to start triggering symptoms, chronic low exposures could damage the epithelial cells of the lungs (Mage et al., 1992). NO_x on the other hand, due to its low solubility in water, can penetrate all parts of the respiratory system resulting in minimal retainment of NO_x in the upper respiratory tract and maximal dosage to the lung tissues offering conducting airways and air exchange regions (Mage et al., 1992). CO is rapidly absorbed in the blood where it

is bound to the hemoglobin to form carboxyhemoglobin (COHb), thus impairing the oxygen-carrying capacity of the blood. The transition from oxyhemoglobin (OHb) to COHb leads to oxygen deprivation in the body tissues. Hemoglobin absorbs CO about just as rapidly as O_2 but the bond is about 245 times stronger (Mage et al., 1992).

Besides the direct impact of air pollution on human health, the social cost associated is also very high (WHO et al., 2017). The annual asthma-related costs incurred by two communities in the USA, especially the ones with children, was as high as $18 million (Brandt et al., 2012). Similarly, the EU was reported to incur $ 1.55 billion for treating children with asthma in 2008 where the quality of the environment was the concern (Bartlett and Trasande, 2014). On the other hand, (Mudarri, 2007) indicated that the social cost of compromised air indoor quality is very high as the asthma-related annual costs incurred in the USA due to dampness and mold exposure was about $3.5 billion.

2.2.5 Air Pollution & Climate Change Nexus

As mentioned earlier, global pollutants prevail in the atmosphere for a very long time and result in long-term global implications. Aerosols and gases in the atmosphere either allow the light and heat energy to pass through them, scatter and provide a shade effect, or absorb them. Gases including CO_2, CH_4, O_3 and N_2O with absorptive wavelengths impede heat, limit the heat transmission back into space and develop the greenhouse effect (Vallero, 2014). Climate change results in stagnation of pollutants without decay in the atmosphere for prolonged periods (Peel et al., 2013). Similarly, CFCs were identified to be capable of disturbing the steady-state concentrations of stratospheric ozone (Vallero, 2014) and scientists observed the ozone hole in the 1980s as a concern to open a larger window for climate change. On the other hand, climate change-induced increases in NO_x emissions (e.g from increased energy use for air conditioning) in summer act as a stable source of precursor for O_3 in the atmosphere (Weaver et al., 2009). Moreover, the higher temperatures result in increased VOC emissions from trees that further stagnate O_3 in the atmosphere and extended lifetime of O_3 in the atmosphere in return increasing the VOC emissions from the trees, thereby forming a perfect nexus (Mickley, 2007; Nolte et al., 2008). Although the anthropogenic sources overshadow the climate change-based penalty of human health impact from pollution (Fang et al., 2013; Silva et al., 2013), Garcia-Menendez et al. (2015) predicted that about 22000 and

95000 air pollution-related deaths could be avoided in the years 2050 and 2100 respectively upon adherence to climate stabilization measures and limiting warming to be below 1.5°.

2.2.6 Policies to Mitigate Air Pollution

2.2.6.1 Controlling Emission Sources

Policies have aimed to regulate sources of emissions from diverse sources including stationary and mobile sources. In the EU, the 2001/80/EC directive was framed to regulate the emissions of NO_x, SO_2 and particulate matter from stationary sources, especially from large combustion plants with thermal input ratings greater than or equaling 50 MW (UNION et al., 2008). A drive for the usage of alternative fuels and the concept of emissions trading was introduced in the US through the Clean Air Act- Amendment of 1990 (Waxman, 1991). Specific to traffic emissions, the Energy Policy Act of 2005 was introduced in the US to incentivize the purchase of hybrid EVs through credits against taxation (Act, 2005). Despite incentives, Mersky et al. (2016) criticized the low market share of EVs associated with individuals' purchase capacity, infrastructure to support EVs and technological limitations surrounding the EV mobility ecosystem. Behavioral interventions include the promotion of public transport usage through logistical (Haque et al., 2013) and financial benefits (Thøgersen, 2009), congestion charges imposed in London (Atkinson et al., 2009) and Stockholm (Johansson et al., 2009). However, off-loading traffic in different cities in specific routes through congestion charging or other measures has reduced and increased emissions in the immediate vicinity and alternate routes, respectively (Atkinson et al., 2009; Johansson et al., 2009; Tang et al., 2017). A more advanced congestion charging system based on distance coverage was introduced in Singapore (Haque et al., 2013). Promotion of 'zero carbon transport' drives is carried out by including infrastructure to support walking and cycling (Han, 2010; Pucher and Buehler, 2005.)

2.2.6.2 Controlling Emission Intensities

EU Directives 70/220/EEC and 88/77/EEC were established for emission regulations for light and heavy-duty vehicles respectively (Directive, 2005). The Directive 88/76/EEC- Luxembourg Agreement, enforced the mandatory requirement of three-way catalysts to reduce CO, VOCs and NO_x (Lubinska, 1985). From

EURO 1 restricting vehicles to emit less than 2.72 g/km (petrol and diesel), 0.97 g/km (petrol and diesel) and 0.14 g/km (diesel only) of CO, HC+ NO_x and PM respectively, the restrictions have been made more stringent as for EURO 6 regulations permitting 1.0 g/km, 0.10 g/km, 0.06 g/km and 0.005 g/km of CO, HC, NO_x and PM (petrol) and 0.50 g/km, 0.17 g/km, 0.08 g/km and 0.005 g/km of CO, HC, NO_x and PM (diesel) respectively. The EU has also enforced a car labeling directive, mandating car manufacturers to showcase complete details of fuel efficiency and CO2 emissions to facilitate informed decision-making from the customer's end (Han, 2010). Also, recommendations are made to distinctly mention carbon-based Vehicle Registration Taxes (VRT) during purchase as they may be camouflaged in the overall price, owing to the observation that Annual Carbon Taxes (ACT) impacted purchases more than the VRTs (Giblin and McNabola, 2009). Innovative neutral revenue policies are also recommended where the high-emitting sources are taxed to incentivize low-emitting energy sources (Galinato and Yoder, 2010). Moreover, cities in the EU have also started implementing Low-Emission Zones (LEZs) where vehicles not meeting specific criteria are not permitted in the region (Zhai and Wolff, 2021).

Besides directive policies, regulatory policies have largely affected the vehicle market, air pollution and the environment. Japanese and American markets have shifted to gasoline engines and the Japanese market dwelling in hybrid vehicles since 2001, has relieved them from the crisis of diesel engine vehicle emissions, unlike the EU (Walsh, 2001). Gallagher et al. (2021) criticized incentivizing the purchase of Diesel vehicles that emit as much as 25- 400 times more PM as compared to gasoline-powered counterparts and about 94 percent of the combustion exhausts are $PM_{2.5}$, which are much more toxic than the larger particles to human health. Gallagher et al. (2021) also highlighted the usage of diesel particle filters as not an efficient option in start-stop type slow-moving traffic as the sufficient temperature in the exhaust is not achieved. Schipper and Fulton (2009) also criticized the incentivization of diesel vehicles in the EU as neither tangible CO_2 nor energy savings were observed as in 2006. In recent years, consideration of hybrid and alternate fuels has received a large focus for AQ-related reasons. Usage of gaseous hydrogen in Fuel Cell Vehicles (FCVs) was studied to emit the least amount of SO_x, CO_2 and PM compared to counterparts including IC Engines and Hybrid Vehicles (Ugurlu, 2020). Since the pollution emission is shifted from traffic to power generation stations for EVs, the comprehensive impact would depend on a multitude of factors including the type of EVs, source of power generation, climate of the region and charging pattern to

mention a few (Requia et al., 2018). This also brings another question to consider, how effective would the EVs be in mitigating (Green House Gases) GHGs if the power source is through fossil fuels (Ghosh, 2020)?

2.3 Urban Environments and Passive Interventions

2.3.1 Air pollution in street canyons & General terminologies

Street canyons are common elements in urban environments where the buildings flank the roads and restrict the dilution of traffic emissions by obstructing the natural airflow. Street canyons with other micro-elements including vegetation and urban building features form the core of micro-scale studies focussed on the turbulent effects within Urban Canopy Layer (UCL). The street canyon geometry determines the nature of the flow to be wake-interfering, skimming, or isolated roughness within them (Oke, 1988) as shown in Figure 2.2. As shown in Figure 2.2, the ambient winds wash down along the windward facade, amass pollution at the street level, rise along the leeward facade infecting the same before mixing with the above roof cleaner air and recirculating back or exiting the canyon forever. This forms the primary recirculation within street canyons. This primary recirculation flow pattern can however change drastically for street canyons with differing Aspect Ratios (ARs). ARs are generally representative of either the H/W ratio, where H and W are the heights of the buildings and width of the street, or the H_1/H_2 ratio, where H_1 and H_2 are the heights of the upwind and downwind buildings. Street canyons with $H_1/H_2 < 1$ $H_1/H_2 < 1$ are referred to as step-up and step-down canyons while canyons with $H_1 = H_2 = W$ are referred to as ideal canyons.

2.3.2 Using passive interventions to engineer street canyon air quality

Both technological and policy-based interventions to mitigate high human exposure to pollution through controlling source and emission intensities have several drawbacks and challenges to overcome. These include high lead time for a new technical intervention as in the case EURO emission regulations, ethical concerns of

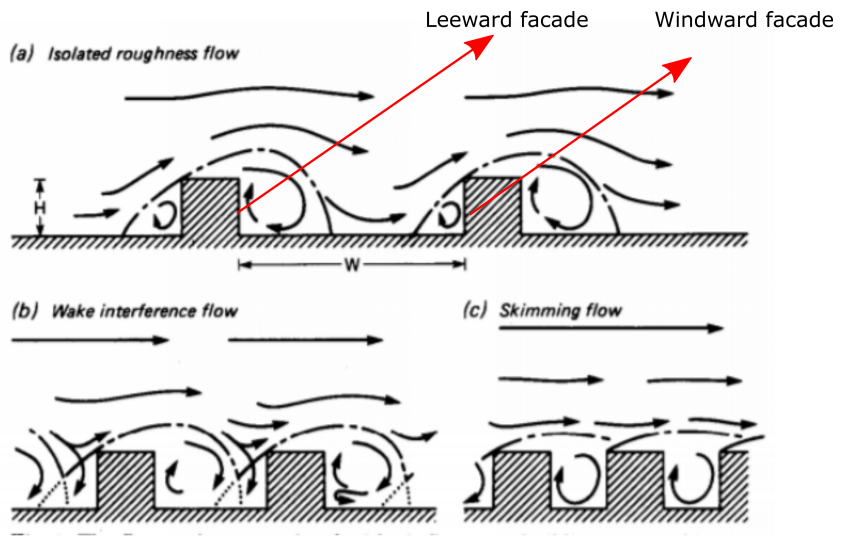

Figure 2.2: Figure showing interference, skimming and isolated roughness flows within street canyons of varying ARs; modified from Oke (1988).

relieving one neighborhood from higher pollution exposure at the expense of another as in the case of congestion charges, increased dependence on human behavior and overall environmental impact in the case of EVs and FCVs to mention a few. On the other hand, passive interventions offer relief from pollution exposure through another strategy, modification of source-receptor pathways. These principally work by engineering the flow pathways in an urban environment to either effectively enhance localized dispersion or divert the pollution-rich air away from human-inhabited regions. Several common urban features including roofs, balconies, advertisement boards, and overhangs when optimally deployed for a micro-environment can assist in reducing human exposure to pollution. The advantages of passive control interventions over the earlier two strategies include ease of implementation and reduced lead time for a solution, cost, dependence on human behavior and regulations to consider. This thesis will focus on passive controls for mitigating human exposure to air pollution. However, it would be best to complement passive interventions with other strategies for realizing better outcomes.

2.3.3 Effect of Asymmetry, Roof Shapes and Other Urban Features

Both wind tunnel and numerical studies have investigated the flow dynamics in wake interference, skimming, isolated roughness and multi-vortex flow within street canyons with differing ARs as shown in Figure 2.3 Li et al., 2009; Li et al.,

2006; Oke, 1988; Vardoulakis et al., 2003; Xiaomin et al., 2006). In regards to pollution exposure, asymmetry strongly influences the initial flushing mechanics and the subsequent flow regime within the street canyons. Narrow street canyons also inhibit the width of large recirculating vortices and vertical mixing (Baratian-Ghorghi and Kaye, 2013). The average pollutant concentration in street canyons with AR=0.5 was recorded to be 67% less than street canyons with ARs of 1 to 2 (Liu et al., 2005). Based on the residence times, a pollutant parcel is estimated to recirculate four times before exiting street canyons with AR=1. In contrast, it recirculates less than 3 times on average for street canyons with AR=0.5 (Liu et al., 2005). Wider street canyons exhibited higher air exchange rates (ACH) but not pollution exchange rates (PCH). From the analysis of the concentration budgets, advection was shown to be responsible for pollution redistributions within the primary recirculation. At the same time, turbulent transport facilitated pollutant penetration between the primary recirculations and the pollutant removal from the street canyons (Li et al., 2009). Large Eddy Simulation (LES) studies have been conducted to understand the contributions from mean and turbulent fluctuations induced fluxes (both mean flow and turbulence aid in the pollution removal process and their mathematical formulations are detailed in section 2.4) for different ARs in idealized street canyons under 2D conditions (Cheng and Liu, 2011; Liu et al., 2005; Liu and Wong, 2014). Cheng et al. (2009) studied the influence of buoyancy on pollution removal mechanisms using a variety of surface heating scenarios and reported that the decrease in Richardson Number (Ri) reflected in an increase in PCH_{mean} and reduction in $\bar{C}_{canyon}$ (average canyon concentration).

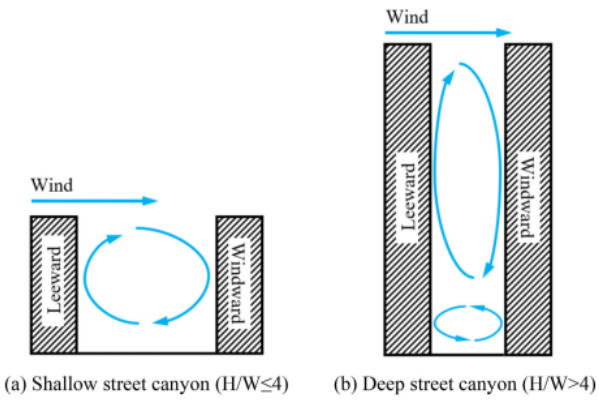

Figure 2.3: Schematic representation of a) single primary recirculation in street canyons with AR<4 and b) formation of multi-vortex recirculation pattern when the AR increases from 4 to 5 (He et al., 2017).

The roof shapes largely determine the amount of ambient air entering and the speed of the vortex formed inside the street canyon. Although slightly slanted roofs improved the street canyon ventilation by reducing the aerodynamic roughness of the street canyons, highly tilted roofs facilitated multiple detached vortices extending over the rooftop, thereby again detrimentally affecting the pollution dispersion (Takano and Moonen, 2013). Huang et al. (2015) and Huang et al. (2009) upon studying a combination of wedge-shaped roofs reported that step-down canyons provided enhanced ventilation as compared to step-up canyons as they tended to form a primary vortex aligned closer to the windward wall and thereby forming a weaker secondary vortex in the canyon's lower part, causing an inhibited transport of pollutants from the source. The upward wedge shapes in the upwind building enhanced the air entry into the canyon while the downward wedge restricted the same. Ding et al. (2019) showed the impact of viaducts on limiting the flow within the street canyons formed by both flat and triangular roof configurations as their elevation was raised such that flow reversal occurred abruptly altering the dispersion. The impact of asymmetry on building typologies can also be a complex function of the amount of built area along with the ARs. Although da Silva et al. (2022) observed a monotonically deteriorating AQ for increasing AR for a single block, detached blocks and courtyard models in general, the courtyard model with a wider AR of 0.8 facilitated 20% better ventilation than the single block model which offered the best ventilation for a symmetric AR configuration suggesting that minimal surface per obstacle in the built environment is crucial (da Silva et al., 2021, 2022). Although roof shape modifications, building asymmetry and typologies can substantially affect pollution dispersion and even promote ventilation in the street canyons holistically, one could say that the findings can be useful guidelines in urban planning in the development phase and rather cannot be applied as solutions to existing street canyons. Moreover, urban features such as asymmetry, roof shapes and building typologies are major infrastructural modifications and can be applied as an adaptive solution to continuously changing environmental conditions.

2.3.4 Effect of wind directions

Changing wind directions can largely influence air exchange and pollution removal from the specific elements of a street canyon and street canyons in their entirety (Huang et al., 2019; Jon et al., 2023). Shapes of the urban built environment were evaluated for the age of the air and air exchange efficiency under varying wind

directions (Hang et al., 2009a). Round city models with two streets developed younger and older air in the street parallel and perpendicular to the upstream winds while the city models developed similarly aged air in the two streets. In a study to evaluate the influence of on-street car parking and vegetation for varying wind directions, having trees along the windward side of the canyon was identified to be beneficial to air quality on footpaths for the oblique wind flow cases (Abhijith and Gokhale, 2015). Similarly, Jon et al. (2023) observed that including balconies only on the leeward side improved the overall ventilation of the street canyon for varying wind directions. Yim et al. (2009) modeled the wall effects to evaluate the retention times and velocity ratios for a densely built environment in Hong Kong for 0° and 22.5° wind incidence scenarios. Yim et al. (2009) showed that the rise in retention times by 45% and 80% by including upstream buildings which are two and four times the height of the subject downstream built environment could reduce up to 30% and 40% when the wind direction changes from 0° to 22.5° respectively. Huang et al. (2009) reported the risk of increased accumulation of pollution along the windward and leeward facades when the ambient winds were aligned more parallel and perpendicular to the street canyon respectively. Jon et al. (2023) observed a deterioration in Net Escape Velocity (NEV) for pedestrians along the leeward side for ambient wind incidence at 0°, 45° and 60° respectively despite an improvement in the street canyon ventilation for oblique cases. Using lift-up building structures is also considered to enhance pedestrian wind availability and increase wind velocities, especially in the low upstream wind velocity zones for orthogonal and oblique winds (Du et al., 2017). Lift-up buildings also experience less exposure to pollution as flow pathways are channelized under the buildings. (Sha et al., 2018) evaluated which floor of the building could be lifted in a city-type environment under oblique wind flow conditions and lifting the first floor was realized to yield maximum relief from pollution exposure by as much as 50% for 30° ambient winds. (Sha et al., 2018) also reported the relatively enhanced benefit of the lift-up structures for oblique winds compared to parallel winds. Finally, despite the strong coupling between the flow above and below the urban canopy, the flows deep within the canopy and in intersections are not aligned with the ambient flows due to several reasons including viscous forces forming an integral part of the flow and the formation of strong helical structures (Claus et al., 2012; Moonen et al., 2012), thus making it a complex scenario for evaluation. However, changes in wind direction can attenuate or aggravate the changes in pollution dispersion brought by a change in any other environmental variables and the response of passive interventions to such changes

in tandem is unexplored.

2.3.5 Other Passive Interventions

Another common urban feature that substantially affects urban ventilation is the viaduct. Raising the elevation of the viaduct from the ground increases the size of the counter-rotating small vortex at the bottom of the windward side to an extent where it enlarges and replaces the predominant vortex. Ding et al. (2019) observed raising the viaducts further upwards would reverse the flow back to the no-viaduct configuration and that these flow reversal properties were observable for roofs including both flat and triangular shapes on both the leeward and windward buildings. By considering the time-activity patterns and breathing rates for three different age groups Hang et al. (2017) estimated the personal exposure to pollution based on street layouts, source locations and viaduct and barrier settings in 3D urban setups. The impacts of viaducts in 3D city-type environments were more complex than in 2D and 3D urban environments. Unlike the observations by Hang et al. (2017), wider ARs in city-type environments did not facilitate improved ventilation of the street canyons (Hang et al., 2018) and the viaducts balanced the pollution distribution between leeward and windward facades (Hang et al., 2017; Hang et al., 2018). Other envelope features including balconies, wing walls and overhangs on the contrary increased and decreased the pollution exposure on the leeward and windward facades respectively. This was consistent for ARs 1-3 (Cui et al., 2020). However, Hang et al. (2018) reported that city-type environments experienced lesser exposure to viaduct-related emissions in the secondary streets due to diluting air flow from the primary street parallel to the wind flow (which was not present for 2D scenarios). Moreover, viaducts can also lead to increased accumulation of pollution below them as they directly restrict the rise of pollutants (Zhi et al., 2020). However, including viaducts in steeper canyons effectively restricted the formation of vertically aligned vortices that elevated the exposure along the near-road building facades (He et al., 2017). Although noise barriers along viaducts can mitigate high pollution exposure along near-road buildings (Hang et al., 2018), increasing the lengths and heights of noise barriers deteriorated the synergistic pollution removal facilitated by the concentration field and velocity in an isolated street canyon environment (Ming et al., 2023) and therefore increased the mean canyon concentrations and also the natural rise-up of pollutants offered by buoyancy in thermally unstable street canyons with ground heating (Zhi et al., 2020). However, partial enclosure

models of the noise barriers along the viaducts mitigated exposure to pollution along crucial pedestrian zones (Ming et al., 2023). Nevertheless, the noise barriers could be beneficial in reducing overall pollution concentration in steeper street canyons (He et al., 2017). Air Quality (AQ) related findings of viaducts are useful for their design. However, viaducts cannot be considered as potential solutions to improve ventilation in a street canyon given their scale of investment and implementation and their structural rigidity restricts them with no scope for adjustment to changes in the environment. Finally, advertisement boards of different configurations including vertical, lateral, single and double layers in aligned and staggered arrangements with pollution sources along primary and secondary streets were shown to decelerate 3D helical wind flows in city-type environments (Lin et al., 2019). The advertisement boards along with decelerating the flow, induced an upward rise of the flow restricting the downward curling flow and dispersion into the secondary streets and therefore invariably increasing the pollution exposure along the building facades for primary street pollution source and an enhanced decay into downwind facades for secondary street pollution source models respectively. Although urban features such as advertisement boards can significantly impact pollution dispersion, they are primarily designed and installed to attract maximum visibility. This again restricts them from being used as a dynamic solution to continuously changing environmental conditions.

2.3.6 Low Boundary Walls & Parked Cars

Low boundary walls were introduced to distance the source (traffic vehicles) and receptors (pedestrians on footpaths) in street canyon environments. McNabola et al. (2008) highlighted the benefit of including a low boundary wall between the road along the Liffey River, Dublin, and the boardwalk adjoining it. The low boundary wall invariably reduced the concentrations along the boardwalk for varying wind flow directions. McNabola et al. (2009) studied the effect of central and footpath low boundary walls on street canyon pollution dispersion for sources on the road's left and right side lanes. The study found the central low boundary walls to effectively reduce about 75% and 40% of concentrations along the leeward and windward pedestrian footpaths. The central and footpath low boundary walls were also evaluated for a range of different building asymmetries (H_1/H_2). The central low boundary walls facilitating two counter-rotating primary vortices generally performed better than the footpath low boundary walls (Gallagher et al., 2012).

However, both the low boundary wall models realized more pronounced concentration reductions along the pedestrian footpaths for higher degrees of asymmetry with step-up street canyon configuration (Gallagher et al., 2012). Gallagher et al. (2011) in an optimization study evaluated the car park models to realize a maximum benefit of about 32% along both leeward and windward facades with parallel parking as compared to oblique and perpendicular parking which detrimentally increased the concentrations along the footpaths. The study also evaluated the effect of occupancy rates and reported a monotonic improvement in pollution reduction along footpaths for an increase in occupancy rates over 50%. In a study to numerically evaluate the practical advantage of including low boundary walls in a real street environment, Gallagher et al. (2013) evaluated the benefit of incorporating low boundary walls and parked cars separately and together in Pearse Street, Dublin geometry model. The study found that the combined influence of the interventions and parked cars alone showed superior performance compared to including footpath low boundary walls alone. The study also mentioned that including parked cars alone reduced footpath concentrations for varying wind directions which the combined intervention did not. The effect of parked cars on the decay rate of pollutants from the street canyons was evaluated using an LES study (Gallagher and Lago, 2019) by calculating the time required to reduce 10% of steady-state concentrations. Reduced decay rates on the leeward side compared to the windward side and for parallel wind flows compared to perpendicular wind flows were reported in the study. The study also highlighted the influence of detailing of the parked cars on the decay rates as the detailed car geometry models included a change in cross-sectional area and the ability to develop secondary vortices that in turn altered the local turbulence and dispersion. The study showed the tendency to overestimate the benefit of utilizing parked cars with simpler geometrical detailing as the more involved geometry facilitated decay rates that were only about half as much as that of the simpler geometry. Studies have also analyzed the combined effect of parked cars and vegetation. Analyzing the effect of continuous and discontinuous vegetation cover with varying porosity in tandem with parked cars under varying wind directions, Abhijith and Gokhale (2015) reported a comprised ventilation upon including vegetation as it decelerated the flow within the street canyons. The ventilation of the street canyons in the study increased with reduced tree-stand density and tree dimensions and increased vegetation porosity. Despite the benefits realized from low boundary walls and parked cars to improve pedestrian ventilation, their potential downside arises from the exclusive focus only on the same. As the surface-level interventions

have limited capability in maneuvering the flow entering the street canyons and therefore the mixing between polluted air contained within the street canyons and ambient cleaner winds, it is reasonable to expect that they could have potentially polluted other elements of the street canyons including the building facades and traffic zones. This idea of therefore relieving pedestrians from pollution exposure at the expense of vehicle commuters and inhabitants of near-road buildings results in ethical concerns from a public health perspective. Finally, as with other passive interventions in general, LBWs are also static interventions making them inflexible to adapt to changes in traffic and environmental conditions. Furthermore, it is a surface-based intervention technique a flexible LBW solution is rather impractical as it could potentially affect mobility.

2.3.7 Noise Barriers

Noise barriers are usually installed on highways to limit sound transmission from high-speed traffic. Noise barriers have also been identified further to separate air pollution sources and receptors downwind of them. They have been studied in both the highway and urban-environment contexts for their efficacy in different forms of installations and under wind, thermal and traffic conditions. Ahangar et al. (2017) investigated a highway model with crosswinds including barriers upwind, downwind, and in both locations to concur to the vertical dispersion and initial mixing promoted by the barrier and the recirculation zone behind the barrier that sweeps the emissions back to the wall. The schematic Figure 2.4 represents the upstream barrier used by Ahangar et al. (2017). Interestingly, a certain downwind distance of H (height of the barrier) from the highway, the upwind and downwind barriers were reported to reduce concentration by 72% compared to a no-barrier case, while the case including barriers in both the locations was reported to reduce concentrations by 78%. Despite the synonymous performance, studies in general have focused only on downstream barriers for highways. However, noise barriers as an urban air pollution control measure are limited as they would potentially hinder roadway mobility, thus making them an impractical solution. Pournazeri and Princevac (2015) reported the promotion of vertical mixing with increasing height of the barrier and enhancement and deterioration of downwind and on-road AQ respectively with sunken road configuration. Gong and Wang (2018) studied the side edge effects of the barriers with different heights under various thermal stability conditions. At a distance of 10m behind the barrier, the 1m high barrier

wall resembled the closest to a Gaussian distribution of pollution along the length of the barrier while no other taller barriers resembled so. Whereas, at 100m from the barriers, all the barriers facilitated pollution distribution which resembled a Gaussian spread. Wang and Wang (2019) evaluated different ARs of the "T-shape" barrier and reported the influence to be profound only 10H distance from the same. On the other hand Venkatram et al. (2021) reported through experimental studies that the effect of vertical mixing could be realized up to a distance of 10H from the barrier and possibly beyond. Through a combination of source and barrier arrangements, Venkatram et al. (2021) highlighted the strong presence of lateral winds around the edges of the barriers for crosswind flow cases. Studies have also incorporated vegetation as a barrier, by themselves and combined with other solid fences. The performance of the barriers has been found to largely depend on the local meteorology and porosity of vegetation respectively. Also, PM of different size ranges were seen to behave differently based on their ability to traverse through the vegetation or get deposited on them and be dispersed downstream by the wind. In a field study, taller and dense vegetation barriers were found to be more effective under lower wind speeds while a combination of barriers including the vegetation (Ranasinghe et al., 2019). Solid fences were found more effective under increased wind speed scenarios to mitigate high downstream concentrations in comparison (Ranasinghe et al., 2019). Ghasemian et al. (2017) concurred with the promotion of vertical mixing offered by the solid barriers and reported that vegetation with denser composition tended to behave similarly to solid fences by facilitating stronger recirculation closer to them. While Leaf Area Density (LAD) of 3.33 reduced only 10% an equivalent solid barrier facilitated 58% reduction in the downstream location of interest. Vegetation with high porosity was reported to deteriorate the downwind concentrations in the study. On the contrary, an LES study revealed that combining a less dense vegetation with a solid barrier could be as effective as combining a highly dense vegetation with a solid barrier (Hashad et al., 2020). The study also reported a better improvement in concentration reduction for smaller particles. Tong et al. (2016) highlighted a higher PM deposition, especially for particulates $< 50nm$ and a subsequent reduced and increased downstream and on-road concentrations with increasing width of the vegetation cover. Hao et al. (2019) studied the combined effect of viaducts, noise barriers, and asymmetry of the canyons. Although the viaducts added more pollution to the street canyons, the noise barriers mitigated them. Also, in a field study conducted by Li et al. (2021) a combination of noise barriers and viaducts were found to be more efficient in mitigating exposure to black

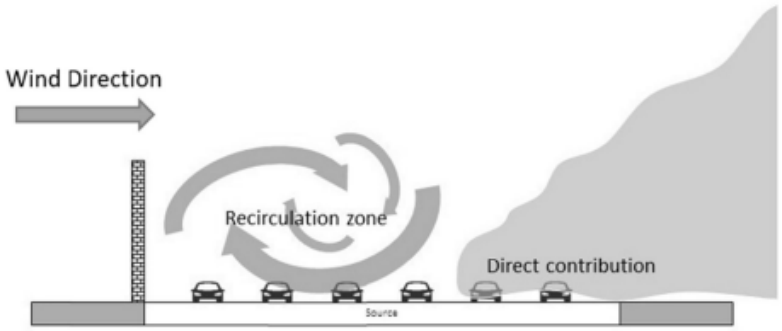

Figure 2.4: Figure showing crosswinds across highways with upstream barrier (Ahangar et al., 2017).

carbon, ultrafine particles and $PM_{2.5}$ respectively. Step-up canyons with increasing asymmetry witnessed a deterioration of air quality along the windward and leeward facades and at pedestrian breathing height. While a mild step-down assisted in flushing the contaminants out of the canyon, increased asymmetry introduced an unfavorable recirculation vortex at the roof of the canyon ventilation and made it the least ventilated combination (Hao et al., 2019). Collins et al. (2022) introduced barriers in street canyons on the windward and leeward sides to realize a general benefit of pollution mitigation along the building facades and a further enhanced benefit while baffles plates were incorporated in the barriers. In a study where the effect of noise barriers and viaducts was analyzed in deep street canyons (ARs ranging from 1 to 6), the effect of viaducts on the flow and dispersion were seen to reduce for increasing ARs as the wind velocities in the vicinity of the same reduced for deeper canyons (He et al., 2017). The study also reported having two sources of pollution (viaduct and ground) always increased the exposure compared to having only one.

Finally, in regards to thermal stability, Gong and Wang (2018) reported that lower concentrations were achieved with unstable conditions as stronger turbulent mixing in the flow aided in recovering the velocity in the flow separation region, hence promoting better dispersion. However, in the study to evaluate the performance of the barriers for both changing flow and thermal conditions the Concentrations Reduction Rates (CRR) were higher in more stable thermal conditions than in unstable thermal conditions (Reiminger et al., 2020). The study also reported higher CRR for oblique cases than for perpendicular wind flow cases.

2.3.8 Wind Catchers

Li et al. (2020) investigated the influence of wind catchers on five different asymmetric canyons under tidal traffic flow conditions in a city-type environment as shown in Figure 2.5. Personal intake fraction (IF_p) of CO gas in the near-road building facades was used as the performance indicator in the study. Wind catchers almost completely removed CO exposure along the leeward facade for shallow and regular canyons. While the wind catchers resulted in a minimum CO exposure reduction along the leeward facades by 30%, the impact along the windward facade was found to be modest. Ming et al. (2021) investigated the response of wind catch-

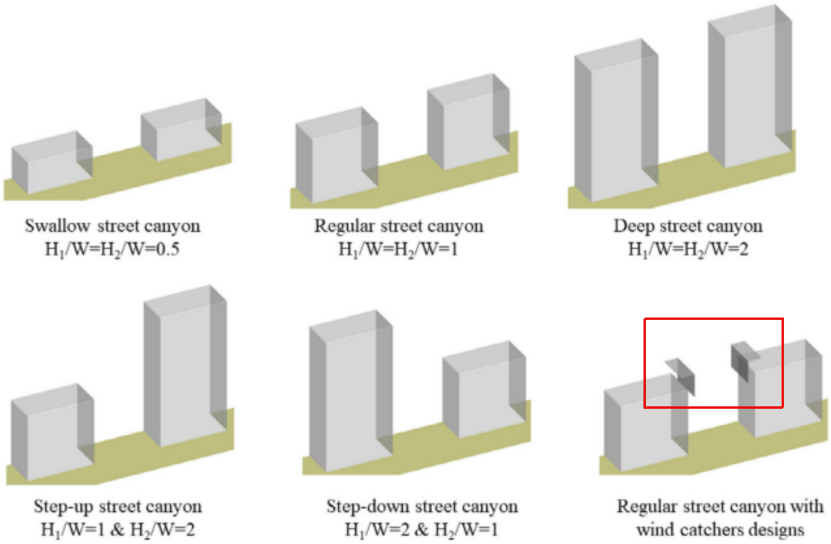

Figure 2.5: Figure showing asymmetric street canyons considered in Li et al., 2020 and inclusion of wind catchers.

ers for varying wind speeds for different asymmetric 2D urban street canyons. The study also correlated the average street canyon CO concentrations with the Sherwood number (Sh). The basis of Sherwood number stems from field synergy theory. In brief, the field synergy theory is an indicator of the synergy between the velocity and concentration gradient vectors in the street canyon. Therefore, larger field synergy means a reduced pollution concentration in the street canyon. The field synergy theory is detailed elaborately in Chapter 5. Ming et al. (2021) recorded that the Sh increased 4 times in a step-down canyon ($H_1/H_2 = 2$). As observed in the studies on asymmetries in street canyons, the steeper canyons experience vertically aligned vortices that result in a complex trajectory for the pollutants to escape. Zhang et al. (2019) introduced wind catchers to street canyons of varying ARs including 1, 3

and 5 and recorded the performance of the wind catchers to be particularly efficient for scenarios of higher ARs. The study also recorded an increase in the normalized wind velocities and a reduction in personal intake fraction at the street level by one or two orders of magnitude respectively. Zhang et al. (2020) analyzed the NO_x- O_3 photo-chemistry to evaluate the influence of urban configurations and background O_3 concentrations on NO_x and O_3 dispersion, and reported the potential of wind catchers to substantially mitigate both reactive and passive NO_2 within the whole canyon region. Chew et al. (2017) reported an increased wind availability by 2.5 times at the street level in the target street canyon and slightly reduced ventilation in the downwind canyons in an ideal 2D street canyon environment. Apart from the street canyon and outdoor ventilation, wind catchers have been extensively used for enhancing natural ventilation and thermal comfort in indoor environments (Montazeri and Montazeri, 2018). From a more practical standpoint, a study by Lauriks et al. (2021) included Roof-shape modification, employment of wind catchers, and electrostatic precipitation units were used as the mitigation strategies to reduce pollution in hotspots in a real street environment in Antwerp, Belgium, and wind catchers facilitated as much as 37% concentration reductions. In another practical study by Gaber et al. (2020), the impact of wind catchers in a real street environment of Alexandria, Egypt was analyzed and the wind catchers were reported to be efficient in channelizing the atmospheric flow into the target street and also increasing near-surface air speed by increasing skin convective heat transfer.
The opportunity to deploy them flexibly for changing environmental conditions has not been explored. Despite the wind catchers' potential to ventilate street canyons in their entirety, the rigid installation models could leave them with the same risk of working detrimentally under environmental conditions that they were not designed for like any other passive intervention. Also, it is worth noting that studies have primarily focused on the performance of wind catchers under orthogonal winds and that oblique wind scenarios have not been considered in detail. Lastly, the wind catchers have been studied using a regular thin plate model or an inverted "L" shape model and other potential shapes have not been explored.

2.4 Urban Ventilation Indices and Applications

Significant research has also been conducted on the development of theoretical ventilation indices for the outdoor environment of cities. These ventilation indices are defined based on the ability of the urban area to dilute pollutants, heat

and moisture by exchanging above-roof ambient winds and air contained within the volume of street canyons. The common considerations in deducing these parameters are that the ambient winds are relatively clean and that they promote cleaner air entering into the street canyons (inhale effect) and remove pollutants from the street canyons (exhale effect). Although this establishes a parallel with indoor ventilation where significant inspiration for modeling ventilation indices for street canyons arose from, outdoor ventilation differs by including open boundaries of the 'ventilated spaces' in question. Ventilation indices are important as they allow for the design of urban spaces to promote greater ventilation and hence lower pollution concentration. They also enable us to gain insight into the fundamental mechanisms behind the success or failure of passive air pollution control measures such as those in question in this thesis. Ventilation indices that have been employed to quantify the pollution dilution capacity of the urban environment include the following.

1. **Volumetric flow rate:** The volumetric flow rate through a canyon opening is defined as follows in Equation 2.1.

$$Q = \int_A \overrightarrow{V}.\overrightarrow{n}\,dA \tag{2.1}$$

Here A is the interface area between the canyon and ambient winds, $\overrightarrow{V}$ is the velocity vector of the flow at the interface and $\overrightarrow{n}$ is the outward-facing unit normal vector of the interface surface. Often normalized flow rates ($Q^* = Q/Q_\infty$) are considered across canyon openings where Q_∞ is the flow rate far upstream. The volumetric air change rate (ACH_{vol}) per hour is defined as follows in Equation 2.2.

$$ACH = \frac{3600Q}{Vol} \tag{2.2}$$

Here, Vol is the volume of the canyon. Hang et al. (2009a) defined air exchange efficiency as the ratio of turnaround time and mean residence time of pollutants in the canyon. Hang et al. (2009a) also studied the round and square city forms with one and two streets for both models and a long rectangular city form. The air exchange efficiency captured the low concentrations developed due to the flush out of pollutants in the long rectangular city model to represent a similar extent of ventilation experienced by the former two city forms. Hang et al. (2009b) reported a difference in the Q^* between the round

and square city forms due to the difference in the wake developed by different city shapes. Hang et al. (2009b) also reported that as the winds were more oblique to the street openings for round city forms with two openings, the magnitude of Q^* across street openings facilitating washout of pollutants monotonically reduced for the main street and the air exchange through the fluctuations and mean flow induced fluxes monotonically increased across the roof surface. For short streets under parallel wind flow, a smooth round city form offered the least concentration within the street as it facilitated minimal Q^* loss along the street compared to sharp-edged and square city forms respectively. The latter two forms offered relatively more air exits through the roofs, prohibiting streamwise washout and thus resulting in higher street concentrations. Although the contribution of Q^* through turbulent and mean flows increased with increasing lengths of the streets in both upward and downward directions for neighborhood scales (47.4W and 79W) similarly under parallel winds, for the city scale cases (333W and 667W) the contributions from the mean flows and fluctuations plateaued and increased in the order of the length of the street respectively Hang et al., 2010). In an analysis of 2 $\times$ 2 and 4 $\times$ 4 building configurations, Hang et al. (2013) observed substantial reduction and nullification of ${Q^*}_{roof}$ through both mean and turbulent contributions for partial and complete roof enclosure models respectively. The 2 $\times$ 2 and 4 $\times$ 4 showcased relatively more deterioration under relatively more parallel winds (0° and 15° wind cases) as opposed to more oblique winds (30° and 45° wind cases). For more complex city-type environments, Hang et al. (2010) observed that variations in building heights, especially including high-rise buildings, vertical flow rates through the roofs and leeward entries in the secondary streets and compromised the same through the primary streets as more wind concentrated toward taller structures. Moreover, multiple studies have highlighted the presence of initial flow adjustment in city-type environments where a substantial loss of Q^* occurs before stabilizing to reach a developed state and that the deterioration of overall ventilation increases with increasing canopy length (Hang and Li, 2011; Hang et al., 2010; Lin et al., 2014).

2. **Air exchange rates (ACH):** ACH indicates the removal of air from the street canyons through open surfaces where the above-roof and in-canyon can mix. These open surfaces can be imagined for example as the interfaces between the roof-level and street-level air (horizontally), or at the ends of the

street (vertically). For a 2D street canyon as shown in Figure 2.6, Cheng et al. (2008) introduced air exchange as in Equation 2.3

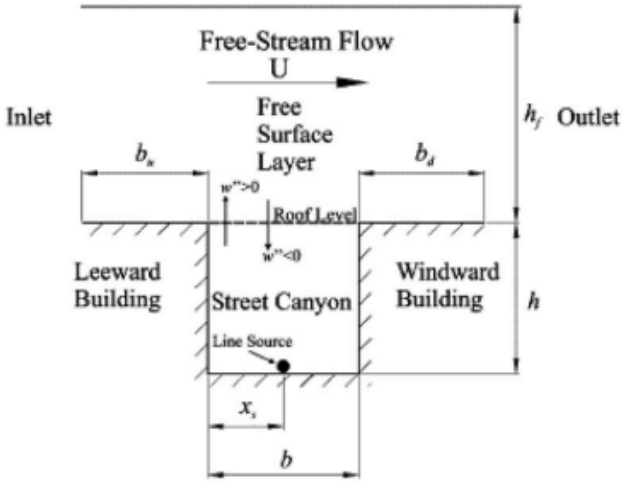

Figure 2.6: a) Schematic figure representing ACH^+ and ACH^- at the roof level in a 2D street canyon (Cheng et al., 2008).

$$ACH = \frac{1}{\lambda}\int_0^{\lambda}\int_{\Gamma_{roof}} w_+ \, dxdt \tag{2.3}$$

Here, w is the vertical velocity component in the wall-normal direction, Γ_{roof} is the roof surface of the 2D canyon, λ is the average time period and + represents only the upward velocity component ($w > 0$). ACH is contributed by both mean flow and turbulent fluctuations and hence was evaluated as in Equation 2.4

$$ACH_{tot} = ACH_{mean} + ACH_{fluc} \tag{2.4}$$

For steady-state modeling, ACH_{mean} could be expressed as in Equation 2.5. Although, ACH^+_{mean} and ACH^-_{mean} counterbalance each other, an increased ACH^+_{mean} indicates a higher mixing rate in a unit time period.

$$ACH_{mean} = \int_0^{\lambda}\int_{\Gamma_{roof}} \overline{w_+} \, dxdt \tag{2.5}$$

However, street canyon ventilation is largely controlled by turbulent fluctuations and is responsible for a majority of pollution removal from the canyons. Liu et al. (2015) while investigating eight different types of building models for the target street canyon, ACH_{fluc} exhibited a linear correlation with fric-

tion factor (ratio of drag to the half of dynamic pressure) with a correlation coefficient greater than 0.9. A similar correlation ($ACH_{fluc} \propto f^{1/2}$) with correlation co-efficient over 0.9 was recorded by Ho et al. (2015) in an investigation on the effect of ARs and Urban Boundary Layer (UBL) depths on aerodynamic resistance and ventilation performance. Ho et al. (2015) also observed a substantial portion as much as 70% of total ACH contributed by ACH_{fluc}. A similar observation was also made by Hang and Li (2010) in an evaluative study to compare the air exchanges in uniform medium and high-rise buildings and buildings with height variations. For taller buildings, a greater wind influx along the windward facade was achieved but the medium-rise buildings in particular experienced greater proportions of air exchange through air exchange via street canyon roofs and interfaces connecting streets that are parallel and perpendicular to the winds via turbulent fluctuations as opposed to via mean flows. Based on the Eddy-viscosity hypothesis, ACH_{fluc} was expressed as in Equation 2.6. Llaguno-Munitxa and Bou-Zeid (2018) introduced a folded normal distribution to calculate ACH from RANS by considering mean vertical velocity $|\overline{w}|$ and vertical turbulence statistics σ_w based on Gaussian distribution. Llaguno-Munitxa and Bou-Zeid (2018) recorded a good agreement (with a maximum error of 4%) between ACH obtained from LES and ACH obtained from the folded normal formulation from RANS for different building shapes.

$$ACH_{fluc} = \int_{\Gamma_{roof}} \sqrt{-\frac{1}{2}\nu_t\left(\frac{\partial \overline{w}}{\partial z}\right) + \frac{k}{6}} dx\, dxdt \tag{2.6}$$

However, before the proposition of ACH^{+}_{fluc} using the Eddy- viscosity formulation by Cheng et al. (2008), Li et al. (2005) had considered isotropy in turbulence and hence as in Equations 2.7-2.9.

$$k = (\overline{u'u'} + \overline{v'v'} + \overline{w'w'})/2 = 3\overline{w'w'}/2 \tag{2.7}$$

$$\overline{w'w'}^{1/2}|_{roof} = \sqrt{\frac{2}{3}K|_{roof}}d\Gamma_{roof} \tag{2.8}$$

$$ACH_{fluc} = \frac{1}{\sqrt{6}}\int_{\Gamma_{roof}} \sqrt{k|_{roof}}d\Gamma_{roof} \tag{2.9}$$

It is worth noting that although the eddy-viscosity-based formulation of ACH is more detailed than the isotropic turbulence-based ACH formulation using RNG $k-\epsilon$ turbulence model (Li et al., 2005) compared well against the LES

predictions simulations by Liu et al. (2005). ACH across the roof modestly deviated from the LES predictions by 5.23%, 16.9% and 17.5% for ARs of 0.5, 1 and 2 respectively. This agreement was certainly good for practical considerations since LES simulations demanded greater computational times of one to two orders of magnitude.

ACH by definition does not deal with the pollution transport into and out of the street canyons. Since it predominantly captures the flow physics at the roof level, ACH sometimes does not indicate the influence of passive interventions at the street level. Mirzaei and Haghighat (2011) witnessed similar ACH rates for different Pedestrian Ventilation System (PVS) strategies for different ARs and thermal stratification conditions. Nazarian and Kleissl (2016) evaluated ACH variation due to thermal effects in a realistic urban environment by considering diurnal changes with solar heating. Nazarian and Kleissl (2016) also observed a majority contribution in ACH by turbulent fluctuations and an increased ACH during leeward wall heating as the mechanical and thermal forcing of the flow complemented each other as opposed to a slightly reduced increase while the windward wall was heated. The least ACH was recorded for the noon setting where the heating was applied to the roofs and was removed from the facades.

3. **Pollution exchange rates (PCH):** Liu et al. (2005) defined PCH in an LES study as the product of fluctuating vertical velocity and the instantaneous resolved-scale pollutant concentration as follows in Equation- 2.10.

$$PCH(t) = \int_{\Gamma} w"(t)|_{roof}\bar{c}(t)|_{roof}d\Gamma \tag{2.10}$$

In a transient observation of PCH, Liu et al. (2005) reported the imbalance between PCH and Q was compensated by the entrainment of pollution in the free stream back into the street canyon. However, Cheng et al. (2008) introduced PCH through the RANS simulation framework as follows in Equation 2.11.

$$PCH = \frac{1}{\lambda}\int_{0}^{\lambda}\int_{\Gamma_{roof}} wc\, dxdt \tag{2.11}$$

Similar to the formulation ACH, both turbulent fluctuations PCH_{fluc} and mean flow PCH_{mean} contribute to the PCH. However, to maintain a steady

state condition, unlike ACH, PCH^{+}_{mean} and PCH^{-}_{mean} do not counterbalance each other. PCH_{fluc} and PCH_{mean} could be expressed as in Equations 2.13 and 2.12.

$$PCH_{mean} = \oint_A U_n C dA \tag{2.12}$$

$$PCH_{fluc} = \oint_A \frac{\nu_t}{Sct}(\frac{dC}{\overrightarrow{dn}})dA \tag{2.13}$$

At steady-state conditions, the total pollutant removal through turbulent and mean fluxes from a canyon will always equal $\dot{Q}$. For the convenience of illustrating the hypothesis considered (discussed in section 2.5) in this thesis, an additional parameter θ is defined as follows in Equation 2.14

$$\theta = \frac{PCH_{mean}}{PCH_{mean} + PCH_{fluc}} \tag{2.14}$$

Under varying conditions of unstable stratification, both ACH_{mean} and ACH_{fluc} increased with decreasing Richardson Number (Ri). However, PCH_{mean} and PCH_{fluc} increased and decreased respectively for the same, such that the PCH_{mean} dominated the pollution removal at lower Ri (Cheng et al., 2009). Decreasing Ri also reduced the residence time of the pollutants in the street canyon (Cheng et al., 2009). Mirzaei and Haghighat (2011) also concurred that buoyancy contributed to enhanced pollution removal in steep canyons by strengthening the secondary vortices. Mirzaei and Haghighat (2011) also observed deteriorated pollution removal from stable stratification facilitated by cooling the ground. Hang et al. (2009c) observed that pollution removal contribution through the roofs under parallel wind conditions was negligible for shorter streets and that for longer streets, PCH_{mean} and PCH_{fluc} were detrimental and supportive respectively.

4. **Air delay τ_d:** Air delay is defined as the time difference between the local mean air age when an urban feature is included and when it is not included as described in Equation 2.15 (Antoniou et al., 2017).

$$\tau_d = \tau_p = \tau_{empty} \tag{2.15}$$

Here, τ_p is the local mean age of the air when a specific geometric feature is

included and τ_{empty} is the local mean age of the air when the feature is not included.

5. **Purging flow rate (PFR):** The purging capacity of a flow represents the total flow rate through mean and turbulence available for completely purging all the pollutants out of a control volume. PFRs have been applied to street canyons and subdomains including pedestrian zones (Peng et al., 2020). The PFR of a street canyon domain is expressed and evaluated as follows in Equation -2.16

$$PFR = \frac{\dot{Q} \times V}{\bar{C}_{canyon}} \tag{2.16}$$

Here, $\dot{Q}$, $\bar{C}_{canyon}$ and V are the source rate of the emission, the average concentration in the canyon and the volume of the canyon respectively. Alternately. for pedestrian zone PFR, the same formulation can be applied with an average concentration in the pedestrian zone ($\bar{C}_{ped}$) and volume of the pedestrian zone (V_{ped}). PFR and ventilation in general improve with larger and shorter street widths and building heights respectively in simple two-building models (Bady et al., 2008). For complex multi-building environments, Bady et al. (2008) reported that except for the canyons formed between two buildings in an aligned arrangement, all other regions showcased better PFR and lower concentration under parallel flow conditions, while the staggered building arrangement outperformed the aligned building model under oblique wind flow conditions with improved PFR in all the areas of assessment as it avoided the circulatory vortices that aligned building model result in. On the contrary, the overall UCL ventilation of an aligned square urban form was observed to be better than that of the staggered form under both parallel and oblique winds (Lin et al., 2014). PFR was used to quantify the extent of ventilation offered by PCH_{mean} and PCH_{fluc} in an environment with building height variations (Hang et al., 2012) and configurations including larger variations were observed to offer higher pedestrian PFR and pedestrian exposure to pollution with more pronounced contributions from the roofs as opposed to lateral entries in uniform configurations. A normalized PFR (PFR^*) as in Equation 2.17 was used to quantify the differences in the reduced PFR values in scaled-down models of ventilation offered by over-hang walls at different heights from the roof including different coverage ratios for 2 $\times$ 2 and 4 $\times$ 4 building

environment under oblique winds (Hang et al., 2013).

$$PFR^* = \frac{PFR}{Q_\infty} \tag{2.17}$$

Where Q_∞ is the volume flow of ambient air entering through the windward street opening. Finally, the length of buildings, lateral widths between building units and street widths largely impact the PFR. You et al. (2017a) reported that middle regions of building units suffered from low PFR with increasing lengths of the buildings and the sides of the same started benefiting from increased lateral widths between the buildings under perpendicular wind flow conditions.

6. **Visitation frequency (VF):** VF is another index of the age of the air from the perspective of the number of visits a pollutant parcel makes to a control domain before exiting for good. The VF can be evaluated using the particle tracking method in the LES formulation or the passive pollution flux method in the RANS formulation as follows in Equation 2.18 (Bady et al., 2008).

$$VF = 1 + \rho \frac{uc + \overline{u'c'}}{S \times Vol} \tag{2.18}$$

Here uc and $\overline{u'c'}$ represent the contributions from the mean and turbulence fluxes. VF holds an inverse relationship with ACH and PFR and therefore Bady et al. (2008) reported reduced and increased VF for increasingly widened gaps and building heights in the simple two-building system. On the same lines, Bady et al. (2008) observed a higher VF for aligned building configurations for parallel winds compared to oblique winds for a system including an array of buildings. As observed in You et al. (2017a) where the middle regions of long building units under perpendicular winds were experiencing lower PFR, You et al. (2017b) in a study to evaluate the aligned and staggered building arrangements confirmed the risk of middle portions of long buildings units experiencing high VF.

7. **Net Escape Velocity (NEV):** As the PFR was inherently dependent on the control volume for assessment, Lim et al. (2013) introduced NEV as a representative velocity of the PFR per unit area as follows in Equation 2.19.

$$NEQ = \frac{PFR}{A/U_\infty} \tag{2.19}$$

Where A is the area of the sides enclosing the control volume considered and U_∞ is the free stream velocity of ambient air at boundary layer height. Hang et al. (2018) evaluated various widths of semi-open roof settings for rectangle and square building forms under varying ambient wind directions. Although the NEQ for overall UCL and pedestrian region deteriorated compared to the reference open roof case with increasing widths of the semi-open roof setting, the reduction substantially reduced for increasingly oblique ambient winds for square and rectangular building forms. The study also reported an increased NEQ for UCL and pedestrian regions with increasingly oblique winds (Hang et al., 2018). Chen et al. (2017) defined in-canopy and exchange velocities that represented horizontal and vertical ventilation and observed that deterioration of the ventilation along the former was more striking than the latter for increasing building packing density in city-type environments. Results by Hang et al. (2010) also concurred with the same as flow rates and air exchanges decelerated quicker for high building density packing compared to medium building packing density environments. The square-form environments facilitate improved overall UCL ventilation over rectangular form under parallel incoming winds and vice-versa for oblique winds indicating the deterioration of overall ventilation with longer UCL (Lin et al., 2014) added evidence to the same.

8. **Age of the air τ_p:** Cheng et al. (2008) defined the average retention times of pollutants in a street canyon as follows in Equation- 2.20.

$$\tau = \frac{\iiint_{vol} c dx dy dz}{\dot{Q}} \tag{2.20}$$

The older age of air represents poor ventilation and the younger one represents new air parcels being constantly replenished in the given control volume by the flow, leading to good ventilation. It is worth noting that this formulation requires a uniform source of pollution from the entire control volume where the age of the air is evaluated. Although the age of the air increased with increasing building packing density (Buccolieri et al., 2010). The hotspots of older air were found to vary for lower and higher packing density environments, as the higher and lower packing density environments witnessed a steady plateau in the downstream regions of the environments and a steady increase under perpendicular wind conditions. The adjustment length of configurations with higher building packing density tends to

be lower than in low building packing density environments (Chen et al., 2017). Buccolieri et al. (2010) also recommended emission guidelines in cities with varying mean air age based on packing density and breathing rate to regulate personal exposure to pollutants. In line with the observations made for NEQ, Hang et al. (2018) and Hang et al. (2013) observed that the increasing widths of the semi-open roof setting and covering the roofs aged the air in the overall UCL and that with increasingly oblique winds, the proportion increase in the age of the air compared to the reference open roof configuration reduced substantially. On the other hand, although the larger urban environments (4 $\times$ 4 buildings) with the same building packing density experienced greater ventilation due to naturally more exposure to ambient winds, they could be as much as 40-250% older than their counterpart small urban environments (2 $\times$ 2 buildings) (Hang et al., 2013). However, the impact of the wind direction on the age of the urban air is largely dependent on the shape of the urban form as Huang et al. (2009) observed an older air age in the street if the urban form was circular as opposed to square form under oblique winds.

2.5 Gaps in literature

The two specific gaps were observed in the literature; one from an application standpoint and another from a theoretical one.

1. **Application-based gap:**

   (a) Wind catchers have largely been investigated in a static setup. This prohibits them from adjusting to changes in the environment and thereby creates the risk of them resulting in detrimental impacts under conditions they are not designed for. The opportunity to deploy them adaptively so that they can be adjusted to different configurations based on environmental conditions remains to be unexplored.

   (b) Passive interventions have largely been evaluated for sensitivity to environmental variables including wind speeds, wind directions, and traffic flow in exclusivity. However, in reality, environmental variables vary in tandem and therefore it is essential to develop response mechanisms with passive interventions that incorporate the combined impact of their changes.

   (c) Flat plate design has been largely considered for the design of wind catch-

ers. Although this design could effectively obstruct the wind flow along its normal direction, its efficacy for winds along other directions is either expected to get attenuated to be modest (for oblique winds) or negligible (parallel to its surface). However, the concept of multi-directional wind deflectors that could promote mixing between the above roof and in-canyon air for all ambient wind directions has not been explored.

2. **Theory-based gap:**

   (a) Previous research has introduced several representative outdoor ventilation indices to illustrate the extent of ventilation. However, only limited investigations have been made on the mechanisms of pollution removal. Cheng et al. (2009) analyzed the direct correlation between θ and $\overline{C}_{canyon}$ and Ming et al. (2021), Ming et al. (2023) analyzed the relationship between Sh and $\overline{C}_{canyon}$. The former demonstrates the improvement in $\overline{C}_{canyon}$ through enhanced PCH_{mean} and suppression of PCH_{fluc}, while the latter demonstrated an improvement in $\overline{C}_{canyon}$ through enhanced and suppressed removal of pollutants through convective and diffusive fluxes. Therefore, as the theoretical basis of the performance of passive interventions is rooted in differing fundamental aspects of the flows, it is crucial to identify the appropriate underlying theories that represent the pollution removal process by wind deflectors well.

Chapter 3

CFD Methodology

3.1 Research Overview

As mentioned in the gaps in the literature, the current study is focused towards addressing both technical and application oriented questions. The fundamental technical pursuits in the study is verification of the inverse correlation hypothesis and understanding the implications of including wind flow deflectors from the perspective of Field Synergy Theory. The application side includes the dynamic deployment of the wind deflectors in street canyons. A logical progression of complexities were incorporated for the same by starting with simple 2D environments and then extending it to ideal and asymmetric city type environments with changing traffic flow directions to finally considering simultaneous diurnal changes in wind and traffic flow directions in city-type environments. Lastly, the best approaches from these studies were utilized to design a multi-direction wind deflector for an ideal and real isolated street canyon environment. This study relies on the use of CFD modelling for the development and assessment of the above concept due to the power nature of the software over experimental and field methods for early stage research. The simulations were performed using ANSYS-Fluent software. The outline of the research overview is presented in a flowchart model in Figure 3.1.

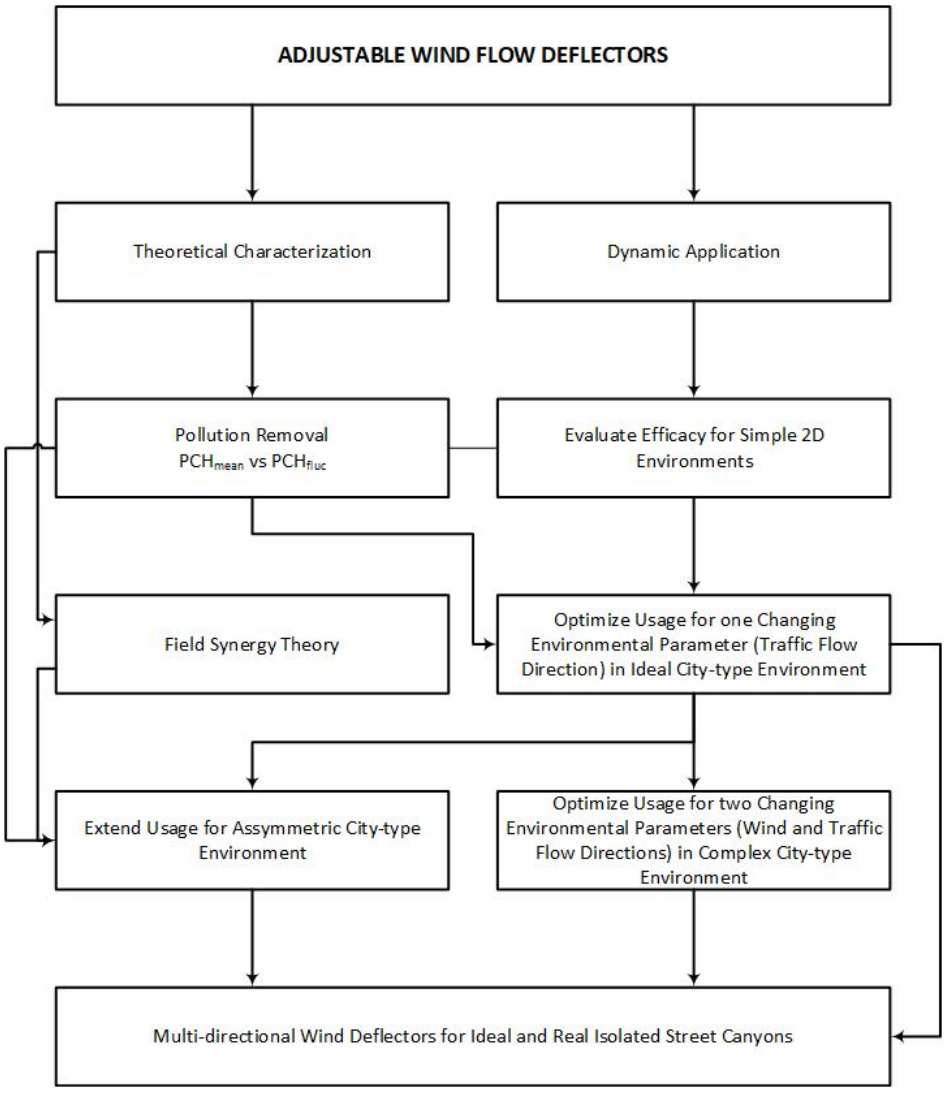

Figure 3.1: Flowchart highlighting the research overview adopted in this study

3.2 Computational Fluid Dynamics

3.2.1 Governing Equations and Closure Problem

In a turbulent flow, instantaneous flow field values including velocity and pressure are always changing in time and hence are expressed as combination of mean and fluctuating components as in Equation 3.1.

$$\phi = \overline{\phi} + \phi' \tag{3.1}$$

The flow fields are substituted with mean and fluctuating components as in Equation 3.1 and time averaged to result in the mass conservation based continuity and the momentum conservation based Navier-Stokes equations as in Equations 3.2 and 3.3.

$$\frac{\partial \overline{u_i}}{\partial x_i} = 0 \tag{3.2}$$

$$\underbrace{\overline{u_j}\frac{\partial \overline{u_i}}{\partial x_j}}_{\text{convective}} = \underbrace{-\frac{1}{\rho}\frac{\partial \overline{p}}{\partial x_i}}_{\text{pressure-gradient}} + \underbrace{\frac{\partial}{\partial x_j}(\nu\frac{\partial \overline{u_i}}{\partial x_j} - \overline{u_i{}'u_j{}'})}_{\text{diffusive}} + S_i \tag{3.3}$$

In Equations 3.2 and 3.3, the velocity field u_i is solved for, $\bar{P}$ is mean pressure and S_i denotes body forces acting on the fluid in the ith direction. The diffusion term in Equation 3.3 including the mean ($\nu\frac{\partial \overline{u_i}}{\partial x_j}$) and fluctuating velocity ($\overline{u_i{}'u_j{}'}$) components are identified as viscous and turbulent (Reynolds) stresses respectively. This is called the closure problem where one would have 4 equations (continuity and Navier Stokes Equations in each of the three directions) and 10 variables (three mean velocities, mean pressure and six fluctuating velocity components). Turbulence models are thus necessary to overcome this closure problem. However, turbulence models vary drastically in their level of resolution and modelling approach, including the number of closure equations developed to compute.

3.2.2 Turbulence Modelling

Turbulence is the phenomenon that results in random fluctuations in the flow fields including velocity and pressure due to excessive kinetic energy. As the flows

transition from laminar to turbulent flows, the viscous and inertial forces become increasingly less and more dominant respectively. This is characterized by Reynolds Number (Re), the non-dimensional ratio of inertial and viscous forces, as in Equation 3.4.

$$Re = \frac{\rho U D}{\mu} \tag{3.4}$$

Where ρ, μ, U and D are the density and dynamic viscosity of the fluid and U and D are the velocity and characteristic length scale of fluid flow. Turbulence results in eddies of different time and length scales and as the largest eddies are as large as in the scale characterized by the computational domain and mean flow, they experience negligible viscous forces. Due to the lack of viscous forces on the large eddies, the shear in the fluid flow would result in an increased and decreased eddy rotation and radius respectively (Schlichting, 1979; Versteeg, 2007). This overall phenomenon is explained by the cascade theory, also shown in Figure 3.4, where the largest eddies in the computational domain derive their energy from the mean flows and this energy is passed on to the smallest scale of eddies (Kolmogorov scale eddies) via medium scale eddies.

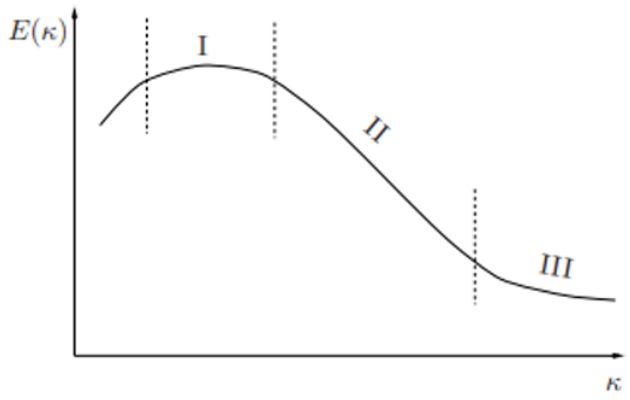

Figure 3.2: The energy cascade; spectral variation of energy of eddies with eddy wave-number, κ ($\kappa \propto L^{-1}$) (Davidson et al., 2011)

Finally, the isotropic Kolmogorov scale eddies dissipate all the energy it derived from the medium scale eddies as heat via friction (Davidson et al., 2011). Ideally, one would not need to model turbulence if the eddies of all the scales are resolved, as in Direct Numerical Simulations (DNS). However, such simulations are computationally very intensive as due to very detailed spatial and temporal discretizations required . As the next option, the Large Eddy Simulations (LES) employs volume filtering techniques to resolve the large and medium-scale eddies and

model the Kolmogorov scale eddies using sub-grid scale models. However, even the LES simulations take more than 13 times longer than traditional RANS (Reynolds Averaged Navier Stokes) turbulence models (Lopes et al., 2024). The RANS turbulence model as a further approximation, models both the medium and Kolmogorov scale eddies. The RANS model predicts the near-wall velocities in the logarithmic region of the flow using the law of the wall-based wall functions. As Figure 3.3 shows the different near-wall regions of the fluid flow, the flow could be seen in independently in the inner and outer regions. The inner region is characterized by strong wall shear (viscous effects) and minimal to negligible inertial effects (no Reynolds shear at the wall as $u' = v' = w' = 0$) and vice-versa for the outer region. Therefore, considering only wall shear in the inner region, a linear increase of velocity from the wall is assumed while as the Reynolds shear forces are constant in the logarithmic region (with no wall shear), a logarithmic law of the wall-wall model is applied here (Davidson et al., 2011). Therefore, the y^+ for these models necessarily needs to be over 30. There have also been the development of hybrid models including Scale Adaptive Simulations (SAS), Detached Eddy Simulations (DES), PANS (Partially Averaged Navier Stokes) as a trade-off for accuracy and computational times. Lastly, there is a separate class of turbulence model called the Reynolds Stress Model (RSM) which is a six-equation model where a transport equation is modeled for all the independent Reynolds stresses.

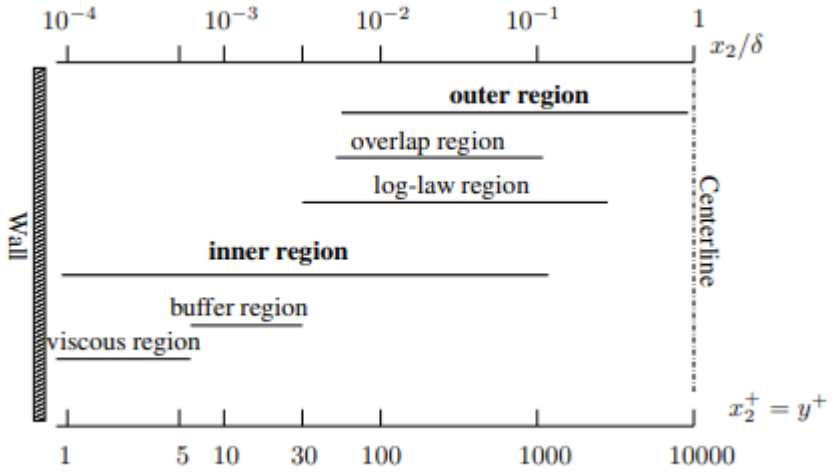

Figure 3.3: Near wall regions of fluid flow v/s y^+ (Davidson et al., 2011)

3.2.2.1 $k-\epsilon$ Turbulence Models

Although the choice of turbulence model is very reliant on the application and resource availability, studies involving wind catchers and many other passive interventions have predominantly used the standard $k-\epsilon$ turbulence model with the standard wall function (Cao et al., 2023; Lin et al., 2019; Ming et al., 2018; Ming et al., 2021; Zhang et al., 2011). The Standard $k-\epsilon$ turbulence model is an eddy viscosity model based on Boussinesq's hypothesis applied to the Reynolds stress assuming isotropic eddy viscosity as in Equation 3.5.

$$\overline{u_i{}'u_j{}'} = \frac{2}{3}k\delta_{ij} - \nu_t(\frac{\partial \overline{u_i}}{\partial x_j} + \frac{\partial \overline{u_j}}{\partial x_i}) \tag{3.5}$$

Here, k is the turbulent kinetic energy, μ_t is the turbulent eddy viscosity and δ_{ij} is Kronecker's delta. The turbulent eddy viscosity is defined as in Equation 3.6, where ϵ is the turbulence dissipation rate.

$$\mu_t = \rho c_\mu \frac{k^2}{\epsilon} \tag{3.6}$$

Although this approximation mitigates the requirement to solve for the fluctuating velocities, it also introduces two variables to solve, k and ϵ. Nevertheless, this brings the complexity of the closure problem down from having 10 variables and four equations to having six variables and four equations. The standard $k-\epsilon$ turbulence model brings closure to the system by modeling transport equations for k and ϵ as in Equations 3.7 and 3.8.

$$\overline{u_i}\frac{\partial k}{\partial x_j} = \frac{\partial}{\partial x_i}[(\nu + \frac{\nu_t}{\sigma_k})(\frac{\partial k}{\partial x_i})] + \frac{1}{\rho}P_k - \epsilon \tag{3.7}$$

$$\frac{\partial \epsilon}{\partial x_j} = \frac{\partial}{\partial x_i}[(\nu + \frac{\nu_t}{\sigma_\epsilon})(\frac{\partial \epsilon}{\partial x_i})] + \frac{1}{\rho}c_{1\epsilon}P_k - c_{2\epsilon}\frac{\epsilon^2}{k} \tag{3.8}$$

P_k is the production source term. $\sigma_k = 1$, $C_{1\epsilon} = 1.44$, $C_{2\epsilon} = 1.92$ and $\sigma_\epsilon = 1.3$ are model constants. The production source term was modeled as in Equation 3.9.

$$P_k = \mu_t S^2 \tag{3.9}$$

Where S_{ij} is the strain rate tensor. Although ReNormalaized Group (RNG) and Realizable $k-\epsilon$ models are improved $k-\epsilon$ models the Standard $k-\epsilon$ turbulence model was predominantly used in this study due to its superior performance in predicting flow fields in sheltered regions involving very low velocities (Lin et al., 2019), such as in street canyon configurations. The Realizable $k-\epsilon$ differs from the Standard $k-\epsilon$ model in only two aspects. First includes a variable c_μ formula as opposed to a constant c_μ for the Standard and RNG $k-\epsilon$ models and the second pertains the model equation for ϵ where the effects of mean rotation on the turbulent viscosity is included. This would result in the following two changes as in Equations 3.10 and 3.11 respectively compared to the Standard $k-\epsilon$ model.

$$c_1 = max[0.43, \frac{\eta}{\eta+5}] \tag{3.10}$$

$$\eta = S\frac{k}{\epsilon} \tag{3.11}$$

On the other hand, the RNG $k-\epsilon$ model differs from the Standard $k-\epsilon$ model through the constant $c_{2\epsilon}$ to capture the smaller length scales of the low Re flows as in Equation 3.12.

$$c^*_{2\epsilon} = c_{2\epsilon} + \frac{c_\mu \eta^3(1-\eta/\eta_0)}{1+\beta\eta^3} \tag{3.12}$$

3.2.3 Species Transport Model

In addition to the six equations and six variables, the species transport model introduces another transport equation for calculating the dispersion of the pollutant gas as in Equation 3.13.

$$\overline{u_j}\frac{\partial C}{\partial x_j} = \frac{\partial}{\partial x_j}((D_m + D_t)\frac{\partial C}{\partial x_j}) + S \tag{3.13}$$

The model tracks the concentration of the pollutant gas by solving for the volume fractions all the mixture gases thus resulting in n-1 species transport equations for n gases in the system. Ansys-Fluent allows the definition of pollution gases through several techniques including fixed source and regular source from a specific region in the computational domain. A 3-D space is identified as the pollution source region

where constant mass flow rate per unit volume of the pollution gas is prescribed to have a volumetric source. As Ansys- Fluent solves for n-1 transport equation, a common transport equation is solved for the diffusion of the pollution gas in air using volume fractions. Therefore, the cell properties including density, material viscosity and thermal conductivity were prescribed to be estimated by the solver using volume weighted averages. Finally binary diffusion coefficient of air and the pollution gas specific to the temperature was defined to characterize the diffusivity.

3.2.4 Other Aspects of CFD Solving

This work comprised steady-state isothermal models of neutrally stratified ABL flow in simple 2D urban environments, 3D isolated street canyons and complex 3D city-type environments. All of the transport equations in the models were solved using second-order discretization schemes. The solutions converged when the residual errors of all the transport equations reached below $1e-6$ and the species transport equation below $1e-8$. Additionally, concentration and velocity monitors were included in critical locations of the computational domain to verify whether the flow achieved steady state. Finally, the SIMPLE solver was used for the pressure-velocity coupling algorithm.

3.3 Validation studies

Experimental studies conducted by Brown et al. (measurement details obtained from Lien and Yee (2004)) at the US Environmental Protection Agency's (EPA) Fluid Modelling Facility (FMC) to measure flow fields in a city-type environment was used as the physical basis for the validation of CFD models used in this study, including flow field including velocity components and TKE. The studies conducted at the ABL wind tunnel of the Meteorological Institute of Hamburg by Meroney et al. (1996) to evaluate ethane gas dispersion and at the Laboratory of Building- and Environmental Aerodynamics of the Institute for Hydromechanics at the Karlsruhe Institute of Technology (CODASC- COncentration DAta of Street Canyons) to evaluate the SF_6 gas dispersion, were used as the physical basis for model validation of pollution dispersion in street canyons for the 2D and 3D models developed, respectively.

3.3.1 Validation of Flow Measurements

3.3.1.1 Experimental Setup

The experiments conducted by Brown et al. (Lien and Yee, 2004) included 77 cubical structures with an edge length of 0.15m in 7 rows and 11 columns for the city-type environment as shown in Figure 3.4a. With a frontal area index of 0.25, the city-type environment completely covered the spanwise width of the wind tunnel. The test section of the FMC was 18.3m long, 3.7m wide and the adjustable height was fixed at 2.1m. The neutral Atmospheric Boundary Layer (ABL) profile from the orthogonal approaching wind was characterized by a reference streamwise velocity of $u_H = 3m/s$, power law coefficient of $\alpha = 0.16$, friction velocity of $u_* = 0.24m/s$, and thickness $\delta = 1.8m$. The building Reynolds Number of the flow, Re_b 30000, is greater than the critical building Reynolds number, $Re_{cr} = 4000$ (Snyder, 1972). The flow is therefore Reynolds-independent and scalable. The velocity components were measured using Pulsed Wired Anemometers (PWA) at a pulsing rate of 10Hz over an averaging time of 120s in each measurement location. Flow field measurements including mean velocity, turbulence velocity variance and turbulent kinetic energy were conducted to ascertain 81 vertical profiles in the study.

3.3.1.2 Numerical model

The mesh independence and model validation study of Brown et al. (Lien and Yee, 2004) were conducted for the full-street scale ($H = 30m$). Figure 3.4b shows the boundary conditions included in the "half-symmetry" model. The "half-symmetry" model utilizes the natural symmetric nature of the problem and allows one to model the problem by including only half the width of the buildings and street parallel to wind flow in the spanwise direction. The results are representative of the flow field around the center column of buildings from Brown et al. (Lien and Yee, 2004) (also marked in Figure 3.4a). Measurements from Lien and Yee (2004) included only flow measurements such as streamwise (u) and wall-normal velocities (w) and TKE along vertical lines in wall-normal direction from ground and building roof-level along the center row of buildings. The measurements included data collection until a distance of 1000mm from the ground level. Lines of comparison of experimental data with numerical measurements are marked as x_1 (upstream to the built environment, 186m from the inlet), x_2 and x_3 (inside the street canyons

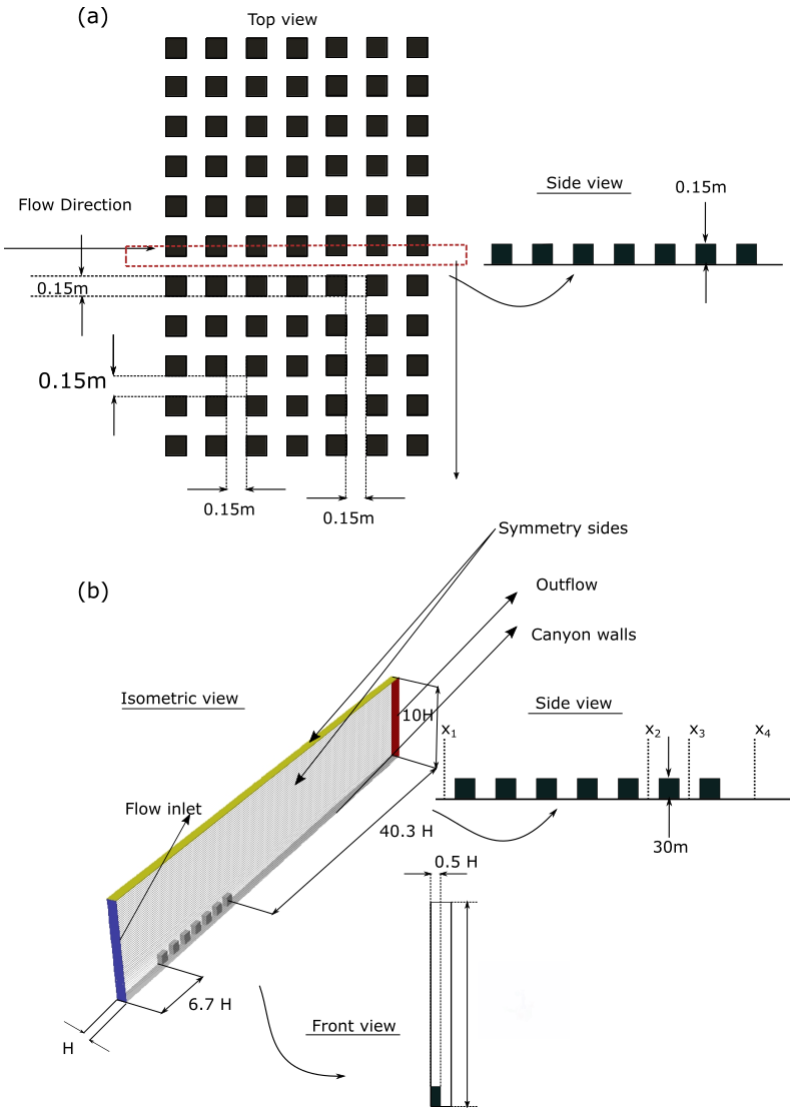

Figure 3.4: a) Schematic arrangement of 77 city-like buildings in the wind tunnel experiment conducted by Brown et al. (top); b) Computational domain and measurement probe locations considered for numerical validation of velocity fields Lien and Yee, 2004 (bottom).

in the built environment, 486 and 546m from the inlet) and x_4 (downstream to the built environment, 696m from the inlet) respectively. A distance of $6.7H$ was provided between the inlet and upwind side of the first row of buildings, $40.3H$ between the downwind side of the last row of buildings and the outflow boundary, and the computational domain's height was $10H$. The computational domains considered for the validation and case studies adhered to the recommended guidelines for urban wind flow computations Franke et al., 2011; Tominaga et al., 2008. The inlet boundaries were modeled by prescribing power-law Atmospheric Boundary Layer

(ABL) profiles using stream-wise velocity component u(z), k(z) and ϵ(z), as in the Equations- 3.14-3.16.

$$u(z) = U_H(\frac{z}{H})^{\alpha} \tag{3.14}$$

$$k(z) = \frac{{u_*}^2}{c_\mu} \tag{3.15}$$

$$\epsilon(z) = {c_\mu}^{3/4} k^{3/2}/\kappa z \tag{3.16}$$

Here, values of α, δ and u_* were prescribed as per experimental conditions mentioned earlier. $c_\mu = 0.09$ and $\kappa = 0.41$ (von Karman number) were model constants. The downstream end of the domain and the top surface were prescribed with outflow and symmetry conditions, respectively. The sides of the domain were prescribed with symmetry conditions. The Grid Convergence Index (GCI) was used using Richardson's extrapolation method for the mesh convergence analyses (Roache, 1994). The computational domain comprised 883,614, 1,695,140 and 3,326,711 hexahedral cells for the coarse, medium and fine meshes. The GCI was evaluated as follows in Equation 3.17.

$$GCI = \frac{1.25\ e_a}{r^p - 1} \tag{3.17}$$

Here, e_a is the approximate relative error, r is the grid refinement ratio and p is the order of convergence. GCI is evaluated at four locations: x_1, x_2, x_3 and x_4. The average GCI for x_1, x_2, x_3 and x_4 were 0.8%, 7.89%, 2.4% and 1.8% respectively, hence proving the conformance in results obtained from the medium and fine grids. Thus medium mesh was deemed converged for further analysis. Figure 3.5 and Table 3.1 show that the numerical predictions of the validation model both qualitatively and quantitatively represent the measurements of streamwise velocity (u), wall-normal velocity (w) and TKE well in four different locations. Although the performance agrees with the recommended statistical metrics for model validation, the w and TKE were not predicted as well as u. The under-prediction of turbulence energy in the validation of the model using the Standard $k - \epsilon$ turbulence model

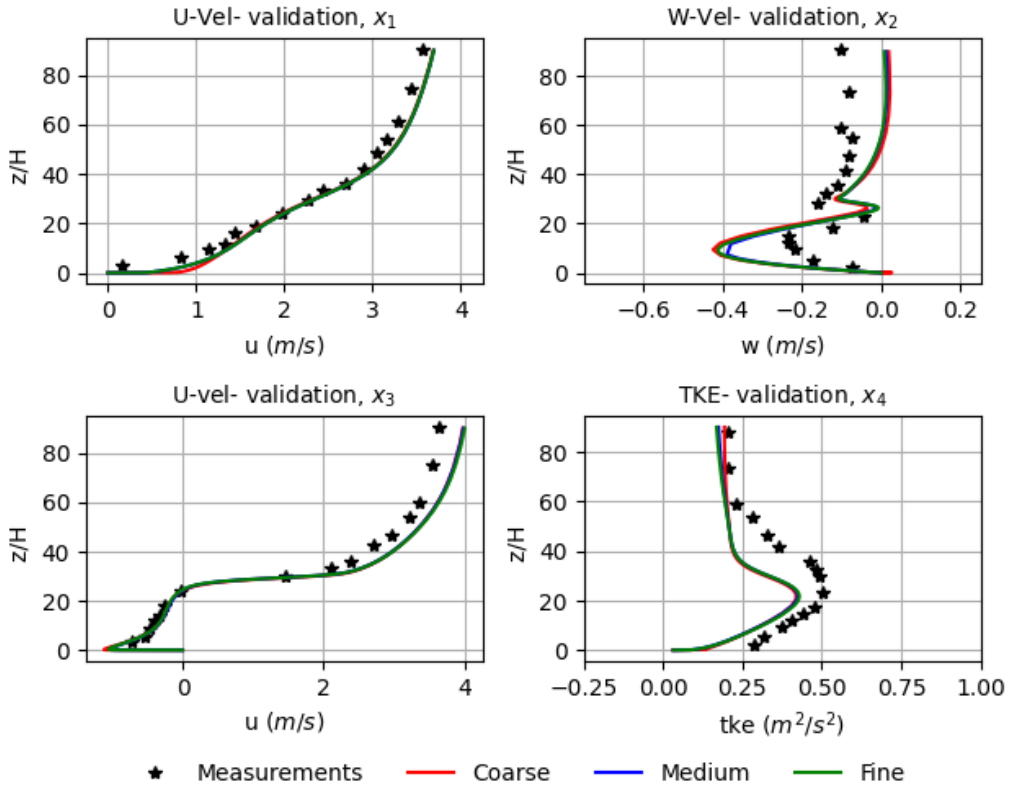

Figure 3.5: Validation of CFD model against flow measurements from Lien and Yee (2004)

in the street canyon and the rooftop of the buildings in the array has also been reported in the literature (Lien and Yee, 2004).

Statistical index	Accepted Result	Target Value	x_1	x_2	x_3	x_4
RNMSE	$< \sqrt{1.5}$	0	0.10	0.67	0.11	0.34
FB	[-0.3,0.3]	0	-0.08	-0.06	-0.13	0.31
FAC2	>0.5	1	1	0.56	0.94	1
MG	[0.7,1.3]	1	0.84	-	-	1.36
VG	<4	1	1.21	-	-	1.13

Table 3.1: Statistical measure of CFD validation of flow measurements conducted by Brown et al. (from Lien and Yee (2004)).

3.3.2 Validation of Concentration Measurements- 2D

3.3.2.1 Experimental Setup

This experiment included two 0.9m long blocks with 0.06 × 0.06m cross-sections positioned 0.06m apart from each other, representing an isolated street canyon that is aligned orthogonal to the incoming winds. Ethane gas was used as the tracer and the concentration was measured at 14 locations as shown in Figure 3.6. Comparison in the current study pertains to the eight probe measurements aligned along the leeward and windward facades at mid-length of the street canyon at 0.01, 0.02, 0.04 and 0.058m from the ground. For the measurements, 4 l/h and 100 l/h of ethane gas and air respectively, in a homogeneous mixture were released from the bottom of the canyon. The experiment conducted by Meroney et al. (1996) included concentration sampling using a flame-ionization type hydrocarbon analyzer and calibration was performed against a laboratory-prepared mixture of air and ethane gas. The reference velocities considered in the experiment were ensured to constitute $Re_b > 3400(Re_{cr})$ to exhibit Reynolds independence. The $U_{ref} = 2m/s$ with AR=1 measurement case was considered for the model validation.

3.3.2.2 Numerical Model

The validation was performed in 2D to reduce computational time. As for the flow field validation, the numerical validation of ethane gas dispersion measurements by Meroney et al. (1996) was conducted in full street scale. The computational domain includes a $5H$ distance between the inlet and the upwind edge of the first building and between the roof of the street canyon and the top boundary, $10H$ distance between the downstream end of the last building and the outflow boundary. The inlet boundaries were modeled by prescribing power-law Atmospheric Boundary Layer (ABL) profiles using stream-wise velocity component u(z), k(z) and ϵ(z), as in the Equations- 3.18-3.20.

$$u(z) = U_{ref}(\frac{z}{\delta})^{\alpha} \tag{3.18}$$

$$k(z) = \frac{{u_*}^2}{c_\mu} \tag{3.19}$$

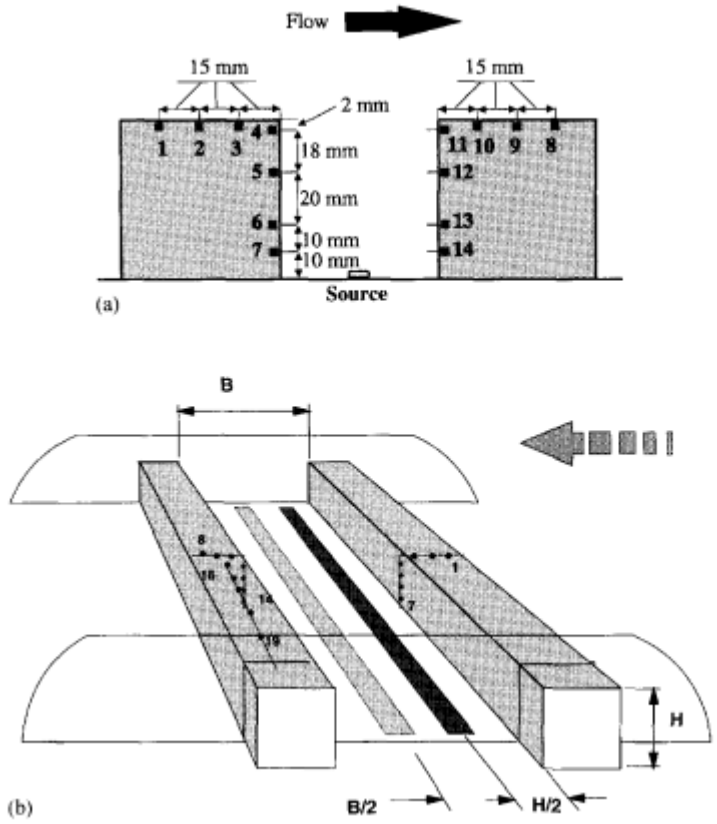

Figure 3.6: Figure from Meroney et al. (1996) showing the ethane gas concentration measurement probe locations and isolated street canyon model under orthogonal ambient wind

$$\epsilon(z) = {u_*}^3/\kappa z \tag{3.20}$$

Here, $\delta = 0.65m$ (in the wind tunnel scale) is the boundary layer thickness of the flow, $c_{mu} = 0.09$. The power law co-efficient (α) and the von Karman constant (κ) were 0.28 and 0.41 respectively. The coarse, medium and fine meshes considered for mesh convergence of the model validation predictions comprised 62,894, 140,594 and 314,444 hexahedral cells. The average GCI errors along leeward and windward facades were 0.8% and 1.8% respectively (grid convergence study was performed using the Standard $k - \epsilon$ turbulence model), hence proving the conformance in results obtained from the medium and fine grids. Thus medium mesh was deemed converged for further analysis. The realizable $k - \epsilon$ model predicted the best on both the windward and leeward sides. The Standard and RNG $K - \epsilon$ models over predicted K on the windward and leeward sides respectively. Figure 3.7 and Table

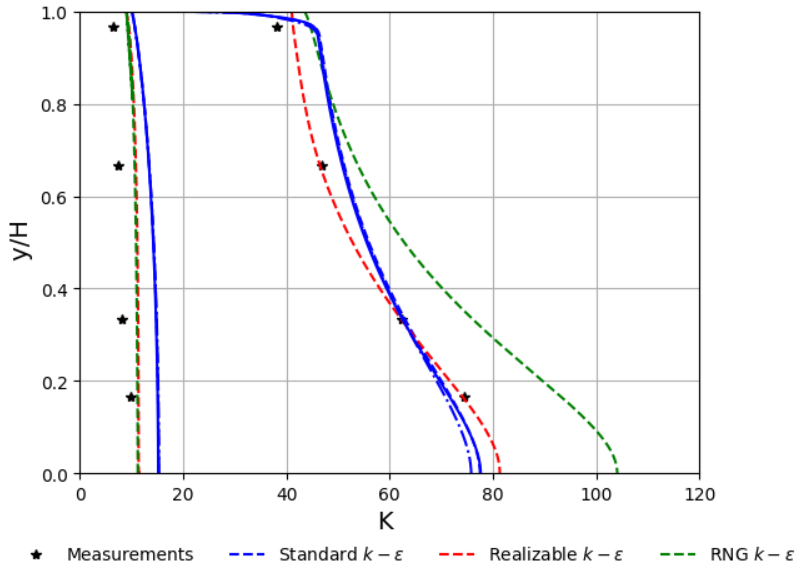

Figure 3.7: Validation of CFD model against concentration measurements obtained by Meroney et al. (1996); *dotted lines (-.), dashed lines (–) and solid lines (-) indicate the coarse, medium and fine meshes respectively.*

3.2 shows the qualitative and quantitative representativeness of the three turbulence models in predicting the no-dimensional concentrations (K) along the leeward and windward facades.

Statistical index	Accepted Result	Target Value	Standard $k-\epsilon$	Realizable $k-\epsilon$	RNG $k-\epsilon$
RNMSE	$< \sqrt{1.5}$	0	0.15	0.06	0.24
FB	[-0.3,0.3]	0	-0.11	-0.16	-0.28
FAC2	>0.5	1	1	1	1
MG	[0.7,1.3]	1	0.74	0.85	0.76
VG	<4	1	1.16	1.06	1.10

Table 3.2: Statistical measure of CFD validation of flow measurements conducted by Meroney et al. (1996).

3.3.3 Validation of Concentration Measurements- 3D

3.3.3.1 Experimental Setup

CODASC database includes concentration fields of SF_6 tracer gas within isolated street canyons including side flows with different ARs, with and without vegetation under different ambient winds directions from wind tunnel measurements. For

the current validation studies, a symmetric isolated street canyon without vegetation under parallel, orthogonal and oblique winds at 45° were chosen as the reference models. The upwind and downwind building dimensions include 12 $\times$12 $\times$120cm (HBL) respectively. SF_6 tracer gas was uniformly injected in the street canyon at a rate of $10gs^{-1}$ through four line sources positioned 0.23H and 0.35H away from the leeward and the windward facades respectively. Figures 3.8a and 3.8b includes the schematics of the street canyon configuration considered for validation under orthogonal ambient winds and the line pollution sources respectively. Measurements of SF_6 for other wind wind directions were performed by rotating the street canyons on the turntable accordingly. The experiment was conducted in a 1:150 reduced scale to the full street model and the CFD validations were performed for full street scale models. SF_6 measurements were conducted across the length ($y/H = -5$ to $y/H = 5$) of both the leeward and windward walls at five specific heights from the ground including $z/H = 0$, $z/H = 0.166$, $z/H = 0.333$, $z/H = 0.5$, $z/H = 0.667$, $z/H = 0.833$ and $z/H = 1$. Measurements were made at 100 points at each height across the length on both the facades. As a standard practice, the vertical dispersion across both the facades were compared at three different locations $y/H = 0$ (mid-canyon), $y/H = -1.26$ (upstream of mid-canyon location) and $y/H = 3.79$ (downstream of mid-canyon location) respectively, as also shown in the Figure 3.8c.

3.3.3.2 Numerical Model

The mesh convergence study was conducted for oblique wind scenario. The coarse, medium and fine meshes comprised of 4588125, 7280622 and 14397953 polyhexacore grid cells respectively. As the difference between the medium and fine meshes were marginal, the medium mesh was considered converged for further analyses. The inlet velocity of the neutrally stratified ABL profile was prescribed as in Equation 3.21.

$$u(z) = u_{ref}(\frac{z}{z_{ref}})^{\alpha} \tag{3.21}$$

Here, $u_{ref} = 4.39$m/s, $z_{ref} = 15$m and $\alpha = 0.30$. For the CFD model, the standard $k-\epsilon$ turbulence model with standard wall function- wall model was employed and the inlet profile was defined using profiles for k and ϵ as in Equations 3.19 and 3.20. The sides and the top surface of the computational domain were prescribed as symmetry surfaces, the downwind exit of the domain was prescribed as outflow condition and the street surfaces and buildings were prescribed as walls. 8H and 7H distances were provided between the upwind edge of the upstream building and

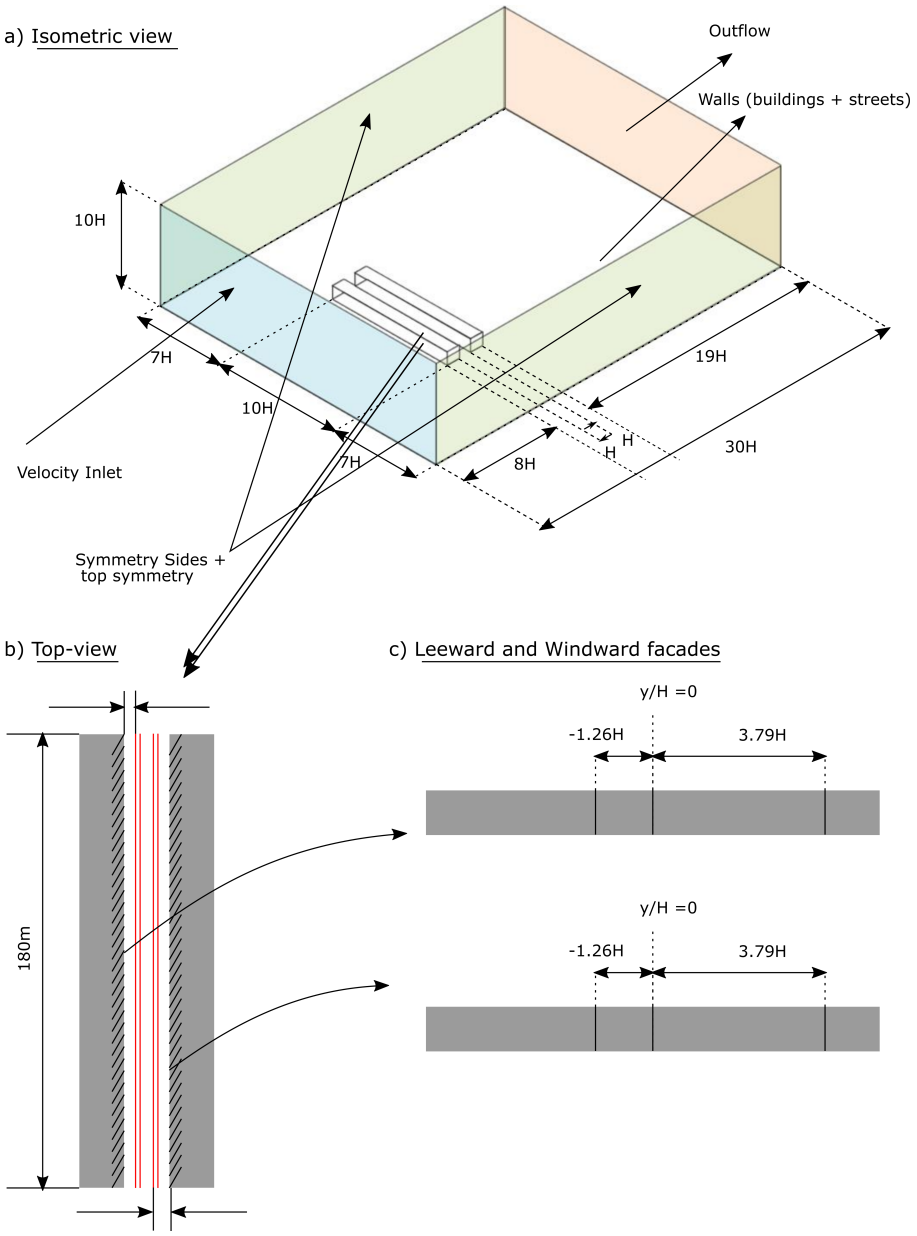

Figure 3.8: a) Schematic of long isolated street canyon in the wind tunnel experiment (CODASC)- computational domain and boundary conditions; b) Top-view showing the line pollution source regions; c) Leeward and windward facades with measurement probe locations (where considered for validation).

the inlet and the sides of the building and the side symmetry surfaces. The height of the computational domain was 10H. Unlike the validation of c_2H_6 measurements by Meroney et al. (1996) where the CFD model used a default Schmidt number of 0.7, the validation of SF_6 gas dispersion was optimal with a Schmidt number of 0.3 for the flow (Schmidt number is a non-dimensional number representing the rate of

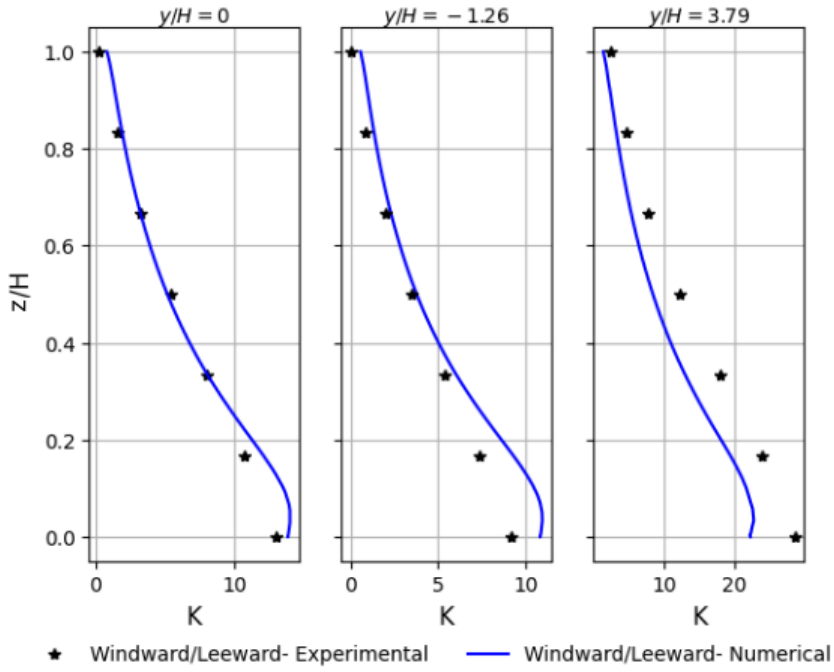

Figure 3.9: Validation of CFD model against concentration measurements from CODASC database pertaining to isolated street canyon under parallel ambient winds

momentum diffusion to mass diffusion). Figures 3.9- 3.11 and Tables 3.3- 3.5 show the qualitative and quantitative comparison of the numerical predictions against CODASC wind tunnel measurements. It can be seen from Figure 3.9 that the numerical predictions were best fitted against measurements for parallel winds. Figure 3.10 indicates that there were over-predictions along the leeward facade for orthogonal winds and there were under-predictions along the leeward facade, especially in the upstream region, for oblique winds at 45°. The over and under predictions from the numerical model is also accounted to the optimal Schmidt number that might be slightly deviant from the common value assumed for all three scenarios. Such variations have also been reported in the literature (Jon et al., 2023). It is worth noting at this point that Lauriks et al. (2021) developed a numerical model including variable Schmidt number and the performance of predictions were substantially improved. Therefore, despite the aberrations from the suggested statistical performance, especially for the oblique winds, the overall validation model was considered satisfactory.

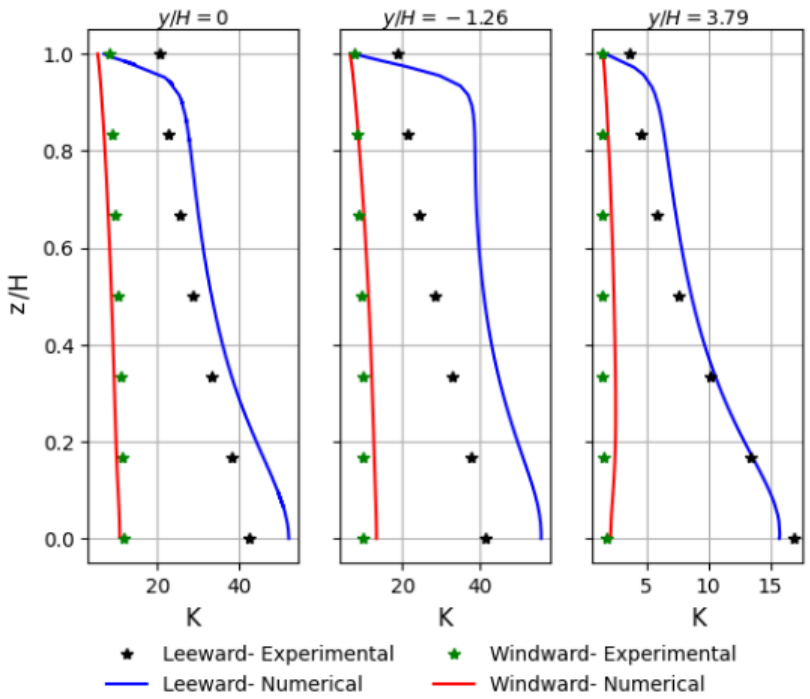

Figure 3.10: Validation of CFD model against concentration measurements from CODASC database pertaining to isolated street canyon under orthogonal ambient winds

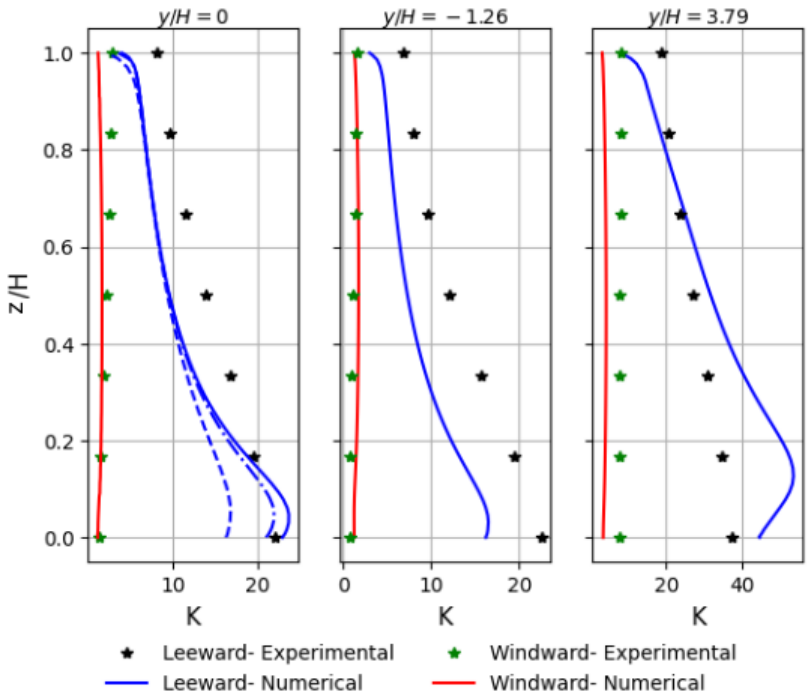

Figure 3.11: Validation of CFD model against concentration measurements from CODASC database for isolated street canyon under oblique ambient winds at 45°. The dashed lines (–) and dash-dotted lines (-.) indicate the coarse and fine meshes respectively.

Statistical index	Accepted Result	Target Value	$y/H = 0$	$y/H = -1.26$	$y/H = 3.79$
RNMSE	$< \sqrt{1.5}$	0	0.04	0.27	0.08
FB	[-0.3,0.3]	0	-0.06	-0.18	0.28
FAC2	>0.5	1	0.86	1	1
MG	[0.7,1.3]	1	0.8	0.82	1.40
VG	<4	1	1.05	1.04	1.12

Table 3.3: Statistical measure of CFD validation of concentration measurements conducted from CODASC database for isolated street canyon under parallel ambient winds.

Statistical index	Accepted Result	Target Value	$y/H = 0$	$y/H = -1.26$	$y/H = 3.79$
RNMSE	$< \sqrt{1.5}$	0	0.04	0.27	0.08
FB	[-0.3,0.3]	0	-0.03	-0.27	-0.08
FAC2	>0.5	1	0.92	0.92	0.92
MG	[0.7,1.3]	1	1.11	0.84	0.85
VG	<4	1	1.01	1.03	1.03

Table 3.4: Statistical measure of CFD validation of concentration measurements conducted from CODASC database for isolated street canyon under orthogonal ambient winds.

Statistical index	Accepted Result	Target Value	$y/H = 0$	$y/H = -1.26$	$y/H = 3.79$
RNMSE	$< \sqrt{1.5}$	0	0.24	0.42	0.42
FB	[-0.3,0.3]	0	0.22	0.36	0.01
FAC2	>0.5	1	0.86	0.93	0.64
MG	[0.7,1.3]	1	1.39	1.09	1.44
VG	<4	1	1.18	1.24	1.43

Table 3.5: Statistical measure of CFD validation of concentration measurements conducted from CODASC database for isolated street canyon under oblique ambient winds at 45°.

Chapter 4

2D and 3D Analyses of Wind Flow Deflectors

The content of this chapter has been accepted for publication in a more concise form: Vasudevan, M., Pilla, F. and McNabola, A., 2023. Enhancing ventilation in street canyons using adjustable roof-level wind flow deflectors. Energy and Built Environment.

4.1 Introduction

As mentioned in the gaps in the literature in Chapter 2, roof-level interventions present several advantages over other passive interventions ranging from independence from surface and subsurface infrastructure and traffic and pedestrian mobility to the promotion of mixing between the polluted air contained within the street canyon volume and cleaner ambient above-roof air to support the dilution of street-level pollution hot-spots. Although studies have extensively worked on demonstrating the ability of wind catchers to reduce personal exposure to pollutants via windows in near-road building facades and pedestrian zones in urban environments, the conceptualization of wind deflectors is pending. Ming et al. (2021) applied the field synergy theory to 2D urban asymmetric environments to correlate the pollution removal from the street canyon and the synergy between the velocity and concentration fields that promote pollution removal through convective fluxes. In the context of urban street canyons, if there is more synergy between the velocity and concentration fields within the street canyon volume, it means that convection

dominates the pollution transport and if not then, diffusion dominates the pollution transport. Although field synergy is a very crucial indicator in informing the internal dynamics within the street canyon (the reason why it is considered in Chapter 5), one could say that it is not a straightforward indicator of the interaction of the in-canyon and above-canyon air that the wind deflector attempts to enhance.

An idealized street canyon experiences the majority of pollution removal through turbulent fluctuations induced fluxes. The Air Exchange rates (ACH) and Pollution Exchange rates (PCH) across the street canyon openings could be as high as an order of magnitude greater than the mean flow induced ACH and PCHs (Cheng et al., 2008). Cheng et al. (2009) illustrated that a decrease in Richarson Number (Ri) resulted in a reduction in retention times of the pollutants in the street canyon and also a transition in a pollution removal mode, from a turbulent fluctuations-dominated (lower θ) process to a mean flow-dominated (higher θ) process. This was considered the starting point for the conceptualization of wind deflectors. By maintaining a constant Ri, it was hypothesized in this study that θ and $\bar{C}_{canyon}$ hold an inverse correlation. The hypothesis is also intuitive as one could expect if the recirculating wind inside the street canyon advects more of the pollutant from the source to the above roof region in its natural trajectory, the pollution removal would depend increasingly less on the turbulent diffusion (which is superficial at the interface surface between the canyon and outside-canyon volumes) to flush the pollutant out of the canyon (washout is more effective than turbulent diffusion). Therefore, the work in this chapter apart from furthering the consideration of θ as a key ventilation index for undertakings about diluting pollution hot spots with cleaner air, also in complex built environments, saliently illustrated the ability of the wind deflectors to steer θ and overall canyon concentrations.

Lastly, from the application point of view, traffic volumes are rarely evenly distributed on all the roads in a city-type environment and traffic intersections are susceptible to air pollution hotspots due to uneven movement of vehicles and spatial variation of air quality (Gokhale and Khare, 2007; Gulia et al., 2019; Gulia et al., 2022). Therefore, an adaptive solution for changing traffic flow direction was considered a straightforward mitigation strategy to reduce the personal exposure of road users and near-road building inhabitants.

4.2 Adjustable Wind Deflectors

The wind deflector could be imagined as a thin and rigid plate that could be moved to any position along the rooftop between two buildings by a cable system and be rotated to any orientation depending on the micro-environment conditions. A functional mode of the wind deflector altering the flow inside a 2D street canyon is shown in Figure 4.1. The deflector was considered 2m long and "thin" (zero thickness). The deflectors had 1m of face width above and below the roof level.

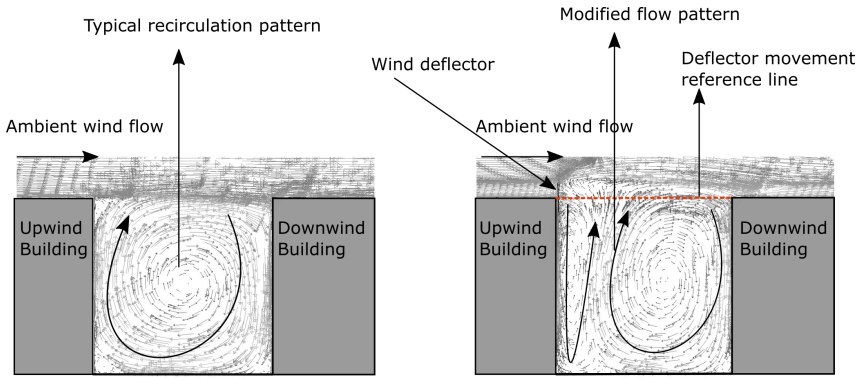

Figure 4.1: a) Conventional flow pattern inside the target street canyon with **no wind deflectors** (left); b) Modified flow pattern with **deflector** washing down both leeward and windward facades with clean rooftop air (right). *Results obtained from 2D CFD simulations.*

4.3 Problem Description

The problem statement in question could be divided into two parts:

1. Verify the hypothesis of an inverse correlation between θ and $\bar{C}_{canyon}$ for a simple 2D and complex 3D city-type environment. This forms the conceptualization of the wind deflectors from a theoretical standpoint.
2. For the application side, the scenarios of considerations are different for the 2D urban and 3D city-type environments. For the 2D urban environment, the question is, how efficient would adjustable wind deflectors be in controlling near-road building exposure if exposure along leeward and windward facades is evenly or unevenly distributed at any given time? Figure 4.2 shows the computational domain, target street canyon and application of wind deflectors in different positions and orientations considered for the performance analysis

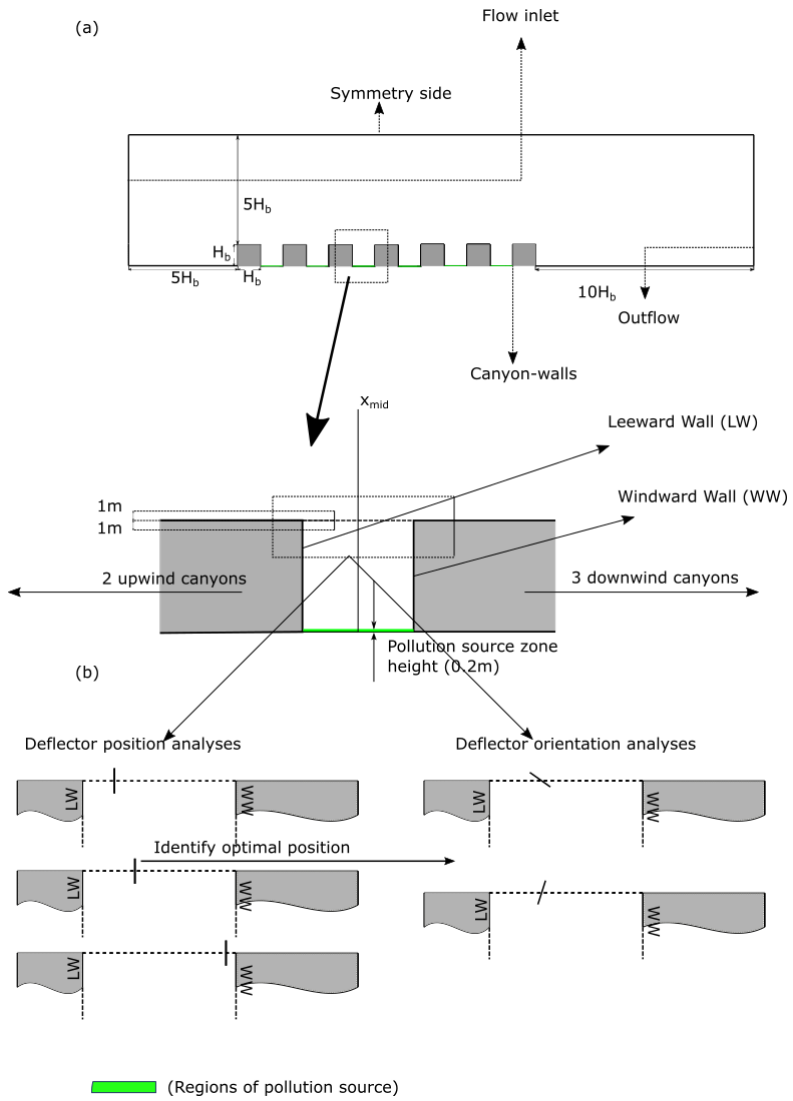

Figure 4.2: a) Computational domain considered for 2D street canyons b) Deflector position and orientation analyses

in a 2D context.

On the contrary, the question for 3D city-type environments is, how efficient would adjustable wind deflectors be in controlling near-road building exposure if the traffic flow direction changes between the cross and side roads in a city-type environment? For convenience, the pollution on cross and side roads are referred to further in this thesis as CRP (Cross Road Pollution) and SRP (Side Road Pollution) source models respectively. Five different traffic flow patterns in the city-type environment were considered for the emission source; CRP, SRP and three other transitional traffic flow types, 8, 12 and 16 hours of CRP source in a day and the rest of the hours of SRP source. In a practical sense,

a city-type environment rarely experiences no traffic flow on any of its roads. Therefore, the current modeling could also be considered as the difference in the traffic flow volume between the two roads. Figure 4.3 schematically shows the CRP and SRP source models and the roof-level inclusion of the wind deflectors.

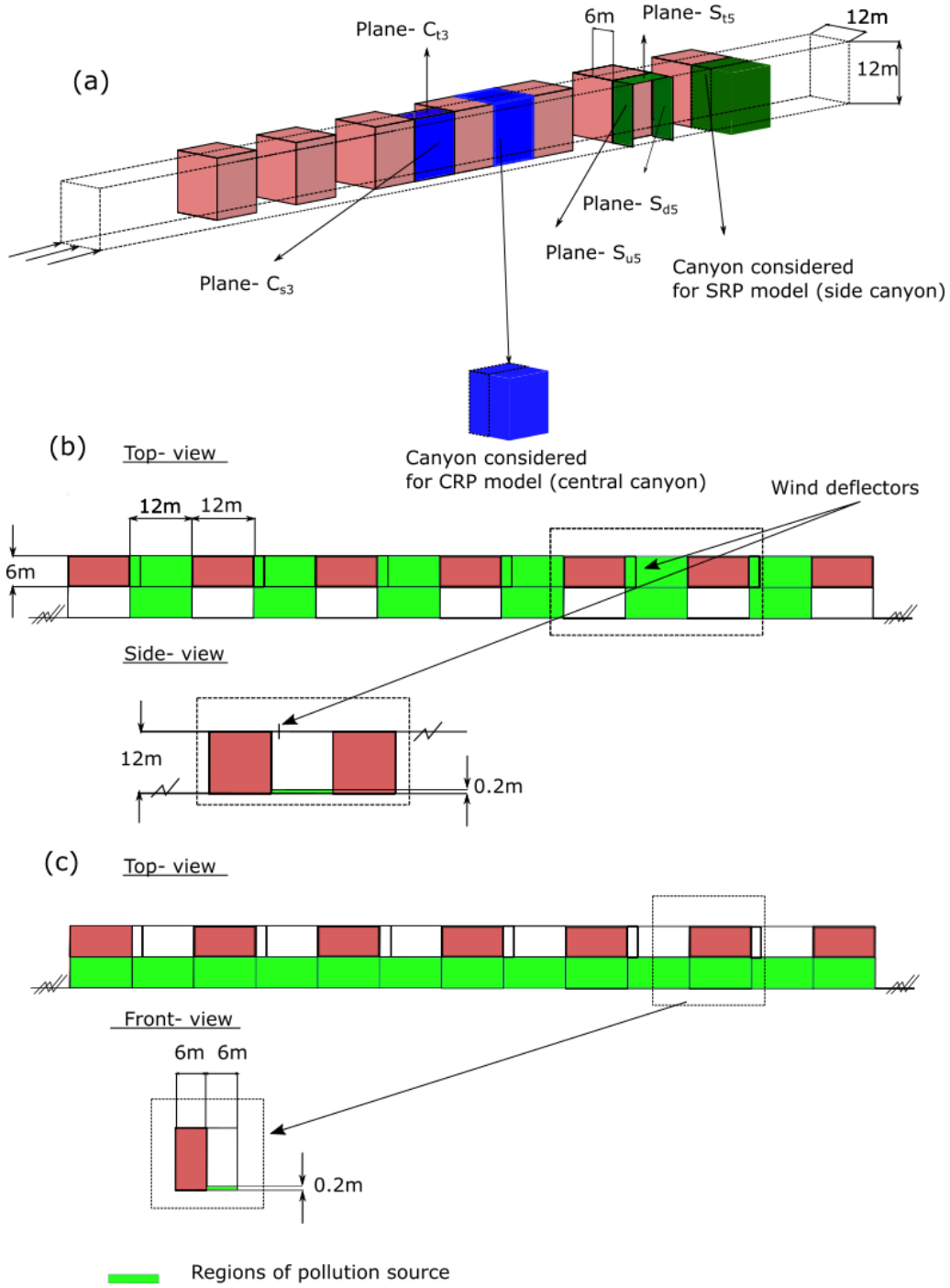

Figure 4.3: isometric view of 3D city-type model with canyons and planes marked for CRP and SRP model analyses (b) CRP model (c) SRP model.

4.4 Computation Domain and Boundary Conditions

H =12m and AR =1 were considered for both the 2D urban street canyon environment and 3D city-type environment. The choices of computational domains and boundary conditions for the validation models and case studies investigated in the work were chosen in line with the best practice CFD guidelines for urban flow modeling (Franke et al., 2011; Tominaga et al., 2008.)

4.4.1 2D Environment

The boundary conditions and choice of the computational domain are similar to the validation model used for bench-marking measurement by Meroney et al. (1996). A $5H$ distance between the inlet and the upwind edge of the first building and between the roof of the street canyon and the top boundary, and a $10H$ distance between the downstream end of the last building and the outflow boundary were prescribed. The velocity inlet boundary condition was prescribed for the inlet boundary to define the neutrally stratified ABL through u, k and ϵ as in Equations 3.18- 3.20. However, the inlet profiles were scaled for $H = 12m$. Other constants including δ, c_μ and α were maintained as in Equations 3.18- 3.20. The building surfaces and streets were similarly modeled as walls, the downwind exit of the domain was modeled as an outflow boundary and the top of the domain were modeled as a symmetry side. Here, the wind deflector and pollution source were introduced to only the target street canyon (third street canyon) to simplify the models and understand its functionality.

4.4.2 3D City-Type Environment

The boundary conditions and choice of the computational domain are similar to the validation model used for bench-marking measurement from Lien and Yee (2004). Furthermore, the schematic shown in Figure 3.4. in Chapter 3 is adopted as the reference for the problem at hand as only the scaling of the domain has changed. A $6.7H$ distance was provided between the inlet and the upwind side of the first row of buildings, $40.3H$ between the downwind side of the last row of buildings and the outflow boundary, and the height of the computational domain was $10H$. The inlet boundaries were modeled by prescribing power-law Atmospheric Boundary Layer

(ABL) profiles using stream-wise velocity component u(z), k(z) and ϵ(z), as in the Equations 3.14- 3.16. Similar to the 2D simulations, the inlet flow profile was scaled for $H = 12m$ and constants including c_μ and α were maintained the same as in Equations 3.14- 3.16.

4.5 Case Description

The 2D simulations included deflector position and orientation analyses. For the deflector position analyses, a reference configuration with no deflector was included, and 10 further configurations with deflectors positioned at 0.25, 0.5, 0.75, 1, 2, 4, 6, 8 and 10m from the leeward wall were considered. The sensitivity of the deflector system to incoming wind velocity was studied by evaluating the deflector performance at ambient wind speeds of 2, 4 and 8m/s. The sensitivity of the results with different turbulence models was assessed using the Standard, RNG and Realizable $k-\epsilon$ turbulence models for reference wind speed of 2m/s.
For the 3D city-type environment simulations, the five different deflector positions of 2, 4, 6, 8, and 10m from the leeward wall were considered along with the reference no-deflector case. The impact of the positioning of the deflectors was evaluated for both CRP and SRP source models. The cases considered for the study are summarized in Table 4.1.

	No- deflector case	Deflector position	Turbulence model	Emission condition	Reference wind velocity
2D simulations					
2D- simulations- AR =1	✓	0, 0.25, 0.5, 0.75, 1, 2, 4, 6, 8 & 10m	Standard $k-\epsilon$, RNG $k-\epsilon$, Realizable $k-\epsilon$	Across the street width, 0.2m high	2m/s
2D- simulations- AR =1 (velocity independence study)	✓	0, 0.25, 0.5, 0.75, 1, 2, 4, 6, 8 & 10m	Realizable $k-\epsilon$	Across the street width, 0.2m high	4, 8m/s
3D simulations					
3-D city-type environment AR =1	✓	2, 4, 6, 8 & 10m	Standard $k-\epsilon$	CRP, SRP	3m/s

Table 4.1: Summary of case studies for conceptualization of wind deflectors

4.6 Mesh convergence

4.6.1 2D simulations

For the mesh convergence study of the 2D study, coarse, medium and fine-resolution meshes comprising 150,027, 237,626 and 314,118 hexahedral cells were considered. As shown in Figure 4.4, non-dimensionalized concentration (K) was compared for the three meshes along the mid-line of the canyon, x_{mid} (marked in Figure 4.2. Despite oscillatory convergence, the conformance between the medium and the fine meshes was convincing for further analysis to be carried out with medium mesh configuration.

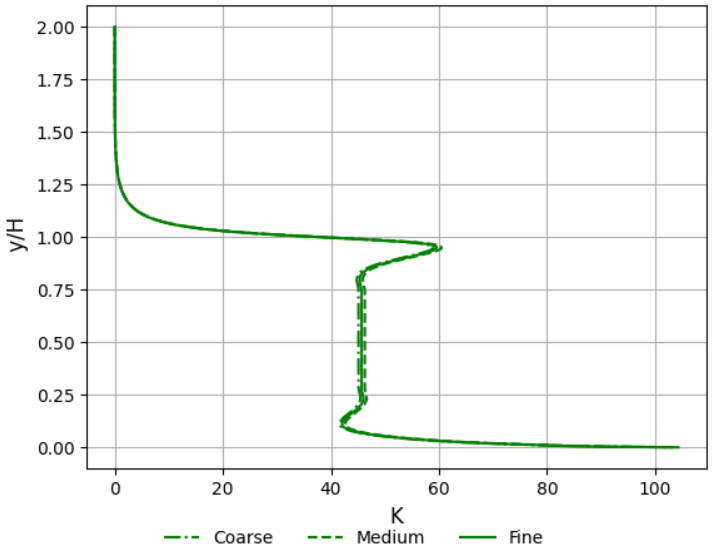

Figure 4.4: a) Mesh convergence study for 2D urban environment comparing the streamwise velocity profile against wall normal distance at the center of the target street canyon (x_{mid} shown in Figure 4.2)

4.6.2 3D simulations

Similarly, the mesh convergence for the 3D study (shown in Figure 5.1) with the city-type environment was conducted using coarse, medium and fine meshes which comprised of 883,614, 1,695,140 and 3,326,711 hexahedral cells. The resolution of the agreement between the medium and fine meshes was satisfactory for the rest of the study to be conducted with medium mesh configuration.

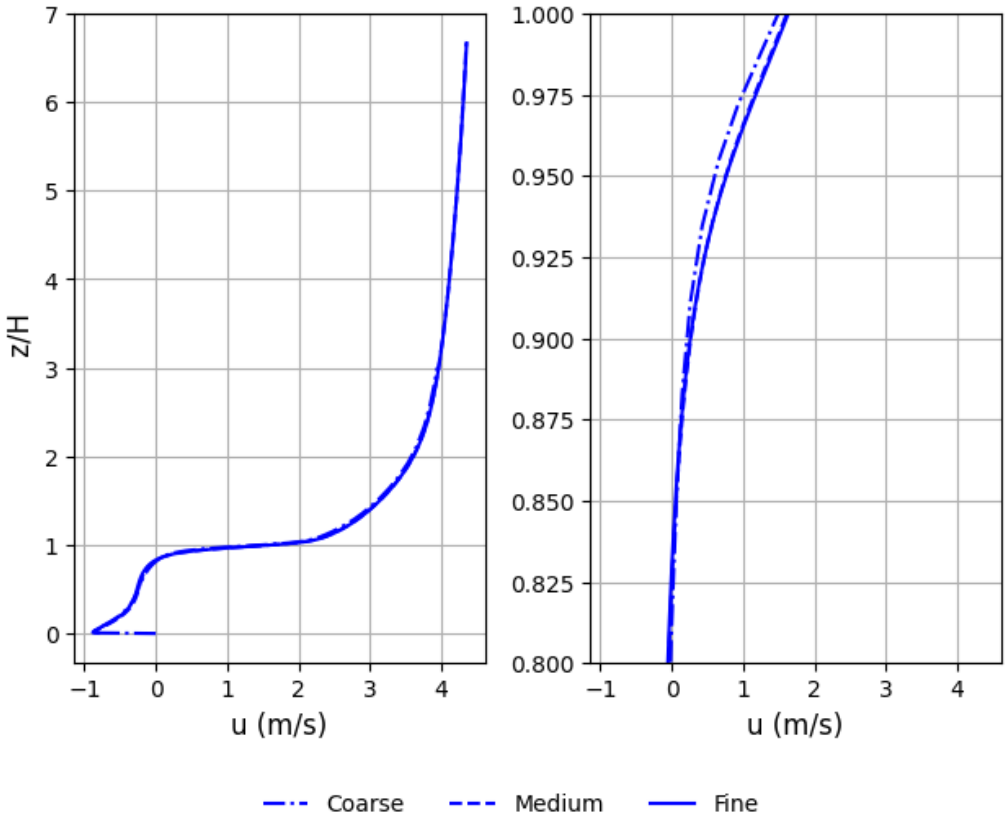

Figure 4.5: a) Mesh convergence study for 3D city-type environment comparing the streamwise velocity profile against wall normal distance at the center of the target street canyon (at x_2, as shown in Figure 3.4, in Chapter 2) in the range $0 \leq$ z/H $\leq$ 7 (on the left). b). Zoomed-in plot of the left in the range $0.8 \leq$ z/H ≤ 1 (on the right)

4.7 Key Assessment Indicators

For quantitative and qualitative interpretation, the impacts of the wind flow deflectors were assessed using the following standard outdoor ventilation indices:

1. **Average pollution concentration:** Area-weighted concentrations for building facades and volume-weighted concentrations for the canyons were evaluated using the Equations 4.1 and 4.2 respectively. The graphical representation of the selected zones for 3D analysis under CRP and SRP source conditions are provided in Figure 4.3.

$$\bar{C}_{2D} = \frac{1}{A} \oint_A C(x, y) dA \tag{4.1}$$

$$\bar{C}_{3D} = \frac{1}{V} \oint_V C(x, y, z) dV \tag{4.2}$$

The concentration (C) of the CO gas in the current work is expressed in mole fraction unless explicitly specified otherwise.

2. **Air Exchange Rates (ACH):** The ACH through turbulent fluxes is computed as Equation 2.6, in Chapter 2. The formulation is based on the eddy viscosity assumption (Cheng et al., 2008) and is an improved version of the isotropic turbulence-based formulation (Li et al., 2005) (Equation 2.9, in Chapter 2). However, in the current study, the ACH due to turbulent fluxes is computed using the isotropic turbulence assumption due to numerical reasons. This decision is taken primarily because of the numerical challenge encountered at the roof level where there are regions where $\sqrt{(k/6) - 0.5 * \nu_t * (\frac{dv}{dn})} < 0$. A plausible explanation is that, according to Boussinesq's assumption which is the foundation for eddy viscosity models, the laminar and turbulent shear stresses align in a direction (Schmitt, 2007) and might have occurred that they are not so here. And unlike in many of the previous studies, the intervention considered here is right on the roof level where the ACH is evaluated and is also where $((k/6) - 0.5 * \nu_t * (\frac{dv}{dn})) < 0$, which could be imagined with the primary aim of the deflector to disturb the ambient flow and potentially skew the alignment of the laminar and turbulent shear stress tensors in its immediate surroundings. Further investigation is not considered in this direction as the truncated formulation with the isotropic turbulence provides satisfactory conformance and more fundamental investigation in this direction is considered out of the scope of this work. The ACH through mean fluxes is computed according to Equation 2.5. Total ACH is the sum of ACH facilitated through turbulent fluctuations and mean flow-induced fluxes, as shown in Equation 2.4 in Chapter 2. ACH is non-dimensionalized by (V/T) where V is the volume of the street canyon and T is the time constant estimated as H/U.
3. **Pollution Exchange Rates (PCH):** The PCH through mean and turbulent fluxes are computed as follows in Equations- 2.12 and 2.13, in Chapter 2.
   At steady-state conditions, the total pollutant removal through turbulent and mean fluxes from a canyon will always be equal to $\dot{Q}$. As outlined in the introduction section, the mode of pollution removal (turbulent fluctuations or mean flow induced) from the street canyon is studied and therefore $PCH_{mean}/\dot{Q}$ (θ) is considered.

4. **Personal intake fraction (IF_p)** IF_p was introduced by Hang et al. (2017) using the Equation 4.3 as follows.

$$IF_p = \frac{\sum_i^N \sum_j^M (P_i)(Br_{i,j})(\Delta t_{i,j})(Ce,j)/m}{\sum_j^M (P_i)} \tag{4.3}$$

Where P is the population exposed to the emission, i refers to the population group (children, adults, or elderly), j refers to the location (indoor- home, other indoor, outdoor- near vehicles or other outdoor locations), Br is the breathability rate, Δt is the time of exposure, C_e is the concentration (kg/m^3) and m is the total mass of emission (kg). The calculations in the paper correspond to the constants used in Hang et al. (2017). However, only indoor-home and outdoor-near vehicles were the environments considered for the analyses.

4.8 Target regions of study

1. **2D simulations:** θ and $\bar{C}_{canyon}$ for the inverse correlation and IF_p for the exposure analyses along the leeward and windward wall pertain to the third street canyon.
2. **3D simulations:** θ and $\bar{C}_{canyon}$ for the inverse correlation for the city-type environment with CRP and SRP source models are assessed for all the central and side street canyons (The schematics of the central and side street canyons are included in Figure 4.3a). For the exposure analyses, indoor IF_p across the near-road building- leeward, windward and side facades were assessed for all the floors through assumed window openings as marked in Figure 4.6a. The near-vehicle outdoor exposure for Canyon 3 is marked in Figures 4.6b and 4.6c. The exposure analysis for the city-type environment was conducted only for the third street canyon.

4.9 Results

4.9.1 2D simulations

The results discussed in this section pertain to simulations performed with the Realizable $k-\epsilon$ turbulence model. Results from the RNG and Standard $k-\epsilon$

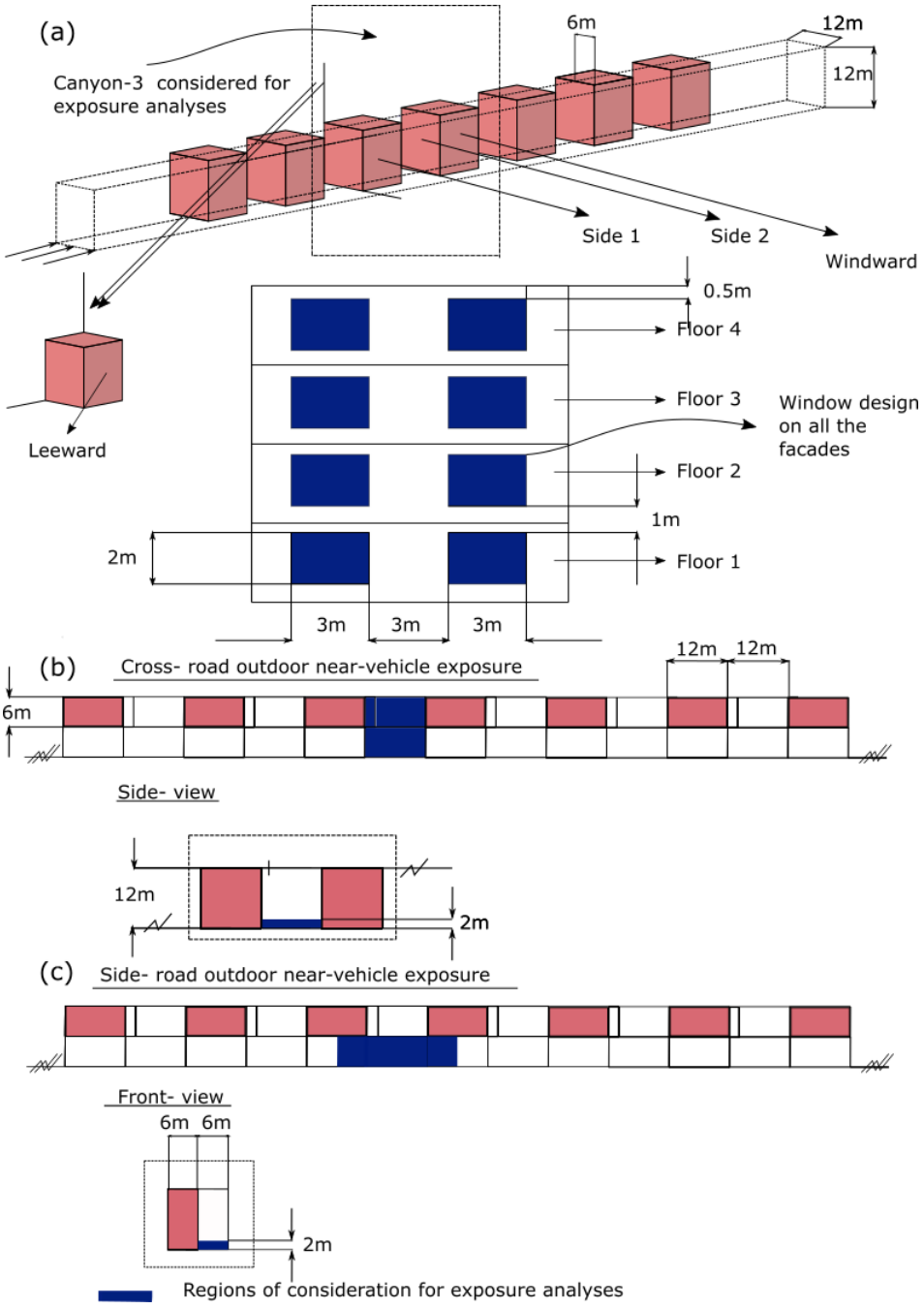

Figure 4.6: (a) Reference floors and windows for indoor IF_p calculations for all the building facades (b) Region of evaluation for near-vehicle outdoor IF_p on crossroads (c) Region of evaluation for near-vehicle outdoor IF_p on the side-roads.

turbulence models can be referred from Figure 4.7a. The variation in K due to turbulence models is regarded in the later part of the section to explain the deviations in θ v/s $\bar{C}_{canyon}$. Figure 4.7b highlights the insensitivity in the performance of wind flow deflectors for change in ambient reference wind velocity.

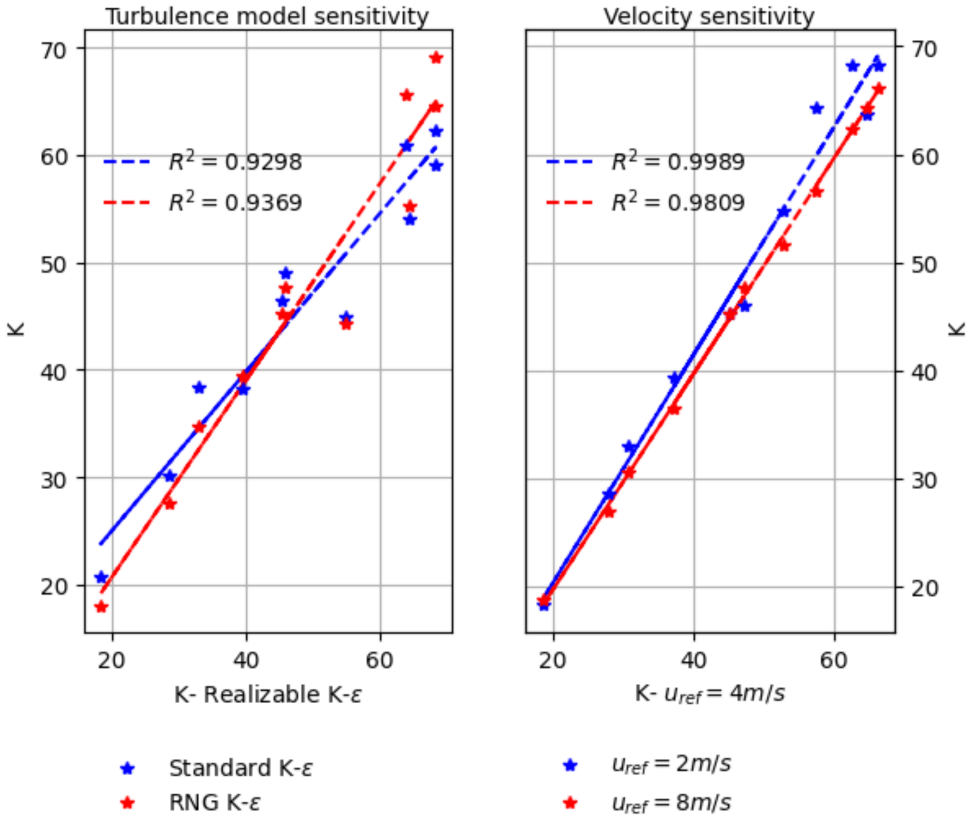

Figure 4.7: a) Sensitivity to turbulence models (2D street canyons), comparing the non-dimensional mean canyon concentration for different deflector positions (on the left); b) Sensitivity to reference wind velocity(2D street canyons), comparing the non-dimensional mean canyon concentration for different deflector positions (on the right).

From Figure 4.8 four flow patterns can be identified when the deflectors are positioned orthogonal to the wind flow direction. The reference no deflector case and when the deflector is attached to the leeward wall constitute flow type 1. This is the regular pattern where the street canyon experiences a standard re-circulation with a large primary vortex. As a result of the re-circulation rising along the leeward wall and mixing with above canyon cleaner air before washing down along the windward facade, the leeward and windward facades experience higher and lower CO exposures respectively ($\bar{CO}_{lee} = 5.17e-7$, $\bar{CO}_{win} = 2.13e-7$ for the no-deflector case

and $\bar{CO}_{lee} = 3.92e-7$, $\bar{CO}_{win} = 1.67e-7$). The deflector when placed at 0.25m constitutes flow type 2. The 0.25m gap between the deflector and the leeward wall offers a passage of air that manages to counterbalance the recirculating flow that traditionally washes down the windward facade. In this configuration, as the flows along the two facades just balance each other, they then rise at the center of the canyon after collecting the pollutants from the ground. In this way, both facades are less polluted. The reduction in average facade concentration for both leeward and windward walls can be seen in Figure 4.8. Deflectors when placed at 0.5, 0.75, 1 and 2m respectively from the leeward wall, constitute flow type 3. In this configuration, the air passing between the leeward wall and the deflector manages to push the traditional re-circulation to establish a reversed re-circulation pattern in the street canyon. As expected, since the flow carries pollutants from the ground before it rises to the windward facade, the windward facade is more contaminated in this case. However, it could also be seen from Figure 4.9 that this rise in average facade concentration along the windward side reduces substantially from when the deflectors are placed at 0.5 to when the deflectors are placed at 2m. Finally, deflectors when placed at 4, 6, 8 and 10m constitute flow type 4. This arguably is the poorest-performing flow type with the deflectors. In these cases, the deflectors are positioned far enough from the leeward wall that the flow adjusts itself to recirculate in a regular way as type 1 flow. However, the deflector limits the re-circulation to mix sufficiently with the above canyon cleaner air.

The percentage reduction of leeward facade concentration is about 86.5% when counterbalancing flows are encountered with passage width between the leeward wall and the deflector limited to 0.25m (flow type 2). This reduction rises to 90% when the deflector is placed 2m from the leeward wall (flow type 3) and further deteriorates to as much about 27% and 22.6% increase to reference case when the deflectors are placed at 6 and 8m from the leeward wall respectively. On the other hand, an 8.45% decrease in facade concentration along the windward wall is noted for type 2 flow. This deteriorated to as much as a 142% increase when the deflector is placed at 0.5 (type 3) and then improved to provide a 90% increase on the windward facade when the deflector is placed at 2m (type 3). The negative impact that flow type 4 provides on the leeward wall means that the marginal improvement it provides on the windward facade is not consequential for further analyses. Previous studies have indicated the low sensitivity of non-dimensionalized (K) concentrations to incoming wind velocities. However, since the deflector performance was substantially dependent on the roof-level wind conditions, a sensitivity study

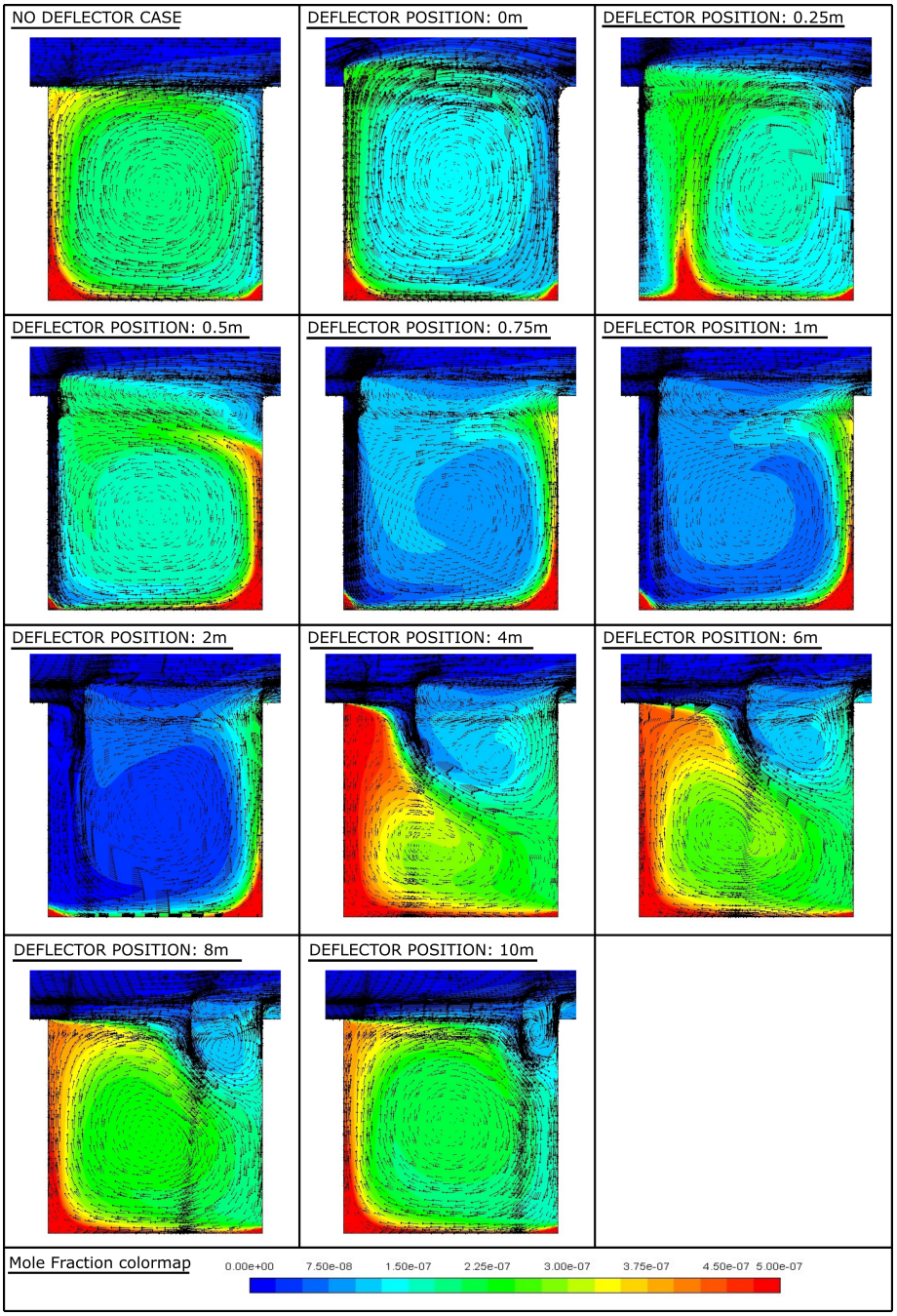

Figure 4.8: Overlayed images of contour plots of the concentration of CO gas and vector plot of velocity magnitude in all 11 deflector configurations studied with AR 1.

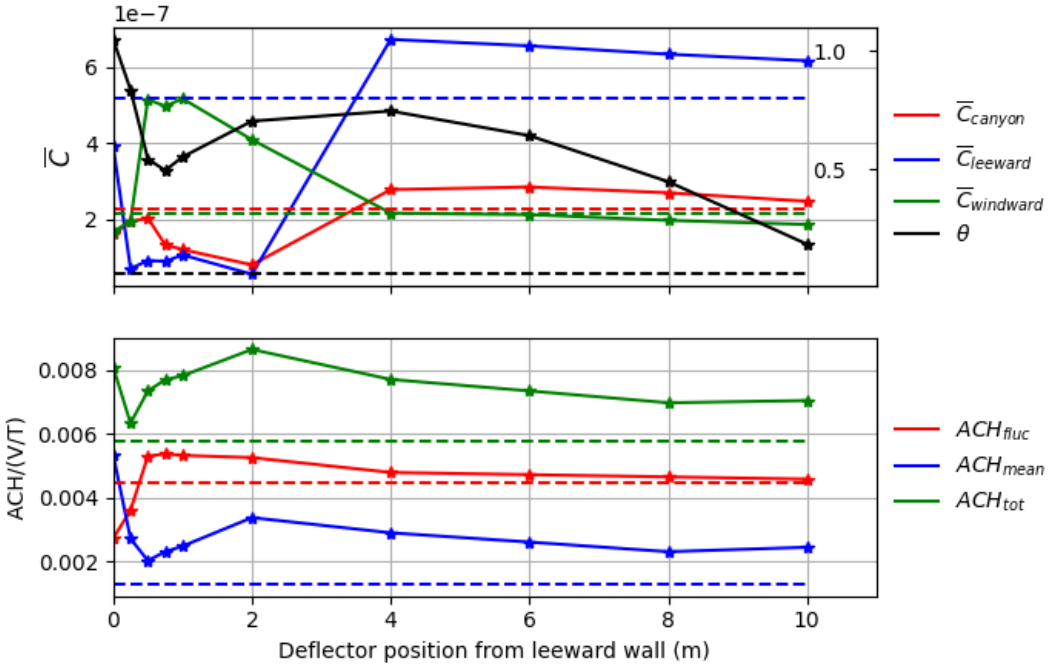

Figure 4.9: (a) Comparison of Windward and Leeward facade concentration, overall street canyon concentrations and θ (top); (b) Comparison of normalized Air Exchange Rates for varying deflector positions (bottom). *Solid lines (-) indicate the cases with the deflectors and the dashed lines (–) indicate the reference case without the deflector*

was conducted. As shown in 4.7, the differences were not strong enough to continue for subsequent analyses.

The inverse correlation between the overall canyon concentration and θ particularly deviated when the deflector was very close to the leeward wall and when it was moved beyond 4m from the same. On the contrary, ACH_{mean} and ACH_{tot} capture the trend better when the deflector was moved beyond 4m from the leeward wall. However, the importance of correlating the overall canyon concentration and θ is justified in the subsequent section involving 3D simulations. Finally, changing the orientation of the deflectors reduced the pollution removal performance and hence was not considered for its evaluation in the 3D city-type environment.

4.9.2 City-Scale 3D simulations

It is worth noting that the city-type environment comprised six canyons and the wind deflectors impacted each of them differently. The primary objective of the analyses was to showcase the benefit of using an adjustable deflector system in street canyons; and a mitigation strategy to prevent the indoor environment exposed via leeward, windward and side walls from prolonged exposure to poor air quality for changing emission source conditions. However, for brevity, repetition of the demonstration for six canyons was not considered. Instead, a canyon where two different deflector positions resulted in maximum CO removal from the immediate central canyon and the two adjacent side canyons was considered. These were the central canyon-3 and side canyons-3 and -4 (results shown in the subsequent subsections). Analyses of the results pertain to this region of the domain.

4.9.2.1 Cross Road Pollution (CRP) Source model

The results from this section reflected similarities to the results from the 2D deflector position analyses. Broadly 3 flow types were identified; the no-deflector case, deflectors when placed 2m away from the leeward walls and deflectors when placed at 4, 6, 8 and 10m from the leeward walls. Figure 4.10 shows the airflow pattern in and around the target street canyon and the influence of the wind deflectors on the same. The resulting CO concentrations on the leeward and windward sides for the no-deflector case and when the deflectors were 2 and 4m away from the leeward walls can be seen in Figure 4.11 (other deflector positions behaved similarly as in the case where deflectors were 4m away from the leeward walls). Figure 4.11 also shows the flow along the canyon mid-section in the streamwise direction for all the cases. The flow field resulting from the no-deflector case was a standard recirculation. The spiral recirculations were oriented such that the wash-down along the windward wall and the rise-up along the leeward wall were aligned closer to the mid-section and the lateral edge of the canyon respectively. The washdown is the downward movement of air streams along the building facades by the fresh above-roof air facilitated through vertical recirculations. This orientation is due to the inward curling of the two air streams laterally entering and exiting the canyons through the sides of the windward and leeward walls respectively. The orientation of the spiral recirculations increased the CO concentrations of the sides of the two walls compared to their central portions. The leeward wall was 2.45 times more polluted than the windward wall ($\bar{C}_{CO,lee3} = 1.46e-7$ and $\bar{C}_{CO,win3} = 5.97e-8$).

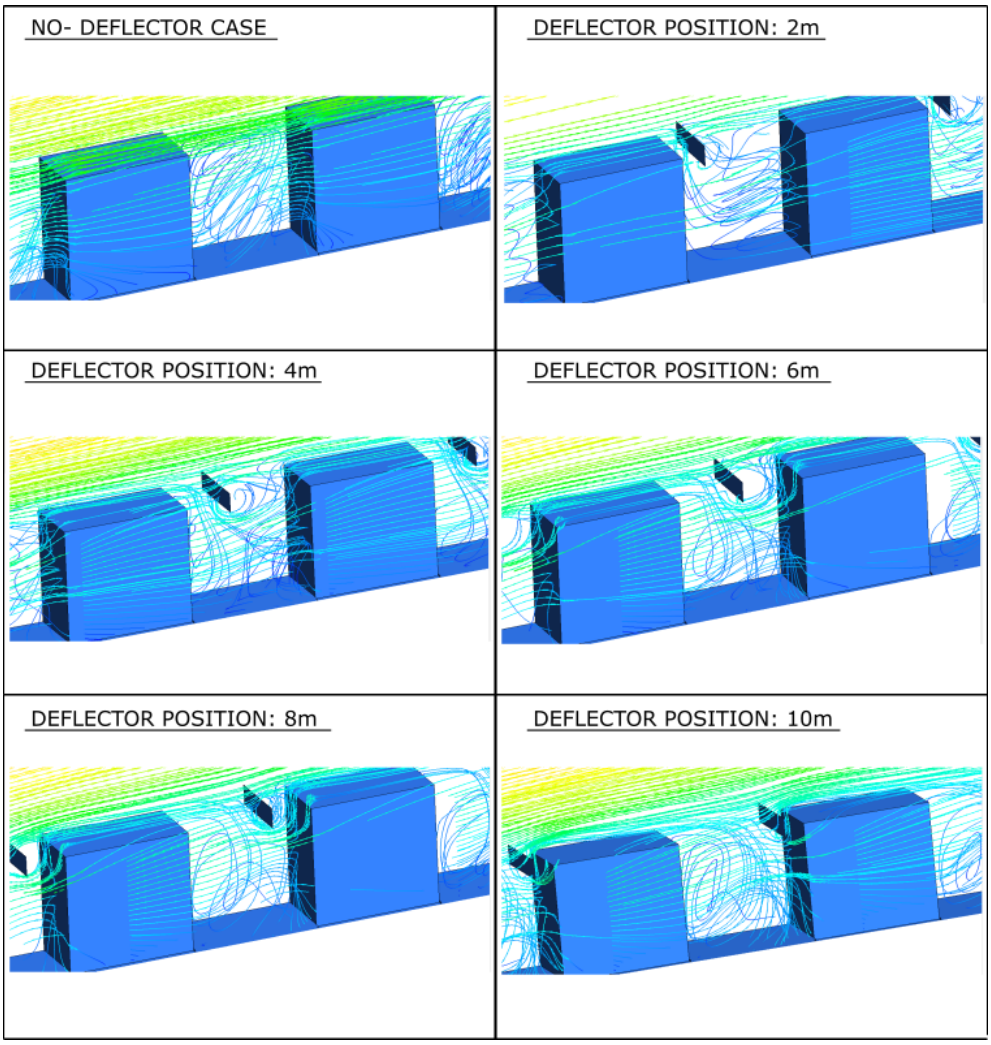

Figure 4.10: Streamlines showing the airflow pattern in the target street canyon and the influence of wind deflectors when placed 2, 4, 6, 8 and 10m away from the leeward walls.

However, this configuration had the benefit of the highest average velocity in the lower canyon region ($z < 1.75$) of about 0.52m/s and hence a substantially lower CO concentration ($\bar{C}_{CO} = 1.17e-7$) in the region than all the deflector configurations except when the deflectors were placed 10m away from the leeward walls.
The flow field was completely altered when the deflectors were placed 2m from the leeward walls. This configuration reflected similarity to Flow type 2 in the 2D simulations where the air streams washing down the leeward and the windward walls counterbalanced to rise through the canyon center. Although Flow type-2 was seen as one of the favorable configurations in 2D flows, the 3D flow nature of the city-type environment made this flow type not particularly favorable for the CRP source

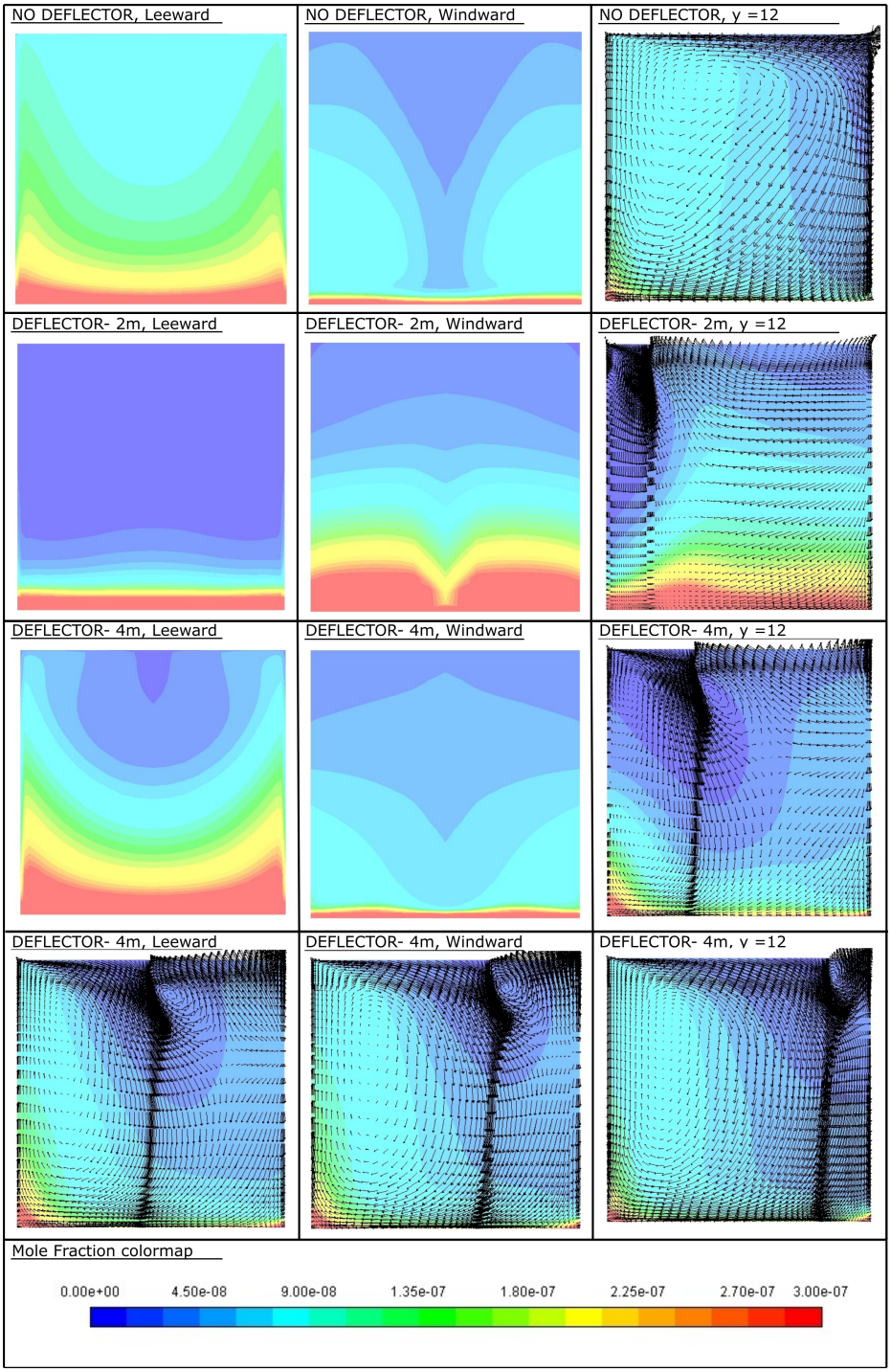

Figure 4.11: Overlayed images of contour plots of the concentration of CO gas and vector plot of velocity magnitude for the CRP source model with deflectors in the third central canyon.

model. Here, the stream of air entering between the leeward wall and the deflector is not strong enough to create a recirculation within the canyon. Therefore, it simply facilitated a wash-down along the leeward wall before it reached the lower part of the windward wall after amassing CO emissions at the street level on its way. The polluted air rose in the canyon in a helical corkscrew-type trajectory in the vicinity of the windward walls. As shown in Figure 4.10, the helical rise-up managed to get as far as only the middle of the canyon (in the streamwise direction) and hence this configuration resulted in a maximum CO concentration reduction of 60.1% along the leeward wall. Subsequently, it also deteriorated the air quality along the windward side by increasing the CO concentration along the same by 119% (comparisons made with no-deflector case). This helical corkscrew-type nature of the flow is the result of the air stream that washed down the leeward wall and the inward curling streams of air from the sides of the canyon. The inward curling air streams from the sides were stronger than the "wash-down air stream" at the middle and higher regions of the canyon and hence the helical corkscrew moved away from the windward wall with the rise-up of the same. At a point where the air streams from the sides became the dominant flow, the two lateral air streams pushed as far as the deflectors to get deflected and recirculated out of the canyon. The "wash-down air stream" being stronger than the lateral recirculations at the lower heights of the canyons and vice-versa is the reason for relatively higher CO centration at the sides of the lower region of the windward wall and central portions of the middle and upper portions of the same. The side portions of the leeward wall were immune to recirculations from the windward wall and hence the marginally lower concentration compared to the central portions of the same. The helical rise-up in tandem with this reduced gap between the leeward wall and the deflector for airflow from the top. This resulted in the lowest average velocity in the lower canyon region ($z < 1.75m$) of around 0.07m/s and hence also the highest concentration in this lower region ($\bar{C}_{CO} = 3.9e-7$). This was also concurred with the results in the following sections where it was identified that the indoor personal exposures were the highest at the ground level floor exposed through the windward and side walls when the deflectors were placed 2m away from the leeward walls for CRP source model.

The cases when the deflectors were placed at 4, 6, 8 and 10m away from the leeward walls reflected similarity to flow type 4 from the 2D deflector position analyses. The air streams entering between the leeward wall and the deflector in these cases were stronger than when the deflectors were placed 2m away from the leeward walls to develop a recirculation. However, unlike in the no-deflector case, the recirculations

were restricted. Flow type 4 was identified to be a disadvantageous flow type in the 2D analyses. However, the 3D nature made this flow type relatively the most effective in this context. As shown in Figure 4.10, the restricted recirculation was very similar to the complete recirculation in the no-deflector case in terms of its orientation. Wash-down occurred closer to the canyon mid-section of the windward wall and rise-up occurred closer to the edge of the leeward wall. When the deflectors were placed 4m away from the leeward wall, spiral recirculations were very weak that they managed to reach only half the distance between the two walls and rose up to only half the height of the leeward wall. The upper region ($z > 6$) of the leeward wall being unaffected by the recirculations showcased a significant CO concentration reduction of about 50% (compared to the no-deflector case). The spiral recirculations that partially rose up the leeward wall and the inward-curling lateral air streams from the sides approached the windward wall. The latter being stronger at the upper portion of the canyon managed a complete recirculation back to the wind deflector to eventually leave the canyon from the roof level just as in the case when the deflectors were placed 2m away from the leeward walls. The restricted airflow from the roof level developed a reduced average velocity in the lower canyon region ($z < 1.75m$) of 0.196m/s and hence produced a substantially large average concentration ($\bar{C}_{CO} = 1.65e - 7$) in the region. This also resulted in higher CO concentration along the lower region of the leeward wall to eventually reduce its overall reduction to 7%. The windward wall did not show a substantial difference. However, this configuration also reduced about 13 and 11% of CO concentration across the upwind and downwind side walls.

The flow patterns were similar when the deflectors were placed 6, 8 and 10m away from the leeward walls except that they progressively tended to mimick the no-deflector case. The recirculations became progressively bigger and the average velocity in the lower canyon region ($z < 1.75$) increased to 0.23, 0.26 and 0.42m/s when the deflectors when were placed 6, 8 and 10m away from the leeward walls respectively. Finally, the average concentration in the region was reduced to be ($\bar{C}_{CO} = 1.11e - 7$) when the deflectors were placed 10m away.

Figure 4.12 shows the difference between the range of values of $\bar{C}_{canyon}$ for the six cases was minimal for canyon -3 unlike canyon -1 and -2, for example. This could explain the reason for modest reductions in the facade CO concentrations. However, the elimination (deflectors 2m away) and restriction of spiral recirculations (deflectors 4, 6, 8 and 10m away) significantly affected the dispersion of CO for SRP source model (illustrated in the next section). It can also be seen from Figure

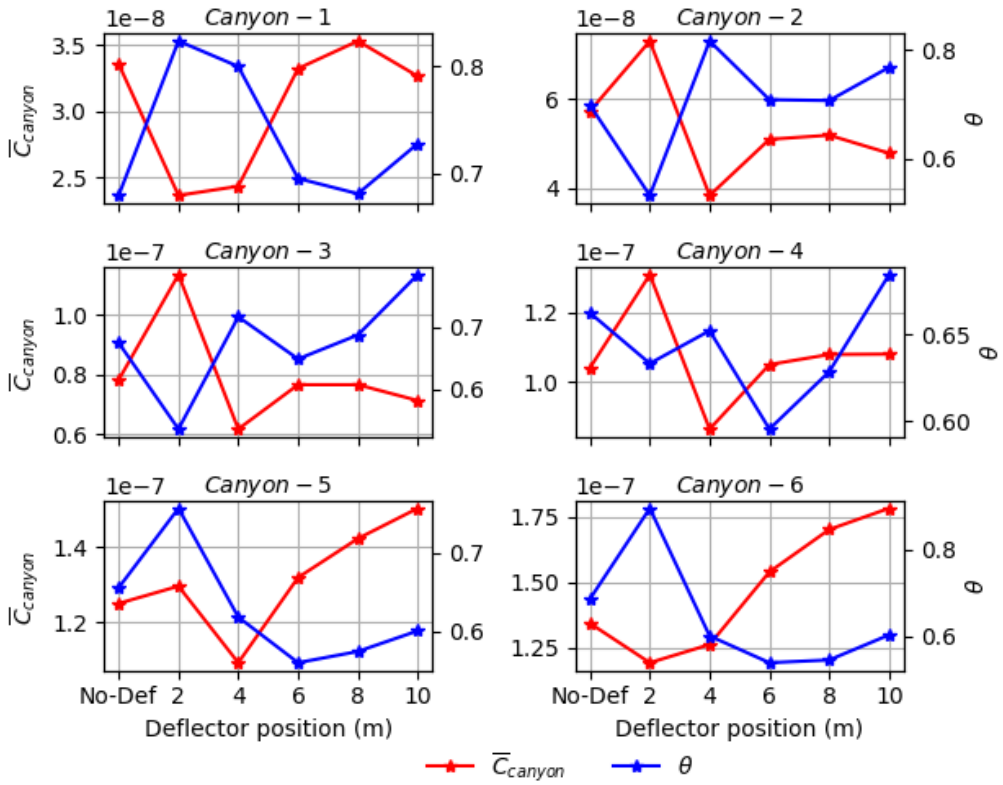

Figure 4.12: Correlation of PCH_{mean}/PCH_{tot} (θ) and average concentration of the entire street canyon for CRP model $\bar{C}_{canyon}$.

4.12, θ maintains the inverse trend with the mean canyon concentration. The planes considered for cumulative PCH_{mean} leaving the canyon are represented in Figure 4.3. For example, the total PCH_{mean} leaving the third central canyon is evaluated as in the equation 4.4

$$PCH_{mean} = PCH_{mean}|_{Ct3} + PCH_{mean}|_{Cs3} \tag{4.4}$$

Here, $Ct3$ and $Cs3$ are the top and side surfaces encasing the third central canyon. The inverse trends were strongly maintained in the first three canyons and the inverse correlation particularly deviated in the latter three canyons. The mesh resolutions were identically maintained in all the canyons and hence eliminated the potential cause of aberration in the inverse correlation.

4.9.2.2 Side Road Pollution (SRP) Source model

SRP source model holds the same flow field as the CRP source model. The primary reason to conduct this assessment was from a physical standpoint. The wind deflectors were seen to be only modestly effective for the CRP source model and it was essential to evaluate its performance for the SRP source model. In addition, from a numerical standpoint, thus far the significance of θ has been illustrated to reflect the ventilation of the canyons. Therefore, to bring generality in the verification of this parameter, the relationship between the mean canyon concentrations (shown in Figure 4.3) and θ has been verified for the SRP source model as well. Figure 4.13 shows the flow pattern at the $y = 5.5m$ planes (i.e., 0.5m away from the side facade of the buildings). This clearly shows that the top recirculation discussed in the CRP source model has a large impact on the washaway of pollution in this model. The magnitude of these recirculations is observed to reduce at planes farther away from the side facades of the buildings and vice-versa. It can also be seen that there is a large re-circulation that is observed in the no-deflector case. This is not observed in the case where the deflector is placed 2m away from the leeward wall. In the case when the deflectors are placed 6 and 10m away from the leeward walls, the re-circulations were observed but they were smaller compared to the no-deflector case. These recirculations are the same inward-curling spiral recirculations discussed for the CRP source model. These recirculations inhibit the natural wash-away of pollutants and accumulate pollution concentrations. The larger the recirculation zones are, the higher the CO concentrations. This is synonymous with the plots in Figure 4.14 where it indicates that the no-deflector case is the worst performing configuration and the deflector performance deteriorates as they are moved from 4m to 10m. When the deflectors were placed 2m away from the leeward walls, there were no recirculations involved and the best performance was observed. This was reflected by the mean CO concentrations on the side wall of the fourth building where the no-deflector case had the highest concentration, ($\bar{C}_{CO,s4} = 9.97e-8$). Deflectors when placed 2m away from the leeward walls offered the maximum reduction of 34%, with ($\bar{C}_{CO,s4} = 6.57e-8$). Subsequently, this impact reduced as the deflectors were moved towards the windward wall as the $\bar{C}_{CO,s4}$ concentration increased to $6.91e-8$, $7.30e-8$, $8.01e-8$ and $8.87e-8$ for the scenarios where the deflectors were placed 6, 8 and 10m away from the leeward walls respectively. In the lower canyon region ($z < 1.75m$), the elimination of recirculations increased the average velocity from 0.35m/s (no-deflector case) to a maximum of 1.44m/s when

the deflectors were placed 2m away from the leeward wall. This also reduced the average CO concentration in the region from 2.78e-7 (no-deflector case) to 2.25e-7.

From a numerical standpoint, the cumulative amount of pollution removed by the mean flow-induced fluxes from the target side canyons as marked in Figure 4.3 was estimated for the third side canyon for example.

$$PCH_{mean} = PCH_{mean}|_{St3} - PCH_{mean}|_{SU3} + PCH_{mean}|_{SD3} \tag{4.5}$$

Here, St represents the top surface of the side canyon and SU and SD represent the upwind and downwind planes of the same target canyon region. As also seen from Figure 4.14, the inverse trend was also upheld for the SRP source model. The plots also indicated the reduction in the natural ability of the ambient winds to wash away CO with every subsequent side canyon having a lesser θ compared to its upwind side canyon. It could also be understood that the recirculations reduced the $PCH_{mean}|_{St} - PCH_{mean}|_{SU}$ value and thereby eventually increased the overall side canyon concentrations.

4.10 Discussions

Despite the understandably lesser environmental factors changing in a 2D environment and the deviations in the inverse correlation, the 2D analysis is considered essential for the following reasons: 1) to demonstrate an opportunity to use an adjustable system that is uncompromising to any specific part of the street canyon over a long period, and that changing the position of the deflectors between street canyon walls result in significantly altered flow patterns that could also be the response to changing conditions under more complex environments for optimal dispersion street canyon ventilation; 2) there is strong evidence of the inverse correlation that it is worth studying under complex 3D conditions and that it gives practical reasoning to understand the performance of deflectors when placed at different locations.

4.10.1 θ Vs $\overline{C}_{canyon}$ relationship

Both the 2D and 3D simulations showed sufficient evidence to support the hypothesis that PCH_{mean} represented the wash-away of the pollutants from the street canyon and that PCH_{fluc} represented the localized removal assisted by the turbu-

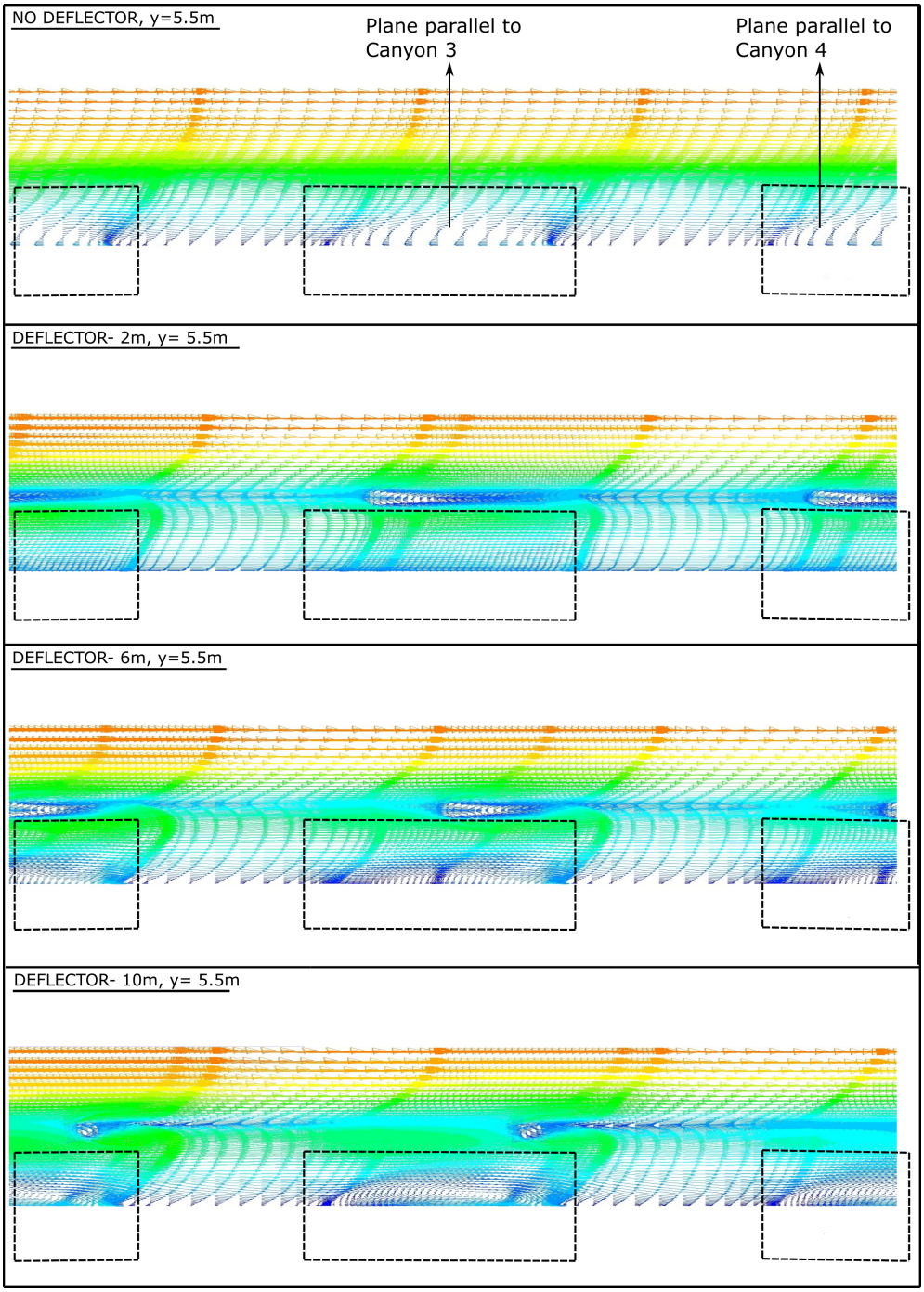

Figure 4.13: streamwise flow for no deflectors and deflectors at 2, 6 and 10m away from the leeward walls.

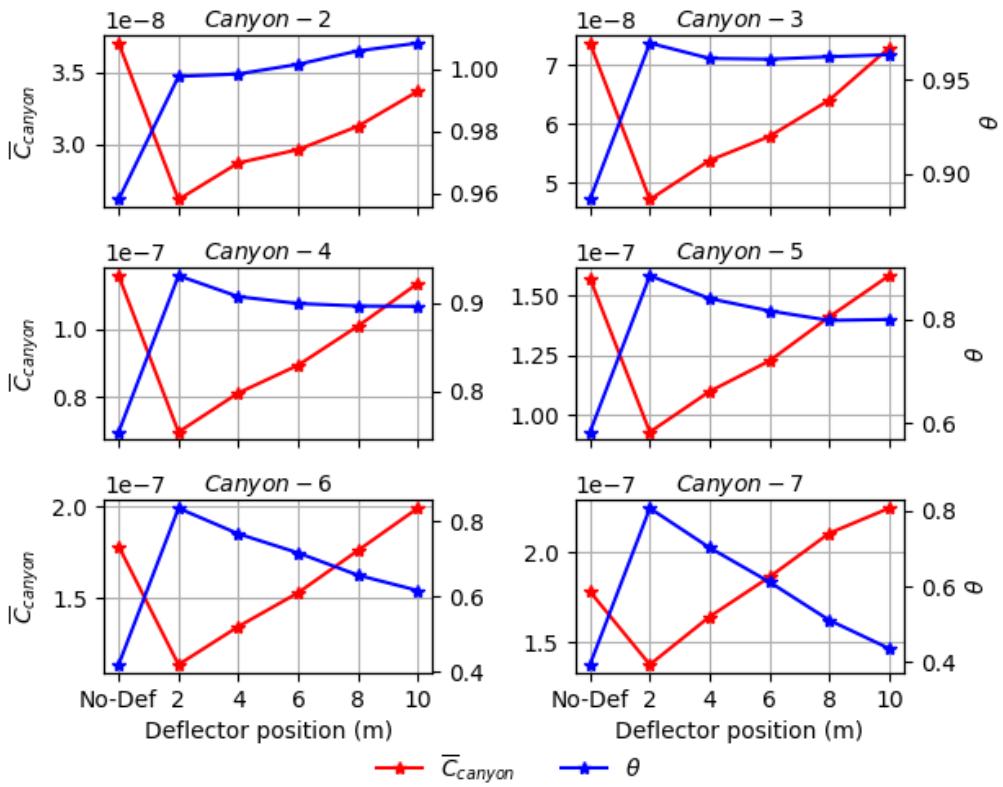

Figure 4.14: Correlation of PCH_{mean}/PCH_{tot} (θ) and average concentration of the entire street canyon for SRP model $\bar{C}_{canyon}$.

lence fluctuations induced fluxes and there is a straightforward benefit in increasing θ. In the 2D simulations, the inverse correlation largely deviated when the deflector was very close to the leeward wall and when it was moved beyond 4m. Although the inverse correlations were more characteristic in the 3D simulations, such deviations as in 2D simulations were observed in the same. The inverse correlations deviated in central canyon-5 when the deflector was placed 2m away from the leeward wall and in central canyons-4, 5 and 6 when the deflector was placed 10m away from the leeward wall respectively. On the contrary, the nature of correlation improved for subsequent downstream canyons for the SRP source model. It can be seen from Figure 4.14 that there is clearly an order of magnitude difference in the difference between the maximum and minimum values of θ and $\overline{C}_{canyon}$ inside canyons 2 and 7 respectively. This indicates that the numerical precision of the solver involved in the formulation could influence the correlation.
The sensitivity of the 2D simulation results with the turbulence model was also considered to be a potential reason for the aberration and hence the sensitivity study with Standard and RNG $K-\epsilon$ turbulence models, refer to 4.7. The $k-\epsilon$ turbulence models have captured the inverse correlation with minimal deviations in 2D and complex 3D environments justifying its suitability, considering the trade-off between numerical accuracy and computational requirements. However, to further the scope of the study, investigating the inverse correlation using more detailed turbulence models including LES or DES is recommended. Finally, in the 2D simulations, as can be seen from Figure 4.9, the ACH_{tot} and canyon concentration proved to be a better indicator in the cases where the deflectors were placed 6, 8 and 10m away from the leeward walls. However, this is not the case with a 3D city-type environment. θ showed inverse trends with the overall canyon concentration and not ACH_{tot} (not shown here for brevity). This accounts for the fact that the lateral inward-curling flows have more direct reach to the pollution source than the top recirculation and θ could be considered a stronger indicator of overall ventilation in complex environments.

4.10.2 Indoor and near-vehicle pollution exposure

4.10.2.1 2D simulations

The deflector when placed 2m away from the leeward wall resulted in the local maximum and minimum of θ and overall canyon concentration respectively.

The flow configuration resulting in a 90% increase in CO concentration along the windward wall illustrated the plausibility of unfavorable localized re-distribution affecting specific elements of the street canyon despite maximum CO removal from the canyon. On the contrary, flow type-2 which resulted in substantially reduced CO concentrations along the leeward and windward facades, increased pedestrian exposure at 1.75m from the street surface to CO gas by 61% compared to when the deflector was placed 2m away from the leeward wall. This situation highlighted the requirement of a system that ventilates the canyon in its entirety and is also adjustable to balance the trade-off of either accumulating the CO concentrations on the windward facade or the street surface. Since the wind deflector is an adjustable system, even the unfavorable positions of the wind deflectors could be seen as a potential solution for the temporarily changing conditions. Therefore, instead of continually accumulating CO on the windward side or at street level, the deflector could be adjusted briefly to operate at Flow type-4 and then revert to operating at Flow type-3 or Flow type-2. The benefit of this flexibility to reduce IF_p in the context of changing traffic flow direction is demonstrated in detail in the 3D city-type environment case.

4.10.2.2 3D simulations

The previous sections showed three distinct flow patterns in the current study and wind deflectors placed at 4m and 2m away from the leeward walls offered maximum relief in the central and side canyons, respectively. Despite the significant reduction in the overall CO concentration in the central and side canyons under CRP and SRP source models, the wind deflectors also inevitably result in a substantial amount of re-distribution of the CO emissions around the building facades like other passive interventions. Therefore, the concern of optimal deflector configurations for CRP and SRP source models detrimentally affecting side and central canyons respectively and the risk of using a fixed deflector position for the two source models were evaluated. This can be seen in Figures 4.15 and 4.16.
The deflectors when placed at 4m did not excessively pollute the side facades. For the CRP source model, the indoor IF_p via side facades was reduced for all of the floors except Floor-1, and the overall CO exposure on side-1 and side-2 was reduced by 11 and 13% respectively. However, deflectors when placed at 2m behaved differently. They substantially reduced and increased the CO concentration on the leeward and windward facade for the CRP source model, as explained in the previ-

ous subsections. However, this configuration increased only the floor-1 IF_p on the windward side and eventually reduced 17% CO exposure on the windward wall in its entirety under SRP source conditions. The configuration reduced IF_p on all the floors exposed via leeward wall and reduced the overall CO concentration along the same by 93%. Being the best configuration for the SRP model, it reduced the maximum amount of CO concentration on the side facades for the SRP source model and increased the CO concentration along the same for the CRP source model. For instance, the increase in the IF_p of floor-1 occupants having exposure to traffic emissions through side facades increased 1.5 fold when the deflectors were placed at 2m for the CRP source model. Therefore, the deflectors while optimally reducing CO exposure along windward and leeward walls did not increase the CO exposure along the side walls to compensate, and vice-versa. They could also be counterproductive if used for an emissions source condition for which they did not yield optimal dispersion patterns. Except for the Floor-1 IF_p, deflectors when placed at 6, 8 and 10m performed worse compared to when placed at 4m. When the deflectors were placed at 4m for the CRP source model, the personal exposure was reduced for Floors- 2, 3 and 4 occupants exposed via leeward, windward and the side facades. For the SRP source model, it produced a similar impact on the side facades and it outperformed the configurations when deflectors were placed 6, 8 and 10m, in reducing the personal CO exposure in all the floors exposed via leeward and windward facades. Since the cumulative CO exposure reduction on all the facades under the considered conditions was best for when the deflectors were placed at 4m, it was sufficient to analyze the no-deflector case and when deflectors are placed at 2 and 4m for the indoor IF_p for the remainder of the analyses. Figure 4.17 shows the response of the wind deflectors for five different traffic flow patterns mentioned in the Problem Description section in the city-type environment, including the CRP, SRP and the three transitional traffic flow types. The cumulative IF_p across all the floors illustrate the trends mentioned in Figure 4.15 when the deflectors are statically placed at 2m and 4m respectively. The adjustable deflector is a concept where the deflectors were placed at 2m for the SRP source model and at 4m for the CRP source model and that was interchangeably moved back and forth based on whether the cross or the side roads were subjected to more traffic. When placed at 4m, the deflector performed better than the no-deflector case, limiting the explanation of the concept in this context. Nevertheless, the adjustable deflector is successful in maintaining the CO concentrations below the reference no-deflector case on all the facades under all five traffic flow models considered. Naturally, the reduction poten-

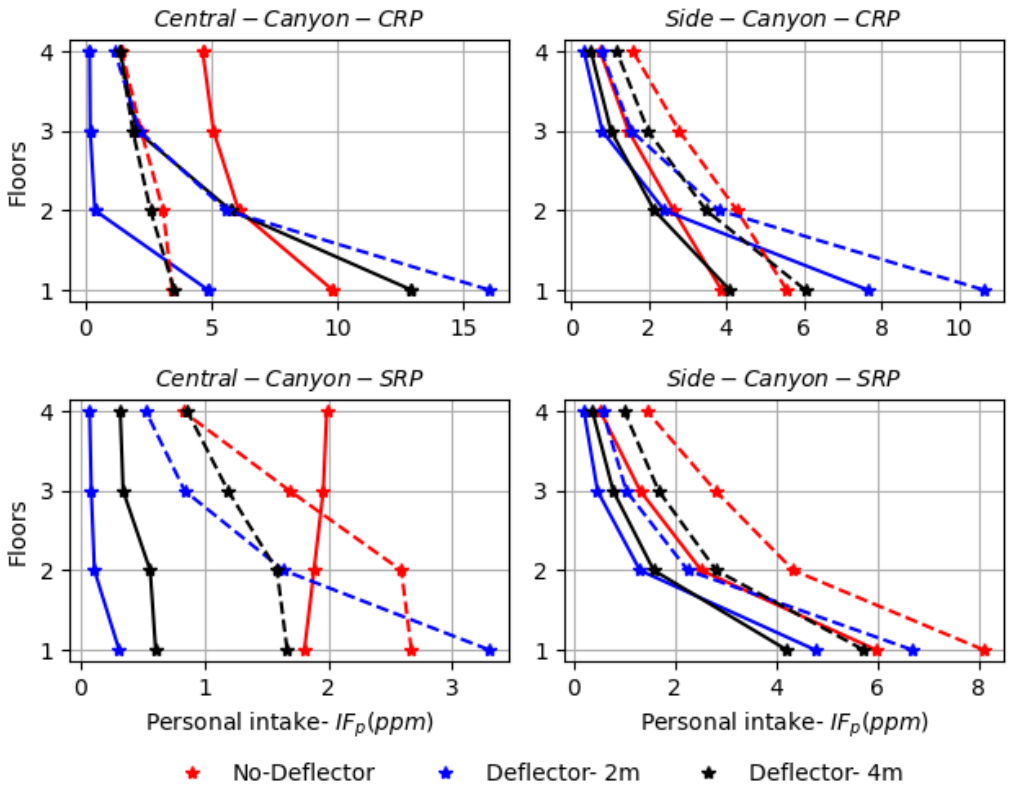

Figure 4.15: Performance of wind deflectors when placed at 2 and 4m from the leeward against the no-deflector case in affecting the indoor air quality in canyon 3 *(Central canyons: solid lines indicate the leeward wall and dashed lines indicate the windward walls. Side canyons: solid lines indicate the side-1 facade and the dashed lines indicate the side-2 facade).*

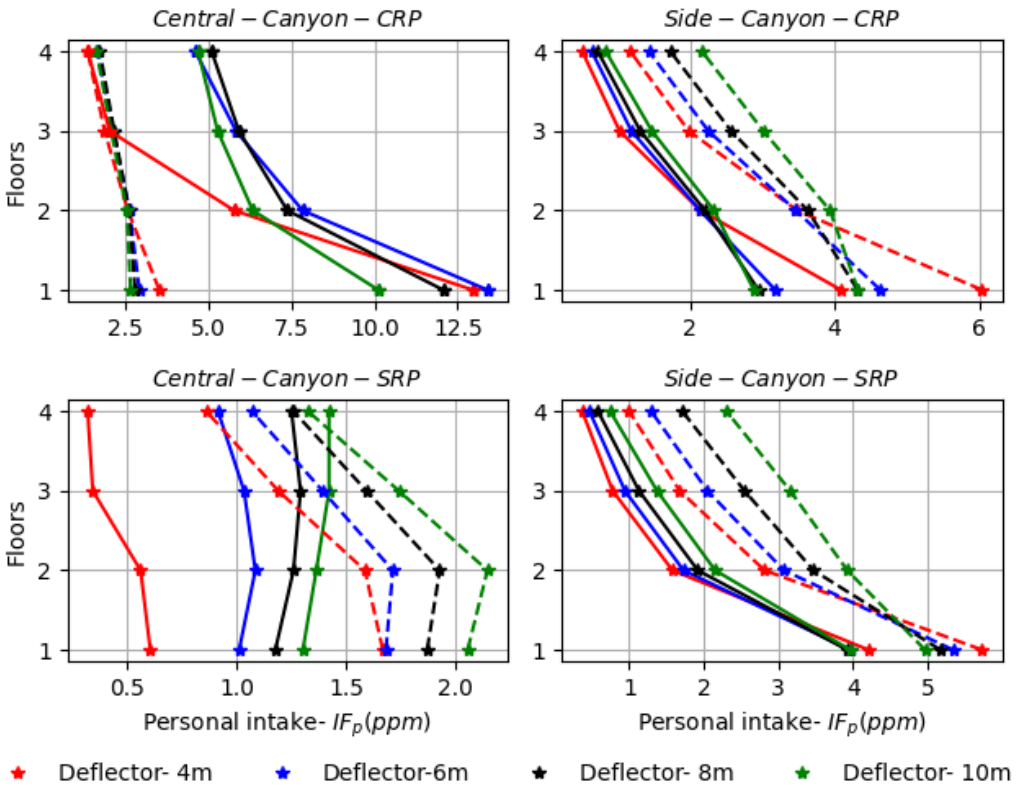

Figure 4.16: Performance of wind deflectors when placed at 4, 6, 8 and 10m the leeward wall in affecting the indoor air quality in canyon 3 *(Central canyons: solid lines indicate the leeward wall and dashed lines indicate the windward walls. Side canyons: solid lines indicate the side-1 facade and the dashed lines indicate the side-2 facade).*

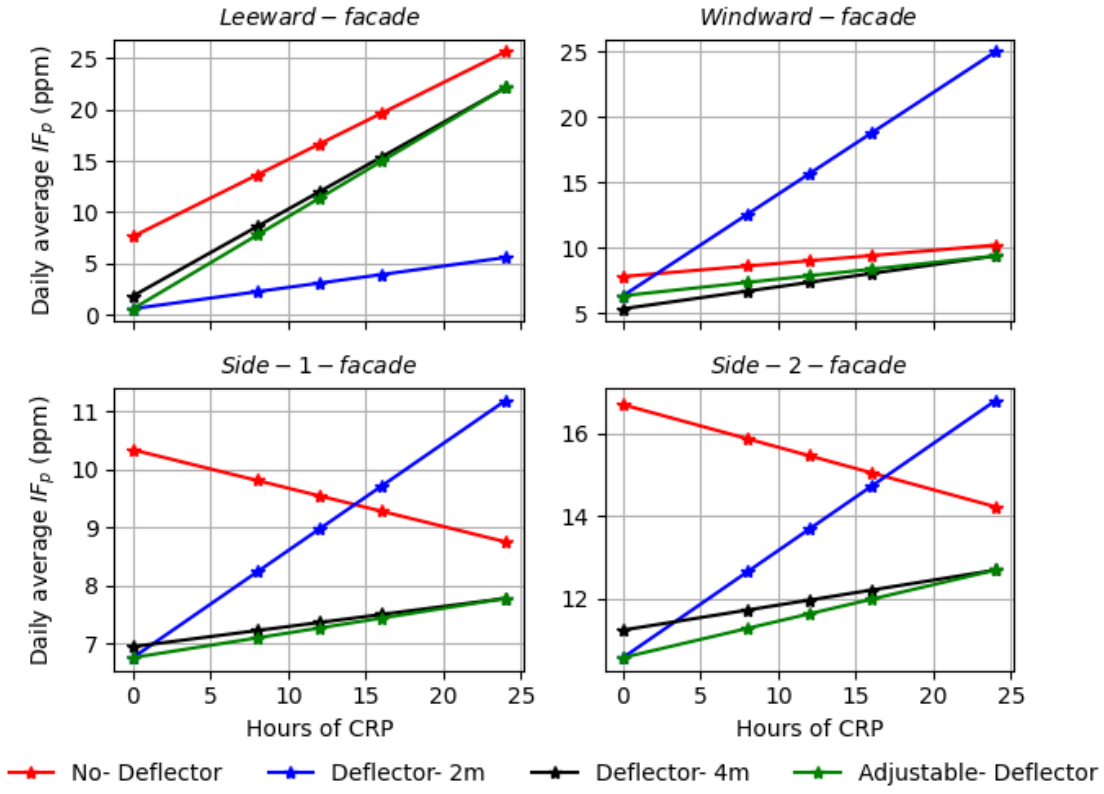

Figure 4.17: Cumulative (for all floors) daily average IF_p of facades due to diurnal changes in traffic flow, comparing no-deflector case with deflectors at 2 and 4m from the leeward wall.

tial on the leeward façade is reduced but the adjustable wind deflector mitigated the risk of higher CO exposure along other facades for increased hours of traffic on the crossroads that the static deflector at 2m would have resulted in. Finally, the indoor exposure has been estimated similarly for all the indoor environments and the exposure pathway was through windows. However, in reality, this could be very different for varying built environments and incorporating such differences is necessary for a more realistic impact of wind deflector systems on indoor exposure. Pedestrians, cyclists and vehicle commuters are exposed to high traffic emissions as well, but for much shorter duration. The average velocity in the lower canyon region was significantly reduced in the central canyons due to the helical corkscrew-type rise-up of the flow and restricted recirculations. However, the helical corkscrew-type rise-up of the flow largely detached the flows in the central canyon and the side streets. Therefore, as can be seen from Figure 4.18, the personal exposure in the crossroad nearly doubled for the CRP source model and witnessed a maximum reduction for

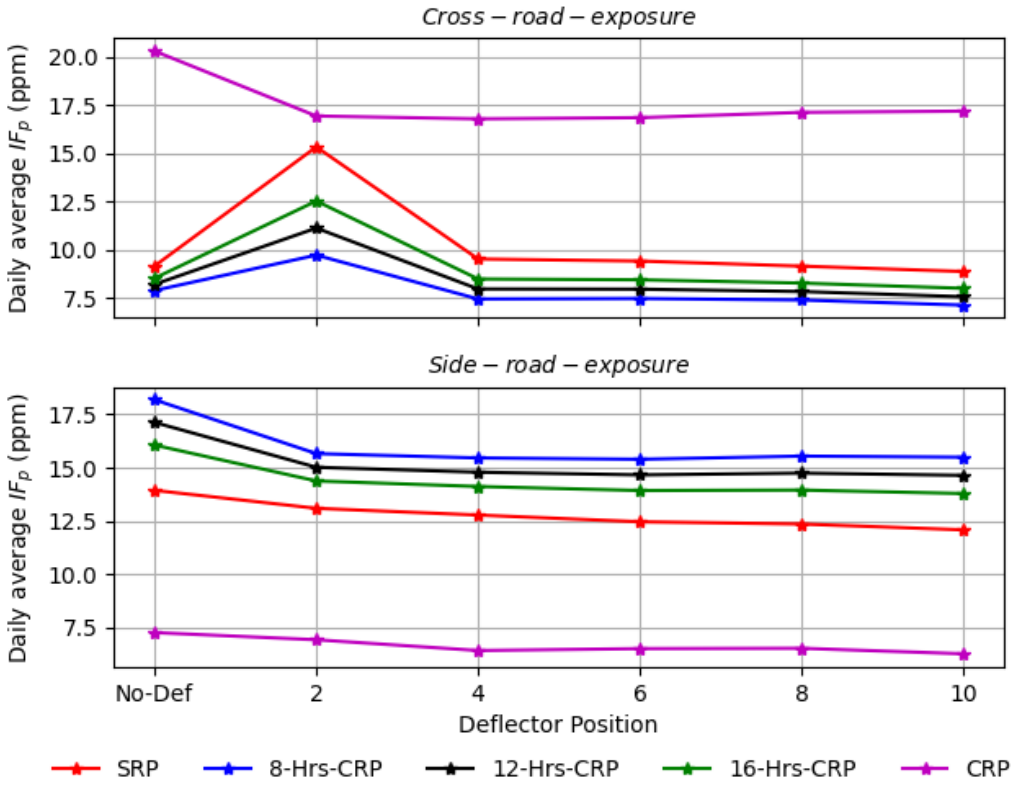

Figure 4.18: Daily average IF_p of the near-vehicle outdoor population due to diurnal changes in traffic flow, comparing no-deflector case with deflectors at 2, 4, 6, 8 and 10m from the leeward wall.

the SRP source model when the deflectors were 2m away from the leeward walls. On the contrary, the sideroad performed substantially better with the deflectors. However, the minimization and the elimination of the inward-curling spiral recirculations did not particularly improve the concentration in the lower canyon region. The reduced airflow in the lower canyon region of the central canyons is expected to be responsible for this trend. A typical urban air pollution hotspot like a traffic intersection can substantially benefit from an adjustable deflector system that can operate on input from vehicle count monitoring, meteorological data and air pollution monitors. Finally, the performance of deflectors varied from one canyon to another for the CRP source model while the deflectors behaved differently for the SRP source condition where the reduction in the overall canyon concentration monotonically increased for every subsequent downstream canyon. This indicated the necessity to consider the interventions to be appropriately suitable to developing and developed regions of urban flow environments.

4.11 Conclusions

Traffic emissions impact both road users and indoor inhabitants occupying near-road buildings. Wind catchers have been effectively introduced in the past to utilize the fresher above-roof winds to ventilate the street canyons in their entirety. However, a street canyon environment is subject to multiple changes including traffic flow patterns, wind speed, wind direction, geometric changes and temperature to mention a few. A methodology to develop mitigation strategies that could adapt to changing conditions has rarely been investigated. The impact of roof-level interventions on the fundamental ventilation indices and their direct relationship with increased air exchange and pollution removal through mean flows has previously not been explored in detail.

Therefore, a systematic methodology was adopted to understand the functionality of the wind deflectors using 2D CFD simulations and then realize its potential in a complex 3D city-type environment. The 2D simulations showed the potential to reduce overall canyon concentration by 2.84 fold when the deflector was placed 2m away from the leeward wall. Nevertheless, the need for an adjustable framework was realized. Despite reducing the overall canyon concentration greatly, the windward wall of the target canyon experienced an 89.3% increase compared to the no-deflector case. When the deflector was placed 0.25m away from the leeward wall, the leeward and the windward walls experienced 86.5 and 8.45% reduction in CO exposure compared to the no-deflector case. However, this configuration experienced 61% more CO exposure at the pedestrian height of 1.75m across the street compared to when the deflector was placed 2m away from the leeward wall.

The adjustable framework of the deflector system was investigated in detail for the 3D city-type environment. The deflectors when placed 4m away from the leeward walls offered a maximum average reduction of 16% across the 6 central canyons for the CRP source condition, and when placed 2m away provided a 34.2% reduction across the 7 side street canyons for the SRP source condition. The inverse relationship between θ and overall canyon concentrations was deemed satisfactory for the 3D simulations. This also reinforced the fundamental ability of the wind deflectors to divert mean air into the canyons and promote a wash-out.

Central canyon-3 and side canyons 3 and 4 were considered for the exposure analyses. When placed 4m away from the leeward walls, the deflector produced a modest impact by reducing the CO exposure by 7, 11 and 13% on leeward, side-1 and side-2 walls. The resulting flow pattern in this configuration was a partially restricted re-

circulation compared to the no-deflector case. The substantial reduction in Floors 3 and 4 (about 50%) indicated the plausible improved potential of the deflectors in the CRP in canyons with higher aspect ratios. However, this configuration experienced poor air quality in the lower canyon region ($z < 1.75m$) due to decreased flow from the top recirculation. When placed 2m from the leeward walls, the deflector reduced 91, 32, 34 and 17% CO exposure across the leeward, side-1, side-2 and windward walls. This configuration also witnessed increased average velocity and reduced CO exposure in the lower canyon region due to the elimination of spiral inward-curling recirculations. The potential to mitigate prolonged exposure due to diurnal changes in the traffic flow pattern was demonstrated by adjusting the deflector position suitably.

Finally, apart from a systematic methodology that was demonstrated in this chapter where the benefit of adjustable wind flow deflectors were shown for 2D simulations and then for changing traffic flow directions in 3D city-type environments, the results indicate the opportunity to use adjustable wind deflectors for other variations in the environment. This has been included in Chapter 6 where the combined influence of changing wind flow and traffic flow directions were considered. Secondly from an air flow dynamics perspective, two major positives were noted. One, that despite the modest CO IFp reductions in the central canyons, the more polluted leeward facade experienced better ventilation in the higher floors deflectors when placed close to the leeward facade as it mitigated the inward curling recirculations to facilitate a regular wash-away along the side road. The side canyons and side facades also largely benefited from deflectors when placed close to the leeward façade for the same reason. As built environment including higher ARs experience higher pollution exposure, Chapters 5 and 6 in this thesis have been dedicated to exposure analysis with adjustable wind deflectors in asymmetric environments with higher ARs to explore the aforementioned two positives.

Chapter 5

Wind Flow Deflectors for Asymmetric City-Type Environments

The content of this chapter has been accepted for publication in a more concise form: Vasudevan, M., Pilla, F. and McNabola, A., 2024. Assessment of pollution removal mechanisms in steep-asymmetric city-type environments using wind deflectors. Energy and Built Environment.

5.1 Introduction

Ventilation indices provide useful information about the extent of aeration in a region within a street canyon or within an entire UCL but seldom have studies focused on mechanisms driving the pollution removal from street canyons. On the contrary, the field synergy theory reflects the mode of ventilation by accounting the amount of pollution removed through convective and diffusive fluxes. In Chapter 4, through both 2D and 3D simulations, θ was correlated to the ability of the ambient mean flow to reach, dilute, and remove the pollutants from street level out of the canyon. Larger θ naturally signified a reduced dependence on turbulent fluctuations induced fluxes that facilitate localized pollution removal at the interfaces of the canyon. Here, the ventilation modes are evaluated using the Field Synergy Number (FS_n, synergy between the velocity and concentration gradient vectors) and Sherwood Number (Sh, ratio of resistance offered by the boundary diffusion

and convective mass transfer) (Chen et al., 2008). Previously, studies have applied field synergy theory to assess urban ventilation in the presence of viaducts and noise barriers in an isolated 3D street canyon (Ming et al., 2023), and with wind catchers in 2D urban street canyons (Ming et al., 2021). These studies demonstrated the increased field synergy and reduced $\bar{C}_{canyon}$ and thereby the advantage of promoting and suppressing the pollution removal through convective and diffusive fluxes respectively. Therefore, analyzing field synergy in the context of a complex city-type environment alongside θ *vs* $\bar{C}_{canyon}$ correlation was considered to aid in understanding specific features of the urban flow that aid and suppress pollution removal from street canyons, thereby also forming the first objective of this chapter.
From an air pollution mitigation standpoint, studies have considered flow dynamics within street canyons with differing Aspect Ratios (ARs) (Cheng and Liu, 2011; Li et al., 2009; Li et al., 2006; Liu et al., 2005; Liu and Wong, 2014; Oke, 1988; Vardoulakis et al., 2003; Xiaomin et al., 2006). Asymmetry strongly affects the initial flushing mechanics, subsequent flow regimes and vertical mixing (Baratian-Ghorghi and Kaye, 2013). With substantial impact on $\bar{C}_{canyon}$ (Liu et al., 2005), residence times, ACH and PCH components (Li et al., 2009), asymmetry in street canyons has been a pivotal feature in built environments for both, implementing passive pollution mitigation measures in general and at the roof level. Roof-level interventions have shown the potential to improve both the fresh ambient wind availability at the street level (Chew et al., 2017; Zhang et al., 2019) and θ (Vasudevan et al., 2023) and the field synergy (Ming et al., 2021). However, whether an adjustable framework of roof-level deflectors would be an effective mitigation strategy for changing traffic conditions in asymmetric environments remains an open question and is therefore considered the second objective of this chapter.

5.2 Problem Description

Conceiving the potential realized from using adjustable wind deflectors in an ideal city-type environment from the previous chapter and the opportunity to consider θ and Sh as representative parameters to explain the impacts of passive interventions on street canyon ventilation, the present chapter is intended to ascertain answers to the following two research questions in the context of applying adjustable roof-level wind flow deflectors for step-up and step-down street canyons.

1. Does $\bar{C}_{canyon}$ exhibit a better inverse correlation with θ or Sh or similarly

with both? Hence providing a conclusive explanation of the pollution removal mechanism facilitated by passive air control interventions.

2. Can poor indoor air quality in near-road asymmetric buildings in a city-type environment with changing traffic flow directions be mitigated using adjustable wind deflectors at roof level?

5.3 Theory

Both FS_n and θ are considered for their representativeness against $\overline{C}_{canyon}$.

5.3.1 Field Synergy Theory

The field synergy principle in convective mass transfer application was introduced for steady state conditions with no mass sources by Chen et al. (2008) as shown in Equation- 5.1.

$$\rho\, U\, .\, \nabla C \;=\; \nabla.(\rho\, D \nabla C) \tag{5.1}$$

By integrating Equation- 5.1 over the entire domain Ω and applying Green's theorem to convert the volume integral to a surface integral, Equation 5.2 can be arrived.

$$\Big\{\int_{\Omega} \rho\, U\, .\, \nabla C\; d\Omega \;=\; \int_{\Omega} \rho\, |\overrightarrow{U}|\, \overrightarrow{\nabla C}\, cos\gamma\; d\Omega\Big\} = \Big\{ \int_{\Omega} \nabla.(\rho\, D \nabla C) = \int_{\Gamma} \overrightarrow{n}.(\rho D \nabla C) d\Gamma \Big\} \tag{5.2}$$

Here, γ is the angle between the velocity and concentration gradient vectors, Γ is the surface enclosing the control volume Ω and $\overrightarrow{n}$ is the unit surface normal vector. By applying non-dimensionalization, FS_n and Sh were defined by Chen et al. (2008) as in Equations- 5.3 and 5.4.

$$FS_n = \frac{\int_{\Omega} \bar{U}.\, \nabla \bar{C}\; d\Omega}{V} \tag{5.3}$$

$$Sh = Re\ S_c\ \frac{\int_\Omega \bar{U}.\ \nabla\bar{C}\ d\Omega}{V} \tag{5.4}$$

Here, R_e is the Reynolds number and FS_n is defined as the synergy between the velocity vector and contamination. Since Sh is defined as the ratio of the resistances offered by the boundary diffusion and convective mass transfer. It represents the relative extent of mass transfer achieved across the boundary surfaces of the street canyon via convective mass transfer compared to that achieved through diffusion. Therefore theoretically, for a constant Re, the overall ventilation can be enhanced by arranging the ventilation mechanism to have high field synergy.

5.3.2 Pollution removal by mean and fluctuations induced fluxes

Pollution removed from the street canyons was assessed through mean and turbulent flow-induced fluxes as in Chapter 4.

5.3.3 Performance of θ v/s Sh

As mentioned in the introduction section, global changes in street canyons as a whole necessitate a more fundamental explanation. A potential explanation for this could stem from the influence of turbulence on the mass transfer of pollutants out of the street canyon. Turbulence can increase and decrease mass transfer in a system based on various ambient factors. To compare the efficacy of θ and Sh as representative parameters, one needs to compare the contributions of PCH_{mean} and PCH_{fluc} and pollution transported out of the canyon via diffusion and convection. Although θ and Sh indicate different mechanisms, the amount of pollution removed out of the canyon remains the same in reality and as shown in Equation- 5.5.

$$\begin{aligned} PCH_{mean}\ +\ PCH_{fluc}\ =\ & Pollution\ removed\ via\ convection \\ & +\ Pollution\ removed\ via\ diffusion \end{aligned} \tag{5.5}$$

In the case where θ and $\overline{C}_{canyon}$ exhibited a stronger correlation than that exhibited by Sh and $\overline{C}_{canyon}$, it can be concluded that resistance offered for enhanced mixing arose more from the turbulent fluctuations in the flow and not the diffusive components. On the contrary, if Sh and $\overline{C}_{canyon}$ exhibited a stronger correlation, it can be

concluded that the turbulent fluctuations induced mixing enhanced the convective mixing and that the resistance to mixing arose from the diffusive elements of the flow regime. The volumes of evaluation of FS_n and Sh are the same as that of the $\overline{C}_{canyon}$, marked as the target street canyons in Figure 5.2. The surfaces where θ were evaluated for the step-down and step-up canyons in the current study can be seen in Figure 5.3. Finally, suppose Sh and θ produced identical trends with $\overline{C}_{canyon}$, it does not mean that PCH_{mean} and PCH_{fluc} are synonymous with pollution removed via convective and diffusive fluxes. It means that both of the mechanisms are individually still valid. This is because turbulence is a multi-characteristic phenomenon that includes rapid diffusivity, high levels of fluctuating vorticity and dissipation of TKE. Therefore, when a passive intervention reduces overall street canyon concentration and exhibits a proportionately higher θ and Sh, one could say that the passive intervention has in general suppressed turbulence-aided pollution removal to reduce both through fluctuations and diffusion.

5.4 Computational Domain & Boundary Conditions

Figure **??** shows the asymmetric city-type environment considered for the study. The choice of the computational domain, boundary conditions, and CO source definition remains the same as in Section 4.3 in Chapter 4. Step-up (H_1 = w =15m, H_2 = 30m) and Step-down canyons (H_1 = 30m, H_2 = w =15m) were included to form an asymmetric third street canyon in a uniformly steep city-type environment ($w_1 = 15m, w_2 = H = 30m$) comprising seven buildings and six street canyons in total as shown in Figure **??**. As a preliminary study, a complete steep city-type environment without any step-down or step-up configuration was compared to an ideal city-type street canyon configuration ($w_1 = w_2 = H_1 = H_2 = 30m$). The ACH through all the street canyons was compromised by 50-55% compared to an ideal city-type street canyon configuration ($w_1 = w_2 = H_1 = H_2 = 30m$). Therefore, such a building morphology was chosen to assess the potential of the wind deflectors when not only the target street canyon, but the whole environment offers the ambient wind to skim over and not interfere substantially with the flow within. Such an analysis has been previously conducted for evaluating the performance of wind catchers in a 2D environment (Zhang et al., 2019), but this study introduces the same in a complex 3D city-type environment.

5.5 Case Descriptions

As the study evaluates the efficacy of adjustable wind deflectors for changing traffic flow directions in asymmetric city-type environments, CRP and SRP source models were independently considered for all the cases studied with the step-up and step-down configurations. The schematics of the pollution source models and regions of CO exposure along the building facades are included in Figure **??**. The wind deflectors considered in this study were 5m high, "thin" and spanned across the entire transverse width between the building roofs. As in the previous chapter, the wind deflectors had half their face area above the roof of the upwind building and the rest below. The reference velocity of the wind flow considered in all the cases was 3 m/s. The inlet boundaries were modeled by prescribing power-law Atmospheric Boundary Layer (ABL) profiles using stream-wise velocity component u(z), k(z) and ϵ(z), as in the Equations 3.14- 3.16. Finally, the deflector positions included in the study are 2.5, 5, 7.5, 10 and 12.5m away from the leeward wall apart from the reference no-deflector case. Table 5.1 shows the summary of cases considered in the study.

	No- deflector case	Deflector position	CRP	SRP
Step-up Canyons	✓	2.5, 5, 7.5, 10 & 12.5 m	✓	✓
Step-down Canyons	✓	2.5, 5, 7.5, 10 & 12.5 m	✓	✓

Table 5.1: Summary of case studies

5.6 Mesh Convergence

The mesh convergence study described in Section 3.3.2.1 in Chapter 3 has been applied to the case studies in this chapter.

5.7 Key assessment parameters & target regions of study

The third street canyon was chosen to be the target street canyon. The upwind and downwind buildings of the target street canyon were marked in blue while the other buildings in the city-type environment are marked in black as shown

in Figures 5.1a and 5.1b. CO exposure was evaluated on the leeward, windward and downwind side facades of the target street canyon at different floors via windows as shown in 5.1c. For the assessment of the pollution removal mechanisms, FS_n, Sh and $\bar{C}_{canyon}$ were evaluated for the central and side street canyons for both the step-down and step-up street canyon configurations under CRP and SRP source models respectively as shown in Figure 5.2. Their respective enclosing surfaces where PCH_{mean} and PCH_{fluc} (for θ) are evaluated can be seen in Figure 5.3.

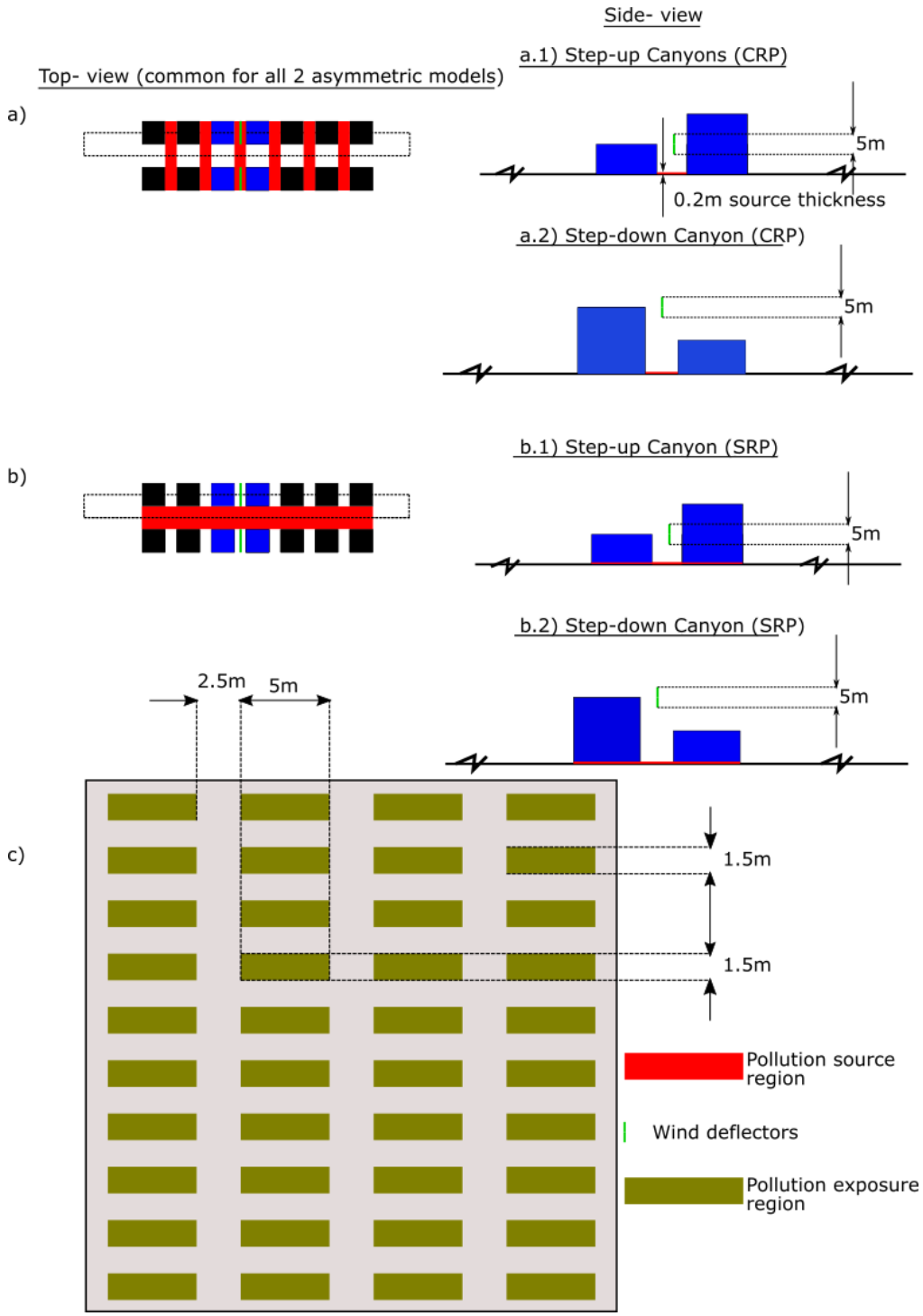

Figure 5.1: a) Computational domain considered for step-up and step-down canyons with CRP source model; b) Computational domain considered for step-up and step-down canyons with SRP source model; c) Window arrangement on all the walls surrounding the target street canyon for estimating the indoor IF_p.

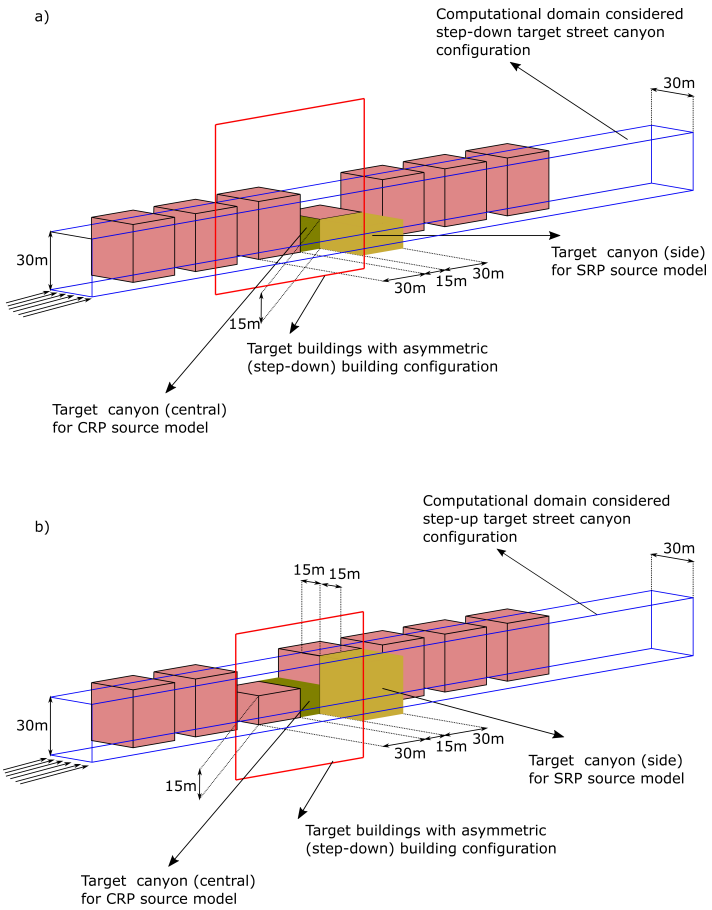

Figure 5.2: a) Schematic figure showing the target central and side street canyons for step-down canyon arrangement; b) Schematic figure showing the target central and side street canyons for step-up canyon arrangement

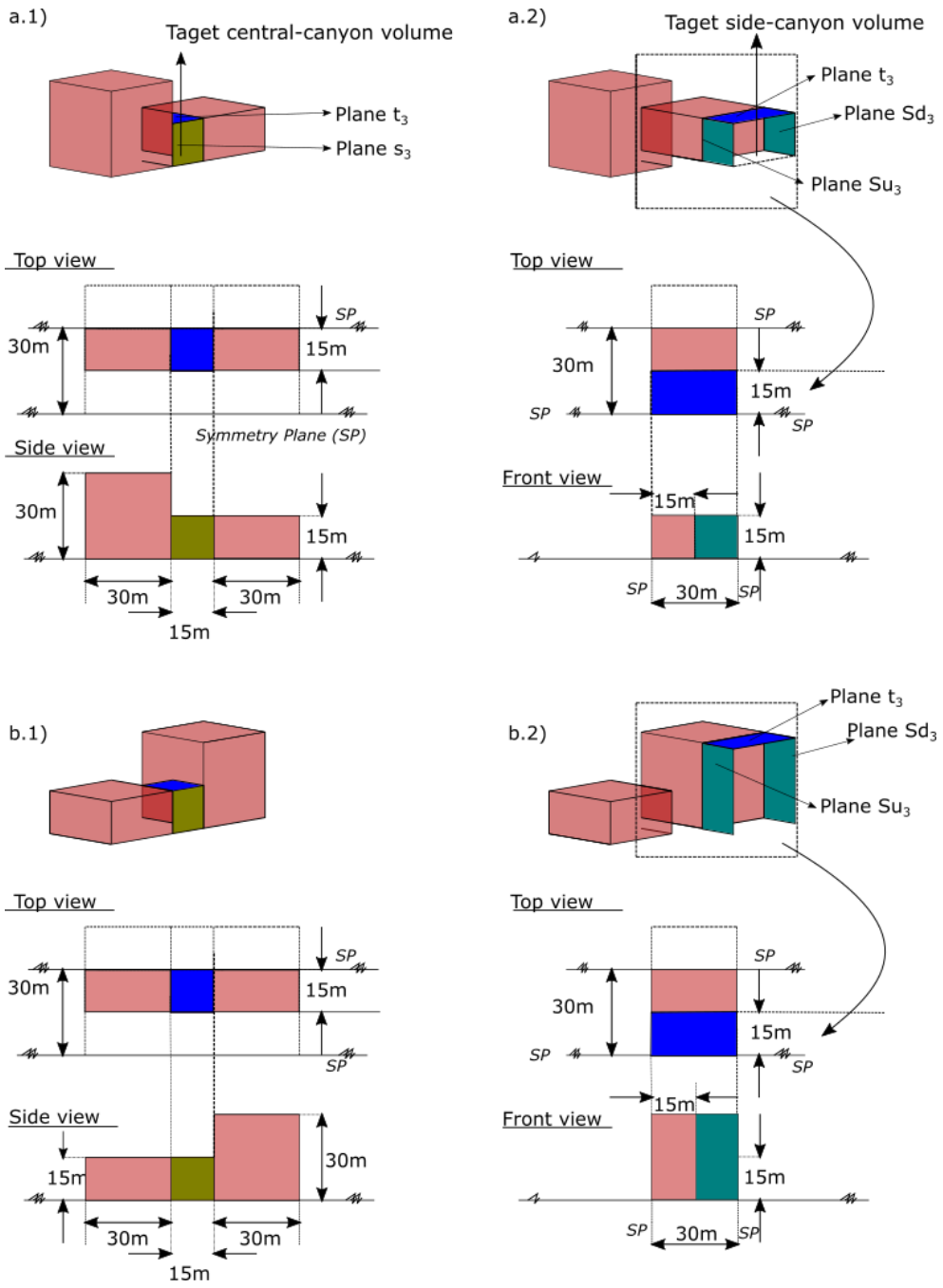

Figure 5.3: a.1) Enclosing planes for the central street canyon in step-down configuration; a.2) Enclosing planes for the side street canyon in step-down configuration; b.1) Enclosing planes for the central street canyon in step-up configuration; b.2) Enclosing planes for the side street canyon in step-up configuration.

5.8 Results

For both the step-down and step-up configurations, the CRP and SRP source models resulted in similar flow patterns. Such an analysis was carried out to evaluate the efficacy of the wind deflectors in mitigating high personal exposure on the immediate building facade. This included changing traffic flow directions (windward and leeward facades for CRP source condition and side facade for SRP source condition). The other reason for this analysis is also to evaluate the efficacy of θ and Sh as parameters to evaluate the change in ventilation conditions in central and side street canyons. Henceforth for convenience, leeward and windward buildings and downwind side facades shall mean the ones in the target street canyon where asymmetry is included.

5.8.1 Step Down Canyons

5.8.1.1 Cross Road Pollution Source Model

The flow is classified into three types here; Flow type 1 includes the reference no deflector case, Flow type 2 includes the cases when the deflectors were placed 2.5 and 5m away from the leeward wall, and Flow type 3 includes the other three cases when the deflectors where placed 7.5, 10 and 12.5m away from the leeward walls respectively. As can be seen from Figure 5.4, Flow type 1 included the majority of its ventilation entering from the sides and minimal contribution from the roof-level opening. Flow type 2 included a washdown along the leeward wall, while Flow type 3 included a vertical recirculation to rise along the leeward wall after a washdown along the windward wall.

The reduced air intake from the roof-level opening and subsequent increased intake from the side openings in Flow type 1 can be attributed to the steep street canyons and asymmetry in arrangement ($W_1 = 0.5\ W_2$). This is unlike the other scenarios including wind deflectors for step-down configurations where recirculation from the roof-level opening and inward curling recirculations from the sides contributed to the ventilation of the street canyon. Therefore, the reference configuration recorded the lowest ventilation at pedestrian exposure level ($z < 2m$) with $v_{avg} = 0.173\ m/s$ and $\overline{C}_{avg} = 6.17e-7$. As can be seen from Figure 5.4, the flow includes two inward curling recirculations from each side of the target street canyon. Since the fresh air enters through the windward side from the side openings

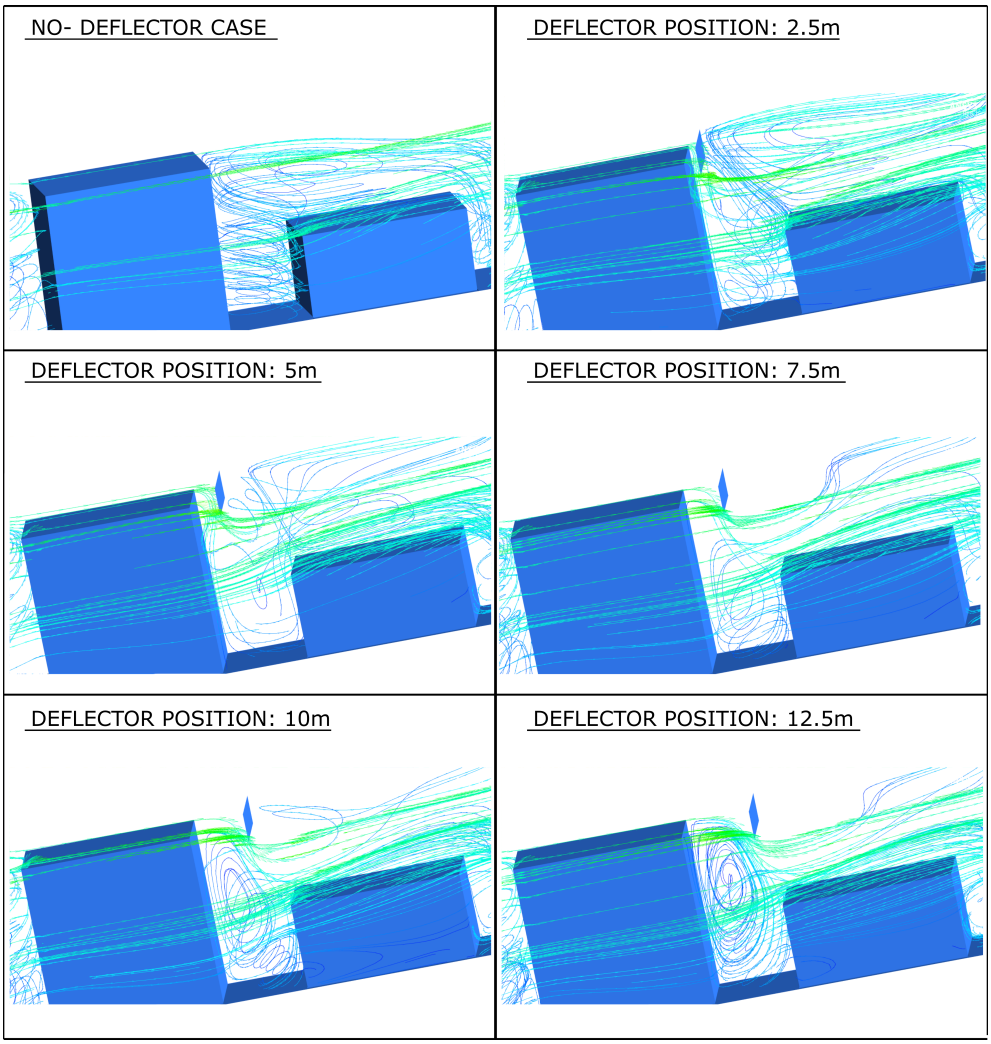

Figure 5.4: Streamlines of the airflow in the target step-down street canyon for the reference no-deflector case and when deflectors were placed 2.5, 5, 7.5, 10 and 12.5m away from the leeward wall.

and reaches the leeward side at the center of the canyon ($y \approx 30$) after amassing CO from the ground, the leeward side is naturally more polluted than the windward side. This nature of recirculation also makes the sides and center of the leeward and windward sides marginally more contaminated than the center and side regions of the same respectively, as shown in Figures 5.5 and 5.6. Apart from the natural rise-up of the recirculating vortices, the step-down configuration of the street canyon pushes the rising recirculation in the downwind direction. Therefore, a helical spiraling rise-up of the flow occurs towards the top of the downwind building.
In Flow type 2, the wind deflector deflects the above roof cleaner air into the canyon. However, the air stream from the roof is just as strong as the ones from the sides.

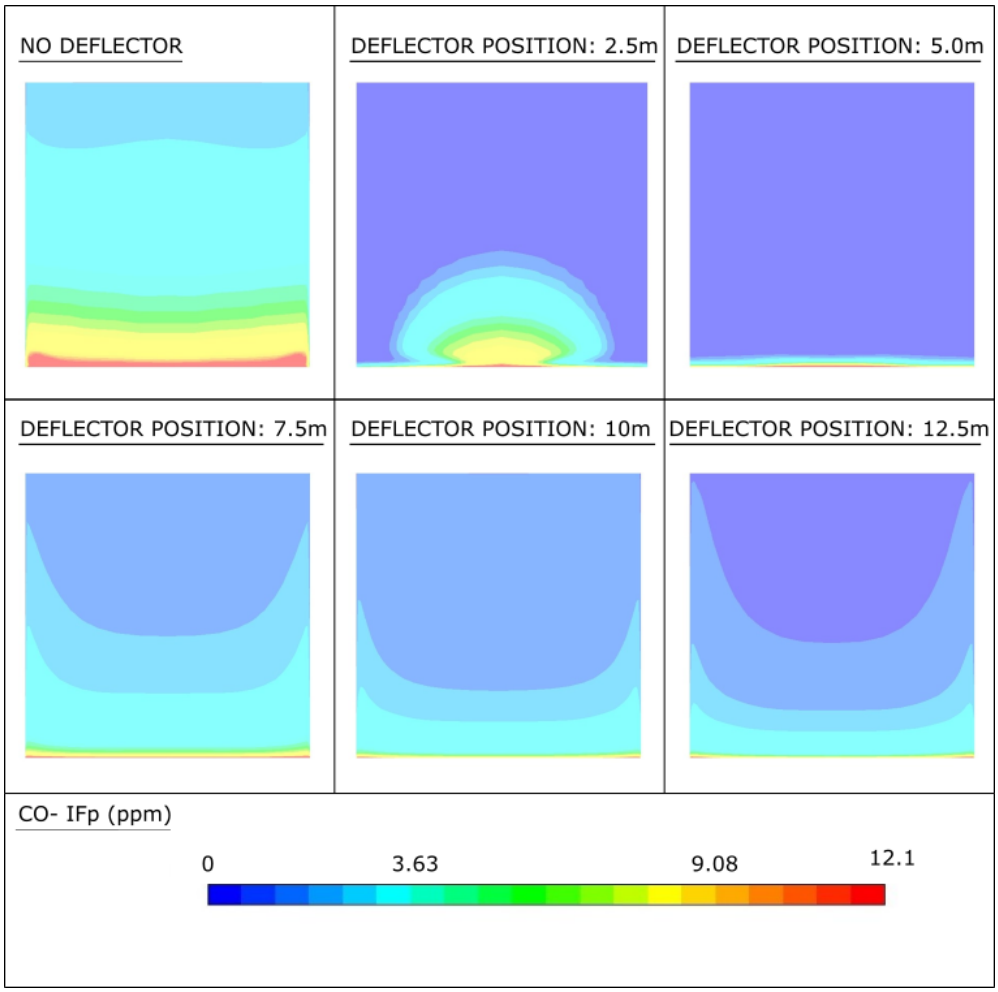

Figure 5.5: Contour plot of IF_p on the leeward facade for reference no-deflector case and when the deflectors were placed 2.5, 5, 7.5, 10 and 12.5m respectively from the leeward wall in step-down street canyons.

Therefore, these air streams from the top fail to complete their natural recirculation and instead washdown along the leeward side. The vertical stream washing down the leeward wall and the inward curling side streams just balance each other in the vicinity of the leeward wall to rise in a helical trajectory to the downwind windward wall. From here it eventually gets deflected back to the wind deflector to be flushed out of the street canyon. As can be seen from Figure 5.4, the helical rise-up occurred only in the vicinity of the lower half of the leeward wall (floors $\leq$ 5) and not the floors above. Figure 5.7 concurred with this observation where the IF_p drastically reduced when going above the fifth floor. This phenomenon is also furthered in Table 5.2 where it shows that the average reduction of CO exposure along the leeward facade by the wind deflector when placed 2.5m away from the

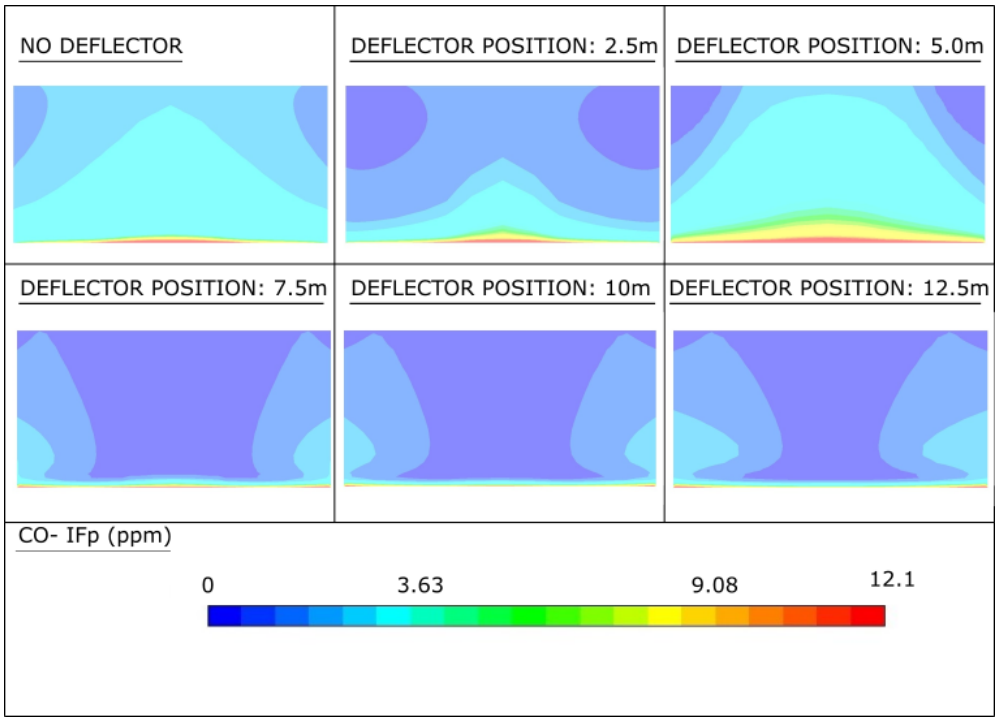

Figure 5.6: Contour plot of IF_p on the windward facade for reference no-deflector case and when the deflectors were placed 2.5, 5, 7.5, 10 and 12.5m respectively from the leeward wall in step-down street canyon.

leeward wall was 60.1% for floors 1-3, while it significantly increased to 92.5% and 99.1% for floors 4-6 and floors 7-10 respectively. When the deflectors were placed 5m away from the leeward wall, the increased flow rate in the passage between the wind deflector and the leeward wall strengthened the air stream to resist the inward curling from the sides. This facilitated a complete wash-down along the leeward wall and directly rose along the windward facade after amassing CO at the ground level. A very high average CO exposure reduction of 95.8%, 98.7% and 99.50% in floors 1-3, floors 4-6 and floors 7-10 was found, as shown in Table 5.2. Furthermore, Figure 5.7 and Table 5.3 highlight the increase in CO exposure along the windward facade compared to the reference Flow type 1. In Flow type 2, the ventilation at the pedestrian exposure level increased in comparison to Flow type 1 because of the additional air stream from the roof and hence the v_{avg} increased to 0.353 m/s and 0.324 m/s. $\overline{C}_{avg}$ reduced to $2.53e-7$ and $1.49e-7$ respectively when the deflectors were placed 2.5 and 5m away from the leeward walls.

In Flow type 3, in all three scenarios where the deflectors were 7.5, 10 and 12.5 m away from the leeward wall, the air stream from the roof underwent a complete recirculation. Because of the air stream from the sides, the recirculation was diago-

nally oriented such that the wash-down along the windward facade and the rise-up along the leeward facade happened at the center ($y = 30\ m$) and edges of the canyon ($y = 15\ m$ & $y = 45\ m$, across symmetry plane). This facilitated a maximum CO removal along the center of the windward facade and maximum addition to the sides of the leeward facades. Despite the addition, it can be seen from Figure 5.7 and Table 5.2 that CO exposure along the leeward facade reduced substantially. This is because the removal was facilitated only by the inward curling air streams from the sides in Flow type 1. However, the inward curling flow is complemented by the vertical recirculation from the roof level in Flow type 3. Flow type 2 demonstrated the best performance in reducing CO exposure along the leeward facade. This indicated that wash-down is superior compared to a recirculation complemented by side and top recirculations. Unlike Flow type 2, all three Flow type 3 scenarios resulted in reducing at least two-thirds of CO exposure along the windward facade, both across floors 1-3 and floors 4-5 (see Table 5.3).

Floors/ Deflector position (m)	% IF_p reduction Floors 1-3	% IF_p reduction Floors 4-6	% IF_p reduction Floors 7-10
No Deflector	-	-	-
2.5	60.1	92.5	99.1
5.0	95.8	98.7	99.5
7.5	58.2	62.6	51.4
10.0	69.7	73.9	60.9
12.5	74.3	80.6	71.1

Table 5.2: Percentage reduction of average CO exposure along the leeward facade in step-down street canyons in step-down street canyons.

Floors/ Deflector position (m)	% IF_p reduction Floors 1-3	% IF_p reduction Floors 4-5
No Deflector	-	-
2.5	32.5	61.8
5.0	-58.8	9.1
7.5	69.1	71.5
10.0	72.6	72.4
12.5	67.3	71.4

Table 5.3: Percentage reduction of average CO exposure along the windward facade in step-down street canyons.

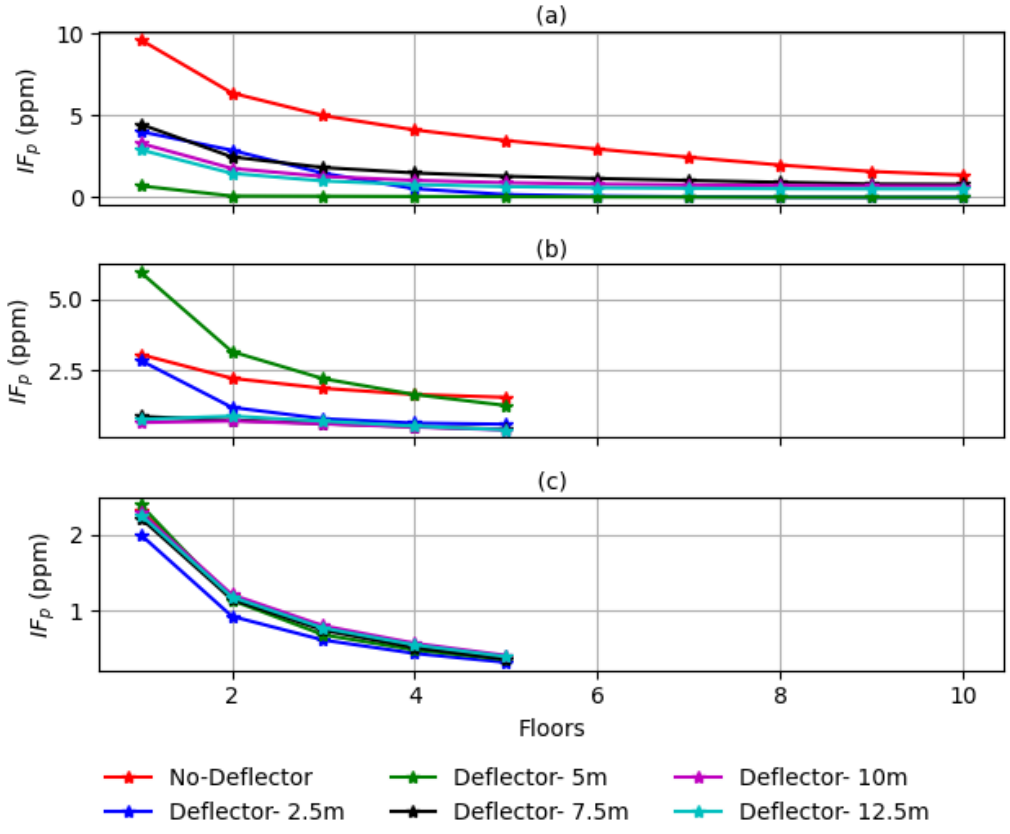

Figure 5.7: Step-down target street canyon- a) IF_p along leeward facade (floors 1-10) under CRP source model; b) IF_p along windward facade (floors 1-5) under CRP source model; c) IF_p along windward facade (floors 1-5) under SRP source model.

5.8.1.2 Side Road Pollution Source Model

In this study, the CO IF_p for side facades is based on only the exposure along the side facade of the downwind building and not the upwind building of the target street canyon, as that is where the influence of the deflector was largely realized. Firstly, along with the streamwise washout of CO in the side road for SRP source models, the asymmetry in building arrangement ($w_1 = 0.5w_2$) allowing wider side roads facilitated a substantially lower CO exposure along the side facade (see Figure 5.7). The inward curling of the air streams from the sides of the central canyons introduces a recirculation in the side roads. This occurred in the vertical plane, referred to henceforth as recirculation 1 for convenience. The reason for enhanced ventilation in the side roads using wind deflectors in the central canyons has been discussed in detail in the previous chapter. However, in the context of wider side roads in the current study, the effects of the wind deflectors on CO exposure along the side walls were not as pronounced as they were when $w_1 = w_2$ in Chapter 4. Figure 5.8 shows the vector plot of the plane 0.5m away in the side from the side facades of the buildings (y =14.5m). This is shown for the reference no deflector case, and when the deflectors were placed 2.5, 5 and 12.5m away from the leeward walls. Figure 5.7 concurred with this observation as they reflect marginal differences between the CO IF_p along the downwind side facade compared to the differences between CO IF_p along leeward and windward walls, when the deflectors were positioned at different locations relative to the leeward wall. This could also be interpreted from Figure 5.9 where the range of $\overline{C}_{canyon}$ and θ values for CRP source model cases were about an order of magnitude greater than that for SRP source model cases.

Finally, one more recirculation in the vertical plane impacted the side canyon ventilation. This was because of the upward-curling nature of the flow to adjust for the subsequent step-up canyon right after the target street canyon (henceforth referred to as recirculation 2 for convenience). Since there is no top-recirculation in the no-deflector case, the inward curling recirculation is horizontally layered (as can be seen from Figure 5.4) and hence only recirculation 2 is observed for this scenario. For flow type 2, there is an increased streamwise push due to the washdown along the leeward wall and hence this increases recirculation 2 whilst recirculation 1 is practically non-existent. As the washdown is stronger for the case when the deflector was placed 5m from the leeward wall compared to the case when the deflector was placed 2.5m away, recirculation 2 is stronger for the former. Recirculation 2 starting at the

downwind building end largely affected the pedestrian ventilation ($z < 2m$) by reducing the v_{avg} from 0.74m/s for the no-deflector case to 0.67 and 0.66m/s for when the deflector was placed 2.5 and 5m away from the leeward wall. This consequently resulted in increasing $\overline{C}_{avg}$ for the three cases from 2.79e-7 for the no-deflector case to 2.78e-7 and 2.79e-7 respectively for the latter two cases. This also concurred with Table 5.4 where CO exposure is lower when the deflector was placed 2.5m away. For cases when the deflector was moved further downstream, top recirculation became the dominant flow in the central canyon thereby making recirculation 1 the crucial one affecting the side facade concentrations. The top recirculation became stronger as the wind deflector was moved closer to the windward wall, so did the recirculation 1. Therefore v_{avg} reduced from 0.71m/s when the deflector was placed 7.5m from the leeward wall to 0.60 and 0.62m/s when the deflector was moved 10 and 12.5m. Accordingly, the concentration increased from 2.76e-7 to 3.00e-7 and 2.99e-7 for the two cases of Flow type 3, respectively. Recirculations 1 and 2 can be distinguished in Figure 5.8 by whether they started at the upwind or the downwind ends of the step-down canyons. Finally, the vertical recirculations can be considered as causes of CO accumulation as they are resistances in the otherwise streamwise washout in the absence of sideward flows that cause these recirculations.

Floors/ Deflector position (m)	% IF_p reduction Floors 1-3	% IF_p reduction Floors 4-5
No Deflector	-	-
2.5	16.9	14.9
5.0	1.2	6.0
7.5	3.6	2.1
10.0	-0.8	-9.6
12.5	1.3	-5.5

Table 5.4: Percentage reduction of average CO exposure along downwind building side facade in step-down street canyons.

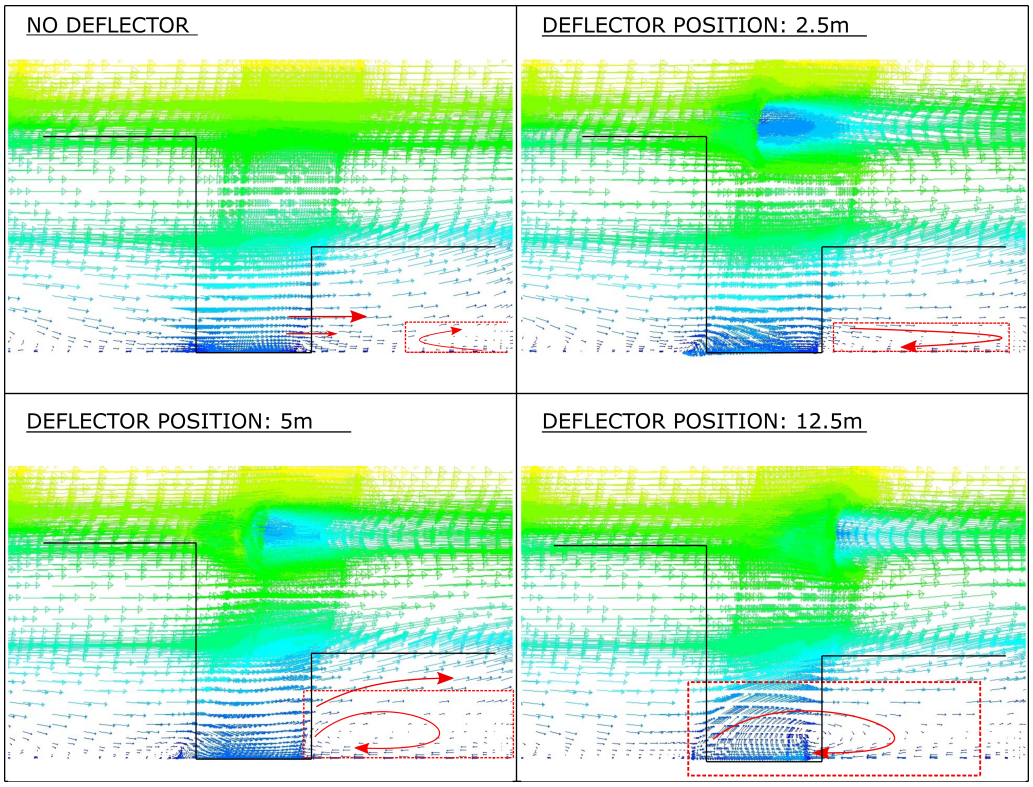

Figure 5.8: Vector plots of velocity magnitude at y = 14.5m plane for no deflector reference case and when deflectors were placed at 2.5, 5 and 12.5m away from the leeward wall in step-down street canyons.

5.8.1.3 θ v/s Sh for step-down canyons

To calculate θ for the target street canyon in the CRP and SRP source models, the total amount of PCH_{mean} exiting the central and side canyons through its virtual enclosing surfaces was individually calculated. The enclosing surfaces and control volume considered as central and side canyons are represented in Figure **??**. In the case of the central canyon, the PCH_{mean} exited the control volume through the side and top surfaces and Equation 5.6 applied to this scenario. For the side street canyon PCH_{mean} exited the control volume through the downwind and top surfaces and entered the same through the upwind surface and Equation 5.7 applied to this scenario.

$$PCH_{mean} = PCH_{mean}|_{Ct3} + PCH_{mean}|_{Cs3} \tag{5.6}$$

$$PCH_{mean} = PCH_{mean}|_{St3} - PCH_{mean}|_{SU3} + PCH_{mean}|_{SD3} \tag{5.7}$$

For $\theta > 1$ in the CRP source model cases indicates that the cumulative PCH_{fluc} from the side and the top surfaces negatively contributed by re-entraining CO back into the control volume. In the CRP source model, all the cases reflected the hypothesized inverse correlation while the increase in θ compared to the no-deflector case when the deflector was placed 2.5m from the leeward wall was not proportional (according to visual observation from Figure 5.9) to the reduction $\bar{C}_{canyon}$. On the contrary, for the SRP source model, the inverse correlation between θ and $\bar{C}_{canyon}$ was proportionately captured for all scenarios except for the no-deflector reference case.

The control volume considered for calculating $\bar{C}_{Canyon}$ is also used for computing FS_n and Sh. The overall inverse correlation between $\bar{C}_{canyon}$ and Sh, according to the field synergy theory, was observed to be very good (see Figure 5.9). Unlike in the case of the θ v/s $\bar{C}_{canyon}$ relationship for the CRP source model, Sh increased proportionately compared to the reference no-deflector case when the deflector was introduced at a distance of 2.5m from the leeward wall. However, as in the θ v/s $\bar{C}_{canyon}$ relationship, the sh v/s $\bar{C}_{canyon}$ relationship captured all of the scenarios correctly except for the no-deflector case for the SRP source model. As discussed in the theory section, since both of the formulations have shown evidence to capture

the changes in $\bar{C}_{canyon}$, the wind deflectors can be considered to be affecting both PCh_{fluc} and removal through diffusion by promoting and suppressing advective removal.

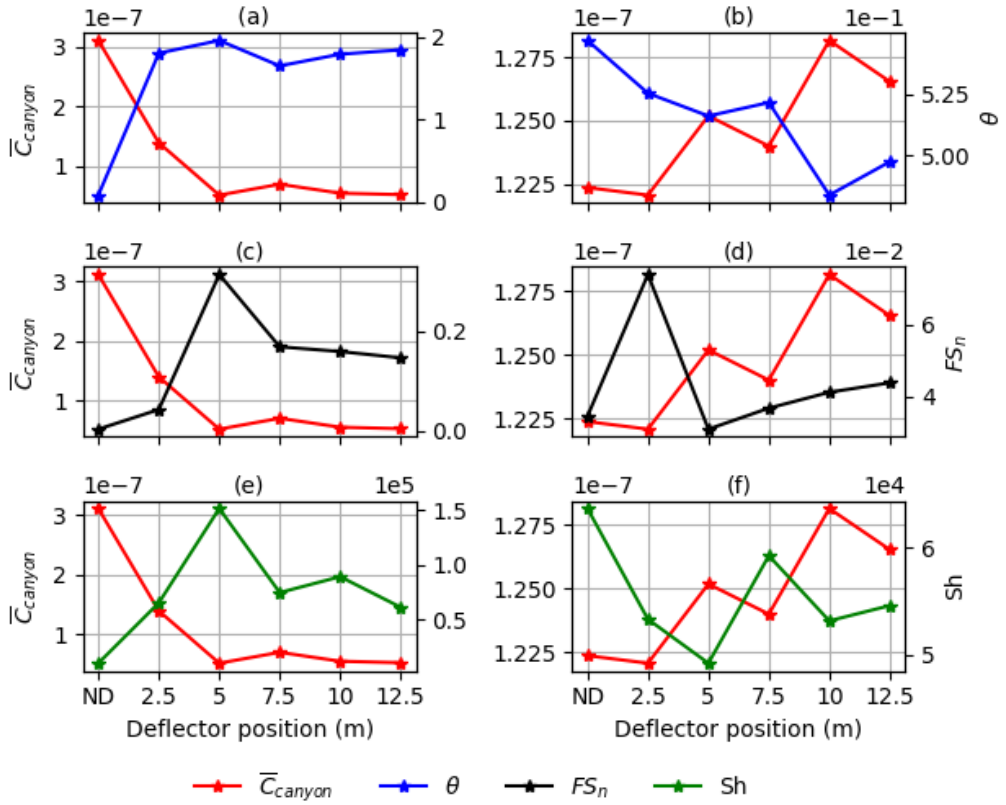

Figure 5.9: Step-down target street canyon- Comparison of $\overline{C}_{canyon}$ against θ under - a) CRP conditions in central street canyon, b) SRP conditions in side street canyon; Comparison of $\overline{C}_{canyon}$ against FS_n under - c) CRP conditions in central street canyon, d) SRP conditions in side street canyon; Comparison of $\overline{C}_{canyon}$ against Sh under - e) CRP conditions in central street canyon, f) SRP conditions in side street canyon.

5.8.2 Step Up Canyons

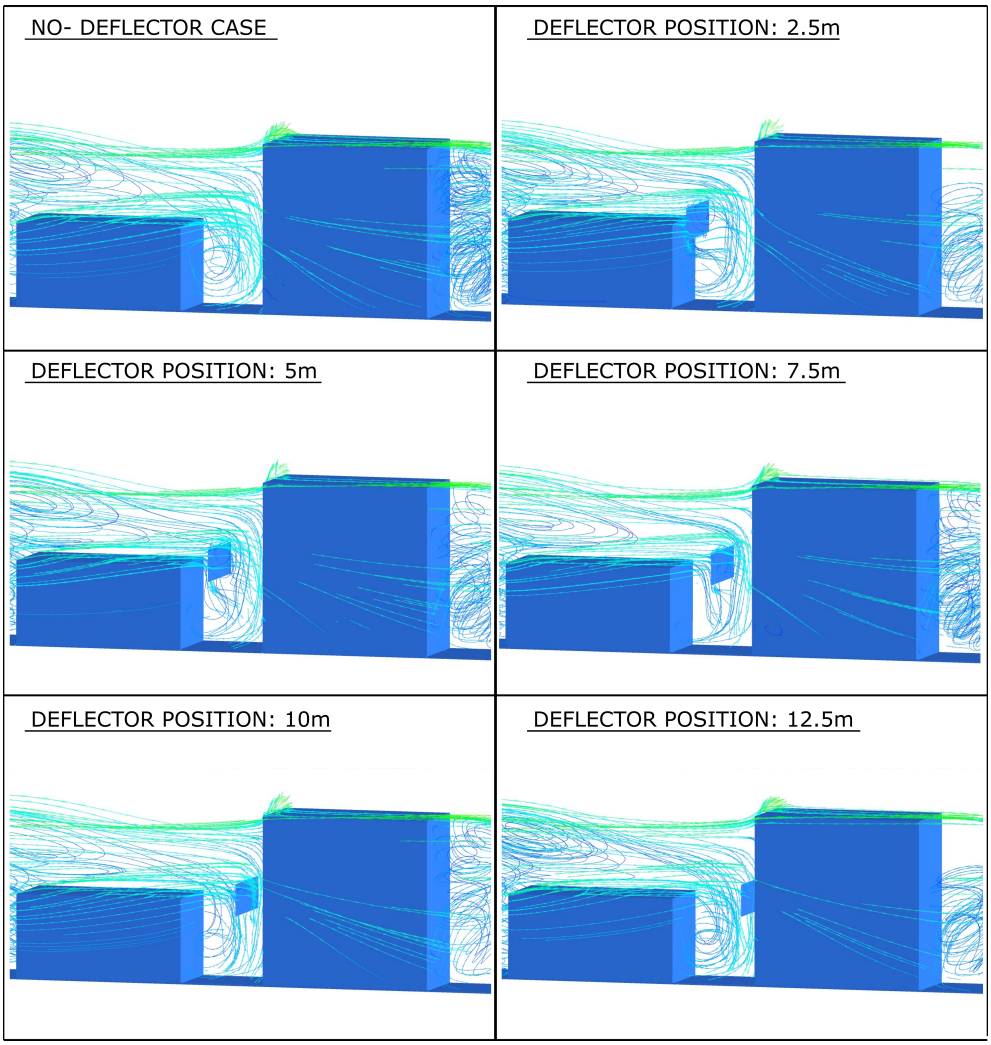

Figure 5.10: Streamlines of the airflow in the target street step-up canyon for the reference no-deflector case and when deflectors were placed 2.5, 5, 7.5, 10 and 12.5m away from the leeward wall.

5.8.2.1 Cross Road Pollution Source Model

As can be seen from Figure 5.10, the flow patterns in step-up street canyons with wind flow deflectors did not qualitatively change much. The step-up nature of the street canyon invariably resulted in a primary top recirculation in both cases including the deflector and otherwise. The inward-curling airstreams from the sides of the street canyons influenced the primary top recirculation to wash down along the center of the windward facade and rise along the sides of the leeward walls. This resulted in higher and marginally lower CO exposure along the side and center

regions of the leeward and windward walls respectively compared to their other regions. This is also seen in Figures 5.11 and 5.12.

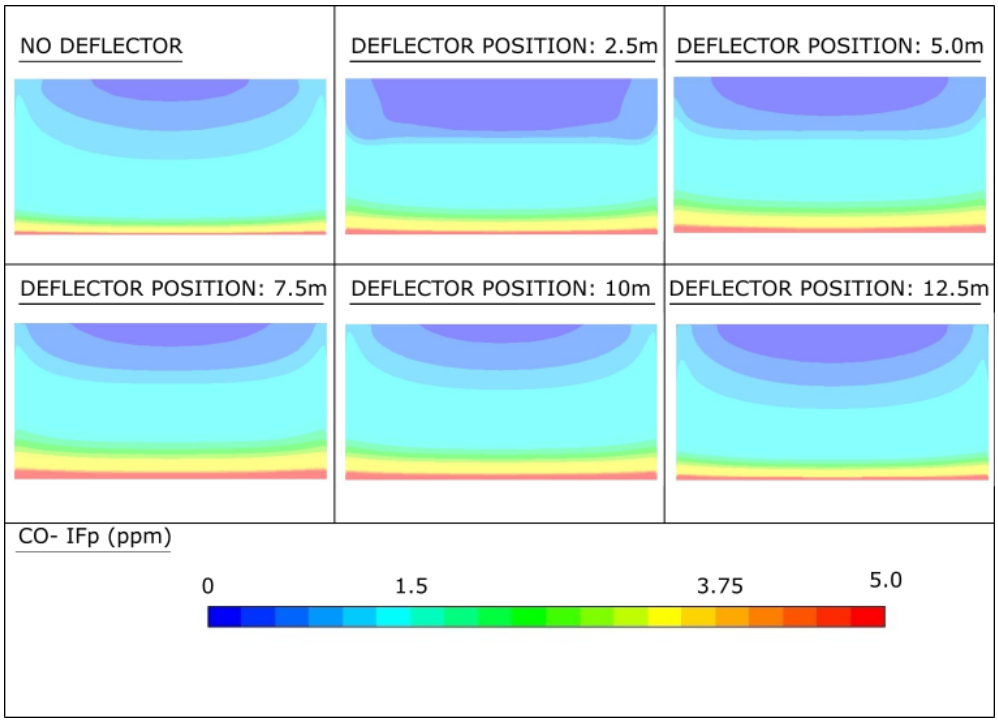

Figure 5.11: Contour plot of IF_p on the leeward facade for reference no-deflector case and when the deflectors were placed 2.5, 5, 7.5, 10 and 12.5m respectively from the leeward wall in step-up street canyons.

For the no-deflector case, a similar top recirculation was observed before the air stream exited through the sides of the canyon after rising along the leeward facade. As the wind deflector was introduced at a distance of 2.5m from the leeward wall, an additional stream of air passed in between the wind deflector and the upwind building to eventually join the primary top recirculation. At first, considering the cases when the deflectors were placed 2.5, 5 and 7.5m from the leeward wall the CO exposure on the leeward wall increased for all three scenarios in the lower part (floors 1-3). More CO accumulated from the recirculation originating from the increasing passage between the leeward wall and the deflector in this case, and was deposited on same. However, the only difference when the deflector was 2.5m away is that floors 4-5 experienced a washdown and hence a 47.9% reduction in CO exposure compared to the no-deflector reference case. When the deflectors were placed 5 and 7.5m away from the leeward wall, the recirculation from the passage strengthened to clean the windward facade further and amassed more CO from the street to eventually pollute the leeward facade more. This can be seen in Tables 5.5 and 5.6.

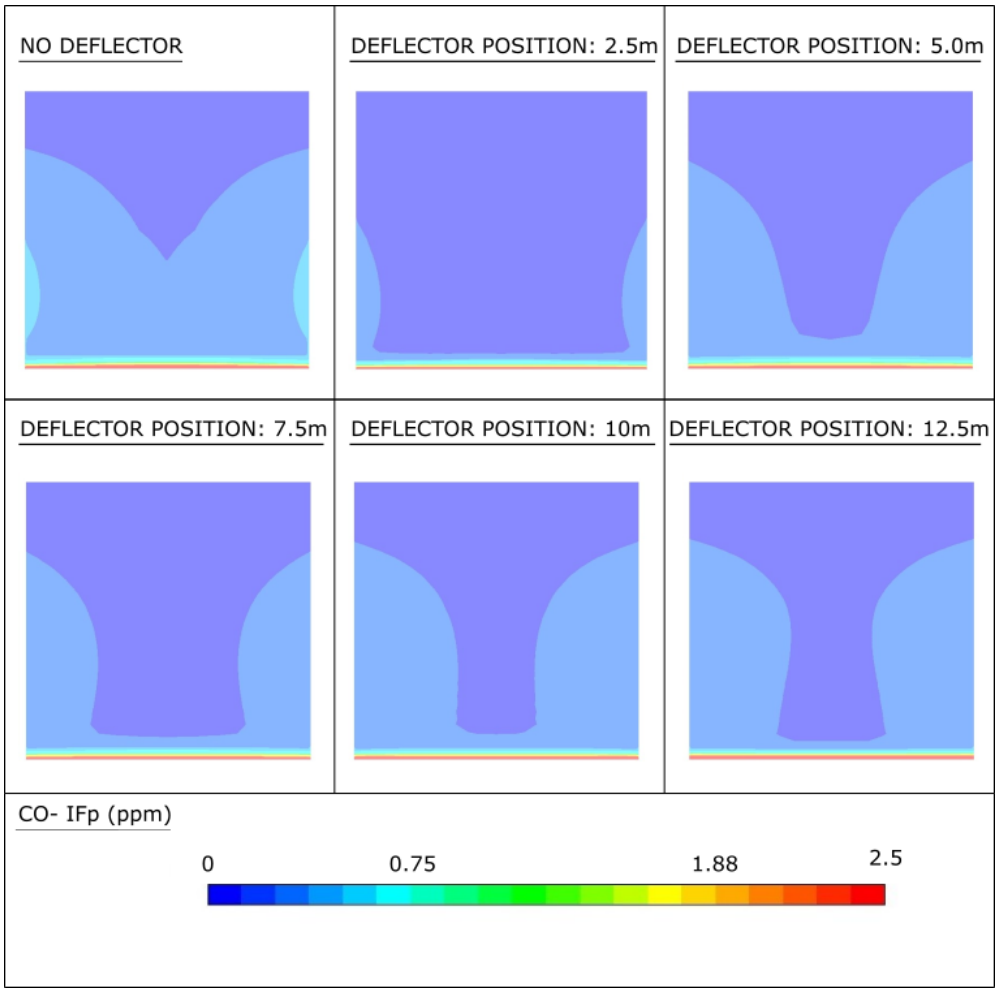

Figure 5.12: Contour plot of IF_p on the leeward facade for reference no-deflector case and when the deflectors were placed 2.5, 5, 7.5, 10 and 12.5m respectively from the leeward wall in step-up street canyons.

This scenario changed when the deflector was moved further to 10 and 12.5m away from the leeward walls. A significant portion of air squeezed in between the wind deflector and the downwind building and exited the canyon through the side without recirculating back to the leeward wall and hence the reduction in increase in CO exposure along the leeward wall. The strengthened washdown further improved the CO reduction along the windward facade compared to the former three scenarios, at least in the lower and middle regions of the windward building, as can be seen from Table 5.6. Finally, the pedestrian exposure trend was found to be coherent with this as $\overline{C}_{avg}$ in the pedestrian exposure zone ($z < 2m$) increased from 7.15e-8 for the no deflector case to 8.35e-8, 8.95e-8 and 9.59e-8 when the deflector was placed at 2.5, 5 and 7.5m away from the leeward wall and subsequently reduced to 8.88e-8

and 7.92e-8 when moved downwind to 10 and 12.5m from leeward wall respectively.

Floors/ Deflector position (m)	% IF_p reduction Floors 1-3	% IF_p reduction Floors 4-5
No Deflector	-	-
2.5	-29.6	47.9
5.0	-39.5	-11.2
7.5	-47.1	0.9
10.0	-29.5	-8.6
12.5	-10.6	-8.1

Table 5.5: Percentage reduction of average CO exposure along the leeward facade in step-up street canyons.

Floors/ Deflector position (m)	% IF_p reduction Floors 1-3	% IF_p reduction Floors 4-6	% IF_p reduction Floors 7-10
No Deflector	-	-	-
2.5	13.8	25.3	-1.3
5.0	15.8	25.8	-3.3
7.5	21.3	29.0	0.7
10.0	21.7	23.0	-9.0
12.5	23.1	25.3	-7.3

Table 5.6: Percentage reduction of average CO exposure along the windward facade in step-up street canyons.

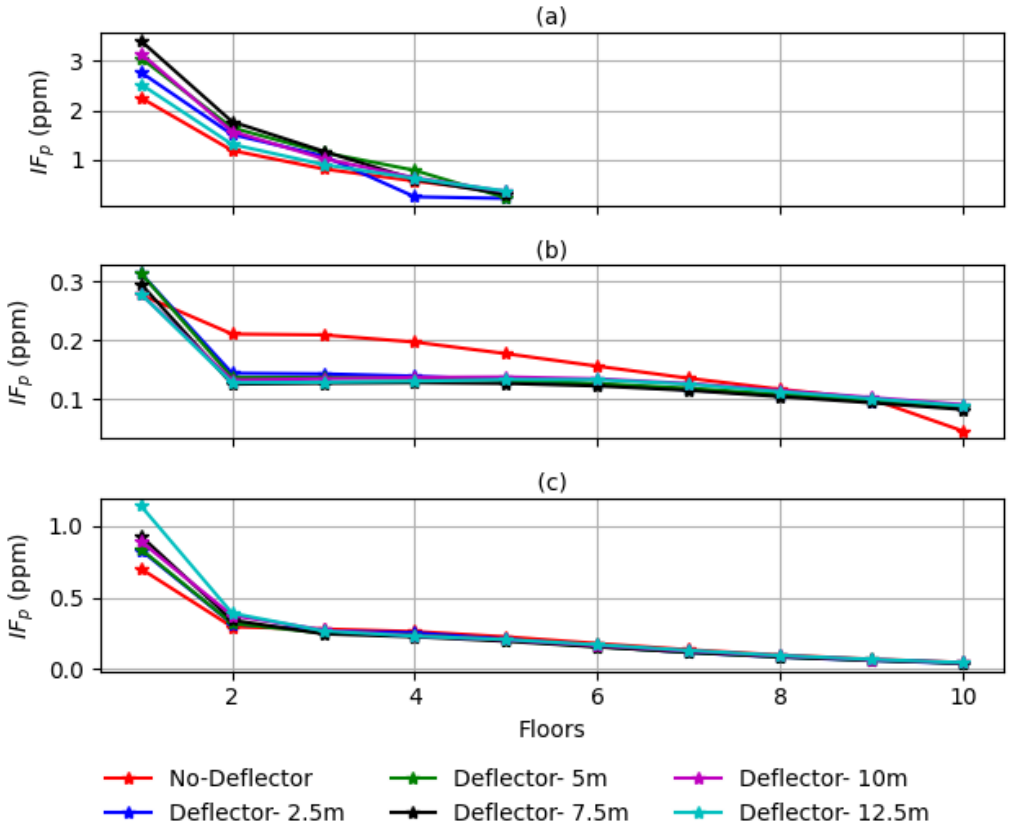

Figure 5.13: Step-up target street canyon- a) IF_p along leeward facade (floors 1-10) under CRP source model; b) IF_p along windward facade (floors 1-5) under CRP source model; c) IF_p along windward facade (floors 1-5) under SRP source model.

5.8.2.2 Side Road Pollution Source Model

The primary top recirculation and the inward-curling air streams that resulted in vertical recirculation 1 in the step-down canyons resulted in a similar influence in the step-up canyons. Figure 5.14 shows the top recirculation 0.5m away from the side facades (y =14.5m plane). In the step-down canyons, the size of the primary top recirculation determined the scale of vertical recirculation 1 . Recirculation 1 increased as the deflectors were moved towards the downwind building. However, in the step-up canyons, the size of the primary recirculation is almost similar in all the cases as it was the downwind building itself and not the wind deflector that determined it. Nevertheless, the wind deflectors played a crucial role in determining how stretched the recirculations were around the downwind building. For instance, the middle portion of the primary circulation in the no-deflector case reached the vicinity of the downwind building whereas when the deflector was placed 12.5m away from the leeward wall, the upper portion of the primary circulation reached the same. This largely influences the height of recirculation 1 which resists the washout along the side road. Table 5.7 concurs with this explanation as the CO exposure reduction in the upper regions (floors 7-10) of the downwind side facade reduced monotonically from 14.2% to 2.5% as the deflector was moved from 2.5 to 12.5m away from the leeward wall. A similar monotonic increase in the lower region (floors 7-10) of the downwind side facade is also observable from Table 5.7. Recirculation 1 was marked in Figure 5.14. Similarly for the pedestrian at $z < 2m$, the $\overline{C}_{avg}$ increased from 1.63e-7 for the no-deflector reference case to 1.77e-7, 1.85e-7 and 1.89e-7 when the deflector was positioned at 2.5, 5 and 7.5m away from the leeward wall. Moving the wind deflector further downstream to 10m from the leeward wall resulted in an increased volume of squeezed air stream between the downwind wall and the deflector resulting in reduced $\overline{C}_{avg}$ to 1.78e-7 in the region. However, moving it 12.5m away from the leeward reduced this exit of air from the passage and hence $\overline{C}_{avg}$ marginally increased to 1.81e-7.

Floors/ Deflector position (m)	% IF_p reduction Floors 1-3	% IF_p reduction Floors 4-6	% IF_p reduction Floors 7-10
No Deflector	-	-	-
2.5	-11.1	7.0	14.2
5.0	-10.7	11.0	12.6
7.5	-18.9	13.7	11.2
10.0	-20.8	10.0	5.6
12.5	-40.9	9.0	2.5

Table 5.7: Percentage reduction of average CO exposure along the downwind-side facade in step-up street canyons.

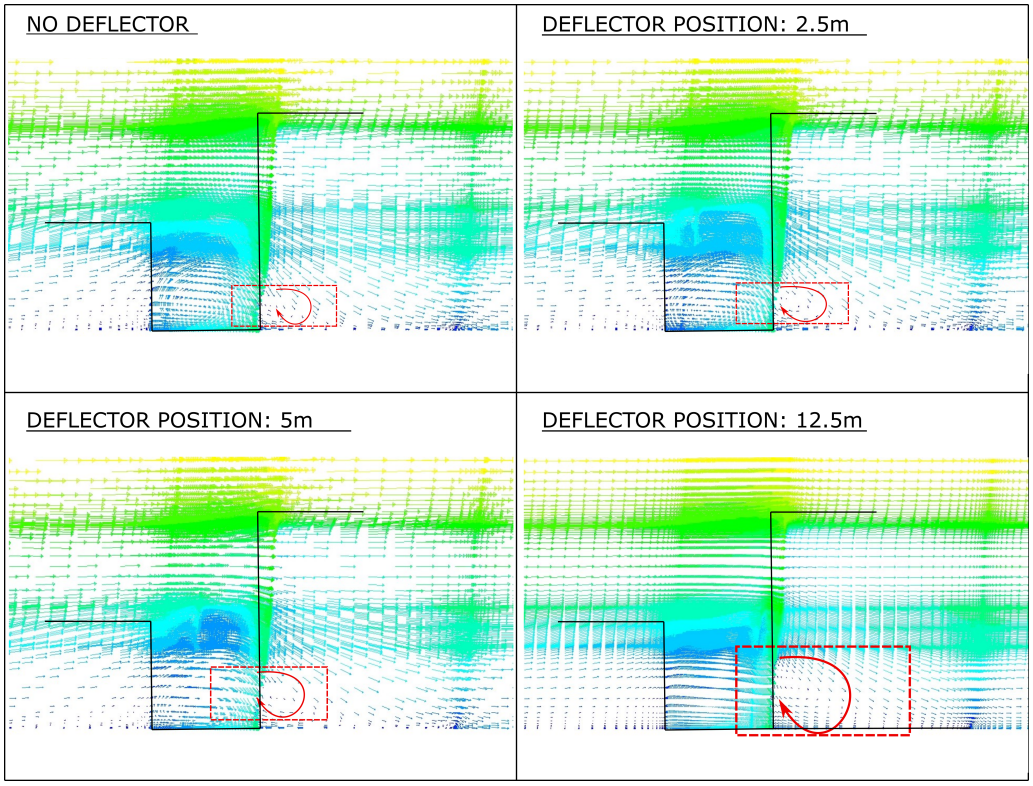

Figure 5.14: Vector plots of velocity magnitude at y = 14.5m plane for no deflector reference case and when deflectors were placed at 2.5, 5 and 12.5m away from the leeward wall in step-up street canyons.

5.8.2.3 θ v/s Sh for step-up canyons

The surfaces and control volumes of evaluation for ventilation indices for the step-up street canyons have also been marked in Figure 5.3. Unlike in the step-down canyons, the θ v/s $\overline{C}_{canyon}$ suffers deviation from an ideal inverse correlation in four cases, three cases in the CRP and one case in SRP source model specifically. In the CRP cases, both θ and $\overline{C}_{canyon}$ increase as the deflector is introduced at a distance of 2.5m from the leeward wall. However, it followed the expected trend until the deflector was moved up to 7.5m from the leeward wall and again suffered deviation when the deflector was positioned at 10 and 12.5m from the leeward wall. On the contrary, θ v/s $\overline{C}_{canyon}$ exhibited an ideal inverse correlation for all of the cases for SRP source model, except for the no-deflector case. With the four different street canyon environments including the two pollution source models for the two asymmetric street canyon geometries, the θ v/s $\overline{C}_{canyon}$ relationship has struggled to capture the appropriate correlation between the cases which included the passive intervention and which did not. However, the relationship has been robust in capturing the extent of ventilation in side and central street canyons except for the two cases of aberration in the step-up CRP source model cases.

On the other hand, Sh v/s $\overline{C}_{canyon}$ performed better as it exhibited the expected trend for the no-deflector cases for both the CRP and SRP source models. However, the correlation suffered deviations for the two cases including when the deflector was placed at 10 and 12.5m from the leeward wall for the CRP source model as did the θ v/s $\overline{C}_{canyon}$ relationship. This also occurred when the deflector was placed at 7.5m from the leeward wall for the SRP source model. Overall, the Sh v/s $\overline{C}_{canyon}$ unlike the θ v/s $\overline{C}_{canyon}$ relationship proved effective in distinguishing the scenarios where intervention was included and where it was not. However, the Sh v/s $\overline{C}_{canyon}$ relationship exhibited exception by deviating from the inverse correlation when the deflector was positioned at 7.5m from the leeward wall for the SRP source model. The relationship proved to be equally robust in representing the ventilation condition of the street canyons.

At this point, it is worth noting that a similar shortcomming in the θ v/s $\overline{C}_{canyon}$ correlation was pointed in Chapter 4. Although the inverse correlation was correctly predicted in most of the cases, the proportionality of increase and decrease of θ for the change in $\overline{C}_{canyon}$ in the cases with and without the wind deflectors were not as convincing as what Sh v/s $\overline{C}_{canyon}$ exhibited in this chapter. Finally, from Figures 5.9 and 5.15, it is essential to note that the synergy between the velocity

and concentration gradient vector (FS_n) does not fully capture the flow physics in its entirety but only when coupled with the Reynolds Number of the flow (SC_t is a constant).

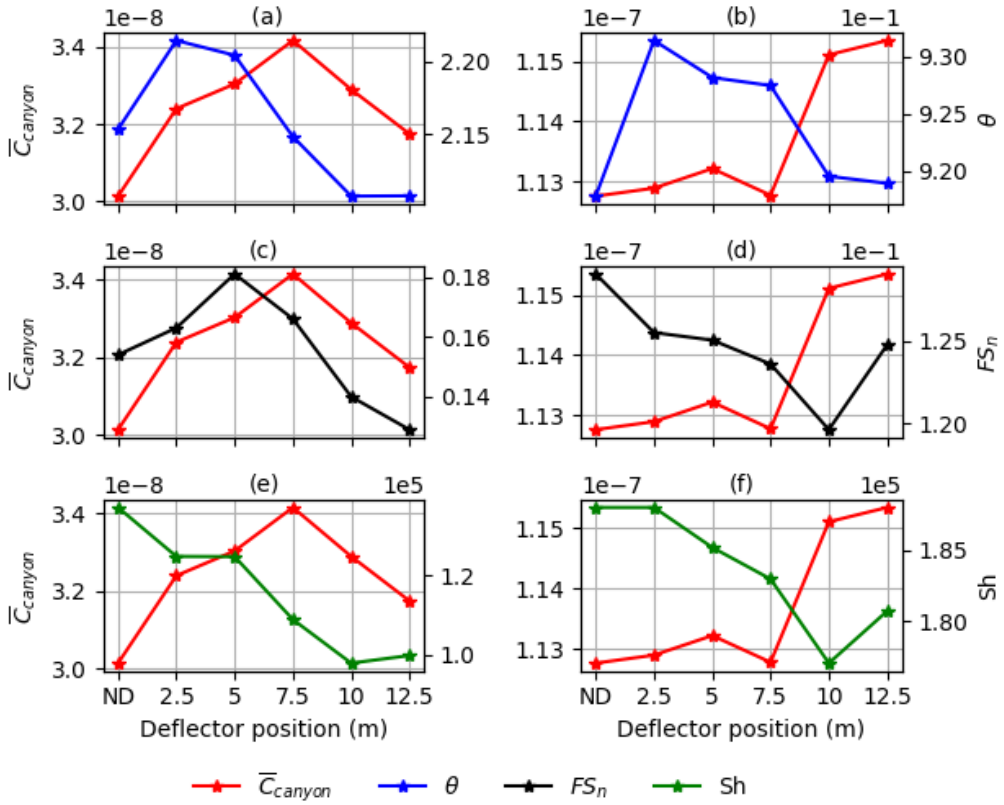

Figure 5.15: Step-up target street canyons- Comparison of $\overline{C}_{canyon}$ against θ under - a)CRP conditions in central street canyon, b) SRP conditions in side street canyon; Comparison of $\overline{C}_{canyon}$ against FS_n under - c)CRP conditions in central street canyon, d) SRP conditions in side street canyon; Comparison of $\overline{C}_{canyon}$ against Sh under - e)CRP conditions in central street canyon, f) SRP conditions in side street canyon.

5.9 Conclusions

Although the comparison of ($\bar{C}_{canyon}$) against Sh and θ reinforces street canyon ventilation theories in general, they have not been applied together in the same study. On the other hand, the literature suggests further investigation into the application of roof-level interventions for non-homogeneous urban environments. Studies in the past have mostly evaluated asymmetric canyons with a single wind catcher set up to realize the challenge of ventilating step-up canyons. The present

study combines the theoretical aspect of assessing the pollution removal mechanisms with the practical application of adjustable wind deflectors to ventilate all asymmetric canyon environments by locating an optimal position for the operation of the same for different traffic flow conditions.
In regards to the pollution removal mechanisms, both θ v/s $\overline{C}_{canyon}$ and Sh v/s $\overline{C}_{canyon}$ correlations performed equally well in predicting the change in overall ventilation of the street canyons for the different configurations once the deflector was introduced in the street canyon system. However, the Sh v/s $\overline{C}_{canyon}$ showed superior performance in distinguishing the system when the wind deflector was introduced and when it was not. As mentioned earlier, turbulence is a complex and multi-characteristic phenomenon, making it difficult to speculate on the underlying physics. However, with the limited data available from the current and previous chapters a reasonable conclusion could be as follows.

1. The inclusion of wind deflectors in the street canyons steered changes in $\overline{C}_{canyon}$ by affecting the proportion of pollution removed from the canyon via diffusive and convective fluxes. This does not mean that the mean and turbulence fluctuations induced fluxes do not change with the inclusion of a wind deflector but the relatively lower proportionate changes in θ v/s $\overline{C}_{canyon}$ as compared to Sh v/s $\overline{C}_{canyon}$ suggest that they are less likely to steer the $\overline{C}_{canyon}$ as much as diffusive or convective fluxes.
2. Changing the location of deflectors steered $\overline{C}_{canyon}$ by also impacting the proportion of pollution removed from the same via mean flow and turbulent fluctuations induced fluxes.

A recommendation utilizing more detailed turbulence models including DES and LES for more nuanced insights into the pollution removal mechanisms in urban environments using passive interventions in future studies is suggested.
Regarding the practical aspect of improving air quality, the wind deflector resulted in the best outcomes for the step-down target street canyon when positioned 2.5m away from the leeward facade by reducing 73.5% and 34.7% of CO IF_p along the leeward and windward facades respectively under CRP and 16.5% along the downwind side facade under SRP source models. For the step-up configurations, the performance predominantly deteriorated with the inclusion of wind deflectors. For the CRP source model, wind deflectors when placed at a distance of 2.5m from the leeward wall (optimal case) increased CO IF_p by 12.7% and decreased by 13.8%

along leeward and windward walls respectively. For the SRP model, the vertical recirculation in the side road stretched as the deflector was moved closer to the windward wall and hence the no-deflector case offered the least CO IF_p across the downwind side facade. Two key takeaways resulted from the CO IF_p analysis of the asymmetric street canyons with adjustable wind deflectors:

1. The effectiveness of the wind deflectors is realized for the step-down target street canyons despite the initial offset of reduced ACH offered by the steep-city environment, hence proving its versatility for usage in step-down canyons.
2. Despite evaluating different locations for optimal performance of the wind deflectors, only a detrimental-to-negligible benefit was realized from the studied configurations for step-up target street canyon environments.

By demonstrating the opportunity and challenges to reduce substantial IF_p in asymmetric canyon configurations and evaluating the operating mechanisms of pollution removal from the same, this study builds on previous investigations on the control of air pollution in idealized city-type street canyon environments and provides further evidence of the potential of wind deflectors at roof level to significantly reduce the CO IF_p in more complex environments as well. However real-world validation of the concept has yet to be conducted and this requires further research, which together with the present results can form the basis of design guidelines for the practical implementation of adjustable deflectors in cities.

Chapter 6

Multi-environmental parameter response of wind deflectors

6.1 Introduction

Previous research involving the performance analyses of passive interventions could be largely classified into the following two approaches.

1. Studies where a particular passive intervention has been evaluated for fixed ambient wind conditions but for different built environments and traffic flow configurations including different Aspect Ratios (ARs), modified roof shapes, building typologies and tidal traffic flow to mention a few. This group of works includes both studies analyzing the performance of a fixed configuration of a passive intervention for a singularly varied feature of the built environment, and studies analyzing multiple configurations of a passive intervention for a singular configuration of the built environment
2. Studies where different configurations of a built environment or a passive intervention in a fixed built environment configuration were evaluated for varying ambient wind conditions including wind speeds and directions.

Although these investigations offer valuable design guidelines for policymakers to include passive interventions in a street canyon based on dominant or critical environmental conditions, the concern that needs further exploration is the simultaneous changing operating conditions in a street canyon environment, including the changes

in the built environment, wind and traffic flow conditions. As it would be a reasonable assumption to say that built infrastructures undergo a permanent transformation as opposed to wind and traffic flow conditions subject to diurnal variations, the latter present themselves as transient environmental features that would necessitate an adaptive pollution mitigation strategy. Studies usually consider constant wind speed as most passive interventions only offer negligible to modest impact on non-dimensionalized concentration (K) for variation in the same. The performance of wind deflectors exhibited a similar trend for changing ambient wind speeds in a 2D environment (as can be seen in Chapter 4). As mentioned apriori in Chapter 2, the ambient wind directions have substantially influenced the pedestrian and overall UCL ventilation of city-type environments with different forms, and performances of passive interventions including parked cars, vegetation and balconies to mention a few. However, wind catchers have not been evaluated for oblique winds. On the other hand, Chapters 4 and 5 also demonstrated the benefit of adjustable wind deflectors for changing traffic flow directions in ideal and asymmetric city-type environments. Therefore, this chapter aims to add another layer of complexity to the problem through performance analyses of adjustable wind deflectors for combined diurnal variations of wind and traffic flow directions in city-type environments.

6.2 Problem Description

Traffic and wind flow directions were considered to fluctuate through their diurnal changes in tandem to evaluate the response of the adjustable wind deflectors. Four different conditions were considered for the traffic and wind flow conditions. Four conditions for the traffic flow included 0, 8, 16 and 24 hours of CRP in a day and SRP for the rest of the day. Similarly, the four conditions for wind flow included 0, 8, 16 and 24 hours of oblique winds at 45° and the rest of the day with orthogonal winds. With four conditions for the two environmental variables, one would arrive at 16 cases as shown in Figure 6.1. Therefore, the extent of pollution removal achieved by the adjustable wind deflectors from different target regions of the city-type environment in this study will be evaluated based on these 16 cases.

Wind direction
Orthogonal (90°) and Oblique ambient winds (45°)

Traffic flow direction
Cross Road Pollution (CRP) and Side Road Pollution (SRP)

	24 hrs - 90° 0 hrs - 45°	16 hrs - 90° 8 hrs - 45°	8 hrs - 90° 16 hrs - 45°	0 hrs - 90° 24 hrs - 45°
0 hrs - CRP 24 hrs - SRP	Orthogonal SRP case - 24 hrs	Orthogonal SRP case - 16 hrs + Oblique SRP case - 8 hrs	Orthogonal SRP case - 8 hrs + Oblique SRP case - 16 hrs	Oblique SRP case - 24 hrs
8 hrs - CRP 16 hrs - SRP	Orthogonal CRP case - 8 hrs + Orthogonal SRP case - 16 hrs	Oblique CRP case - 8 hrs + Orthogonal SRP case - 16 hrs	Orthogonal CRP case - 8 hrs + Oblique SRP case - 16 hrs	Oblique CRP case - 8 hrs + Oblique SRP case - 16 hrs
16 hrs - CRP 8 hrs - SRP	Orthogonal CRP case - 16 hrs + Orthogonal SRP case - 8 hrs	Orthogonal CRP case - 16 hrs + Oblique SRP case - 8 hrs	Oblique CRP case - 16 hrs + Orthogonal SRP case - 8 hrs	Oblique CRP case - 16 hrs + Oblique SRP case - 8 hrs
24 hrs - CRP 0 hrs - SRP	Orthogonal CRP case - 24 hrs	Orthogonal CRP case - 16 hrs + Oblique CRP case - 8 hrs	Orthogonal CRP case - 8 hrs + Oblique CRP case - 16 hrs	Oblique CRP case - 24 hrs

Figure 6.1: A Matrix illustrating the 16 possible combinations of scenarios from two variations in traffic flow (CRP and SRP) and wind flow directions (orthogonal and oblique).

6.3 Computational Domain and Boundary conditions

6.3.1 Orthogonal winds

As prescribed for the ideal and asymmetric city-type environments under orthogonal ambient winds in Chapters 4 and 5, a $6.7H$ distance was provided between the inlet and the upwind side of the first row of buildings, $40.3H$ between the downwind side of the last row of buildings and the outflow boundary, and the computational domain's height was $10H$. The computational domain included 6 street canyons with 7 buildings. A steep ($H/w_1 = 2$) asymmetric ($w_1 = 0.5w_2$) city-type environment was considered. The schematic of the computational domain considered for this study is shown in Figure 6.2. For the neutrally stable ABL, orthogonal to the cross roads, the inlet boundary conditions including the u ($U_{ref} = 3m/s$, $\alpha = 0.16$ and $u_* = 0.24m/s$), k and ϵ were the same as in Equations 3.14- 3.16 in Chapter 3. The other boundary conditions including the symmetry sides and top surface, exit outflow surface, and streets and buildings as walls were also maintained as in Chapters 4 and 5. With a constant addition of 10^{-7} kg/m^3s of CO gas from designated regions for CRP and SRP source models (as shown in Figure 6.2), CO gas was used as the pollutant in this study.

6.3.1.1 Oblique winds

The computational domain and boundary conditions prescribed for the oblique wind cases are represented in Figure 6.3. The computational domain included 7 rows and 4 columns of buildings. Although all the features of the city-type environment included for the oblique wind flow conditions were the same as that for the orthogonal wind conditions, the boundary conditions of the sides of the domain were modified. The side faces on the upwind and downside directions of the city-type environment are prescribed as velocity inlet and outflow conditions respectively. A $6.7H$ distance was provided between the inlet sides (including both the inlet surfaces) and the upwind side of the first row and column of buildings. Similarly, $40.3H$ and $41H$ distances were provided between the downwind side of the last row and column of the buildings and the outflow boundaries. The height of the computational domain was $10H$. The velocity components on the two velocity inlets were prescribed as follows in Equations 6.1 and 6.2 respectively.

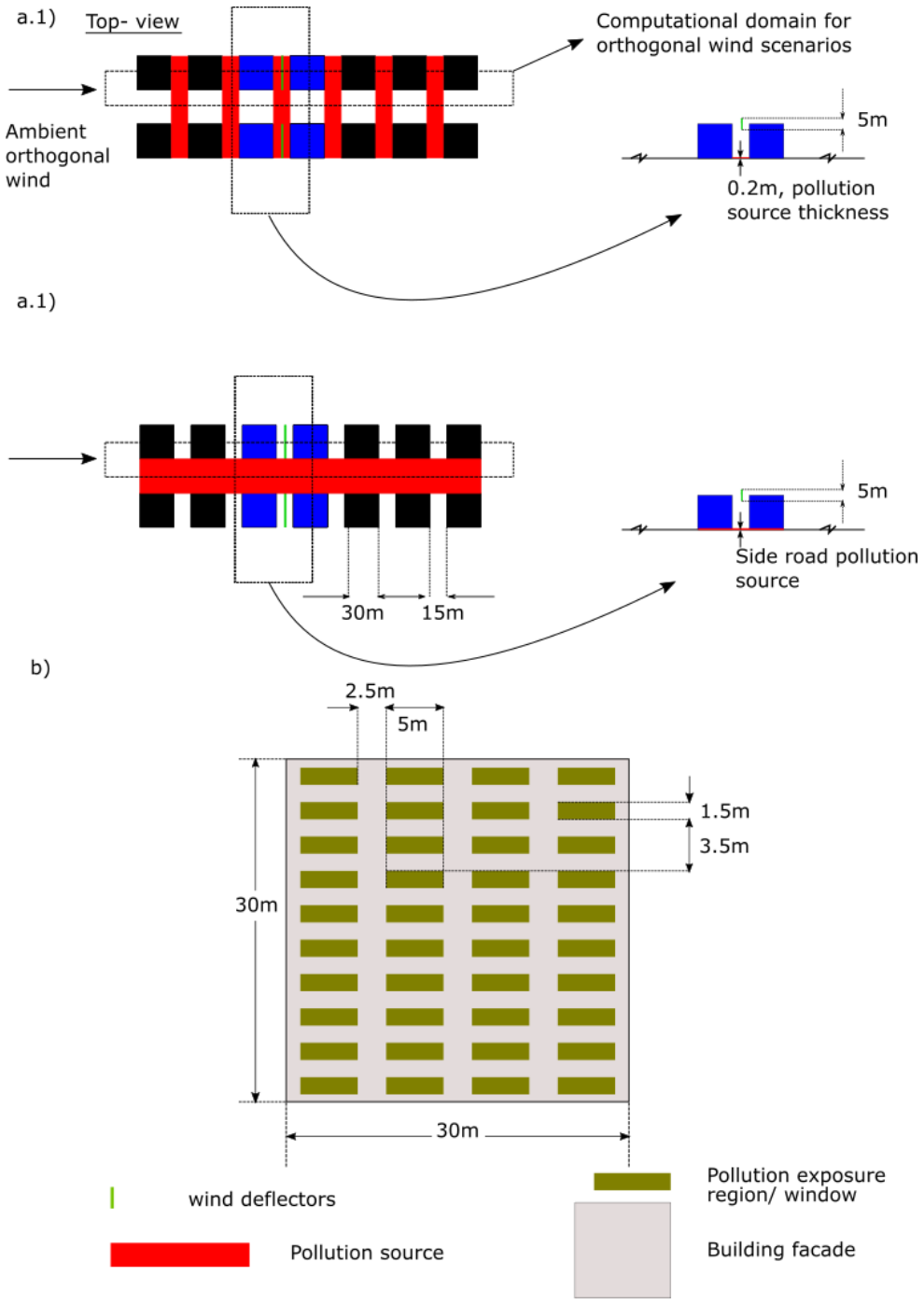

Figure 6.2: Schematic representation including top and side views of the computational domain considered for steep-asymmetric canyons with a.1) CRP source model; a.2) SRP source model; b) regions where exposure of pollutants are evaluated for each building facade (windows).

$$u_x(z) = U_{ref}(\frac{z}{\delta})^{\alpha} cos\alpha \tag{6.1}$$

$$u_y(z) = U_{ref}(\frac{z}{\delta})^{\alpha} sin\alpha \tag{6.2}$$

Here, α is the angle of incidence of the incoming ambient wind.
It is worth noting that direct comparisons of the orthogonal wind conditions and oblique wind conditions are included in the study. A more realistic solution of orthogonal wind conditions from the computational domain considered for oblique wind flow cases may be modestly deviant from the results presented here. The configuration considered for oblique wind conditions included 4 columns of buildings and buildings along rows 2 and 3 (where the comparisons are made) could be influenced by the side flows under orthogonal wind conditions which would not be the case when modeled as per the configuration illustrated for the orthogonal wind scenarios with symmetry conditions on the side faces. However, this approximation was performed because it is part of the methodology to develop a solution for a basic scenario (changing traffic under orthogonal wind conditions) and use it as a starting point to derive solutions for more complex problems (simultaneously changing traffic and wind flow directions as in this case). This is explained further in the case description subsection to follow. This concern eliminated the possibility of conducting orthogonal wind condition simulations using the computational domain considered for oblique wind flow scenarios. The other possible methodology of correcting the approximation was by including more columns in the city-type environment so that the effect of the side flows is minimized on the middle rows of the buildings. However, this would drastically increase the computational requirements and thus the current methodology of analyses was deemed a satisfactory approximation for a quantitative study that aims to develop and illustrate an approach to solve a multi-parameter environmental problem.

Figure 6.4 shows the schematic of the CRP and SRP models for the oblique wind flow scenarios with standard and tilted configurations of the wind deflector. The regions where the personal exposure to CO gas is evaluated along the building facades remains the same as in orthogonal wind conditions (previously shown in Figure 6.2b).

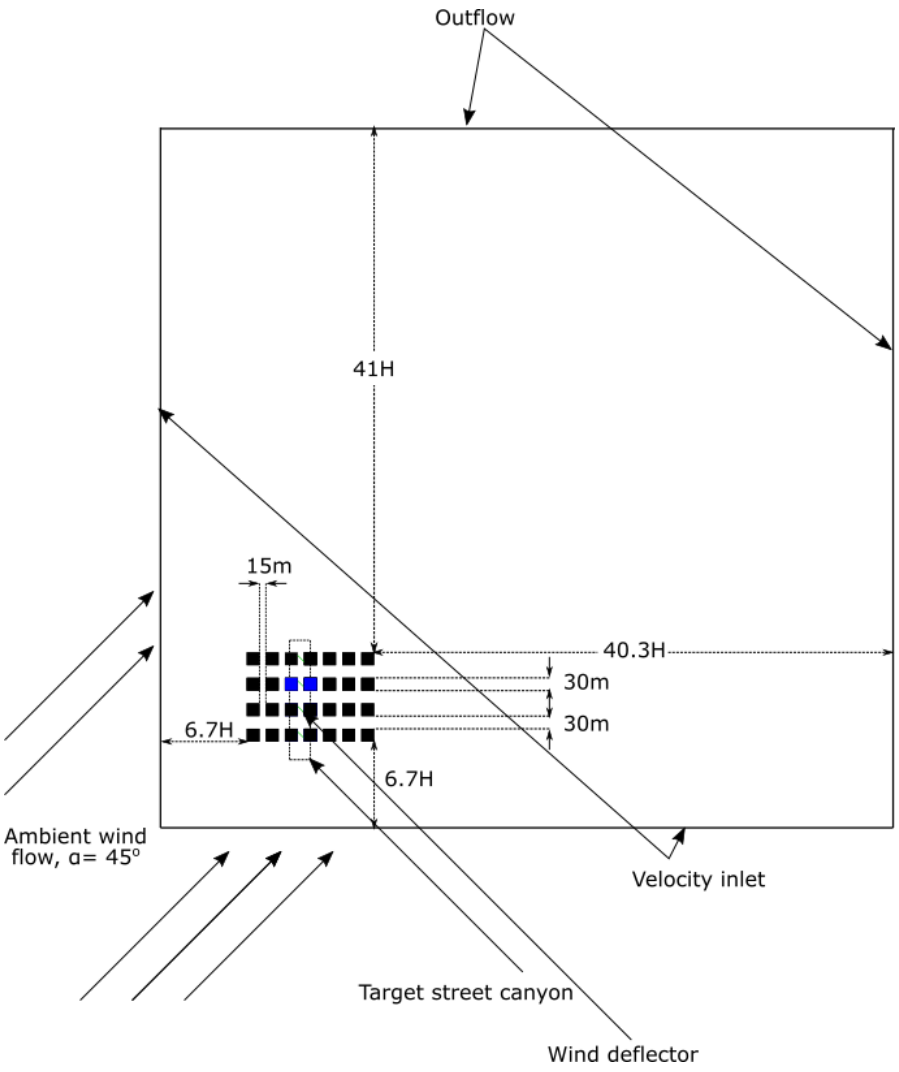

Figure 6.3: Top view of the computational domain of the city-type environment considered for the oblique wind conditions.

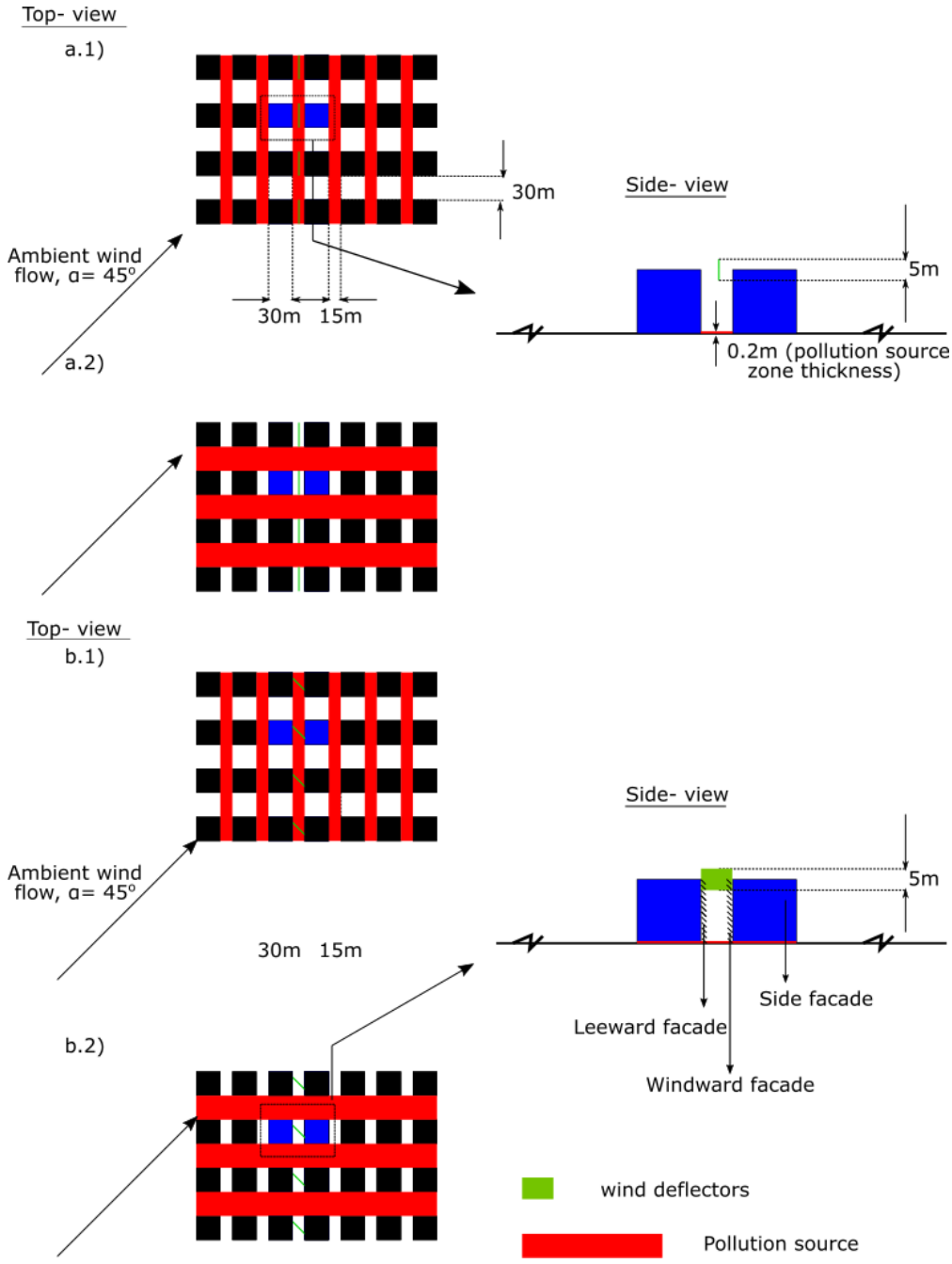

Figure 6.4: a) Schematic representation with top and side views of standard deflector orientation under oblique wind conditions for CRP and SRP source models (top); b) Schematic representation with top and side views of standard deflector orientation under oblique wind conditions for CRP and SRP source models (bottom).

6.4 Case Descriptions

Performance analyses of wind flow deflectors under orthogonal wind and oblique wind conditions form the two parts of this study. As in the previous chapter, the wind deflectors were 5m tall, "thin" and spanned across the entire width of the building roofs. The wind deflectors had half its face area above the roof of the upwind building and the rest below. The CRP and SRP source models were independently considered for both orthogonal and oblique ambient winds to test the efficacy of the adjustable nature of the wind deflectors. Exposure reduction for the orthogonal wind condition was achieved by varying the position of the wind deflector at the roof level. The locations of the deflectors included 2.5, 5, 7.5, 10 and 12.5m from the leeward walls apart from the reference no-deflector case. For the oblique wind flow condition, wind flow was at 45°. The analyses in this part included three configurations, the reference no-deflector case, the "standard" configuration where the wind deflectors were parallel to the crossroads, and the "tilted" configuration where the wind deflectors were oriented at 45° to orthogonally obstruct and maximize the wind availability inside the street canyons. For the CRP and SRP source configurations with oblique winds, the wind deflectors were tilted at their respective optimal locations (evaluated from orthogonal wind scenarios cases). Table 6.1 comprises the summary of all the cases considered in the present work.

	No- deflector case	Deflector position	deflector orientations	CRP	SRP
Orthogonal winds					
Steep Canyons	✓	2.5, 5, 7.5, 10 & 12.5 m	standard	✓	✓
Oblique winds					
Steep Canyons	✓	x_1 m	Standard & Tilted	✓	
Steep Canyons	✓	x_2 m	Standard & Tilted		✓

Table 6.1: Summary of case studies

Finally, a combined sensitivity analysis is performed for changing wind and traffic flow directions as shown in Figure 6.5.

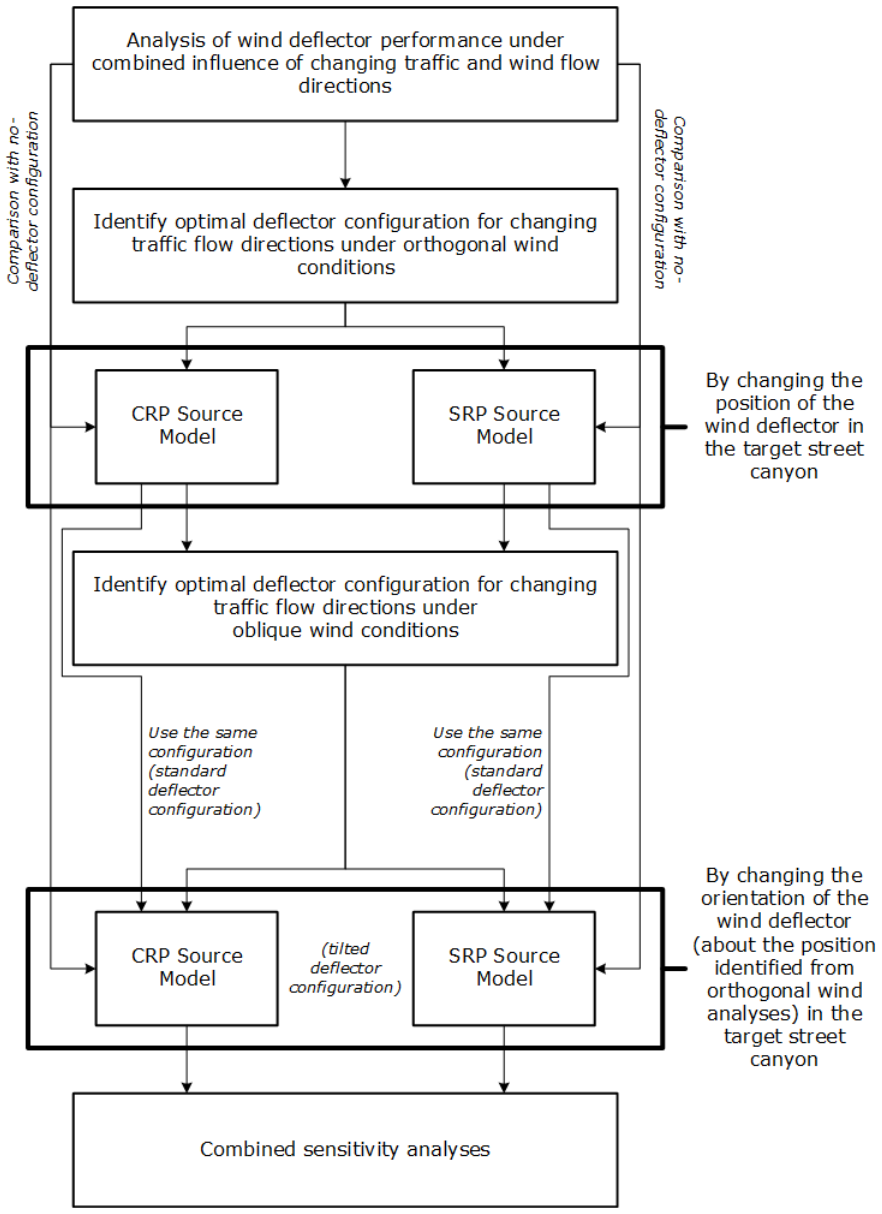

Figure 6.5: Flow chart representing the two-step strategy adopted in the current work to optimize the wind deflector performance for simultaneous changes in traffic and wind flow directions.

6.5 Mesh Convergence

The mesh convergence study described in Section 3.3.2.1 in Chapter 3 was again applied to the case studies in this chapter.

6.6 Key assessing parameter & target regions of study

CO IF_p (as defined in Chapter 4) is considered as the primary parameter of investigation in this chapter.

6.7 Results

6.7.1 Orthogonal Winds

6.7.1.1 Orthogonal Winds and CRP

For the no-deflector case, the recirculations resulted in distinct flow patterns in the upper, middle and lower regions. With strong interaction with the ambient winds at the roof level, a strong top recirculation forced a wash-down along the upper part of the windward wall. The side recirculations largely affected the flow in the middle region of the canyon where the wash-down along windward and leeward walls were oriented from the sides to the center of the canyon and vice-versa respectively. Despite the alignment of the top recirculation with the side recirculation, the exit of the former through the sides at the ground level indicated that the effect of the downward push from the top recirculation was more pronounced throughout the canyon. In the lower region, due to the reduced influence of the side recirculation on the top recirculation, the downward push from the latter managed to achieve a distorted and vertically oriented sideward recirculation to rise along the canyon in a cork-screw type trajectory. This observation of the stronger influence of the top recirculation in the upper and lower regions and that of the side recirculation in the middle region concurred with the nature of cork-screw type helical rise-up in Figure 6.6. When the deflector was placed 2.5m away from the leeward wall, the above-roof air entered the passage between the wind deflector and the leeward wall to facilitate a wash-down along the same. The airflow from the sides substantially influenced the flow in the middle and lower regions of the canyon to align it laterally. While a part of the wash-down exited the canyon through the sides at the ground level, the alignment primarily created a wake region in the central portion of the lower and middle regions of the leeward facade. This increased the CO IF_p in the lower and middle regions of the leeward facade by about 90% and 84% respectively. However, the rise-up followed the top recirculation in the middle and upper regions along the

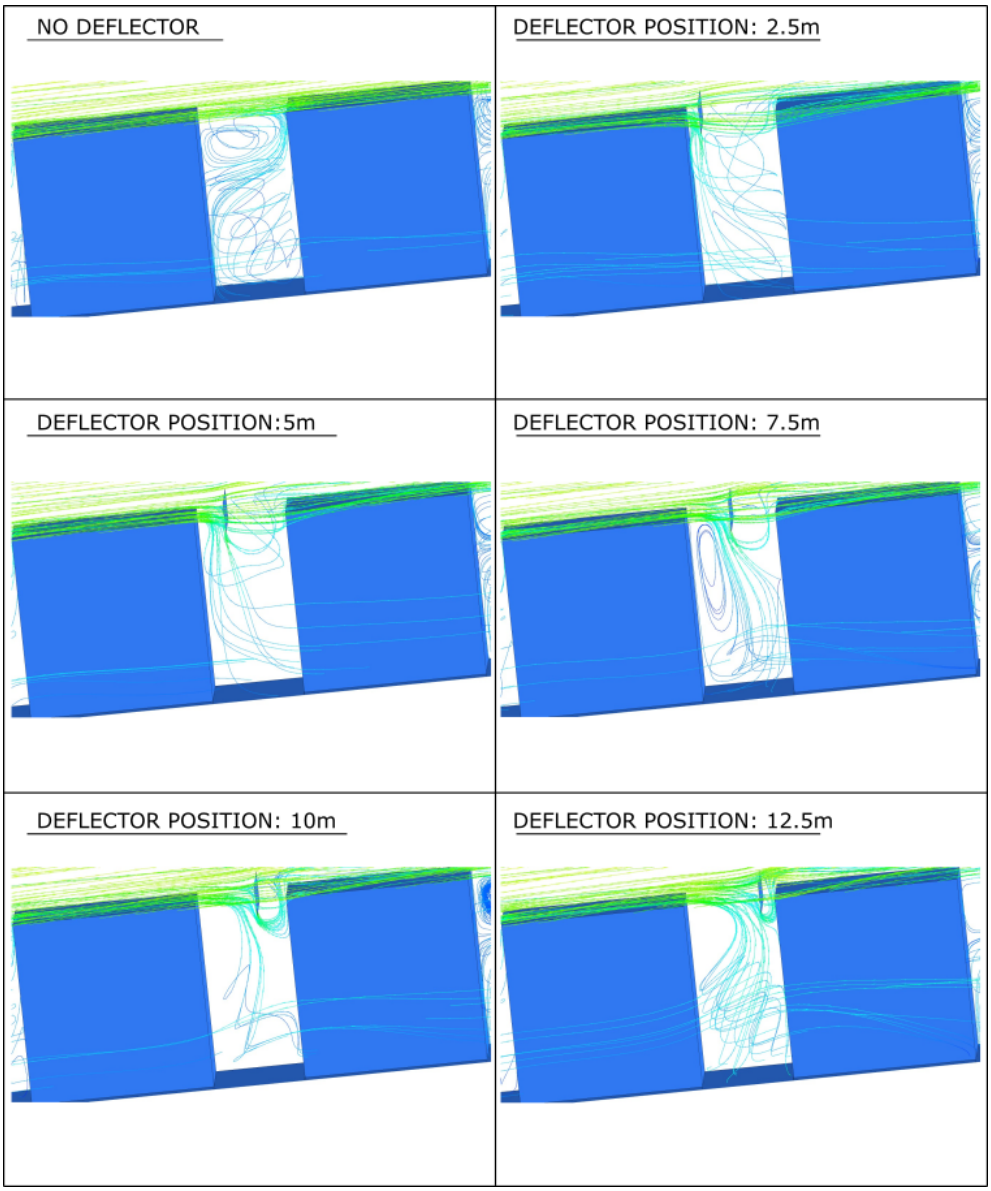

Figure 6.6: Streamlines of the airflow in the target steep street canyon for the reference no-deflector case and when deflectors were placed 2.5, 5, 7.5, 10 and 12.5m from the leeward wall under orthogonal wind conditions.

windward wall increasing 38% and 82% (also shown in Table 6.3) of CO IF_p in the middle and upper regions of the windward wall.

When the deflector was 5m away from the leeward wall, the flow pattern in the canyon was similar to the case when the deflector was 2.5m away from the leeward wall. However, the widened passage for wind catchment provided a stronger top recirculation and the overall flow roughly resembled a counter-clockwise top recirculation (reversed to traditional clockwise recirculation in an ideal 2D or pseudo-3D

street canyon) aligning lesser to the side recirculations. The stronger wash-down reduced the influence of the lateral recirculation and mitigated the rise-up including a recirculation unlike when the deflector was placed 2.5m away from the leeward wall. Further, the reduced influence of the lateral recirculation and alignment with the same also reduced the wake zone in the lower and middle regions of the leeward facade. Therefore, the leeward wall benefited substantially with a 77% and 99% CO IF_p reduction in its middle and upper regions compared to the no-deflector case. Due to the more pronounced influence of the top recirculation, the rise-up of the top recirculation along the windward wall after amassing CO at the street level increased the CO IF_p along the facade by 51%.

When the deflector was moved further away to 7.5 10m from the leeward wall, the wind catchment passage between the leeward wall and the deflector increased enough to change from facilitating a wash-down along the leeward wall to a traditional recirculation. However, in both cases, the air flows from the sides were strong enough to align the recirculations to enter and exit along the windward and leeward walls from the sides to the center and vice-versa respectively. As the air streams amassed CO from the streets before they rose along the sides of the leeward walls, the sides of the leeward walls were more polluted than the central regions. However, the passage for air entry through the sides widened when the deflector was 10m away, the side recirculations enabled a substantial portion of the recirculations to be swept through the sides and not rise along the leeward walls and hence the lower IF_p of CO gas along the leeward walls than when the deflector was 7.5m away from the leeward wall. This reduced the CO IF_p along the leeward by 32% compared to when the deflector was 7.5m away from the leeward wall. However, the deflector configuration was still unfavorable as the leeward wall was exposed to 32% more CO IF_p than the reference no-deflector case. Finally, when the deflector was placed 12.5m away from the leeward, the flow pattern in the canyon resembled that of the no-deflector case but for one difference. In this case, the top deflector was restricted by the wind deflector so that the top recirculation could not initiate a cork-screw type helical rise-up in the lower region near the windward wall as in the no-deflector case. This mitigated higher IF_p of CO gas along the sides of the leeward wall in the middle and upper regions respectively. Although the lateral recirculations in the lower region caused a 60.9% higher CO IF_p exposure in the leeward facade, the middle and upper regions benefited from the mitigation of the helical cork-screw type rise-up of the flow and hence the overall CO IF_p reduced by about 15.8% compared to the no-deflector case. The top and side recirculations

facilitating a wash-down along the windward facade reduced CO IF_p along the facade by 83%, thus making it the most favorable configuration for mitigating higher personal exposure with CRP source under orthogonal wind conditions.

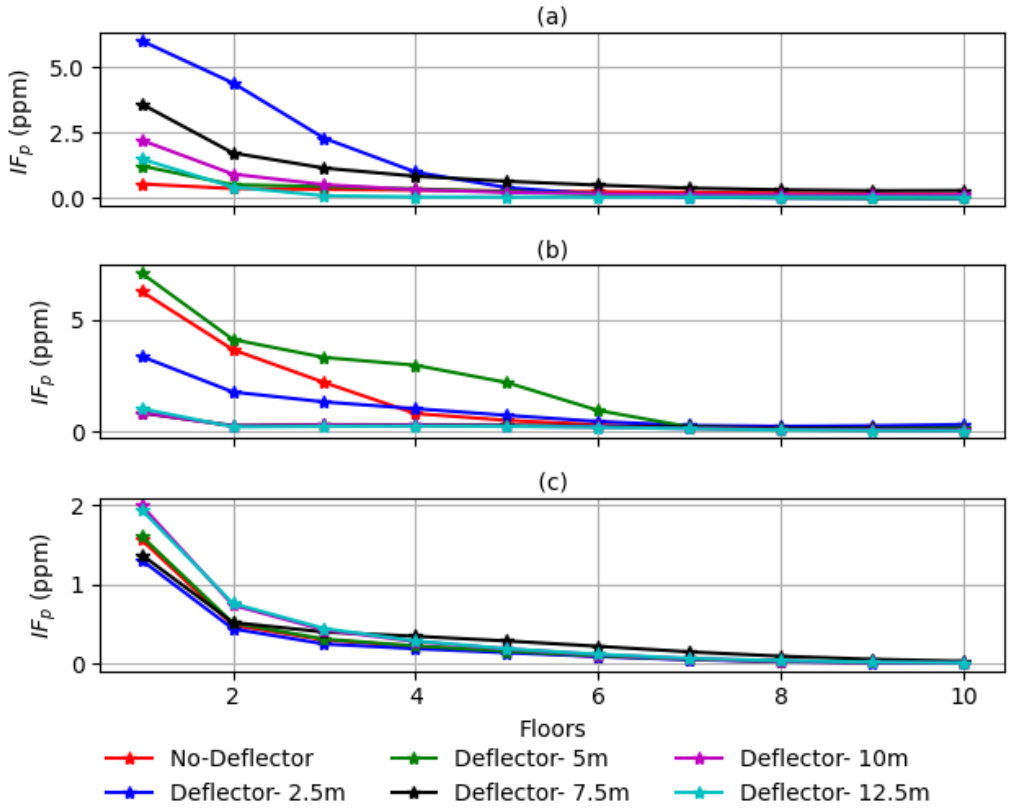

Figure 6.7: Steep target street canyon- a) IF_p along leeward facade (floors 1-10) under CRP source model; b) IF_p along windward facade (floors 1-10) under CRP source model; c) IF_p along downwind side facade (floors 1-10) under SRP source model and orthogonal winds.

Floors/ Deflector position (m)	% IF_p reduction Floors 1-3	% IF_p reduction Floors 4-6	% IF_p reduction Floors 7-10
No Deflector	-	-	-
2.5	-90.5	-84.6	99.2
5.0	-74.3	77.1	95.1
7.5	-41.2	-13.6	-12.4
10.0	-190	14.3	4.21
12.5	-60.9	81.9	65.9

Table 6.2: Percentage reduction of average CO exposure along the leeward facade in the steep street canyons under orthogonal wind conditions with CRP source model.

Floors/ Deflector position (m)	% IF_p reduction Floors 1-3	% IF_p reduction Floors 4-6	% IF_p reduction Floors 7-10
No Deflector	-	-	-
2.5	46.9	-38	-82.2
5.0	-19.8	-287	-398
7.5	88.7	50.1	-184
10.0	88.9	56	-54.8
12.5	88.2	59.8	21.7

Table 6.3: Percentage reduction of average CO exposure along the windward facade in the steep street canyons under orthogonal wind conditions with CRP source model.

6.7.1.2 Orthogonal Winds and SRP

The exposure of CO gas along the side facade is also substantially affected by the side and top recirculations. It is worth noting from Figure 6.7 that the exposure of CO gas along the side facades is lesser than its counterparts along leeward and windward walls since the side roads are wider than the cross roads. The best case scenario for ventilation along the side road would be a case where streamwise flow along it is as minimally influenced by its interaction with the flow between the buildings. Figure 6.8 shows the vector plot of the flow 0.5m (y= 14.5m) upstream of the side walls for all the cases. As can be seen in Figure 6.8, for the no-deflector case, the inward curling (also mentioned for the CRP cases for the alignment of the top recirculation) of the side recirculations resulted in vertical recirculation along the plane mentioned. However, the air stream exiting the sides forced down by the top recirculation limits the extent of this vertical recirculation to only along the side facades of the building. When the deflector was 2.5m away from the leeward wall, the wash-down of the top recirculation along the leeward wall resisted the inward curling as can be seen from Figure 6.8. The recirculation in the vertical plane was completely mitigated causing it to be the scenario offering the maximum CO exposure reduction along the side facade. A similar influence was expected when the defector was positioned 5m away from the leeward wall. However, a small recirculation was observed at the upwind edge of the side facade. A plausible explanation for this difference is that the inward curling side recirculation and the wash-down top recirculation balanced each other to completely mitigate any recirculation in the side road region when the deflector was positioned 2.5m from the leeward wall. On the contrary, when the deflector was 5m away from the

leeward wall, the further strengthened top recirculation due to the increased wind catchment at the roof level overcompensated the inward curling side recirculations to result in small vertical recirculations in the side road region. While 34.7% of the CO IF_p was reduced when the deflector was 2.5m away from the leeward wall, the reduction was compromised to a modest 14.6% when the deflector was 5m away. It is worth noting that the top recirculation resulted in flow against the streamwise flow when the deflector was 7.5, 10 and 12.5m away from the leeward wall. When the deflector was 7.5m away from the leeward wall, the side recirculation was not strong enough to prohibit a complete vertical-clock-wise recirculation. This can be seen in Figure 6.8 as two distinct recirculations in the vertical plane (one parallel to the canyon side opening and one in the vicinity of the side facade). Two vertical recirculations decelerated the wash-down along the side road and resulted in about a 67.9% increase in the side facade. However, when the deflector was 10 and 12.5m away from the leeward facade, side recirculations were strong enough to restrict a complete clockwise top recirculation, resulting in the side recirculations to exit the canyon along the streamwise flow and mitigating the vertical recirculation parallel to the canyon side entrance. This substantially reduced the CO IF_p along the side wall compared to when the deflector was 7.5m away from the leeward wall. The two scenarios also included a wash-down of the windward facade by the side recirculation entering the region between the deflector and the windward facade as shown in Figure 6.6, resulting in a vertical recirculation in front of the side facade. As the wash-down exited at a higher elevation when the deflector was 12.5m away, a larger vertical recirculation was formed as shown in Figure 6.8 resulting in a relatively CO IF_p (also seen in Table 6.4).

Floors/ Deflector position (m)	% IF_p reduction Floors 1-3	% IF_p reduction Floors 4-6	% IF_p reduction Floors 7-10
No Deflector	-	-	-
2.5	36.8	31.9	20.4
5.0	13.9	24	-7.25
7.5	-44.5	-73.7	-300.6
10.0	23.1	-22.3	-63.7
12.5	-17.4		-94.6

Table 6.4: Percentage reduction of average CO exposure along the side facade in the steep street canyons under orthogonal wind conditions with SRP source model.

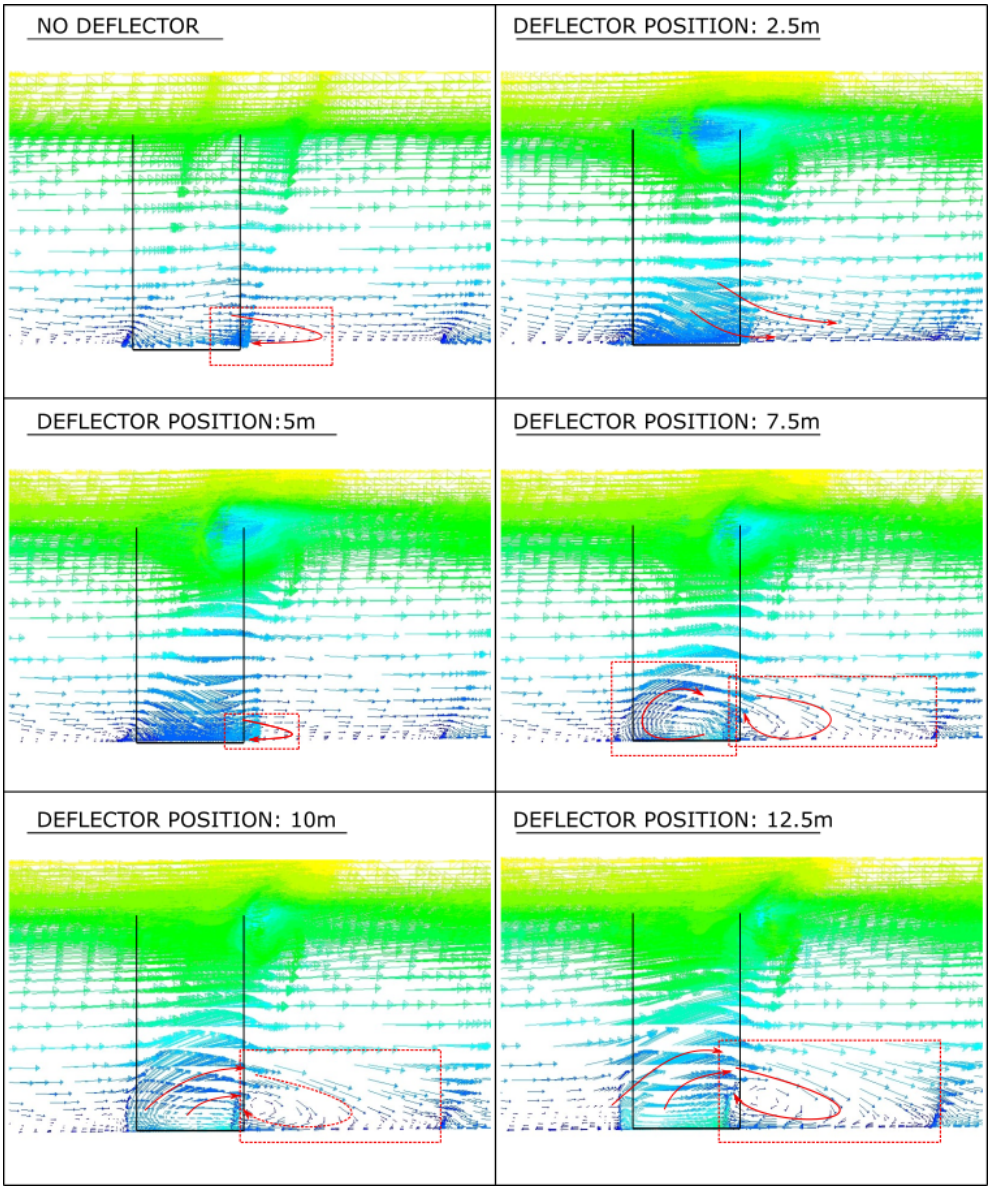

Figure 6.8: Vector plots of velocity magnitude at y = 14.5m plane for no deflector reference case and when deflectors were placed at 2.5, 5, 7.5, 10 and 12.5m away from the leeward wall in the target steep street canyons.

6.7.2 Oblique Winds

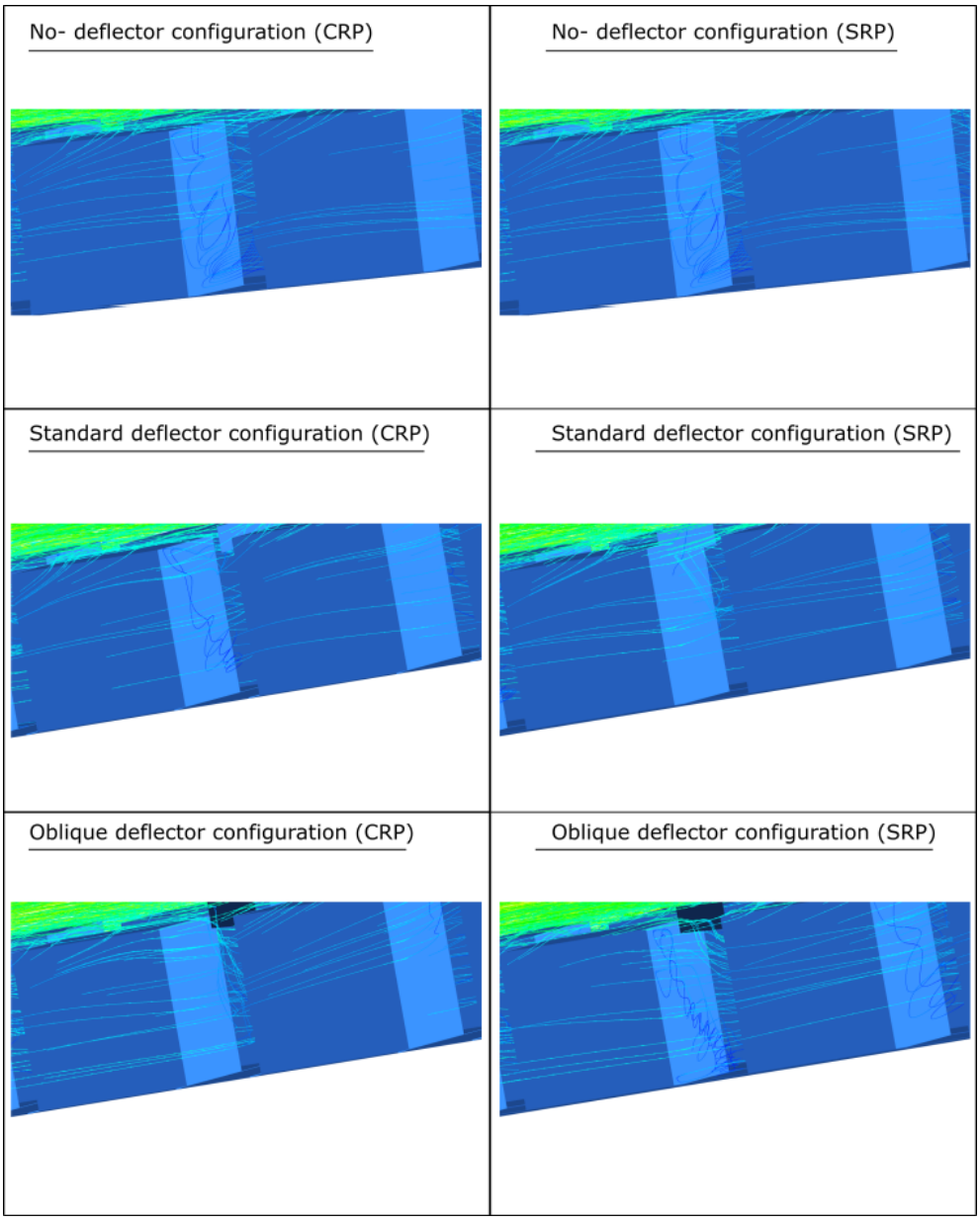

Figure 6.9: Steep target street canyon under oblique wind conditions with no-deflector, standard deflector and tilted deflector configurations for CRP and SRP source models.

As mentioned apriori, the analyses for scenarios including oblique winds are carried out by considering the results from orthogonal winds as the starting points. However, it is worth mentioning that the flow field for no-deflector configuration under CRP and SRP source models is the same while it is not for the standard deflector configurations. The standard deflector configuration under CRP and SRP

source models corroborates to including the deflector in the target street canyon 12.5 and 2.5m away from the leeward facade. Similarly, the tilted deflector configuration corroborates tilting the deflectors by 45° from their respective positions under standard deflector configurations for the two source models.

6.7.2.1 Oblique Winds and CRP

When the incoming ambient wind direction is oblique with 45° incidence to the city-type environment, wind flow through the side entrances of the street canyons offers primary ventilation as opposed to the orthogonal cases where both, the wind flow through the roof and side entrances were equally important. As can be seen from Figure 6.9, where the streamlines of the no-deflector, standard deflector (12.5m away from the leeward facade, based on orthogonal wind analyses results) and tilted deflector configurations are shown, the ambient wind mainly entered and exited through the sides apart from the rise-up near the upwind edge of the leeward wall exiting through the roof. Unlike the orthogonal wind scenarios where the top recirculations substantially contributed to the pollution washout, the 45° oblique wind case did not result in such top recirculations as the streamwise flow of the ambient winds aligned with the side entrances of the canyons. Therefore, the streamwise flow and the inward curling recirculations were the only two major features of the flow under 45° oblique winds. Upon encountering the city-type environment, the streamwise flow naturally rose upwards in the region and CO exposure along the windward, as shown in Figure 6.10. However, the inward curling recirculations were oriented downwards. There are two aspects worth noting here. First, the target street canyon with 45° oblique wind featured only one inward curling lateral recirculation, unlike the orthogonal wind cases, thus pushing flow behind the upwind building. Second, the side recirculations in the 45° oblique wind case were more contaminated than the orthogonal cases as they amassed CO from upwind cross roads. The no-deflector and standard deflector configurations largely resulted in similar flow patterns and subsequently similar CO IF_p along the leeward, windward and side facades respectively. In both scenarios, the inward curling recirculations and the streamwise flows counterbalanced each other near the leeward wall resulting in a strong recirculation zone and flow rising along the upwind edge of the leeward wall through the roof. As the recirculations amassed CO from the street level, the lower region of the leeward wall and the upwind side in the middle region of the same experienced higher CO IF_p as shown in Figure 6.10. As

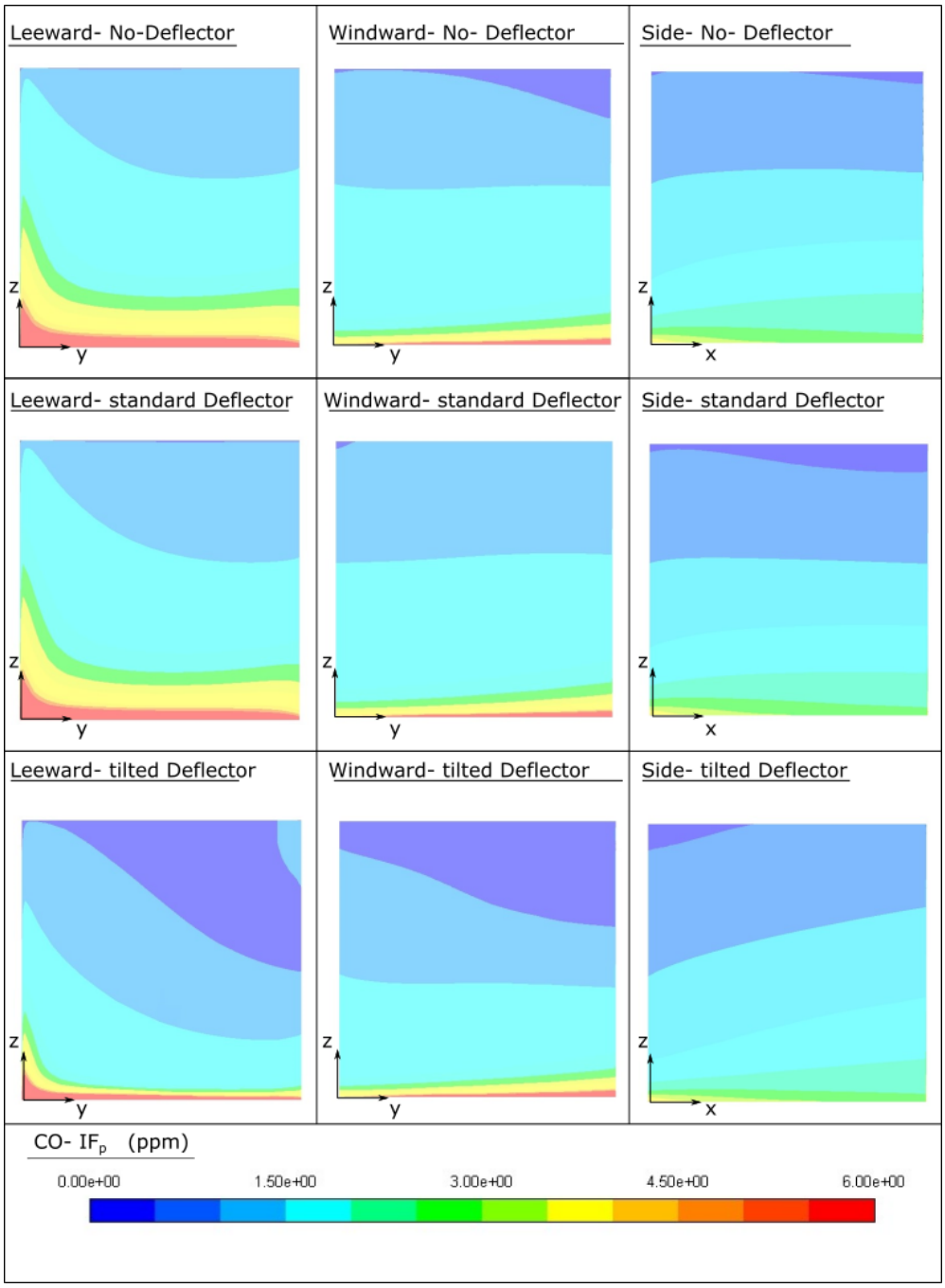

Figure 6.10: Steep target street canyon- IF_p along the leeward facade, windward and downwind side facade for no-deflector case (left), and scenarios including standard (center) and tilted deflector configurations (right) under oblique winds with CRP source model.

can be seen in Figure 6.11, the lower region accounted for about 56% and 57% of overall leeward CO IF_p for the no-deflector and standard deflector configurations respectively. The standard deflector configuration reduced 2.3% and 7.8% of CO

IF_p along the leeward and side facades while it increased 4.4% along the windward wall. The tilted deflector configuration orthogonally obstructed the ambient wind and pushed the air directly into the canyon to facilitate a more vertically oriented lateral recirculation in the target street canyon. This allowed for a vertical rise-up of the flow along the upwind edge of the leeward wall without much lateral recirculation at the street level. Although the lower region of the leeward wall still accounted for nearly 57% of the total leeward CO IF_p, this configuration offered about a 48% reduction in the region compared to the other two configurations. The tilted deflector configuration offered a substantial reduction of about 52% along the leeward wall and a nominal and minimal reduction of about 16% and 5% along the windward and side facades. The downward push facilitated by the tilted deflectors along the z-direction is also seen from the CO IF_p contours across leeward and windward facades shown in Figure 6.10.

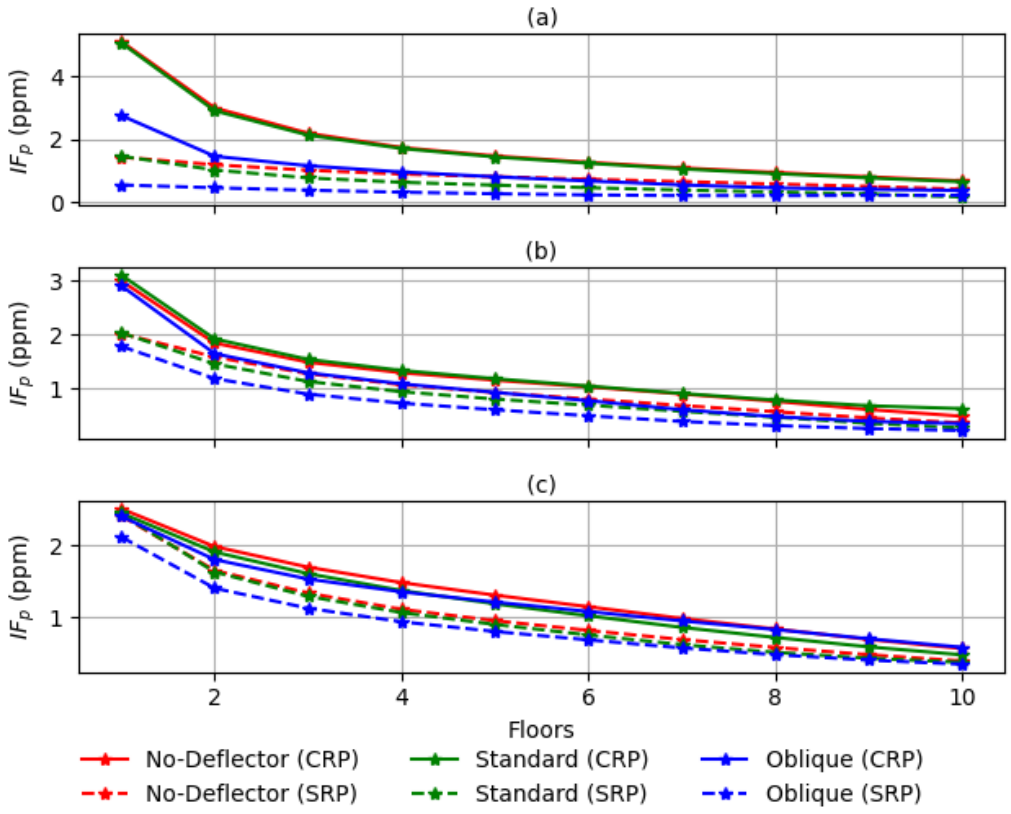

Figure 6.11: Steep target street canyon under oblique winds- a) IF_p along leeward facade (floors 1-10) under CRP and SRP source model; b) IF_p along windward facade (floors 1-10) under CRP and SRP source model; c) IF_p along downwind side facade (floors 1-10) under CRP and SRP source model.

6.7.2.2 Oblique Winds and SRP

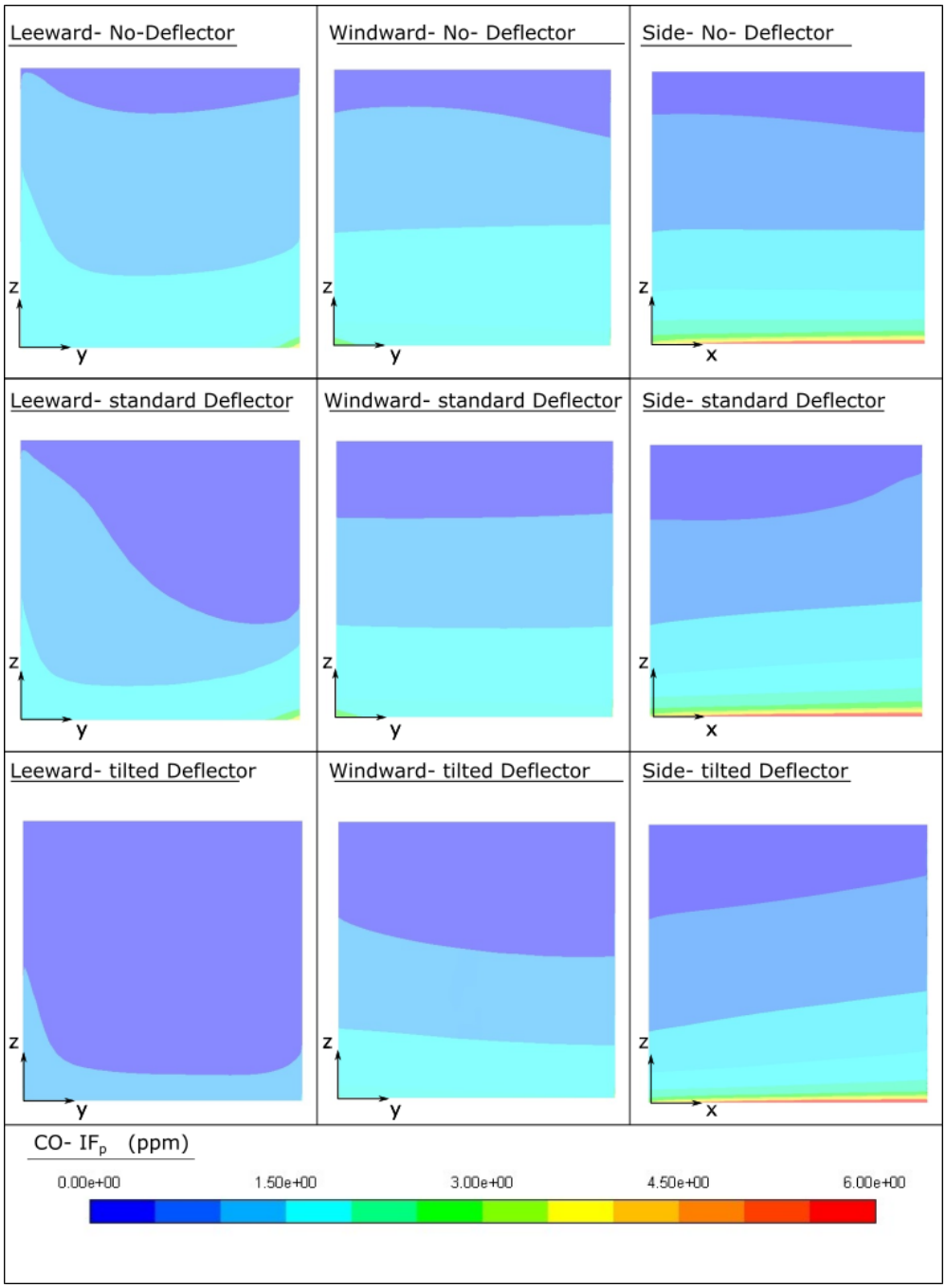

Figure 6.12: Steep target street canyon- IF_p along the leeward facade, windward and downwind side facade for no-deflector case (left), and scenarios including standard (center) and tilted deflector configurations (right) under oblique winds with SRP source model.

Figure 6.12 shows similar trends of CO IF_p along leeward, windward and the side facades for the no-deflector case with SRP as in Figure 6.10, representing the

CRP source model. Here again, the leeward facade suffered the maximum CO IF_p amongst the three facades considered due to the strong recirculation in its vicinity at street level. However, the extent of contamination in these facades differed from the CRP source model depending on the amount of CO amassed from the different source regions on the ground. Only two differences were particularly noted for the SRP model under oblique wind flow conditions. One, since the deflector was placed close enough to the leeward facade (2.5m away, based on results from the orthogonal wind analyses results), the deflector was able to divert a portion of the above-roof ambient winds into the canyon to induce vertically oriented recirculations that enable a flow rise-up without undergoing strong lateral recirculations as in the no-deflector case. This facilitated a 35.8% CO IF_p reduction across the leeward facade compared to a negligible 2.3% when the deflector was included with the standard configuration with CRP source and oblique winds. The tilted configuration by orthogonally obstructing the flow diverted more fresh above-roof air into the canyon and facilitated stronger ventilation for the leeward facade particularly by reducing up to 62.2% CO IF_p. Interestingly, the relative extent of reduction of CO IF_p across the leeward facade by the tilted configuration under oblique wind conditions was higher for the SRP source model compared to the CRP source model. This indicated that although orthogonally obstructing the above-roof ambient winds was an effective strategy in mitigating high exposure across the facade under maximum risk, further optimization could be evaluated to obstruct the ambient flow in more upstream locations than assessed here.

In regards to the CO IF_p along the facade under orthogonal winds, the inward curling recirculations primarily disrupted the wash-out of pollutants in the streamwise direction along the side road, and deflector configurations that mitigated the same through wash-down along the leeward facade substantially cleansed the side facade. However, under oblique wind flows, the changes to the inward curling air flows were localized within the street canyons and did not affect the entry into them. Therefore, as shown in Figure 6.12, the tilted deflector configuration negligibly impacted the side facade. This phenomenon was common for both the CRP and SRP source models and hence the tilted configurations only resulted in modest reductions of 6.8% and 17.2% respectively.

6.8 Discussion

The analysis includes three regions of three specific facades under three different deflector operational systems. The regions were grouped as lower, middle and upper with the same definition as in the previous sections. The leeward, windward and downwind side facades of the third street canyon in the third column (as marked in Figures 6.2 and 6.4) were selected as the facades of interest. As compared in Figures 6.13, 6.14 and 6.15, the configurations include the no-deflector (left column), standard deflector (middle column) and tilted deflector (right column) scenarios. The no-deflector scenario in Figures 6.13, 6.14 and 6.15 represents the reference cases under orthogonal and oblique wind cases with CRP and SRP source models with no deflectors. The standard deflector configuration in Figures 6.13, 6.14 and 6.15 represents a scenario where the optimal deflector configurations identified for CRP and SRP source models under orthogonal winds were used without further modifications for their respective cases under oblique winds also. The tilted deflector configuration represents a scenario where the deflectors were operated the same as the standard deflector configuration under orthogonal winds but were additionally tilted to orthogonally obstruct the ambient winds only when the winds were oblique to the city environment.

Therefore, each small box in Figures 6.13, 6.14 and 6.15 are area averaged CO IF_p values of three (lower and middle regions) or four (upper region) floors from a single simulation or two simulations that are linearly interpolated according to Figure 6.1. The common features in Figures 6.13, 6.14 and 6.15 indicate a homogeneous trend across the three regions and this concurs with the findings from the impact of the deflectors under orthogonal and oblique winds as the facades predominantly exhibited monotonic responses (also seen in Figures 6.7 and 6.11). Secondly, the impact of the deflector is more crucial in the lower region than in the middle and upper regions respectively. It can be seen from Figures 6.13 and 6.14 that the no deflector configuration exhibited higher CO IF_p across the leeward and windward walls predominantly for more oblique and orthogonal winds respectively. As discussed in the previous sections, this is due to the influence of strong recirculations in the vicinity of the respective facades for the two cases. However, what specifically characterizes the two facades for the no-deflector configuration is their sensitivity to the two environmental variables. It is seen from Figure 6.13 that the leeward facade is far more sensitive to the wind direction while it is not so for the traffic flow direction. While there is about 63% and 28% reduction of CO IF_p in the lower region when switching

from 24 hours of CRP to 24 hours of SRP under orthogonal winds, switching from 24 hours of orthogonal to oblique winds results in an order of magnitude rise in the CO IF_p along the facade, under both constant CRP and SRP source models. On the contrary, the windward wall shows relatively more sensitivity to the traffic flow direction than the wind flow direction. Apart from the striking difference when the cases which included complete CRP or SRP and orthogonal and oblique winds, four boxes in the second and third rows and columns of the first subplot in Figure 6.14 representing the mixed cases where both the environmental variables feature both alternatives on a particular day illustrated this difference substantially. Moving from 8 hours of oblique SRP and 16 hours of orthogonal CRP to 8 hours of oblique CRP and 16 hours of orthogonal SRP (complete traffic flow direction inversion case) reduced the CO IF_p along the lower region of the windward facade by about 80%, whereas moving from the former to 8 hours of orthogonal SRP (complete wind flow direction inversion case) and 16 hours of oblique CRP increased CO IF_p by 59%. It is worth noting that, despite having a strong recirculation in its vicinity under oblique winds, unlike the windward facade under orthogonal winds, the leeward facade exhibited much lesser sensitivity to the traffic flow direction. This meant that recirculations resulted in a more localized impact under the orthogonal winds than under the oblique winds. This also concurs with the streamlines in Figure 6.9, where the recirculations for oblique winds extended behind the upwind building of the target street canyon. This can also be inferred from Figures 6.13, 6.14 and 6.15 in general for all facades as the difference between 0 and 24 hours of CRP is substantially higher for the three facades when the winds are orthogonal than when the winds are oblique.

The second aspect of comparison arises from the influence of the various configurations of the deflector in the vicinity of the windward and leeward walls. For the leeward wall under orthogonal winds, the deflectors resulted in an increased CO IF_p reduction in the middle and upper floors. Although the deflector when placed 12.5m away from the leeward wall reduced the overall CO IF_p along the leeward facade, the lower region experienced a 60% increase compared to the no-deflector configuration when the traffic operated along the cross roads for the entire day. When the traffic operated completely along the side roads under orthogonal winds, the reduction of CO IF_p increased from about 45% in the lower region to 73% and 96% in the middle and upper regions respectively. However, the standard deflector configuration did not effectively mitigate CO exposure along the leeward wall under oblique winds. Whereas the tilted deflector configuration reduced concentrations

by 47%, 45% and 48% in the lower, middle and upper regions of the leeward wall under oblique winds with complete cross road pollution. Figure 6.13 also shows the potential reduction in the daily intake of CO by about 26% and 41% in the lower region of the leeward wall when the winds were oblique for 8 and 16 hours a day if the tilted deflector configuration was used. Both the middle and upper regions experienced 45% and 50% reduction in CO exposure when the winds were oblique for 8 and 16 hours respectively. It is worth noting that the tilted deflector configuration reduced about 60% CO exposure in the lower region of the leeward wall for 8 and 16 hours of oblique winds in a day with a complete SRP source. On the other hand, the windward facade benefited more from the standard deflector configuration under orthogonal winds than from both the standard and tilted configurations under oblique winds. As can be seen from Figure 6.14, the orthogonal winds contaminated the windward facade more during the CRP source scenarios than during the SRP source scenarios. The standard deflector configuration reduced 88%, 58% and 27% of CO exposure along the windward wall under with complete CRP source under orthogonal winds. However, the tilted deflector configuration reduced only about 8%, 19% and 33% of CO exposure in the lower, middle and upper regions of the windward wall with complete CRP source under oblique winds. This reiterates the more localized nature of the problem under orthogonal winds. It can also be seen from Figure 6.11, that the tilted deflector under oblique winds with SRP source models reduced substantial CO exposure along the leeward facade as well. In alignment with the aforementioned discussions, it would be reasonable to make an informed assumption that this particular tilted configuration could have been efficient for the CRP source model under oblique winds as well. Lastly, as in the case of the leeward facade, Figure 6.14 also highlights the potential of CO reduction along the windward facade with the combination of CRP source and orthogonal winds for even a minimum of 8 hours by a substantial 46% in the lower region.
Lastly, the side facades experienced relatively reduced CO IF_p compared to the leeward and windward facades under both orthogonal and oblique winds due to the wider and narrower side and cross roads respectively. Although the absolute CO concentration on the side facade under orthogonal winds was higher with the CRP source condition than with the SRP source condition, the lower CO IF_p illustrates the relatively lesser severity on the facade from SRP source due to the wide side roads ($\dot{m}_{srp} = 2\ \dot{m}_{crp}$). Although the standard deflector configuration highlights a consistent CO IF_p reduction along the facade for all combinations of traffic flows under orthogonal winds, the percentage of reduction increases from about 36% for

complete SRP conditions to 46%, 56% and 68% for 8, 16 and 24 hours of CRP source. This furthered the argument of the relatively more decoupled nature of the flow in amassing CO from the streets in the side road and within the street canyon regions under orthogonal winds compared to when the winds were oblique. Otherwise, the standard deflector configuration offering 68% reduction of CO IF_p along the side facade when operating for CRP source model (12.5m away from the leeward) would have resulted in the highest reduction when the traffic operated completely along the side roads. When the deflector was 12.5m away from the leeward wall, it deteriorated the air quality along the side facade. As in the case of the windward walls, the deflectors were not very effective in reducing the exposure along the side facades under both the CRP and SRP source models under oblique winds(also seen in Figure 6.15). As mentioned earlier in the results section, unlike orthogonal winds, the deflectors managed to mitigate the inward curling recirculations only within the street canyons and not while they entered the street canyons under oblique winds. Therefore under the complete influence of oblique winds, the reductions by tilted deflector configurations only ranged between 7- 14%, 7-16% and 0.5-16% in the lower, middle and upper regions respectively.

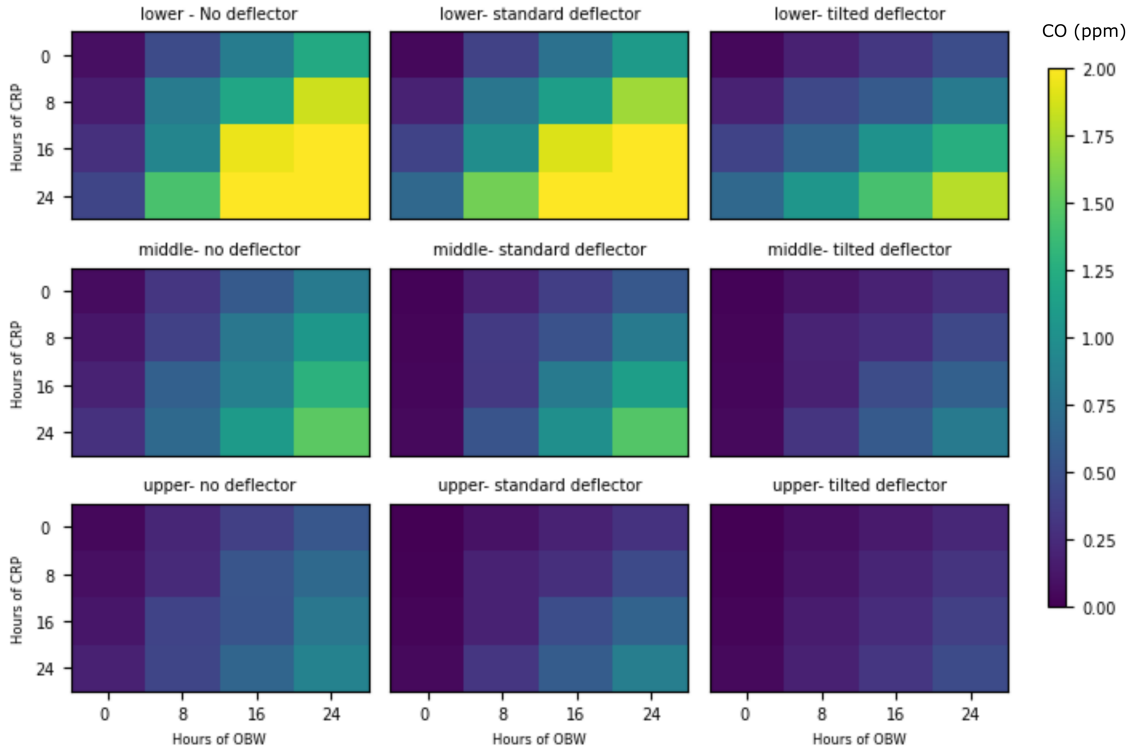

Figure 6.13: Combined sensitivity chart for the performance of wind deflector across the leeward facade for combined changes in traffic and wind flow directions.

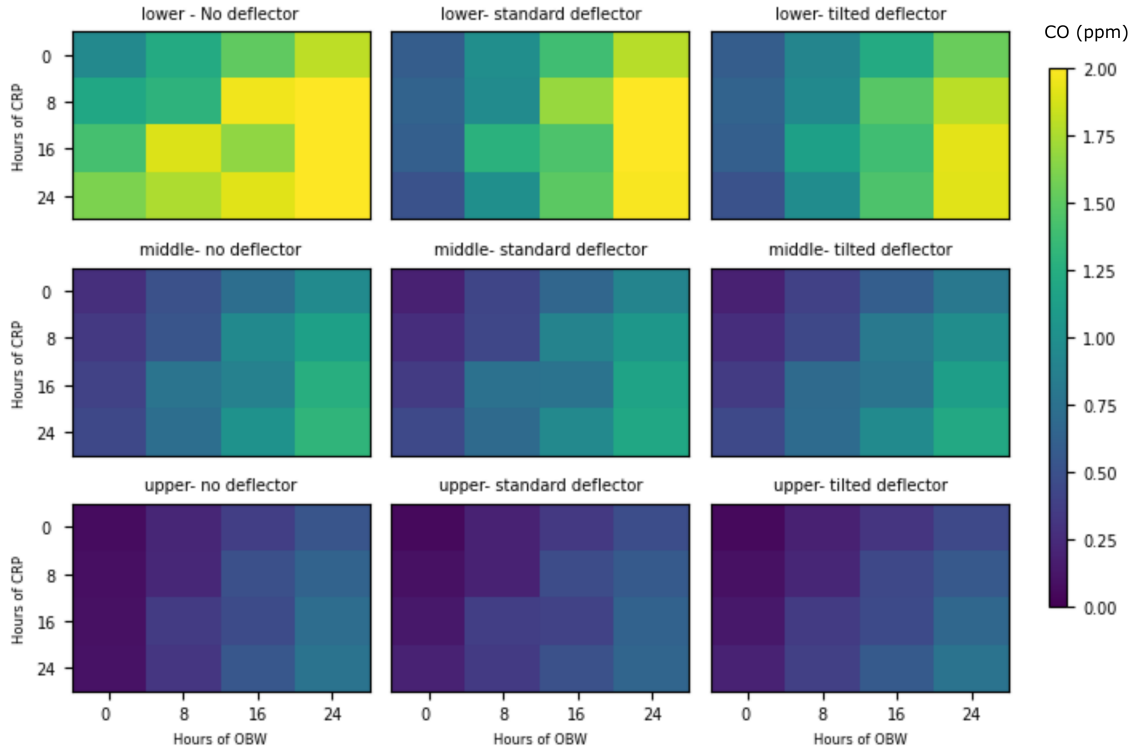

Figure 6.14: Combined sensitivity chart for the performance of wind deflector across the windward facade for combined changes in traffic and wind flow directions.

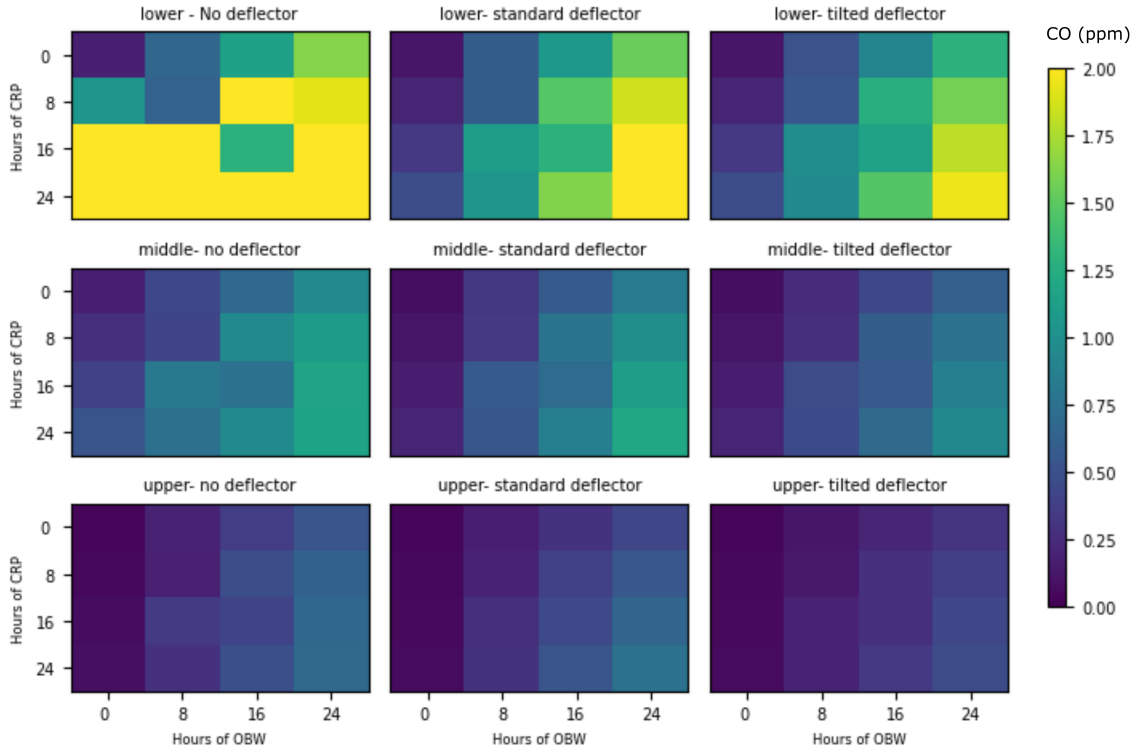

Figure 6.15: Combined sensitivity chart for the performance of wind deflector across the side facade for combined changes in traffic and wind flow directions.

6.9 Conclusions

Vehicular emissions are the primary concern for air quality in near-road buildings in city environments. Often, the efficacy of a passive intervention is evaluated through the prism of one variable environmental parameter including the wind speed, wind direction, asymmetry of the street canyons and traffic to mention a few. A combined influence of wind direction and traffic flow direction was considered in this study to evaluate the efficacy of adjustable wind flow deflectors in this study. A systematic approach was undertaken to develop a two-fold solution methodology; first, to identify the optimal position of the wind deflectors in the target street canyon for the two traffic flow configurations under orthogonal wind conditions and second, to evaluate the efficacy of standard and tilted installations of the wind deflectors under oblique winds about the optimal positions previously identified under orthogonal wind conditions. The advantage of the methodology included reducing computational time and resources by arriving at preliminary solutions before performing more computationally intensive simulations including a 2D array of buildings in the city-type environment. The limitation includes the physical implication of symmetry boundaries in the half-symmetry model which the middle row of buildings in the 2D array may not adhere to. Nevertheless, the study is a demonstration of the methodology to conceive a logical solution strategy that reduces the computational resources on such computationally intensive problems.

In the first step towards optimization of the deflector configurations, the standard deflector configuration offered a modest 15.8% and a substantial 48.2% reduction of CO IF_p across the leeward and windward facades respectively with CRP source model under orthogonal wind conditions (when the deflector was 12.5m away from the leeward wall). Similarly, the standard deflector configuration reduced CO IF_p across the downwind side facade by about 34% under SRP source model. The oblique winds under no-deflector scenarios resulted in contaminating the leeward facade the most through a strong recirculation in its vicinity. Conceiving the optimal positions from the standard deflector configurations, the tilted deflector configuration resulted in 47.3% and 16.6% reduction across the leeward and windward facades respectively with CRP source and only 17.8% across the side facade with SRP source. The following conclusions were deduced based on the combined sensitivity analyses.

1. The leeward and windward facades were at increased risk of experiencing higher CO IF_p during the orthogonal and oblique winds with CRP source model respectively. The limitations of the standard deflectors were realized under oblique winds where for example with CRP source model, it increased and decreased CO IF_p across windward and leeward facades by 4.4% and a mere 2.3%. On the contrary, the tilted deflectors reduced about 47.3% and 16.6% respectively across the leeward and windward facades. The advantage was further reinforced with SRP source model where the standard and tilted deflector configurations offered 35.8% and 62.2% across the leeward façade which was under maximum risk of CO exposure due to the inward curling recirculations. Finally, the side facades experience maximum risk from SRP source models where the tilted deflectors reduced 17.8% of CO IF_p across the same as compared to the standard deflectors which performed similarly as the no-deflector scenario.
2. The facades under immediate risk high CO IF_p experienced a drastic reduction in exposure when the traffic flow direction was changed when the winds were orthogonal. However, the leeward facade exhibited relatively stable behavior when the traffic flow direction was changed under oblique wind flow conditions. This indicated that the flow within the canyons was more decoupled to have stronger variations with changes in traffic flow directions when the ambient wind flows were orthogonal than when they were oblique to the city-type environment. However, it is worth noting that the leeward facade an order of magnitude higher difference CO IF_p when the wind directions were changed for both source models as compared to switching the sources for a fixed wind direction. Therefore, it can be inferred that the combined changes in traffic and wind flow directions have a complex relationship where the changes in changes in traffic flow are more pronounced under orthogonal wind conditions while the changes in wind directions are itself more influential for any given source model.
3. The sensitivity of the facades to changing traffic flow direction under different flow directions also implied the influence of the wind deflectors to reduce CO IF_p. The optimal deflector configurations to mitigate high CO IF_p under orthogonal winds warranted the deflector location based specifically on the pollution source region. However, the leeward facade experienced an even higher 62.2% CO IF_p under SRP tilted configuration than the CRP tilted configuration which reduced 47.3% exposure. This implied that, although

changing the orientation of the wind deflector was an effective strategy, the optimal design for the two source models could result from exploring a common flow challenge, the inward curling recirculation for example.
It is important to note that the current approach modified flow substantially across all three facades considered under orthogonal wind conditions, while so across the leeward facade under oblique winds.

Lastly, the real environment is a very dynamic system and this work aimed at developing simple strategies using passive interventions to adapt to different conditions without losing the benefit of high efficiency under predominant and crucial conditions for which they are usually designed. The authors recommend further study in the direction of the current research by incorporating more environmental parameters in tandem to develop an advanced understanding of both the environments and passive interventions and their response to environmental changes.

Chapter 7

Adjustable Wind Flow Deflectors in Dublin City- A Real World Analyses

7.1 Introduction

Chapters 3, 4 and 5 were extensively focussed on developing adaptive solutions with roof-level wind flow deflectors for diurnal changes in traffic and wind flow directions. This approach could be extended in multiple ways. A real-time feedback loop for performance tuning including sensors for pollutants and ambient variables can give indication whether a passive intervention is actually improving or deteriorating an environmental condition and can be used to provide adaptive strategies including adjusting traffic flow, adjusting the passive interventions or have supplementary systems like an air purifier to engage. State-of-the-art AI/ ML modeling strategies could be deployed on historical data to spatio-temporally ascertain the concentration build up and prevent it from reaching the thresholds. Furthermore, hyperlocal optimization approached could provide detailed understanding on the exposure extents and performance of passive interventions and if further attention is required for a hotspot. However, there are both practical and technical challenges associated with this approach. As mentioned in Chapter 6, it is impractical to develop a solution for every combination of environmental settings and the idea was to increase the face area of contact of the wind deflectors to enhance the wind

availability in the street canyons by tilting the same for oblique ambient winds. From a technical standpoint, urban winds are transient, gusty and rarely oriented in a particular direction for a long enough duration. The adjustable wind deflectors experience the challenge of deploying a sensor and response system to work efficiently under continuously changing conditions by facilitating maximum face area at the optimal location. Apart from the cost and implementation, if the response system is not swift enough to adapt to operating the wind deflectors at the optimal setting, it could leave the micro-environment at risk of experiencing higher pollution exposure. Apart from that, adjustable wind deflectors mean that the mechanical and structural integrity of the system is crucial as it is exposed to heavy wind loads and changing weather conditions with the risk of wear and tear. Despite it being a passive intervention from an air pollution mitigation perspective, it is not purely passive but requires energy input, thus making cost a question for installation and operation. Therefore, extensive usage of adjustable wind deflectors requires careful financial viability for sustained operation. Adjustable wind deflectors especially in tilted configurations could congest the roof-top area and the ventilation and sunlight availability of the top-floor house. Lastly, the designs and functionals modes of the adjustable wind deflectors need to comply with the safety and also in some cases the aesthetic standards. Therefore, this chapter explores the possibility of developing a common solution for changing ambient wind directions in a long-isolated street canyon. A static multi-directional wind deflector system is introduced which could mitigate high pollution exposure arising from changing ambient wind directions. However, the solution could not be as efficient as adjustable wind flow deflectors under each environmental setting as it is not a derived case-based solution unlike the former. An octagonal multi-directional wind deflector was introduced in this study as shown in Figure-7.1 to offer orthogonal deflecting surfaces for 0°, 45° and 90° respectively. The study includes the performance assessment of the octagonal wind deflector system under theoretical and real street canyon environments respectively.

7.2 Problem Description

The present chapter is intended to ascertain answers to the following research questions in the context of applying multi-directional static roof-level wind flow deflectors in a long-isolated street canyon.

1. How beneficial or detrimental are the multi-directional wind deflectors in re-

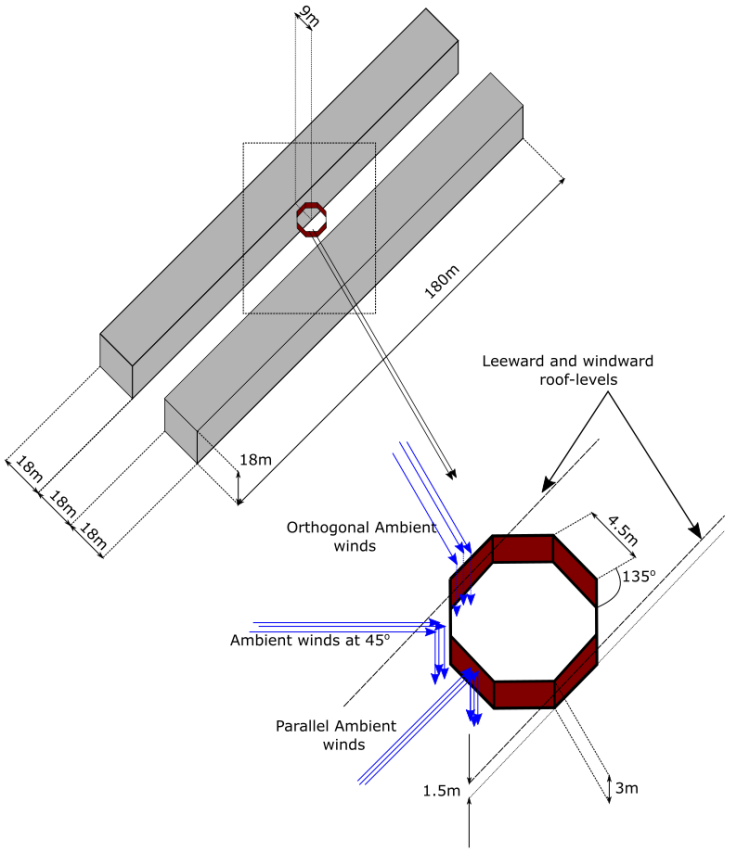

Figure 7.1: Schematic of a hexagonal multi-directional wind deflector to orthogonally deflect incoming ambient winds at 0°, 45° and 90° respectively.

ducing pollution exposure along leeward and windward facades for changing wind directions in a theoretically isolated street canyon setup?

2. How beneficial or detrimental are the multi-directional wind deflectors in reducing pollution exposure along leeward and windward facades forming at busy city centre street in Dublin, Ireland (Pearse Street) under predominant wind conditions?

7.3 Computational Domain and Boundary Conditions

7.3.1 Theoretical cases

Figure 3.8 shows the symmetric isolated street canyon environment chosen for performance analyses of multi-directional wind deflectors for the initial theoretical street canyon setting. The choice of the computational domain and boundary conditions remains the same as in section 3.3.3 in Chapter 4. The pollutant source definition changed as CO gas was used as the pollutant instead of SF_6 and a uniform surface source of 12m width centrally located along the street surface was used instead of four independent line sources.

7.3.2 Pearse Street Environment

For the performance analyses of multi-directional wind deflectors in the simulation of a real world environment (Pearse Street), the choices of the computational domain were similar with a pollution source width of 10.5m. Pearse Street is aligned in the East-West direction with approximately a 16° inclination towards the south. The tallest building in the domain was 40m high and therefore 280m, 320m and 760m distances were prescribed between the side ends of the street canyon and the symmetry sides, upwind edge of the street and the velocity inlet boundary and the downwind distance. The computational domain was 400m high. The geometry of Pearse Street was obtained through a combination of sources. As a preliminary step, the plan view layout of the street was obtained by marking the plan outlines of all the buildings in the street from Google Earth on AutoCAD. Additionally, lidar data of Pearse Street was obtained from the 2015 aerial laser and photogrammetry survey of Dublin city collection record. The lidar data for Pearse Street was available from six different datasets representing the region as compressed datasets. They were incorporated together in ArcGIS software where they were cured to separate the street surface, vegetation, buildings and outlier noise points. The building points were used to create a building Raster from where building polygons and raw building models were generated. The raw building model footprints were regularized before a building multipatch was generated that was again exported in AutoCAD. The building layouts from Google Earth images and building height and roof shape information from lidar data were then correlated to develop the Pearse Street ge-

ometrical model. Finally, this geometrical model was imported into SpaceClaim software where the street geometry was rotated appropriately and subtracted from the larger volume to result in the final computational domain considered for this study. Pearse street was chosen as the case-study real environment due to the availability of associated data, its heavy traffic usage in Dublin city and the canyon-like nature of the street.

Wind data from Met Eireann, the Irish Meteorological Service recorded at Dublin Airport From January 1, 2024, to June 30, 2024, was used for the current analysis. The winds in Dublin city were predominantly south-westerly (from south-west to north-east). As can be seen from Figure 7.3, the winds were 22.5° offset from the West-East direction. With the natural 16° inclination of Pearse Street, it created a 38.5° incidence with the predominant wind direction in the city. Therefore, the computational domain was adjusted to additionally account for this.

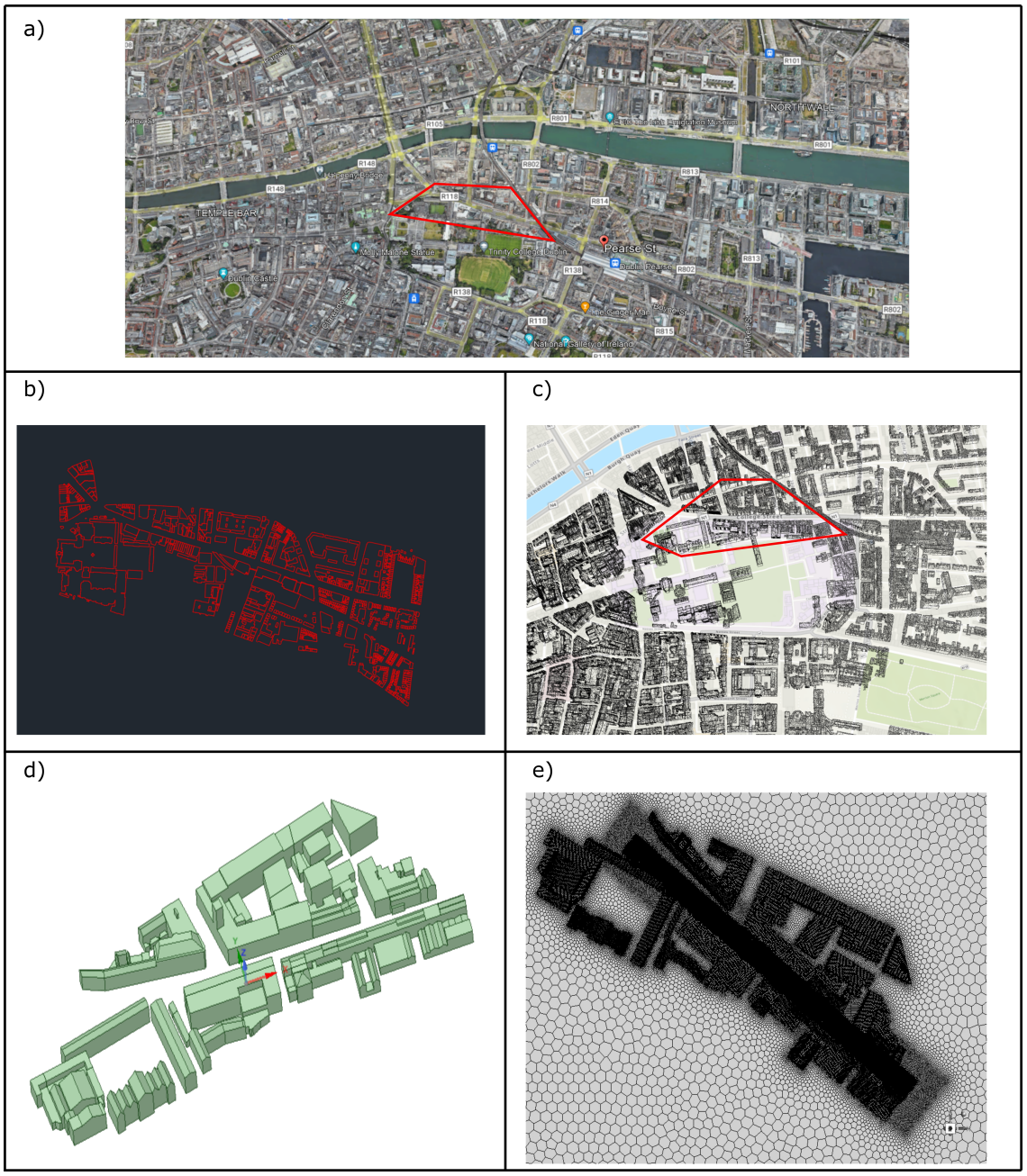

Figure 7.2: Methodological sequence of developing a CFD model for flow in Pearse Street environment from 2D plan layout and 3D information from lidar data of the neighborhood; a) Plan view of Pearse Street neighborhood from Google Earth; b) 2D plan view layout of Pearse Street neighborhood mapped in AutoCAD; c) 3D Lidar data of buildings in Pearse Street neighborhood in ArcGIS; d) 3D solid models of buildings in SpaceClaim; e) Polyhexacore mesh of Pearse Street neighborhood in Ansys Fluent.

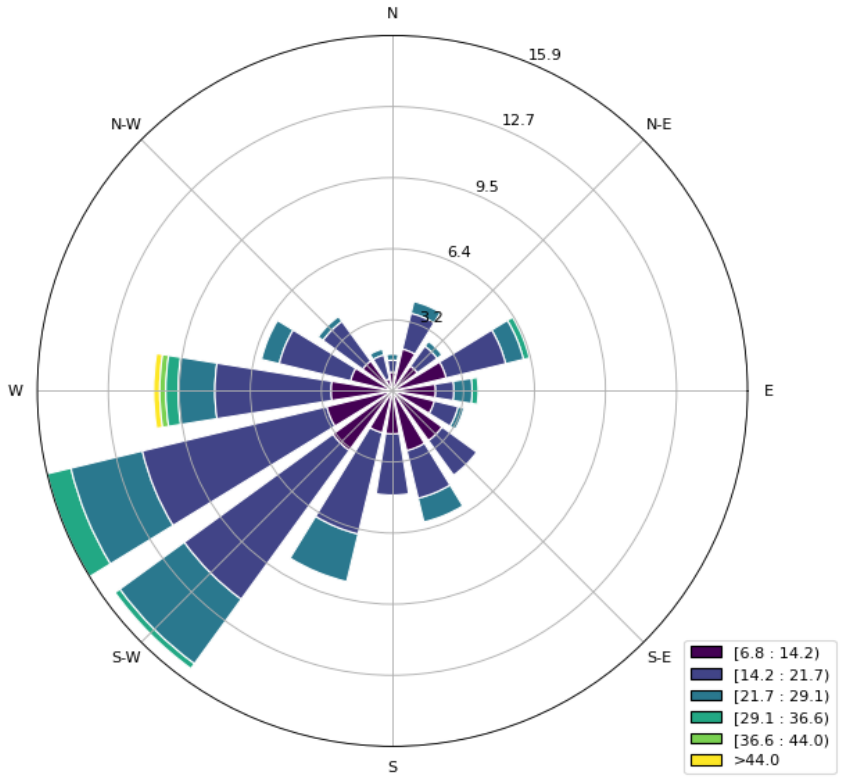

Figure 7.3: Wind rose diagram representing the statistical distribution of speeds and directions of ambient wind flows in Dublin.

7.4 Case Description

Three different directions including 0°, 45° and 90° of the ambient winds were considered for the performance assessment of multi-directional wind deflectors in the ideal environment. For each wind direction, four different conditions were assessed including the no-deflector configuration, 1-deflector configuration (included at the center of the street, $y/H = 0$), 2-deflectors configuration (included towards the sides of the street, $y/H = -0.25$ and $y/H = 0.25$) and 3-deflectors configuration (included at the center of the street, $y/H = 0$ and included towards the sides of the street, $y/H = -0.25$ and $y/H = 0.25$) respectively. The multi-directional wind deflectors as schematically shown in 7.5 were initially chosen to be 4.5m long along its sides and 3m high. The deflectors were symmetrically placed about the roof of the street canyon buildings as it included 1.5m of depth both below and above the same. The schematic of the case studies considered for the theoretical assessment of the multi-directional wind deflectors is shown in Figure 7.4. However, as these deflectors managed to result only in marginal impact on the street canyon

ventilation, a modified deflector design which was 6.2m long along each side and 6m high (symmetrically placed about the roof of the street canyon buildings with 3m above and below the roofs) was chosen for evaluation. Finally, four multi-directional wind deflectors were included in Pearse Street where potential street-canyon-like micro-environments were formed. The summary cases studied included the ideal and real street scenarios are summarized in Table 7.1

	0°	45°	90°	Predominant direction
Ideal environment				
No-deflector case	✓	✓	✓	-
1-deflector case	✓	✓	✓	-
2-deflectors case	✓	✓	✓	-
3-deflectors case	✓	✓	✓	-
Real street environment				
No-deflector case	-	-	-	✓
4-deflectors case	-	-	-	✓

Table 7.1: Summary of case studies for performance analyses of multi-directional wind deflectors

7.5 Mesh Convergence

The mesh convergence study described in Section 3.3.3.2 in Chapter 3 has been applied to the case studies in this chapter.

7.6 Key Assessing Parameters

CO IF_p (as defined in Chapter 4) is considered as the primary parameter of investigation in this chapter.

7.7 Target regions of study

Figures 7.5 and 7.6 illustrate the target regions where CO IF_p is assessed for the theoretical and real street environments respectively.

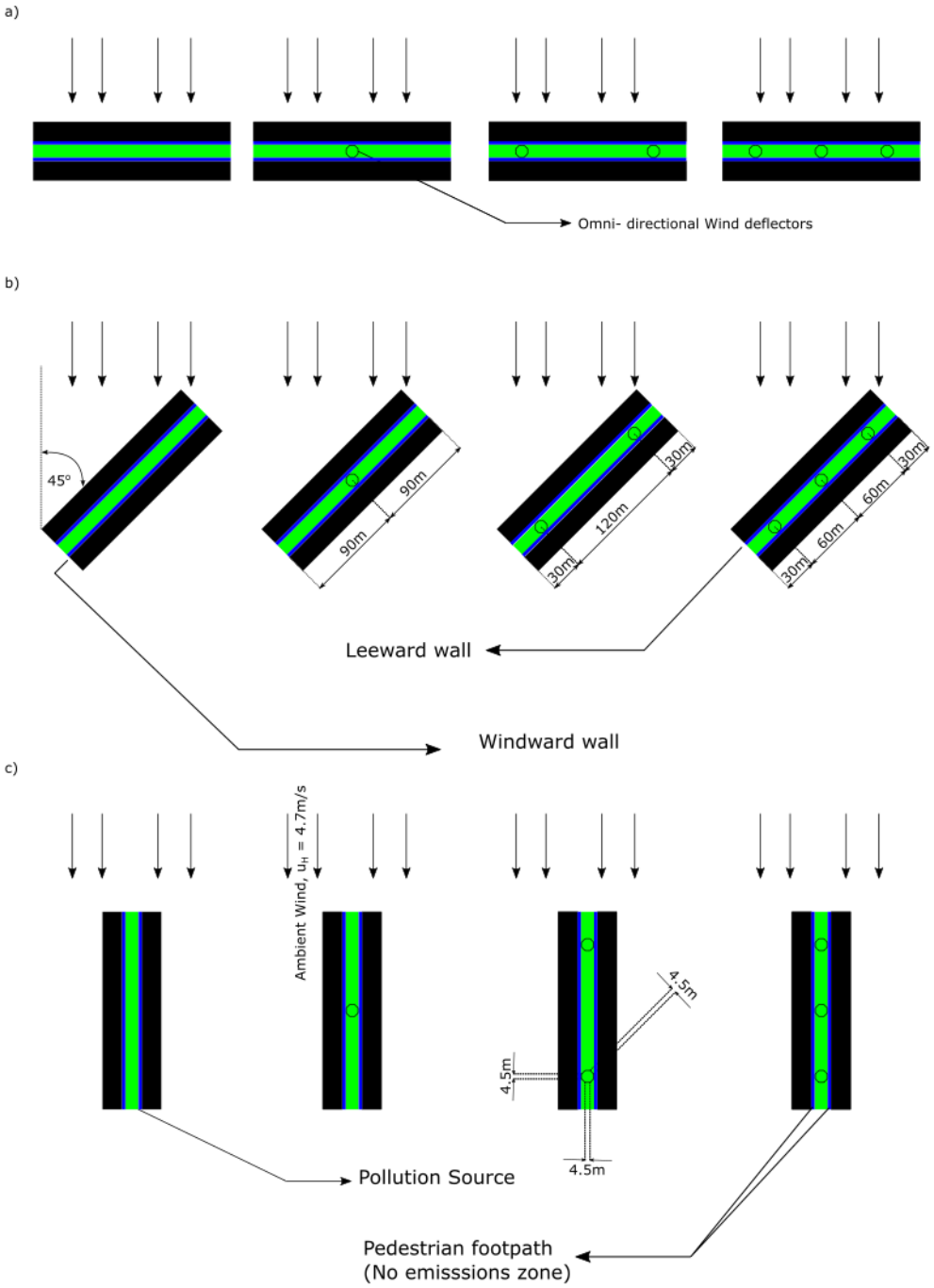

Figure 7.4: Schematic of case studies considered for the performance assessment of multi-directional wind deflector under ambient winds at a) 0°, b) 45° and c) 90° respectively in ideal street canyon environment.

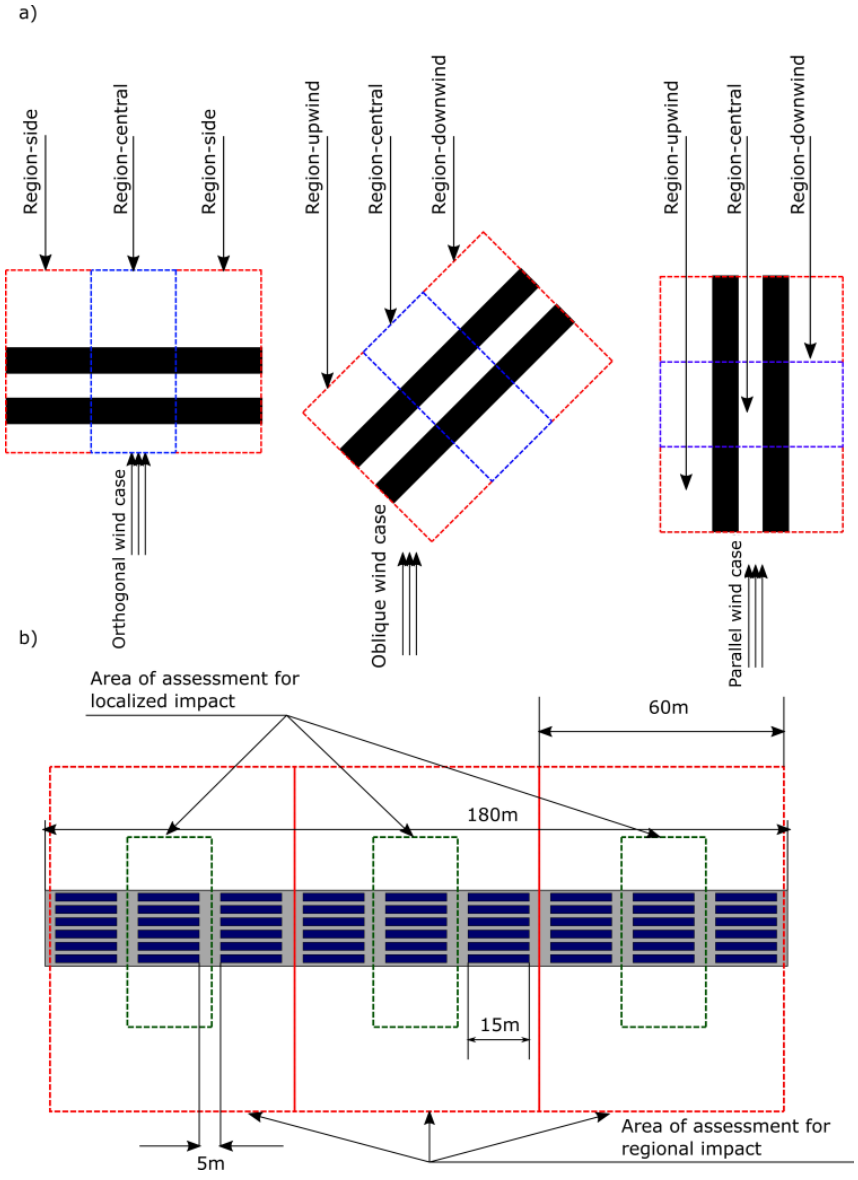

Figure 7.5: a) Schematic representing the different regions of the isolated street canyon under different ambient wind directions; b) Schematic representing the arrangement of windows considered in the study for the evaluation of near-road building CO IF_p.

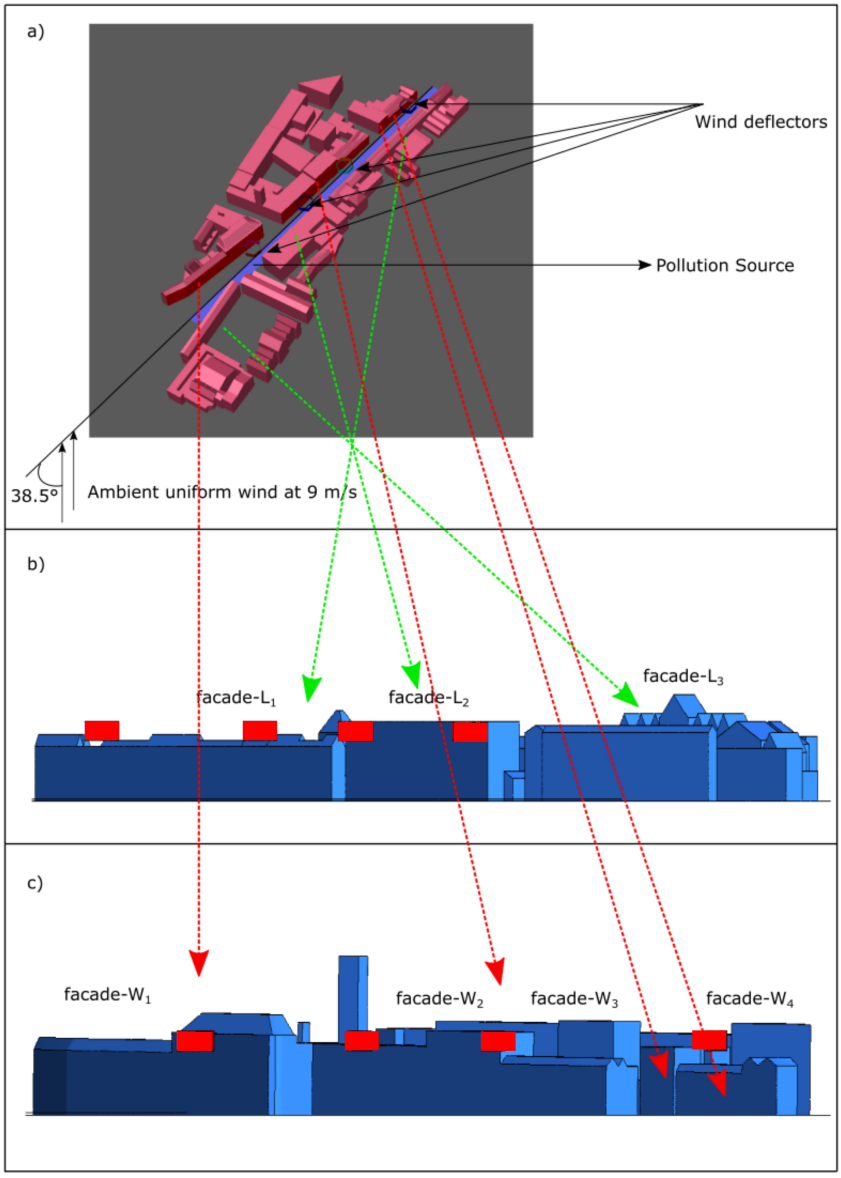

Figure 7.6: a) Isometric view of the Pearse Street environment and direction of the ambient wind; b) Front view of target leeward facades ;c) Front view of target windward facades

7.8 Results & Discussions

7.8.1 Theoretical cases

7.8.1.1 0° ambient winds

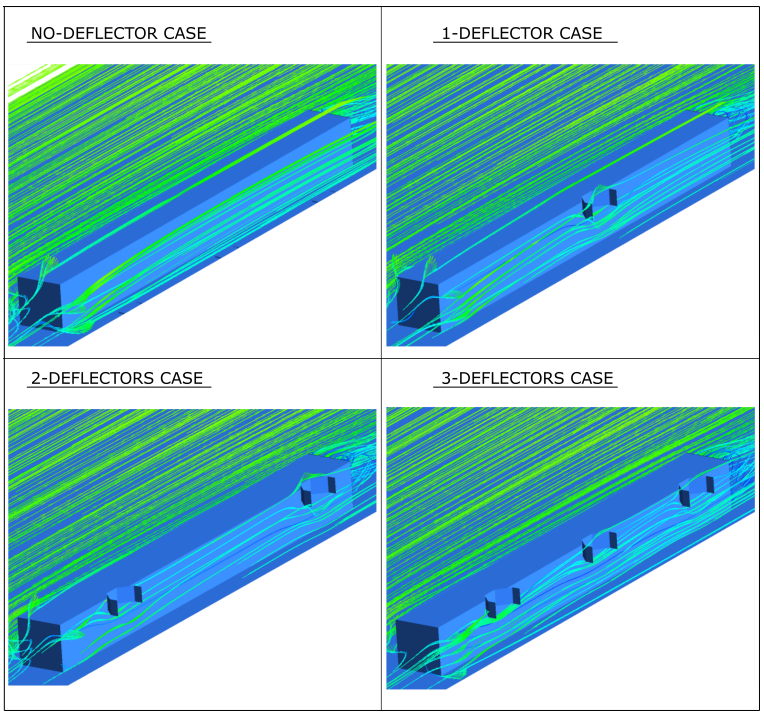

Figure 7.7: Streamlines of the flow (plotted $0 \leq y/H \leq 10$) under parallel ambient winds with no deflectors and one, two and three deflectors respectively.

When the ambient wind was parallel to the street canyon, the multi-directional wind deflectors facilitated a downward push of the air stream. This maximized the cleaner above-roof air flowing into the street canyons, especially in the lower floors where CO was accumulated. The downward push of the ambient winds facilitated by the deflectors can be seen in Figure 7.7, showing the flow streamlines in the street canyon. Figure 7.8 shows the contour of CO IF_p on the leeward/ windward walls. Figure 7.9 shows the localized variation of CO IF_p across six floors in the upwind, central and downwind regions. The downward push of cleaner air into the canyon concurred with Figure 7.9, where the 2-deflectors and 3-deflectors cases, respectively, reduced about 25.7% to and 48.5% of CO IF_p in Floors 1, 2 and 3 in the upwind region. Although it is not obvious from Figure 7.9 due to the ranges of the values involved, the 2-deflectors and 3-deflectors cases also reduced about 27% of CO IF_p on Floor 6 in the upwind region and are noticeable in Figure 7.8. The

subsequent downstream areas including the central and downwind regions have benefited from wind deflectors upstream of them. The upwind deflector reduced ground level CO IF_p in the central region. However, it could not be reduced to as much as if a deflector were introduced in the central region, especially on the higher floors. The 2-deflector case reduced 21% CO IF_p in Floor-1 compared to the no-deflector case but resulted in 6% higher CO than the latter in Floor-4. On the contrary, the 1-deflector case facilitated similar exposure in Floor-1 as the no-deflector case and reduced about 30% and 17% on Floors 4 and 5 respectively. A similar trend was observed in the downwind region where the 1, 2 and 3-deflectors cases facilitated increasingly better ventilation at the ground level, and thus lesser CO IF_p in the downwind region.

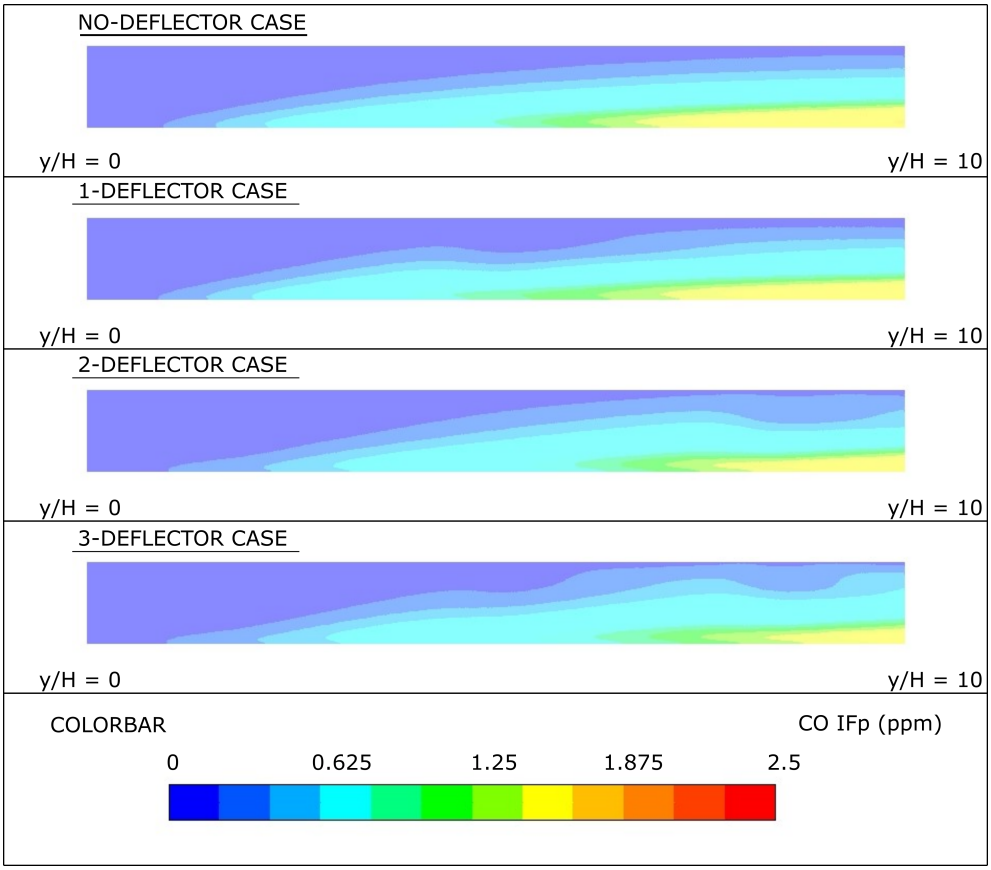

Figure 7.8: Contour of CO IF_p across the windward/ leeward facade (plotted $0 \leq y/H \leq 10$) under parallel ambient winds with no deflectors and one, two and three deflectors respectively.

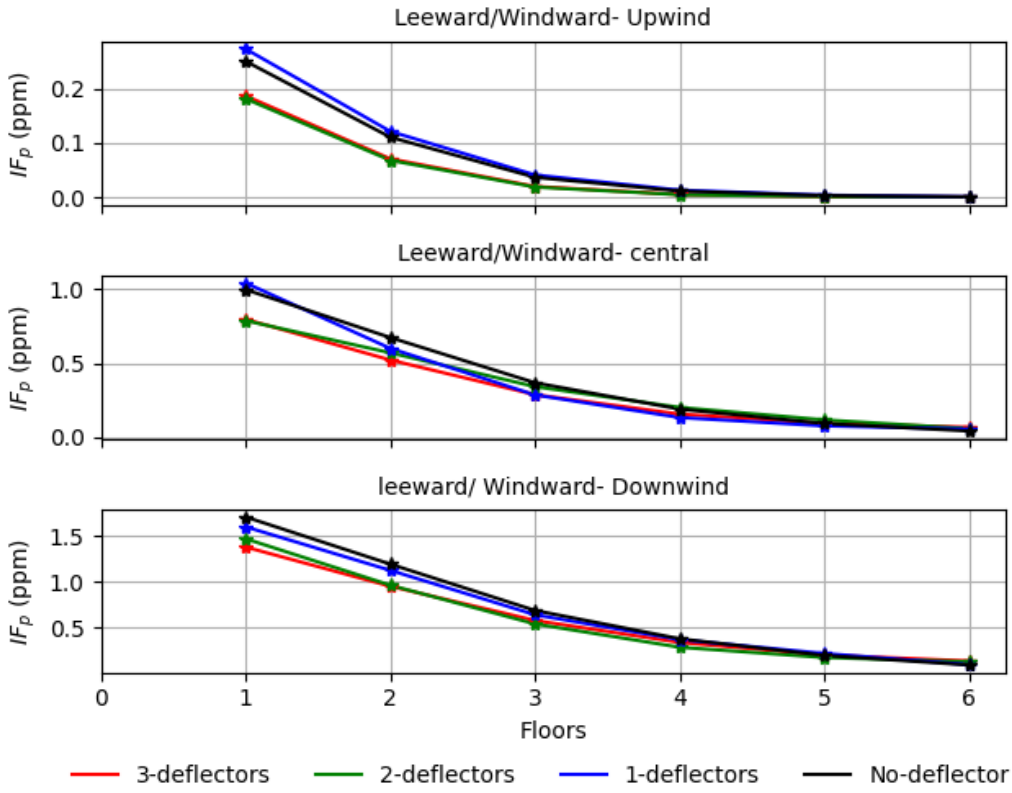

Figure 7.9: Localized variation of CO IF_p across the height of the leeward and windward facades under parallel ambient winds with no deflectors and one, two and three deflectors respectively.

7.8.1.2 90° ambient winds

Figure 7.10 shows the streamlines representing the flow in the isolated street canyon under perpendicular ambient winds when no deflectors and one, two and three deflectors were included. Figure 7.11 shows the contour of CO IF_p along and leeward and windward facades for the four cases. While the flow scenarios including the wind deflectors seemed to follow a similar pattern as the no-deflector case, their characteristic differences are more distinctly observed in Figure 7.12 where the CO IF_p across the height of the buildings on the leeward and windward facades were compared. Two distinct flow features characterize the impact of multi-directional wind deflectors on the leeward and windward sides respectively.

The CO IF_p on the leeward side for the central and side regions was substantially reduced in the higher floors (4-6). The CO IF_p was reduced by 47.4% and 80.3% and 56.7% and 85.6% on floors 5 and 6 for the 3-deflectors and 1-deflector

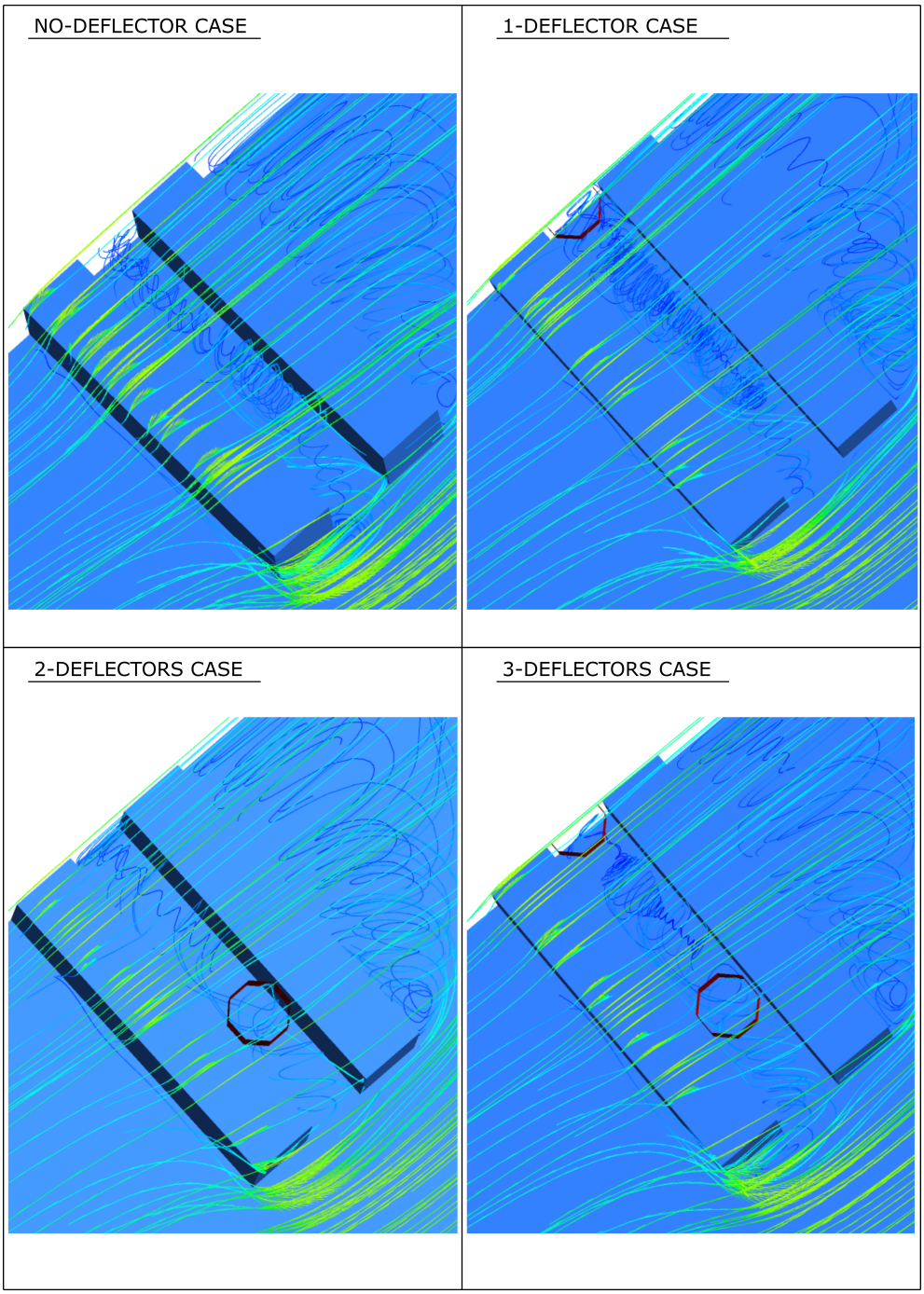

Figure 7.10: Streamlines of the flow (plotted $0 \leq y/H \leq 5$, as symmetry about y/H= 0) under perpendicular ambient winds with no deflectors and one, two and three deflectors respectively.

cases respectively. As can be seen from Figure 7.11, the multi-directional wind deflectors facilitated a washdown of ambient perpendicular winds between itself and the leeward facade in the target region. The substantially increased CO IF_p re-

ductions in the higher floors indicated that the washdown could offset the lateral washaway of the pollutants towards the center of the street canyon in the higher elevations, and was not successful in doing the same across the entire building height. On the other hand, the 3-deflectors and 1-deflector cases offered negligible changes to CO IF_p along floors 1-4 in the side region as they respectively offered a monotonically increasing CO IF_p reduction between 16.4% and 44.9% and 20.3% and 45.6% in the same area with increasing distance from the ground at the centre. It is also worth noting that the average CO IF_p across six floors of the leeward facade in the central region was 3.73 folds higher than in the side region for the no-deflector case. It can be seen from Figure 7.11 that the side flows from the side entrances of the isolated street canyon increasingly approach the leeward facade in their vertical recirculations towards the center. Figure 7.11 also shows that the multi-directional wind deflectors apart from ventilating the leeward facade by facilitating wash-down along the higher floors, redirect the vertical recirculations to rise within them and therefore reduce the CO exposure across the lower floors from vertical recirculations that was enriched with CO concentration at the ground level. This explained both the naturally reduced CO IF_p along the side regions of the leeward facade compared to the central area, and the inability of the multi-directional wind deflectors to reduce CO IF_p along the side regions of the leeward facade respectively.

The windward facade is also progressively more polluted from the sides to the center of the street canyon as the vertical recirculations continuously amass CO from the ground level. The multi-directional wind deflector impacts the windward side in two ways. Firstly, as in the case of the leeward facade, it limits the reach of the vertical recirculation toward it and secondly, it deflects the washdown of the vertical recirculation to orient towards the center of the street canyon, thereby resulting in a wake. Limiting the reach of the progressively polluted vertical recirculations restricts the CO exposure along the windward facade and the wake increases the CO exposure by limiting the dispersion. The latter dictates the flow in the central region that the multi-directional wind deflectors increase CO IF_p on the windward facade. However, the former offered localized relief on the windward side under the 3- and 2-deflector configurations in the side region. All three configurations including the deflectors deteriorated air quality regionally on the windward side compared to the no-deflector configuration.

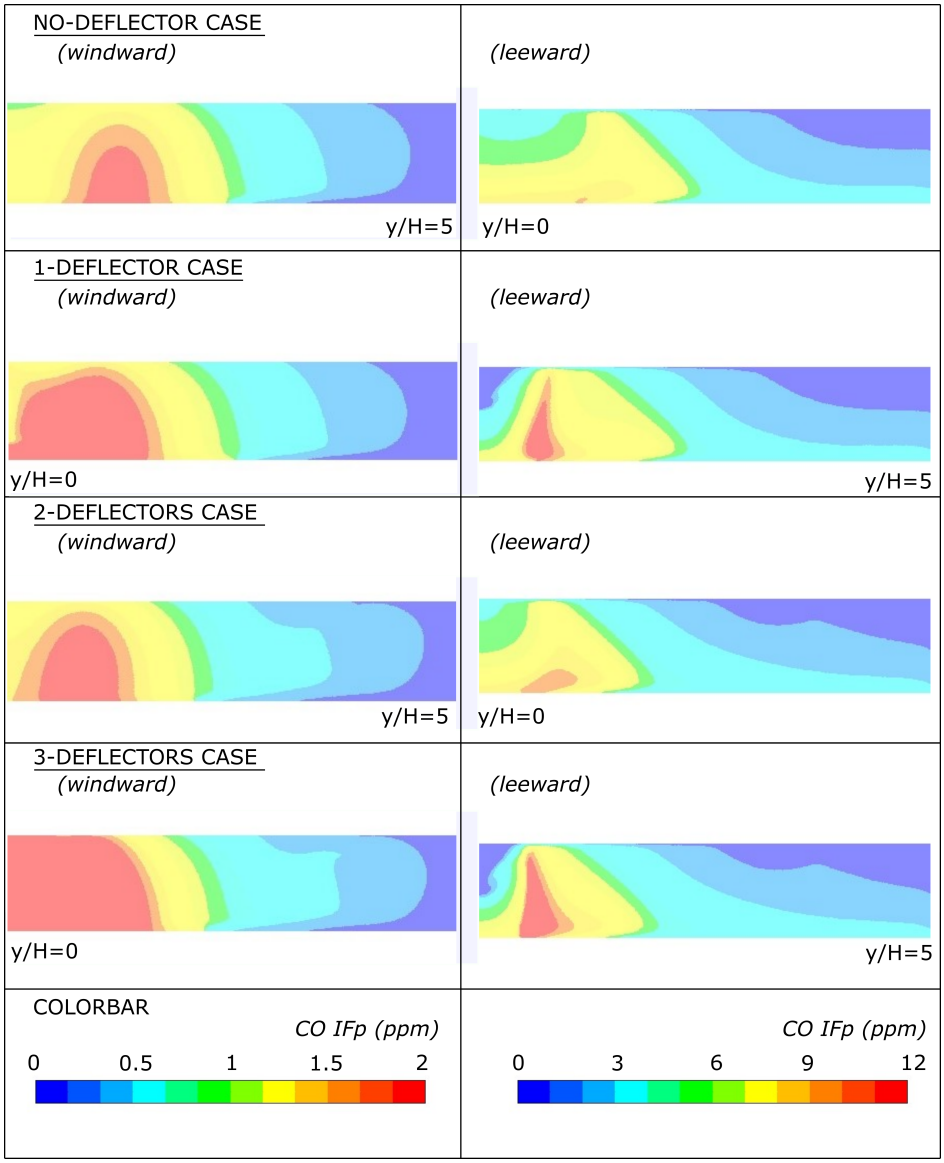

Figure 7.11: Contour of CO IF_p across the windward and leeward facade (plotted $0 \leq y/H \leq 5$, as symmetry about y/H= 0) under perpendicular ambient winds with no deflectors and one, two and three deflectors respectively.

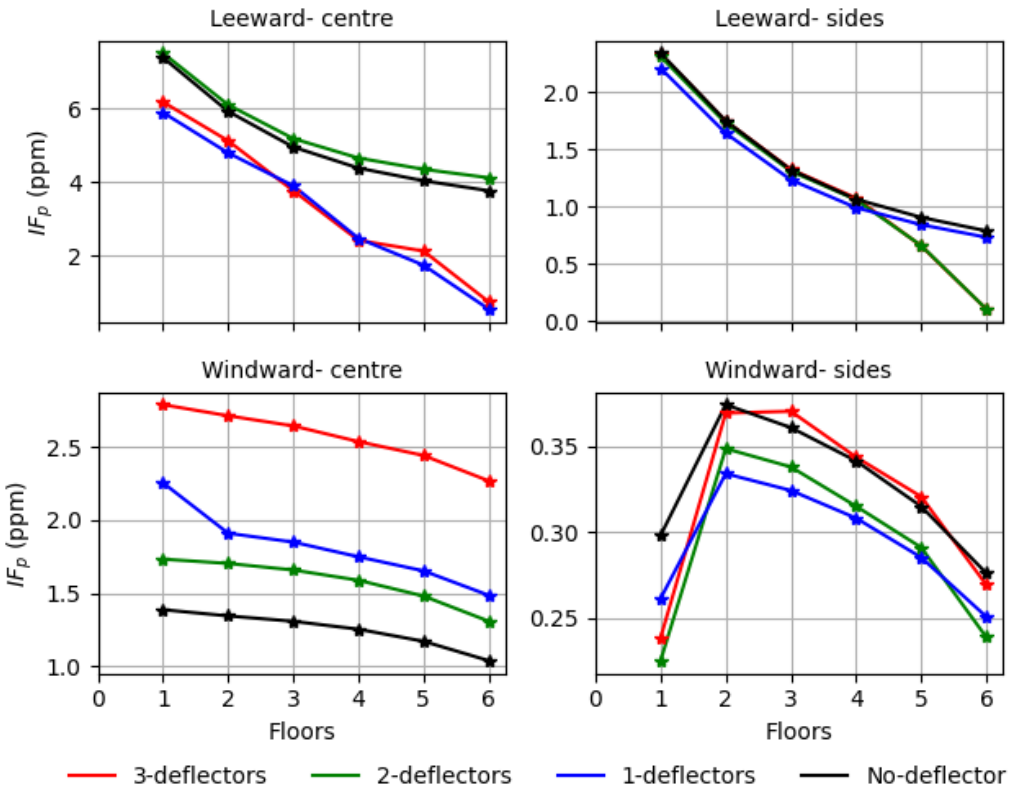

Figure 7.12: Localized variation of CO IF_p across the height of the leeward and windward facades under perpendicular ambient winds with no deflectors and one, two and three deflectors respectively.

7.8.1.3 45° ambient winds

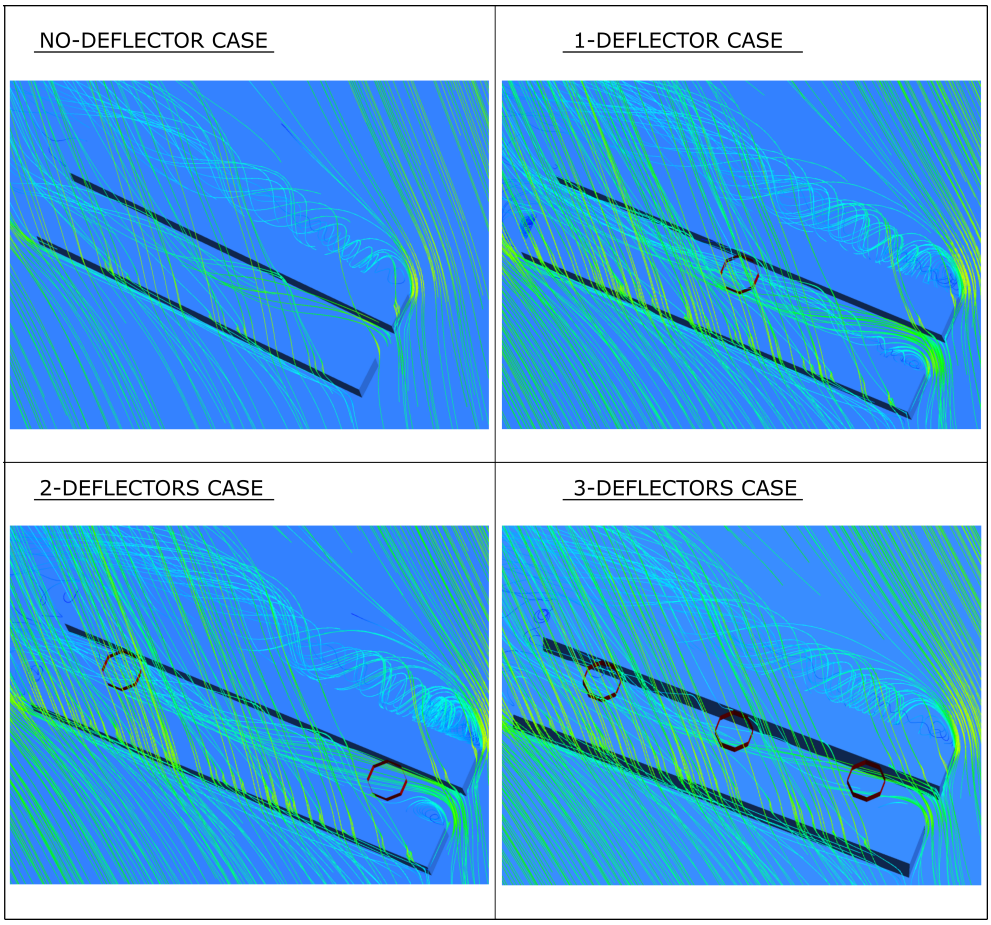

Figure 7.13: Streamlines of the flow (plotted $0 \leq y/H \leq 5$, as symmetry about y/H= 0) under oblique ambient winds at 45° with no deflectors and one, two and three deflectors respectively.

Figure 7.13 shows the streamlines representing the flow in the isolated street canyon under oblique ambient winds at 45° when no deflectors and one, two and three deflectors were included. Figures 7.14 and 7.15 show the contour of CO IF_p along and leeward and windward facades for the four cases. The contour plots of CO IF_p showed similar behavior for the case with no deflectors and when one, two and three deflectors were introduced, except for the local and regional impacts around the multi-directional wind deflectors. Unlike in the perpendicular wind scenario where the laterally traversing vertical recirculations from the sides to the centre of the street canyons dominated the flow, streamwise flow from the upwind to downwind side entrances dominated the flow within the street canyon when the ambient wind was oblique at 45°. Figures 7.16 and 7.17 show the regional impact of multi-directional wind deflectors on the CO IF_p across all six floors of

the leeward and windward facades in the upwind, downwind and central regions of the street canyon, respectively. For the no-deflector case, the streamwise flow enters the canyon through the upwind side entrance, impacts the windward wall, the leeward wall and again the windward wall before it exits through the downwind side entrance. As a combination of perpendicular and parallel wind conditions, the flow comprises both oscillatory an trajectory of the streamwise flow between the two facades (as in the perpendicular flow scenario) and rising between the two facades (as in the parallel wind scenario). Due to both accumulation of upstream CO and the flow rising, the central and downwind sides of the canyon experienced high CO IF_p respectively, compared to the upwind region. It can be seen from Figure 7.16 that the wash-down facilitated by the 3-deflector and 2-deflector case sufficed to similarly achieve monotonically increasing CO IF_p reduction from Floor 1 to Floor 6 by 23.4% to 60.1% respectively on the leeward facade in the upwind region. It is worth noting that the CO IF_p reductions in the central and downwind regions were noticeable only on the upper floors. Such reduction of the impact of deflectors is owed to the strengthened streamwise flows in the central and downwind region which increasingly develop higher resistance to the vertical wash-down of the ambient winds offered by the deflectors.

As far as the windward facade is concerned, the multi-directional wind deflector maximized the contact of polluted stream (by streamlining the flow parallel to the windward facade) from the leeward facade in the vicinity of the windward facade by before they divert back to the leeward facade. The multi-directional wind deflector facilitated this by guiding the flow parallel between itself and the windward facade. Unlike the vertical recirculation under perpendicular winds that facilitate washdown along the windward facade, the oblique winds sweep through the pollution source region to pollute the windward facade. The 3-deflector and 2-deflector cases increased the CO IF_p in Floors 1, 2 and 3 of the windward facade by 24-60% in the upwind region. This is contrary to the perpendicular wind scenario where they reduced CO IF_p in their immediate vicinity. The 1-deflector case (as in the 3-deflector case) substantially deteriorated CO exposure on the windward facade in the central regions. While the 2-deflector (as also in the 3-deflector case) case deteriorated CO exposure on the windward facade in the downwind region.

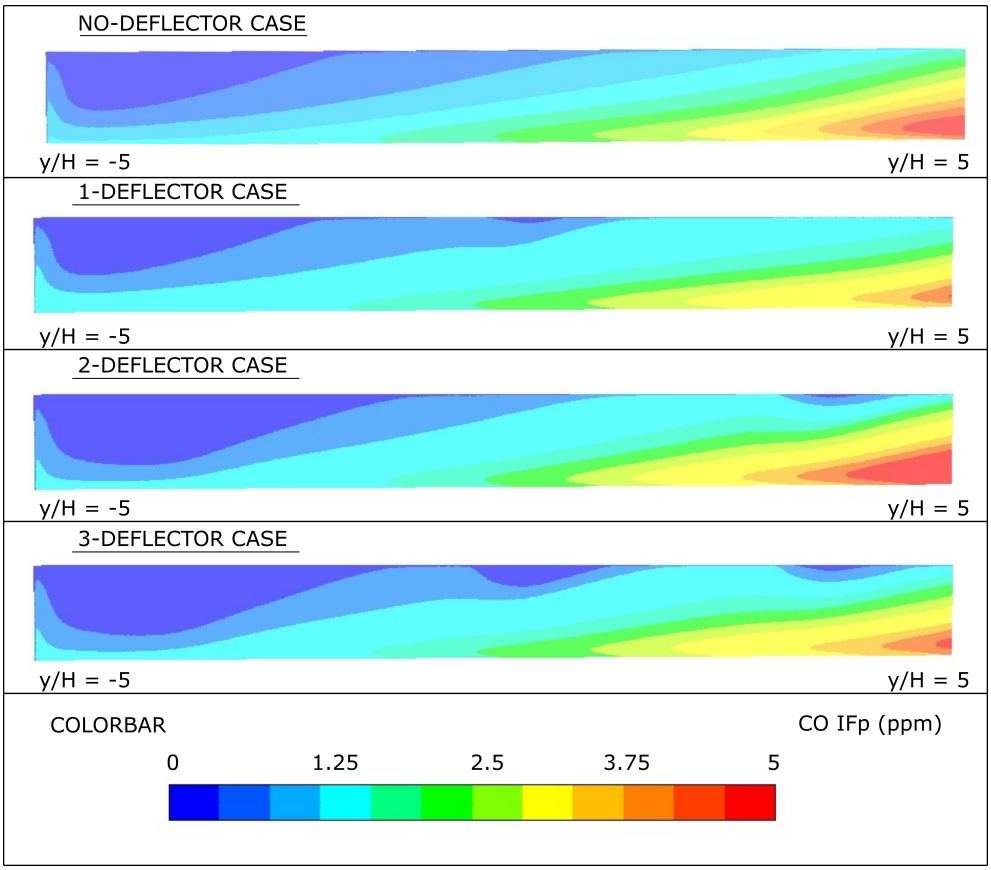

Figure 7.14: Contour of CO IF_p across the leeward facade (plotted $-5 \leq y/H \leq 5$) under oblique ambient winds at 45° with no deflectors and one, two and three deflectors respectively.

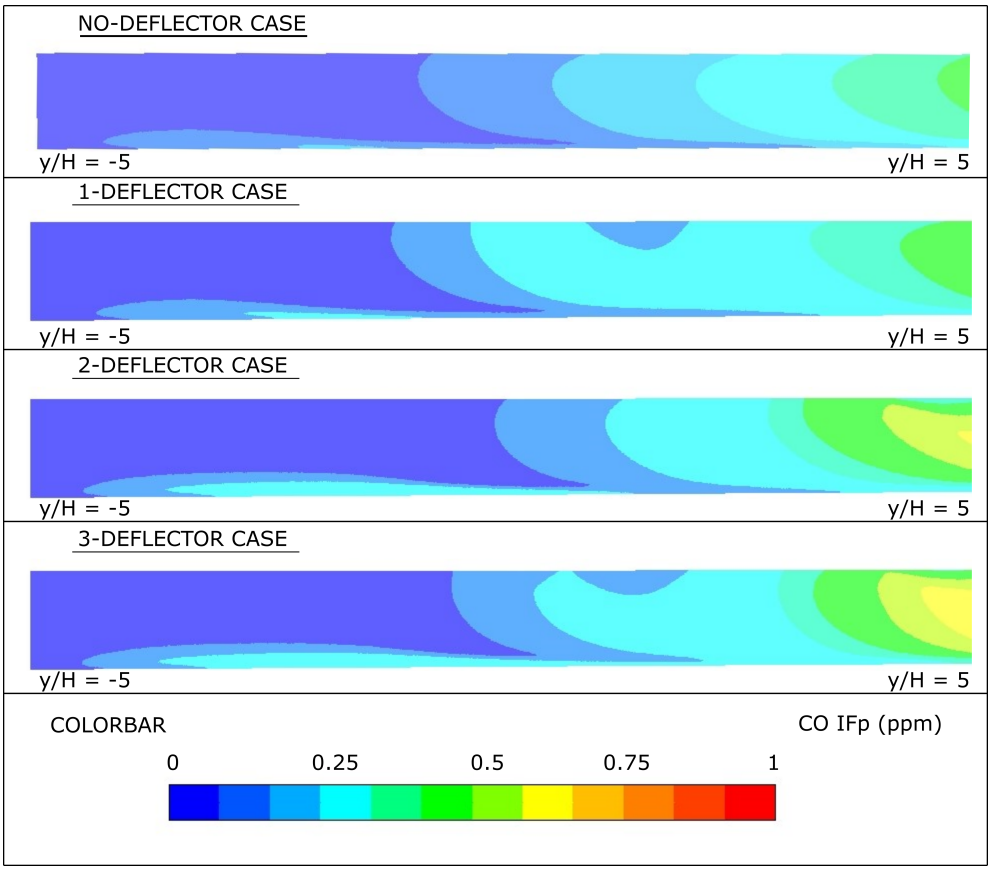

Figure 7.15: Contour of CO IF_p across the windward facade (plotted $-5 \leq y/H \leq 5$) under oblique ambient winds at 45° with no deflectors and one, two and three deflectors respectively.

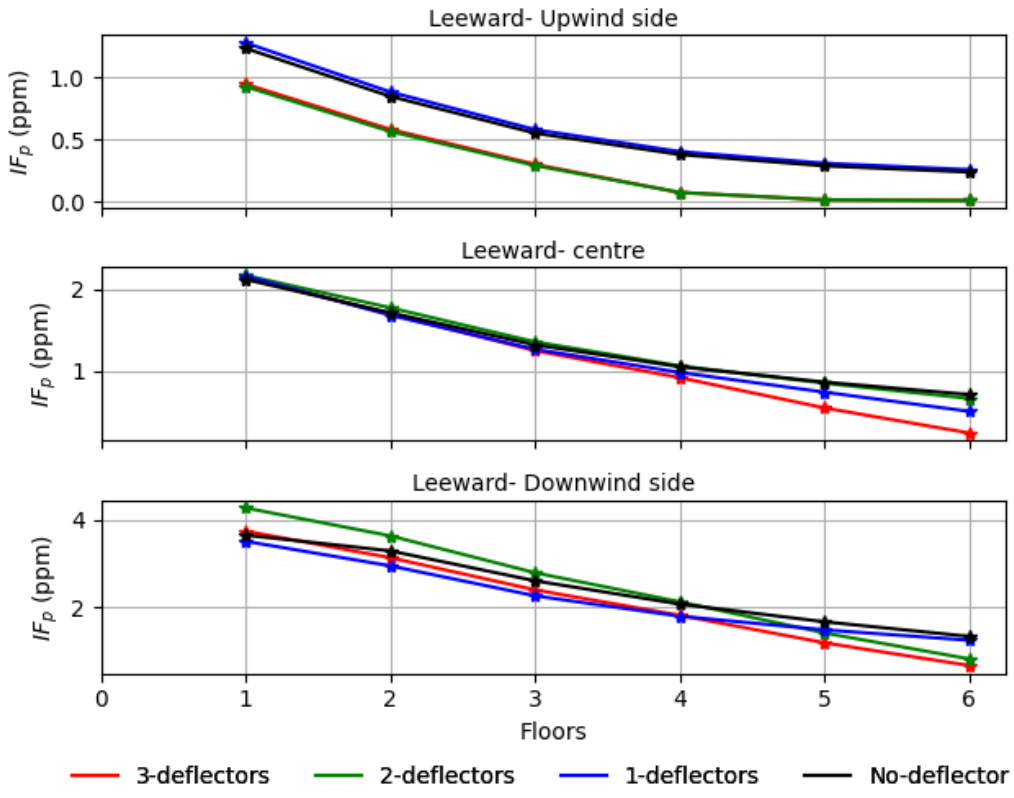

Figure 7.16: Localized variation of CO IF_p across the height of the leeward under oblique ambient winds at 45° with no deflectors and one, two and three deflectors respectively.

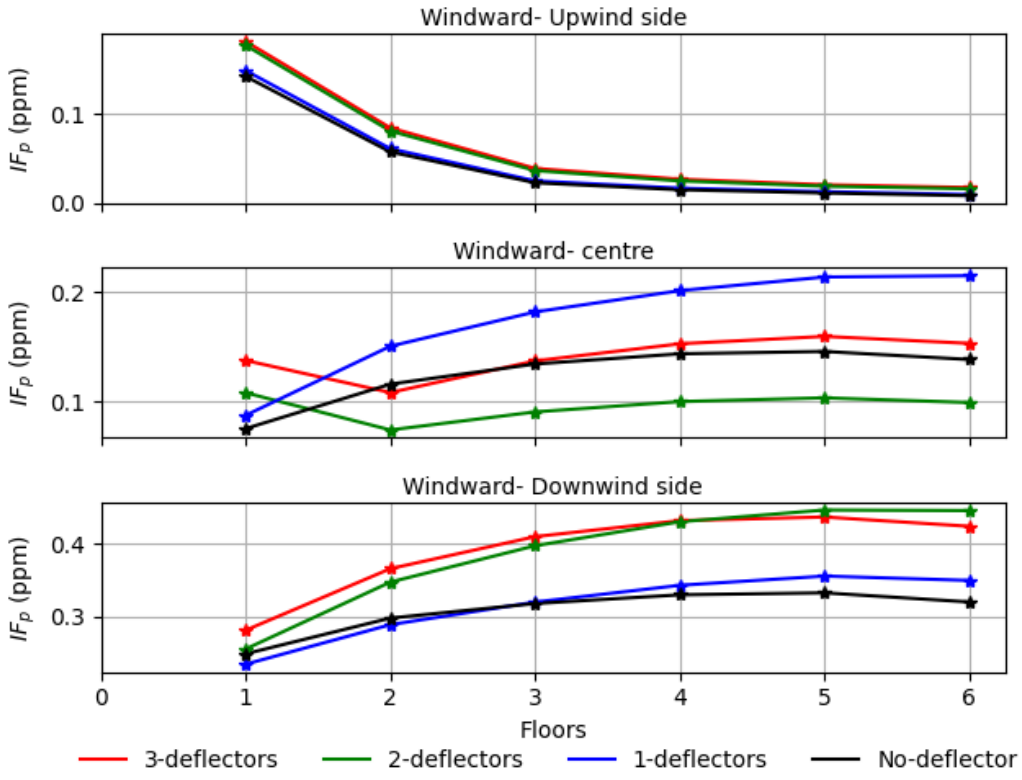

Figure 7.17: Localized variation of CO IF_p across the height of the windward under oblique ambient winds at 45° with no deflectors and one, two and three deflectors respectively.

7.8.2 Pearse Street environment

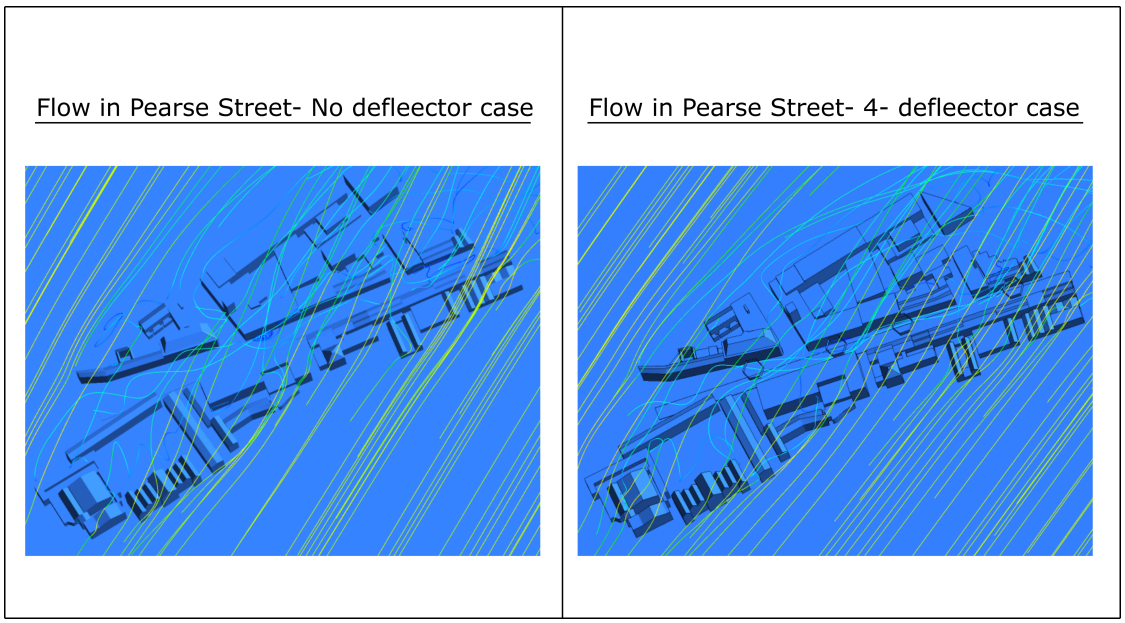

Figure 7.18: Comparison of flow streamlines in the Pearse Street environment with and without the inclusion of multi-directional wind flow deflectors.

As in the case of the oblique incident wind for the ideal isolated street canyon in the theoretical case, the ambient wind was seen to both rise through and be oscillating between the leeward and windward facades in the Pearse Street environment. Figure 7.18 shows the streamlines of the flow when no-deflectors and 4-deflectors in potential street canyon hotspots were included. Figure 7.19 shows the contour of CO IF_p and velocity magnitude at $z = 0.5m$ and $z = 10m$ respectively. As can be seen from Figure 7.19, the multi-directional wind deflectors did not substantially change the nature of the flow regime. Figure 7.20 shows the average CO IF_p along the target leeward and windward facades marked in Figure 7.6 (facade numbering in ascending order from upwind to downwind region). As can be seen in Figure 7.20, the the multi-directional wind deflectors had a mixed impact on the windward facades where negligible changes were observed in windward facades 1 and 3. CO IF_p changes across the windward facades 2 and 4 experienced an increase and reduction of 19.5% and 15.3% respectively. However, the leeward facades with the multi-directional deflectors experienced a modest CO IF_p reduction throughout. Leeward facades 2 and 3 experienced 16.1% and 12.1% reductions, while leeward facade 1 experienced similar CO exposure as the no deflector scenario. Such an influence is accounted to the two major influences imparted by the multi-directional

wind flow deflectors. One, as Figure 7.18 shows, the ambient wind has been pushed downwards and this has particularly benefited the leeward side facades with reduced CO exposure. The other major influence is similar to the observation made in the theoretical cases. As the wind oscillates between the leeward and windward facades, especially downstream after leaving leeward facade-2, the deflector stretches out the region of contact of polluted air before it leaves windward facade-2 by aligning the flow parallel to the facade. However, the wind deflector by pushing the ambient wind downwards again in the downwind end of the canyon reduces exposure in windward-facade 4.

There are few considerations here that are worth mentioning again to further the understanding of the deflectors and the scope of the present work. Unlike in the theoretical case studies, an explicit ABL profile using UDF for the velocity-inlet boundary condition was not included for simplicity, but a uniform ambient wind velocity was considered. This means that the performance could have been better in reality as for now the difference in velocity of wind at the polluted ground level and the roof level where the deflector pushes the wind downward is lesser than if an ABL were included. Secondly, it would be essential to incorporate the influence of built environment in the surrounding streets and vegetation to represent the reality more closely.

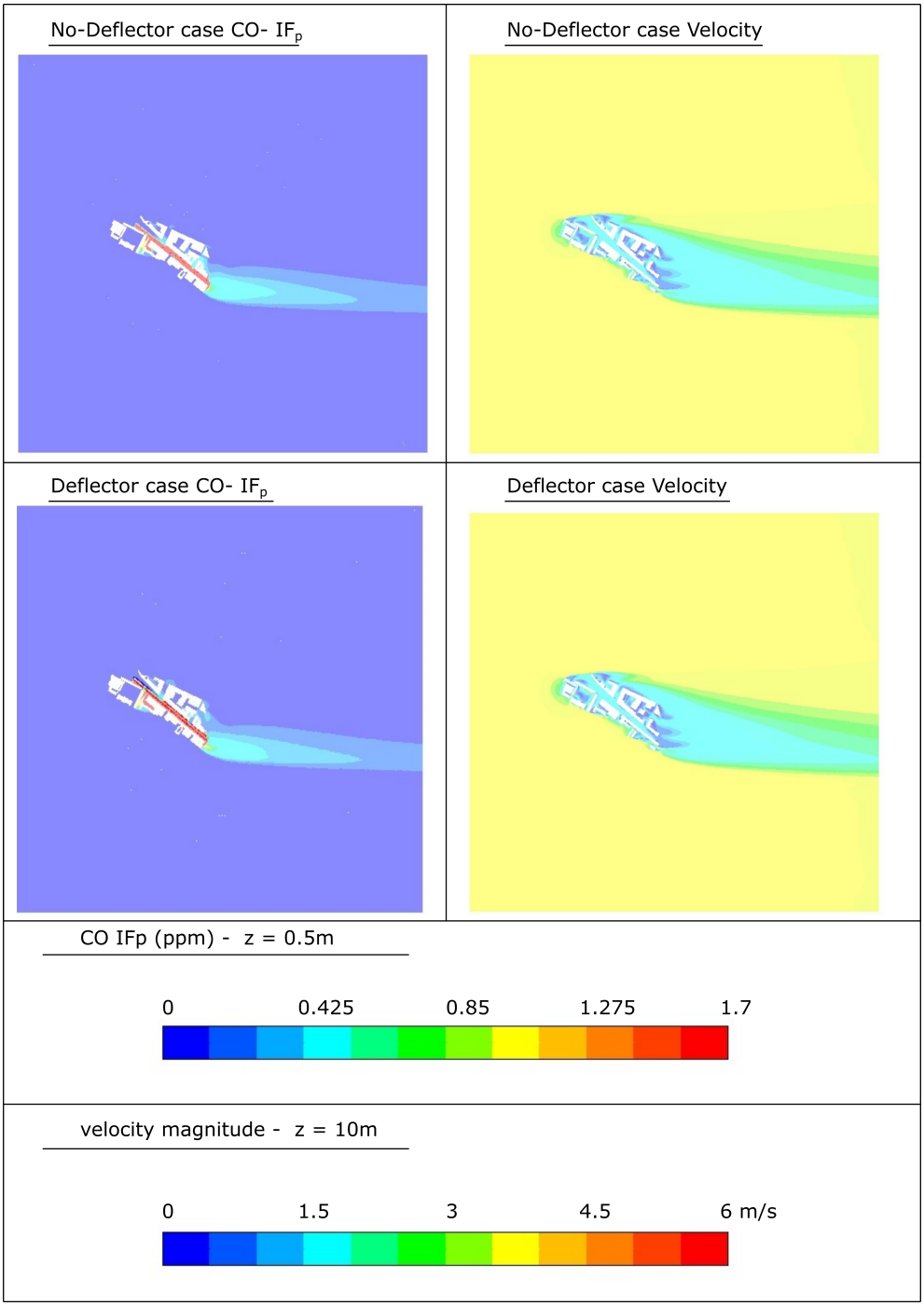

Figure 7.19: Contour plots of CO IF_p and velocity magnitude in the Pearse Street environment with and without the inclusion of multi-directional wind flow deflectors.

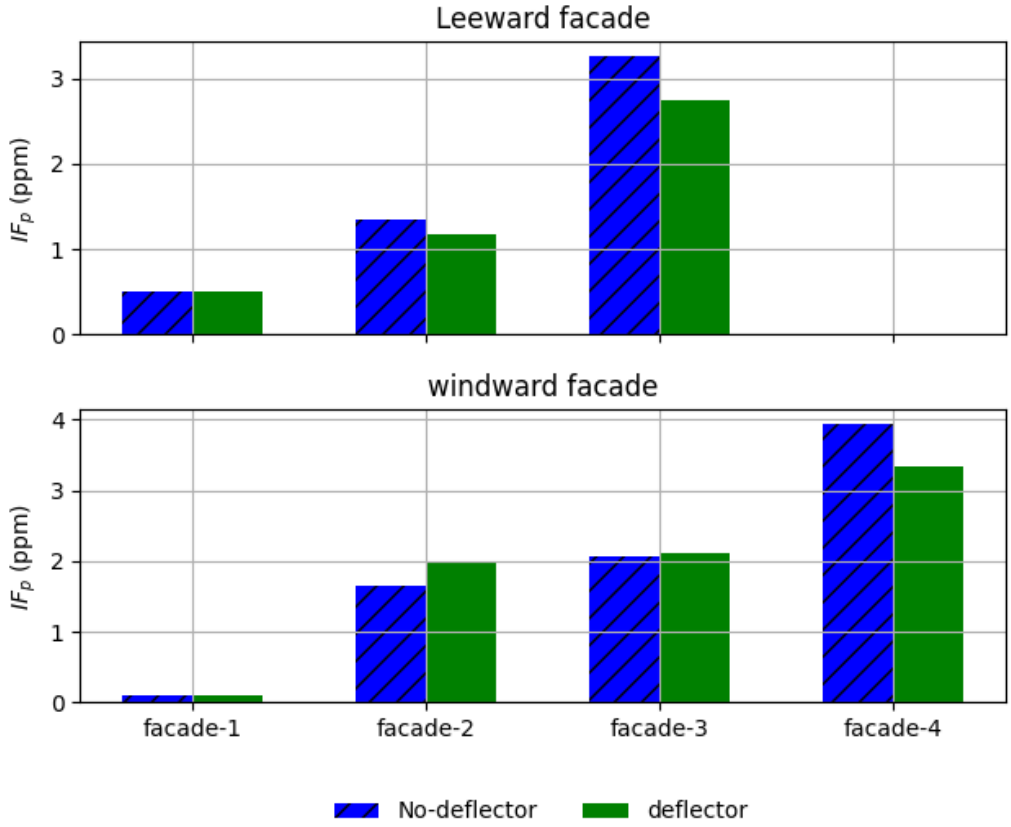

Figure 7.20: Comparison of average CO IF_p across the target windward and leeward facades in the Pearse Street environment with and without the inclusion of multi-directional wind flow deflectors.

7.8.3 Conclusions

Previous chapters were dedicated to developing adaptive solutions for changing environmental conditions. However, in this chapter, the efficacy of a common solution for changing wind directions was evaluated by conceptualizing a multi-directional wind deflector system. The multi-directional wind deflectors were more efficient in pushing the ambient winds downward when the winds were parallel to the ideal street canyon and that CO IF_p reduced as much as 45-50% in the upwind region even in Floor 1 on both the leeward and windward facades. However, the effect of the deflectors facilitated minimal wash-down across leeward facade when the ambient wind was orthogonal to the street canyon. This was less prominent in the side regions of the street canyon as compared to the central region as the strong side recirculations overshadowed this. The windward facade experienced higher CO IF_p when the deflectors were included as compared to the no deflector scenarios. On the contrary, the wash-down influence of the wind deflectors along the leeward facade weakened as the flow rose and strengthened downstream.
In general, the results from this chapter have demonstrated that although the multi-directional wind deflectors in principle are capable of handling ambient winds with differing angles of incidence, their walls offer minimal area of obstruction to effectively enhance the interaction between the air contained within the street canyons and the above-roof ambient winds. Perhaps, the flat plate deflectors if oriented to obstruct the ambient winds orthogonally could have benefited more in enhancing mixing of in and above canyon air. Although, it might appear premature to conclude so for isolated street canyon models based on the implications of flat plate deflector models for city-type environment, the fundamental idea of the multi-directional wind deflector was rooted in the same. It is also worth mentioning at this stage that the multi-directional wind deflectors were initially designed to be 3m high (1.5m above and below the canyon roof) before the design with 6m height was adopted. The design with 3m deflector height resulted in negligible influence on flow field and CO IF_p across the leeward and windward facades. This furthered the understanding that the same deflector-height/building-height ratio of multi-directional wind deflector as the flat plate deflector resulted in lesser efficiency and that a reasonable amount of air mixing enhancement had to be achieved through doubling the height of the deflector. However such large deflector system may be less practical if it came to installation. Future work on the practical implementation of deflector systems should consider the following:

1. How often does the real street environment undergo changes in the wind direction. In a scenario where the ambient wind approaches the target street canyon in the predominant direction for 20-24 hours a day, it would be practical to consider the implementation of flat plate deflectors orthogonally obstructing the same.

2. If the scenario involved a more complex distribution of wind patterns, where a substantial amount time included ambient winds not along the predominant wind direction, a necessity for either adjustable or multi-directional wind flow deflectors is rational. Furthermore, the choice between adjustable and multi-directional wind flow deflectors could be based on factors including frequency of ambient wind direction, responsiveness of the adjustable wind flow deflectors to adapt and opportunity for including larger design of multi-directional wind deflectors as the available contact surface is a crucial parameter for the efficacy of the same.

Chapter 8

Conclusions and future work

8.1 General summary

Near-road buildings experience elevated levels of exposure to traffic pollution. Various passive interventions have been studied in the past for their efficacy in mitigating high personal exposure in near-road buildings. Roof-level interventions offer superior characteristics because they can naturally promote the mixing between the above-deck ambient winds and the air contained within the street canyons and because they practically do not depend on the surface and subsurface infrastructure and negatively impact on mobility. However, roof-level wind catchers have generally been implemented in a static setup despite the dynamic nature of the environment. The conceptualization of roof-level passive interventions is also pending. Therefore, the present work was outlined with different application and theoretical research questions through four independent chapters. This included analyzing the efficacy of the wind deflectors:

1. with a dynamic setting in 2D environments under orthogonal ambient winds.
2. with a dynamic setting in ideal 3-D city-type environments under orthogonal ambient winds.
3. with a dynamic setting in asymmetric 3-D city type environments under orthogonal ambient winds.
4. with a dynamic setting in asymmetric 3-D city type environments under orthogonal and orthogonal ambient winds.

5. with a static wind multi-directional wind deflector setup in ideal with different ambient wind flow directions and real isolated street canyons with predominant wind flow wind direction in Dublin.

8.2 Major findings

Based on the research undertaken, it can be concluded that

1. There is sufficient evidence for the PCH_{mean} vs $\bar{C}_{canyon}$ inverse correlation hypothesis from urban 2D and 3D city-type environments with ideal and asymmetric street canyons (step-down and step-up). This also emphasized that adjustable wind deflectors were able to regulate $\bar{C}_{canyon}$ by altering PCH_{mean} and PCH_{fluc} by their operational location at the roof level.
2. From the application of field synergy theory to asymmetric street canyons in 3D city-type environments, an inverse correlation between Sh and $\bar{C}_{canyon}$ is demonstrated. This explains that when the removal of pollution through convective fluxes was increased, $\bar{C}_{canyon}$ was reduced, meaning that these facilitated the global removal of pollutants from the canyon. of the street. It is worth noting that in a simultaneous evaluation of θ vs $\bar{C}_{canyon}$ and Sh vs $\bar{C}_{canyon}$, the latter performed specifically better in distinguishing between the scenarios which included the wind deflector and which did not.
3. The adjustable wind flow deflectors proved to reduce the $\bar{C}_{canyon}$ by 2.84 fold in the target street canyon in 2D street canyon environment. Despite a significant the $\bar{C}_{canyon}$ reduction at a particular location, the requirement of adjustable wind flow deflector of was conceptualized based on varying CO exposures across the building facades in the target street canyon. This concept was furthered by demonstrating the opportunity to mitigate mitigate prolonged exposure due to diurnal changes in the traffic flow pattern. It was demonstrated by adjusting the deflector position suitably in an ideal 3D configuration ($H_1 = H_2 = w = 12m$). This was done by considering the CRP and SRP source models in the 3D city-type environment.
4. While applying the adjustable wind flow deflectors for the steep asymmetric environments including step-down ($H_1 = 2H_2 = w = 30m$) and step-up ($2H_1 = H_2 = w = 30m$) target street canyons, the concept proved to be effective for step-down target street canyons despite the initial offset of reduced ACH offered by the steep-city environment. However, the adjustable wind

deflectors resulted in generally detrimental results for the step-up target street canyons. Nevertheless, it is worth noting that the deflectors were presently evaluated at the upwind building roof level. Inclusion of passive interventions at the roof level presents flexibility as there are no restrictions to surface mobility and any indoor or outdoor infrastructure.

5. The combined sensitivity of the wind deflector for changes in traffic and wind flow directions was evaluated using a two-step optimization process. As in Chapters 4 and 5, the best location for the deflector in a steep asymmetric city-type canyon ($H_1 = H_2 = 2w_1 = w_2 = 30m$) with CRP and SRP source models was evaluated by considering different locations at the roof level. The optimal locations indicated an opportunity to mitigate a modest 15.8% and a substantial 48.2% reduction of CO IF_p across the leeward and windward facades respectively with CRP source model. This was 34% across the downwind side facade with the SRP source model under orthogonal wind conditions. As a second step, for the oblique winds with CRP and SRP source models, the deflectors were pivoted by 45° about their respective optimal locations (as identified from the orthogonal wind conditions) to perpendicularly obstruct and deflect the ambient winds into the street canyons. With modest influence on the windward and downwind side facades, this technique mitigated about 47.3% and 62.2% of CO IF_p across the leeward facade in the target street canyon with CRP and SRP source models respectively.
6. The multi-directional wind deflectors were not as effective as the flat plate deflectors in general, simply because of the reduced contact area it offered to deflect the ambient above roof winds into the street canyon. Although conceptually it offered equal potential to deflect parallel, oblique and orthogonal winds, the street canyons benefited from it the most under parallel wind conditions where even the ground level ventilation improved as the above roof winds were pushed downwards. The leeward facade experienced varying level of relief from the deflector depending on how much wash-down could be achieved amidst the lateral wind and streamwise flows. The windward facade generally experienced detrimental impact for oblique and orthogonal winds with the multi-directional wind deflectors. The results of the multi-directional wind deflectors in Pearse Street environment reflected the results from the ideal isolated street canyons. A modest 15% CO IF_p reduction across the target leeward facades and mixed minimal influence to subject target windward facades to experience about -20 to 15% CO IF_p was observed in the Pearse

Street environment. Although, the study included several simplifications including constant wind speeds, lack of vegetation cover and lack of inclusion of effects of surrounding street built environments, it presented some crucial understanding in correlating the results conducted based on ideal and real street environments. Furthermore, as in the case of the theoretical cases, it is important to conduct floor wise analyses of CO IF_p across the target facades in real street environment and include more details including actual windows to better the understanding of the implications of wind deflectors on IAQ.

8.3 Future work

The study intended to develop a methodology that establishes a fundamental understanding of wind deflectors in simplified contexts that can be evaluated for efficacy of utilizing these in scenarios involving varying complexities. Both numerical and application-based choices added to the scope and limitations of the current research. The numerical limitations of the work are discussed in Chapter 4 where the methodology is detailed. Traffic, local meteorology, pollutants and micro-environment detailing present scenarios and parameters that could sharply affect the current research findings.

The buildings considered in the study were monolithic and devoid of explicitly modeled features including open doors, windows, balconies and overhangs. The exposure outside the demarcated windows on the building facades was considered indoor exposure of the building occupants in specific regions on a particular floor. Therefore, no specific correlations between indoor and ambient AQ were employed for analyses. The simplification of detailing also extended to street layouts where dedicated pedestrian footpaths were considered only for isolated street canyon scenarios in Chapter 7. Furthermore, no additional details in the canyons including vegetation, viaducts, noise barriers, arcades or elevated building designs were included in the analyses of the current research. Traffic-related scenarios that affect the models include the dynamic effects of Vehicle Induced Turbulence (VIT), fleet compositions from both design and emission perspectives and the inclusion of car parks in the street canyon models. From the meteorological side, the buildings were subject to neutrally stratified stable Atmospheric Boundary Layer (ABL) flows under isothermal conditions. This meant that diurnal temperature changes in the facades and streets due to surface heating and cooling were not incorporated in the analyses of this research. Although the effect of wind speeds was studied, the ambient winds

were always considered to be steady involving no transient gusts. It is worth noting that although the wind deflectors were evaluated in a dynamic framework from a practical standpoint where they were either moved or rotated about an axis for varying environmental conditions, only the static influence of wind deflectors was evaluated for each of its configurations and not dynamic implications of moving or tilting. The performance evaluation of the wind deflectors was applied to only the dispersion of gaseous pollutants and not the particulates. The study was completely based on results from computational work and no experiments or field measurements were conducted, albeit all models were rigorously validated using available and relevant wind tunnel data.

Finally, from an optimization standpoint, the adaptivity of wind deflectors was evaluated for simultaneously changing two environmental variables, wind direction and traffic flow changes. However, in reality, these changes could be accompanied by other changes including wind gusts, humidity and temperature changes which substantially affect pollution dispersion. Considering a multi-variate optimization with several variables in the context of developing CFD solutions could be both computationally exhaustive and time-consuming. Therefore, high-fidelity CFD simulations could be utilized for developing reference data and surrogate modeling techniques could be used for rapid decision making. This approach would allow one to develop a comprehensive database of optimal configurations of wind deflectors to be employed for a variety of environmental conditions.

Bibliography

Abhijith, K., & Gokhale, S. (2015). Passive control potentials of trees and on-street parked cars in reduction of air pollution exposure in urban street canyons. *Environmental pollution*, *204*, 99–108.

Abhijith, K., Kumar, P., Gallagher, J., McNabola, A., Baldauf, R., Pilla, F., Broderick, B., Di Sabatino, S., & Pulvirenti, B. (2017). Air pollution abatement performances of green infrastructure in open road and built-up street canyon environments–a review. *Atmos. Environ.*, *162*, 71–86.

Act, E. P. (2005). Energy policy act of 2005. *US Congress*, 1–27.

Ahangar, F. E., Heist, D., Perry, S., & Venkatram, A. (2017). Reduction of air pollution levels downwind of a road with an upwind noise barrier. *Atmospheric Environment*, *155*, 1–10.

Alam, M. S., & McNabola, A. (2014). A critical review and assessment of eco-driving policy & technology: Benefits & limitations. *Trans. Policy*, *35*, 42–49.

Antoniou, N., Montazeri, H., Wigo, H., Neophytou, M. K.-A., Blocken, B., & Sandberg, M. (2017). Cfd and wind-tunnel analysis of outdoor ventilation in a real compact heterogeneous urban area: Evaluation using "air delay". *Build. Environ.*, *126*, 355–372.

Atkinson, R. W., Barratt, B., Armstrong, B., Anderson, H. R., Beevers, S. D., Mudway, I. S., Green, D., Derwent, R. G., Wilkinson, P., Tonne, C., et al. (2009). The impact of the congestion charging scheme on ambient air pollution concentrations in london. *Atmospheric Environment*, *43*(34), 5493–5500.

Bady, M., Kato, S., & Huang, H. (2008). Towards the application of indoor ventilation efficiency indices to evaluate the air quality of urban areas. *Build. Environ.*, *43*(12), 1991–2004.

Baratian-Ghorghi, Z., & Kaye, N. B. (2013). The effect of canyon aspect ratio on flushing of dense pollutants from an isolated street canyon. *Sci. Total Environ.*, *443*, 112–122.

Bartlett, E. S., & Trasande, L. (2014). Economic impacts of environmentally attributable childhood health outcomes in the european union. *The European Journal of Public Health*, *24*(1), 21–26.

Beig, G., Sahu, S. K., Singh, V., Tikle, S., Sobhana, S. B., Gargeva, P., Ramakrishna, K., Rathod, A., & Murthy, B. (2020). Objective evaluation of stubble emission of north india and quantifying its impact on air quality of delhi. *Science of The Total Environment*, *709*, 136126.

Bodansky, D. (1993). The united nations framework convention on climate change: A commentary. *Yale J. Int'l l.*, *18*, 451.

Brandt, S. J., Perez, L., Künzli, N., Lurmann, F., & McConnell, R. (2012). Costs of childhood asthma due to traffic-related pollution in two california communities. *European Respiratory Journal*, *40*(2), 363–370.

Brimblecombe, P. (1978). Air pollution in industrializing england. *Journal of the Air Pollution Control Association*, *28*(2), 115–118.

Buccolieri, R., Carlo, O. S., Rivas, E., Santiago, J. L., Salizzoni, P., & Siddiqui, M. S. (2022). Obstacles influence on existing urban canyon ventilation and air pollutant concentration: A review of potential measures. *Building and Environment*, *214*, 108905.

Buccolieri, R., Sandberg, M., & Di Sabatino, S. (2010). City breathability and its link to pollutant concentration distribution within urban-like geometries. *Atmospheric Environment*, *44*(15), 1894–1903.

Cao, Z., Yang, X., Wang, Y., Zhao, T., Zhai, C., & Wu, S. (2023). Analysis of fugitive emission dispersion from urban industrial buildings and optimization using wind catchers. *Journal of Wind Engineering and Industrial Aerodynamics*, *239*, 105448.

Challoner, A., & Gill, L. (2014). Indoor/outdoor air pollution relationships in ten commercial buildings: Pm2. 5 and no2. *Building and Environment*, *80*, 159–173.

Chen, L., Hang, J., Sandberg, M., Claesson, L., & Di Sabatino, S. (2017). The influence of building packing densities on flow adjustment and city breathability in urban-like geometries. *Procedia engineering*, *198*, 758–769.

Chen, Q., Ren, J., & Guo, Z. (2008). Field synergy analysis and optimization of decontamination ventilation designs. *Int. J. of Heat Mass Transf.*, *51*(3-4), 873–881.

Cheng, W., & Liu, C.-H. (2011). Large-eddy simulation of flow and pollutant transports in and above two-dimensional idealized street canyons. *Bound. Layer Meteorol.*, *139*, 411–437.

Cheng, W., Liu, C.-H., & Leung, D. Y. (2008). Computational formulation for the evaluation of street canyon ventilation and pollutant removal performance. *Atmos. Environ.*, *42*(40), 9041–9051.

Cheng, W., Liu, C.-H., & Leung, D. Y. (2009). On the correlation of air and pollutant exchange for street canyons in combined wind-buoyancy-driven flow. *Atmos. Environ.*, *43*(24), 3682–3690.

Chew, L. W., Nazarian, N., & Norford, L. (2017). Pedestrian-level urban wind flow enhancement with wind catchers. *Atmos.*, *8*(9), 159.

Claus, J., Coceal, O., Thomas, T. G., Branford, S., Belcher, S. E., & Castro, I. P. (2012). Wind-direction effects on urban-type flows. *Boundary-layer meteorology*, *142*, 265–287.

Collins, C. M., Otero, A., & Woodward, H. (2022). Shape matters: Reducing people's exposure to poor air quality using sculpted infrastructure elements. *Cities & Health*, *6*(2), 275–281.

Costa, L. G., Cole, T. B., Dao, K., Chang, Y.-C., Coburn, J., & Garrick, J. M. (2020). Effects of air pollution on the nervous system and its possible role in neurodevelopmental and neurodegenerative disorders. *Pharmacology & therapeutics*, *210*, 107523.

Cui, D., Li, X., Du, Y., Mak, C. M., & Kwok, K. (2020). Effects of envelope features on wind flow and pollutant exposure in street canyons. *Build. Environ.*, *176*, 106862.

da Silva, F. T., Reis Jr, N. C., Santos, J. M., Goulart, E. V., & de Alvarez, C. E. (2021). The impact of urban block typology on pollutant dispersion. *J. Wind Eng. Ind. Aerodyn.*, *210*, 104524.

da Silva, F. T., Reis Jr, N. C., Santos, J. M., Goulart, E. V., & de Alvarez, C. E. (2022). Influence of urban form on air quality: The combined effect of block typology and urban planning indices on city breathability. *Sci. Total Environ.*, *814*, 152670.

Dat, N.-D., & Chang, M. B. (2017). Review on characteristics of pahs in atmosphere, anthropogenic sources and control technologies. *Science of the total environment*, *609*, 682–693.

Davidson, L., et al. (2011). Fluid mechanics, turbulent flow and turbulence modeling. *Chalmers University of Technology, Goteborg, Sweden (Nov 2011)*.

Delbeke, J., Runge-Metzger, A., Slingenberg, Y., & Werksman, J. (2019). The paris agreement. In *Towards a climate-neutral europe* (pp. 24–45). Routledge.

Ding, S., Huang, Y., Cui, P., Wu, J., Li, M., & Liu, D. (2019). Impact of viaduct on flow reversion and pollutant dispersion in 2d urban street canyon with different roof shapes-numerical simulation and wind tunnel experiment. *Sci. Total Environ.*, *671*, 976–991.

Directive, E. (2005). Directive 2005/55/ec of the european parliament and of the council of 28 september 2005 on the approximation of the laws of the member states relating to the measures to be taken against the emission of gaseous and particulate pollutants from compression-ignition engines for use in vehicles, and the emission of gaseous pollutants from positive-ignition engines fuelled with natural gas or liquefied petroleum gas for use in vehicles. *Official Journal of the European Communities L*, *275*, 1–163.

Du, Y., Mak, C. M., Liu, J., Xia, Q., Niu, J., & Kwok, K. C. (2017). Effects of lift-up design on pedestrian level wind comfort in different building configurations under three wind directions. *Building and Environment*, *117*, 84–99.

Ellison, R. B., Greaves, S. P., & Hensher, D. A. (2013). Five years of london's low emission zone: Effects on vehicle fleet composition and air quality. *Transportation Research Part D: Transport and Environment*, *23*, 25–33.

Ernst, A., & Zibrak, J. D. (1998). Carbon monoxide poisoning. *New England journal of medicine*, *339*(22), 1603–1608.

Fang, Y., Mauzerall, D. L., Liu, J., Fiore, A. M., & Horowitz, L. W. (2013). Impacts of 21st century climate change on global air pollution-related premature mortality. *Climatic Change*, *121*, 239–253.

Franke, J., Hellsten, A., Schlunzen, K. H., & Carissimo, B. (2011). The cost 732 best practice guideline for cfd simulation of flows in the urban environment: A summary. *Int. J. Environ. Pollut.*, *44*(1-4), 419–427.

Fu, P., Guo, X., Cheung, F. M. H., & Yung, K. K. L. (2019). The association between pm2. 5 exposure and neurological disorders: A systematic review and meta-analysis. *Science of the Total Environment*, *655*, 1240–1248.

Gaber, N., Ibrahim, A., Rashad, A. B., Wahba, E., El-Sayad, Z., & Bakr, A. F. (2020). Improving pedestrian micro-climate in urban canyons: City center of alexandria, egypt. *Urban Climate*, *34*, 100670.

Galinato, G. I., & Yoder, J. K. (2010). An integrated tax-subsidy policy for carbon emission reduction. *Resource and Energy Economics*, *32*(3), 310–326.

Gallagher, J., Gill, L. W., & McNabola, A. (2012). Numerical modelling of the passive control of air pollution in asymmetrical urban street canyons using refined mesh discretization schemes. *Build. Environ.*, *56*, 232–240.

Gallagher, J., Gill, L., & McNabola, A. (2013). The passive control of air pollution exposure in dublin, ireland: A combined measurement and modelling case study. *Sci. Total Environ.*, *458*, 331–343.

Gallagher, J., & Lago, C. (2019). How parked cars affect pollutant dispersion at street level in an urban street canyon? a cfd modelling exercise assessing geometrical detailing and pollutant decay rates. *Sci. Total Environ.*, *651*, 2410–2418.

Gallagher, J. (2013). *An investigation of the passive control of air pollution in the urban environment* (Doctoral dissertation). Trinity College Dublin.

Gallagher, J., Gill, L. W., & McNabola, A. (2011). Optimizing the use of on-street car parking system as a passive control of air pollution exposure in street canyons by large eddy simulation. *Atmos. Environ.*, *45*(9), 1684–1694.

Gallagher, M., Basu, B., Ghosh, B., Alam, M. S., Gill, L., Kamber, B., & McNabola, A. (2021). Particulate matter from diesel vehicles: Emissions and exposure.

Garcia-Menendez, F., Saari, R. K., Monier, E., & Selin, N. E. (2015). Us air quality and health benefits from avoided climate change under greenhouse gas mitigation. *Environmental Science & Technology*, *49*(13), 7580–7588.

Ghasemian, M., Amini, S., & Princevac, M. (2017). The influence of roadside solid and vegetation barriers on near-road air quality. *Atmospheric Environment*, *170*, 108–117.

Ghosh, A. (2020). Possibilities and challenges for the inclusion of the electric vehicle (ev) to reduce the carbon footprint in the transport sector: A review. *Energies*, *13*(10), 2602.

Giblin, S., & McNabola, A. (2009). Modelling the impacts of a carbon emission-differentiated vehicle tax system on co2 emissions intensity from new vehicle purchases in ireland. *Energy Policy*, *37*(4), 1404–1411.

Goel, A., & Kumar, P. (2015). Zone of influence for particle number concentrations at signalised traffic intersections. *Atmos. Environ.*, *123*, 25–38.

Gokhale, S., & Khare, M. (2007). Statistical behavior of carbon monoxide from vehicular exhausts in urban environments. *Environ. Model. Softw.*, *22*(4), 526–535.

Gong, L., & Wang, X. (2018). Numerical study of noise barriers' side edge effects on pollutant dispersion near roadside under various thermal stability conditions. *Fluids*, *3*(4), 105.

Gulia, S., Goyal, P., Goyal, S., & Kumar, R. (2019). Re-suspension of road dust: Contribution, assessment and control through dust suppressants—a review. *Int. J. Environ. Sci. Technol.*, *16*(3), 1717–1728.

Gulia, S., Kaur, S., Mendiratta, S., Tiwari, R., Goyal, S., Gargava, P., & Kumar, R. (2022). Performance evaluation of air pollution control device at traffic intersections in delhi. *Int. J. Environ. Sci. Technol.*, *19*(2), 785–796.

Haerens, M. (2011). *Air pollution*. Greenhaven Publishing LLC.

Han, S. S. (2010). Managing motorization in sustainable transport planning: The singapore experience. *Journal of Transport Geography*, *18*(2), 314–321.

Hang, J., & Li, Y. (2010). Ventilation strategy and air change rates in idealized high-rise compact urban areas. *Building and Environment*, *45*(12), 2754–2767.

Hang, J., & Li, Y. (2011). Age of air and air exchange efficiency in high-rise urban areas and its link to pollutant dilution. *Atmospheric Environment*, *45*(31), 5572–5585.

Hang, J., Li, Y., Sandberg, M., Buccolieri, R., & Di Sabatino, S. (2012). The influence of building height variability on pollutant dispersion and pedestrian ventilation in idealized high-rise urban areas. *Build. Environ.*, *56*, 346–360.

Hang, J., Li, Y., Sandberg, M., & Claesson, L. (2010). Wind conditions and ventilation in high-rise long street models. *Building and Environment*, *45*(6), 1353–1365.

Hang, J., Luo, Z., Sandberg, M., & Gong, J. (2013). Natural ventilation assessment in typical open and semi-open urban environments under various wind directions. *Building and environment*, *70*, 318–333.

Hang, J., Luo, Z., Wang, X., He, L., Wang, B., & Zhu, W. (2017). The influence of street layouts and viaduct settings on daily carbon monoxide exposure and intake fraction in idealized urban canyons. *Environ. Pollut.*, *220*, 72–86.

Hang, J., Sandberg, M., & Li, Y. (2009a). Age of air and air exchange efficiency in idealized city models. *Building and Environment*, *44*(8), 1714–1723.

Hang, J., Sandberg, M., & Li, Y. (2009b). Effect of urban morphology on wind condition in idealized city models. *Atmospheric environment*, *43*(4), 869–878.

Hang, J., Sandberg, M., Li, Y., & Claesson, L. (2009c). Pollutant dispersion in idealized city models with different urban morphologies. *Atmospheric Environment*, *43*(38), 6011–6025.

Hang, J., Xian, Z., Wang, D., Mak, C. M., Wang, B., & Fan, Y. (2018). The impacts of viaduct settings and street aspect ratios on personal intake fraction in three-dimensional urban-like geometries. *Build. Environ.*, *143*, 138–162.

Hao, C., Xie, X., Huang, Y., & Huang, Z. (2019). Study on influence of viaduct and noise barriers on the particulate matter dispersion in street canyons by cfd modeling. *Atmos. Pollut. Res.*, *10*(6), 1723–1735.

Haque, M. M., Chin, H. C., & Debnath, A. K. (2013). Sustainable, safe, smart—three key elements of singapore's evolving transport policies. *Transport policy*, *27*, 20–31.

Hashad, K., Yang, B., Baldauf, R. W., Deshmukh, P., Isakov, V., & Zhang, K. M. (2020). Enhancing the local air quality benefits of roadside green infrastructure using low-cost, impermeable, solid structures (liss). *Science of the total environment*, *717*, 137136.

He, L., Hang, J., Wang, X., Lin, B., Li, X., & Lan, G. (2017). Numerical investigations of flow and passive pollutant exposure in high-rise deep street canyons with various street aspect ratios and viaduct settings. *Sci. Total Environ.*, *584*, 189–206.

Hime, N. J., Marks, G. B., & Cowie, C. T. (2018). A comparison of the health effects of ambient particulate matter air pollution from five emission sources. *International journal of environmental research and public health*, *15*(6), 1206.

Ho, Y.-K., Liu, C.-H., & Wong, M. S. (2015). Preliminary study of the parameterisation of street-level ventilation in idealised two-dimensional simulations. *Build. Environ.*, *89*, 345–355.

Huang, Y.-d., He, W.-r., & Kim, C.-N. (2015). Impacts of shape and height of upstream roof on airflow and pollutant dispersion inside an urban street canyon. *Environ. Sci. Pollut. Res.*, *22*, 2117–2137.

Huang, Y.-D., Hou, R.-W., Liu, Z.-Y., Song, Y., Cui, P.-Y., Kim, C.-N., et al. (2019). Effects of wind direction on the airflow and pollutant dispersion inside a long street canyon. *Aerosol and Air Quality Research*, *19*(5), 1152–1171.

Huang, Y., Hu, X., & Zeng, N. (2009). Impact of wedge-shaped roofs on airflow and pollutant dispersion inside urban street canyons. *Build. Environ.*, *44*(12), 2335–2347.

Iwata, H., & Okada, K. (2014). Greenhouse gas emissions and the role of the kyoto protocol. *Environmental Economics and Policy Studies*, *16*, 325–342.

Johansson, C., Burman, L., & Forsberg, B. (2009). The effects of congestions tax on air quality and health. *Atmospheric Environment*, *43*(31), 4843–4854.

Jon, K. S., Luo, Y., Sin, C. H., Cui, P.-y., Huang, Y.-d., & Tokgo, J. (2023). Impacts of wind direction on the ventilation and pollutant dispersion of 3d street canyon with balconies. *Building and Environment*, *230*, 110034.

Kharol, S. K., McLinden, C. A., Sioris, C. E., Shephard, M. W., Fioletov, V., van Donkelaar, A., Philip, S., & Martin, R. V. (2017). Omi satellite observations of decadal changes in ground-level sulfur dioxide over north america. *Atmospheric Chemistry and Physics*, *17*(9), 5921–5929.

Khomenko, S., Cirach, M., Pereira-Barboza, E., Mueller, N., Barrera-Gómez, J., Rojas-Rueda, D., de Hoogh, K., Hoek, G., & Nieuwenhuijsen, M. (2021).

Premature mortality due to air pollution in european cities: A health impact assessment. *The Lancet Planetary Health*, *5*(3), e121–e134.

Kim, H., Kim, W.-H., Kim, Y.-Y., & Park, H.-Y. (2020). Air pollution and central nervous system disease: A review of the impact of fine particulate matter on neurological disorders. *Frontiers in Public Health*, *8*, 575330.

Krzyzanowski, M., & Cohen, A. (2008). Update of who air quality guidelines. *Air Quality, Atmosphere & Health*, *1*, 7–13.

Landrigan, P. J. (2017). Air pollution and health. *Lancet Public Health*, *2*(1), e4–e5.

Lauriks, T., Longo, R., Baetens, D., Derudi, M., Parente, A., Bellemans, A., Van Beeck, J., & Denys, S. (2021). Application of improved cfd modeling for prediction and mitigation of traffic-related air pollution hotspots in a realistic urban street. *Atmos. Environ.*, *246*, 118127.

Li, B., Qiu, Z., & Zheng, J. (2021). Impacts of noise barriers on near-viaduct air quality in a city: A case study in xi'an. *Build. Environ.*, *196*, 107751.

Li, X.-X., Liu, C.-H., & Leung, D. Y. (2005). Development of ak–ε model for the determination of air exchange rates for street canyons. *Atmos. environ.*, *39*(38), 7285–7296.

Li, X.-X., Liu, C.-H., & Leung, D. Y. (2009). Numerical investigation of pollutant transport characteristics inside deep urban street canyons. *Atmos. Environ.*, *43*(15), 2410–2418.

Li, X.-X., Liu, C.-H., Leung, D. Y., & Lam, K. M. (2006). Recent progress in cfd modeling of wind field and pollutant transport in street canyons. *Atmos. Environ.*, *40*(29), 5640–5658.

Li, Z., Shi, T., Wu, Y., Zhang, H., Juan, Y.-H., Ming, T., & Zhou, N. (2020). Effect of traffic tidal flow on pollutant dispersion in various street canyons and corresponding mitigation strategies. *Energy and Built Environment*, *1*(3), 242–253.

Lien, F.-S., & Yee, E. (2004). Numerical modelling of the turbulent flow developing within and over a 3-d building array, part i: A high-resolution reynolds-averaged navier—stokes approach. *Bound. Layer Meteorol.*, *112*, 427–466.

Lim, E., Ito, K., & Sandberg, M. (2013). New ventilation index for evaluating imperfect mixing conditions–analysis of net escape velocity based on rans approach. *Build. Environ.*, *61*, 45–56.

Lin, M., Hang, J., Li, Y., Luo, Z., & Sandberg, M. (2014). Quantitative ventilation assessments of idealized urban canopy layers with various urban layouts and the same building packing density. *Building and environment*, *79*, 152–167.

Lin, Y., Chen, G., Chen, T., Luo, Z., Yuan, C., Gao, P., & Hang, J. (2019). The influence of advertisement boards, street and source layouts on co dispersion and building intake fraction in three-dimensional urban-like models. *Build. Environ.*, *150*, 297–321.

Liu, C.-H., Leung, D. Y., & Barth, M. C. (2005). On the prediction of air and pollutant exchange rates in street canyons of different aspect ratios using large-eddy simulation. *Atmos. Environ.*, *39*(9), 1567–1574.

Liu, C.-H., Ng, C.-T., & Wong, C. C. (2015). A theory of ventilation estimate over hypothetical urban areas. *Journal of hazardous materials*, *296*, 9–16.

Liu, C.-H., & Wong, C. C. (2014). On the pollutant removal, dispersion, and entrainment over two-dimensional idealized street canyons. *Atmos. Res.*, *135*, 128–142.

Llaguno-Munitxa, M., & Bou-Zeid, E. (2018). Shaping buildings to promote street ventilation: A large-eddy simulation study. *Urban climate*, *26*, 76–94.

Lopes, D., Puga, H., Teixeira, J., Lima, R., Grilo, J., Dueñas-Pamplona, J., & Ferrera, C. (2024). Comparison of rans and les turbulent flow models in a real stenosis. *International Journal of Heat and Fluid Flow*, *107*, 109340.

Lubinska, A. (1985). Auto emissions: Europe agrees at last.

Mage, D., Ozolins, G., Peterson, P., Webster, A., Orthofer, R., Vandeweerd, V., & Gwynne, M. (1996). Urban air pollution in megacities of the world. *Atmospheric environment*, *30*(5), 681–686.

Mage, D. T., Zali, O., Organization, W. H., et al. (1992). *Motor vehicle air pollution: Public health impact and control measures edited by david mage and olivier zali* (tech. rep.). World Health Organization.

Mayer, H. (1999). Air pollution in cities. *Atmospheric environment*, *33*(24-25), 4029–4037.

McCreddin, A., Gill, L., Broderick, B., & McNabola, A. (2013). Personal exposure to air pollution in office workers in ireland: Measurement, analysis and implications. *Toxics*, *1*(1), 60–76.

McNabola, A., Broderick, B., & Gill, L. (2008). Reduced exposure to air pollution on the boardwalk in dublin, ireland. measurement and prediction. *Environment international*, *34*(1), 86–93.

McNabola, A., Broderick, B., & Gill, L. (2009). A numerical investigation of the impact of low boundary walls on pedestrian exposure to air pollutants in urban street canyons. *Sci. Total Environ.*, *407*(2), 760–769.

Meroney, R. N., Pavageau, M., Rafailidis, S., & Schatzmann, M. (1996). Study of line source characteristics for 2-d physical modelling of pollutant dispersion in street canyons. *J. Wind Eng. Ind. Aerodyn.*, *62*(1), 37–56.

Mersky, A. C., Sprei, F., Samaras, C., & Qian, Z. S. (2016). Effectiveness of incentives on electric vehicle adoption in norway. *Transportation Research Part D: Transport and Environment*, *46*, 56–68.

Mickley, L. J. (2007). A future short of breath? possible effects of climate change on smog. *Environment: Science and Policy for Sustainable Development*, *49*(6), 32–43.

Ming, T., Fang, W., Peng, C., Cai, C., De Richter, R., Ahmadi, M. H., & Wen, Y. (2018). Impacts of traffic tidal flow on pollutant dispersion in a non-uniform urban street canyon. *Atmos.*, *9*(3), 82.

Ming, T., Han, H., Zhao, Z., de Richter, R., Wu, Y., Li, W., & Wong, N. H. (2021). Field synergy analysis of pollutant dispersion in street canyons and its optimization by adding wind catchers. *Building Simulation*, *14*, 391–405.

Ming, T., He, F., Wu, Y., Shi, T., Su, C., Wang, C., Li, Z., Chen, W., & de Richter, R. (2023). The effect of noise barriers on viaducts on pollutant dispersion in complex street canyons. *Energy Built Environ.*, *4*(5), 589–600.

Mirzaei, P. A., & Haghighat, F. (2011). Pollution removal effectiveness of the pedestrian ventilation system. *Journal of Wind Engineering and Industrial Aerodynamics*, *99*(1), 46–58.

Montazeri, H., & Montazeri, F. (2018). Cfd simulation of cross-ventilation in buildings using rooftop wind-catchers: Impact of outlet openings. *Renewable Energy*, *118*, 502–520.

Moonen, P., Dorer, V., & Carmeliet, J. (2012). Effect of flow unsteadiness on the mean wind flow pattern in an idealized urban environment. *Journal of wind engineering and industrial aerodynamics*, *104*, 389–396.

Mudarri, D. (2007). Public health and economic impact of dampness and mold.

Nazarian, N., & Kleissl, J. (2016). Realistic solar heating in urban areas: Air exchange and street-canyon ventilation. *Building and Environment*, *95*, 75–93.

Nolte, C. G., Gilliland, A. B., Hogrefe, C., & Mickley, L. J. (2008). Linking global to regional models to assess future climate impacts on surface ozone levels in the united states. *Journal of Geophysical Research: Atmospheres*, *113*(D14).

Oke, T. R. (1988). Street design and urban canopy layer climate. *Energy Build.*, *11*(1-3), 103–113.

Park, H., Lee, B., Ha, E.-H., Lee, J.-T., Kim, H., & Hong, Y.-C. (2002). Association of air pollution with school absenteeism due to illness. *Archives of pediatrics & adolescent medicine*, *156*(12), 1235–1239.

Peel, J. L., Haeuber, R., Garcia, V., Russell, A. G., & Neas, L. (2013). Impact of nitrogen and climate change interactions on ambient air pollution and human health. *Biogeochemistry*, *114*, 121–134.

Peng, Y., Buccolieri, R., Gao, Z., & Ding, W. (2020). Indices employed for the assessment of "urban outdoor ventilation"-a review. *Atmospheric environment*, *223*, 117211.

Polivka, B. J. (2018). The great london smog of 1952. *AJN The American Journal of Nursing*, *118*(4), 57–61.

Pournazeri, S., & Princevac, M. (2015). Sound wall barriers: Near roadway dispersion under neutrally stratified boundary layer. *Transportation Research Part D: Transport and Environment*, *41*, 386–400.

Pu, Y., Yang, C., Liu, H., Chen, Z., & Chen, A. (2015). Impact of license plate restriction policy on emission reduction in hangzhou using a bottom-up approach. *Transportation Research Part D: Transport and Environment*, *34*, 281–292.

Pucher, J., & Buehler, R. (2005). Cycling trends and policies in canadian cities.

Ranasinghe, D., Lee, E. S., Zhu, Y., Frausto-Vicencio, I., Choi, W., Sun, W., Mara, S., Seibt, U., & Paulson, S. E. (2019). Effectiveness of vegetation and sound wall-vegetation combination barriers on pollution dispersion from freeways under early morning conditions. *Science of The Total Environment*, *658*, 1549–1558.

Ravindra, K., Sokhi, R., & Van Grieken, R. (2008). Atmospheric polycyclic aromatic hydrocarbons: Source attribution, emission factors and regulation. *Atmospheric environment*, *42*(13), 2895–2921.

Reiminger, N., Jurado, X., Vazquez, J., Wemmert, C., Blond, N., Dufresne, M., & Wertel, J. (2020). Effects of wind speed and atmospheric stability on the air pollution reduction rate induced by noise barriers. *Journal of Wind Engineering and Industrial Aerodynamics*, *200*, 104160.

Requia, W. J., Mohamed, M., Higgins, C. D., Arain, A., & Ferguson, M. (2018). How clean are electric vehicles? evidence-based review of the effects of electric mobility on air pollutants, greenhouse gas emissions and human health. *Atmospheric Environment*, *185*, 64–77.

Reyes, V., Martınez, O., & Hernández, G. (1923). National center for biotechnology information. *Plant Breeding. Universidad Autónoma Agraria Antonio Narro, Calzada Antonio Narro*.

Roache, P. J. (1994). Perspective: A method for uniform reporting of grid refinement studies.

Roy, A., Sheffield, P., Wong, K., & Trasande, L. (2011). The effects of outdoor air pollutants on the costs of pediatric asthma hospitalizations in the united states, 1999 to 2007. *Medical care*, *49*(9), 810–817.

Rydin, Y., Bleahu, A., Davies, M., Dávila, J. D., Friel, S., De Grandis, G., Groce, N., Hallal, P. C., Hamilton, I., Howden-Chapman, P., et al. (2012). Shaping cities for health: Complexity and the planning of urban environments in the 21st century. *The lancet*, *379*(9831), 2079–2108.

Schipper, L., & Fulton, L. (2009). Disappointed by diesel? impact of shift to diesels in europe through 2006. *Transportation research record*, *2139*(1), 1–10.

Schlichting, H. (1979). Boundary layer theory, mcgraw-hill, new york, 1979. *FIGURE CAPTIONS solid curve displays the exact solution. The difference be-*

tween the exact solution and the eighth QLM iteration for all t in the figure is less than, 10–10.

Schmitt, F. G. (2007). About boussinesq's turbulent viscosity hypothesis: Historical remarks and a direct evaluation of its validity. *Comptes Rendus Mécanique*, *335*(9-10), 617–627.

Sha, C., Wang, X., Lin, Y., Fan, Y., Chen, X., & Hang, J. (2018). The impact of urban open space and 'lift-up'building design on building intake fraction and daily pollutant exposure in idealized urban models. *Science of the Total Environment*, *633*, 1314–1328.

Silva, R. A., West, J. J., Zhang, Y., Anenberg, S. C., Lamarque, J.-F., Shindell, D. T., Collins, W. J., Dalsoren, S., Faluvegi, G., Folberth, G., et al. (2013). Global premature mortality due to anthropogenic outdoor air pollution and the contribution of past climate change. *Environmental Research Letters*, *8*(3), 034005.

Snyder, W. H. (1972). Similarity criteria for the application of fluid models to the study of air pollution meteorology. *Bound. Layer Meteorol.*, *3*(1), 113–134.

Srivastava, R. K., Neuffer, W., Grano, D., Khan, S., Staudt, J., & Jozewicz, W. (2005). Controlling nox emission from industrial sources. *Environmental progress*, *24*(2), 181–197.

Takano, Y., & Moonen, P. (2013). On the influence of roof shape on flow and dispersion in an urban street canyon. *J. Wind Eng. Ind. Aerodyn.*, *123*, 107–120.

Tang, J., McNabola, A., Misstear, B., & Caulfield, B. (2017). An evaluation of the impact of the dublin port tunnel and hgv management strategy on air pollution emissions. *Transportation Research Part D: Transport and Environment*, *52*, 1–14.

Tang, J., McNabola, A., Misstear, B., Pilla, F., & Alam, M. S. (2019). Assessing the impact of vehicle speed limits and fleet composition on air quality near a school. *International journal of environmental research and public health*, *16*(1), 149.

Thøgersen, J. (2009). Promoting public transport as a subscription service: Effects of a free month travel card. *Transport Policy*, *16*(6), 335–343.

Tominaga, Y., Mochida, A., Yoshie, R., Kataoka, H., Nozu, T., Yoshikawa, M., & Shirasawa, T. (2008). Aij guidelines for practical applications of cfd to pedestrian wind environment around buildings. *J. Wind Eng. Ind. Aerodyn.*, *96*(10-11), 1749–1761.

Tong, Z., Baldauf, R. W., Isakov, V., Deshmukh, P., & Zhang, K. M. (2016). Roadside vegetation barrier designs to mitigate near-road air pollution impacts. *Science of the total environment*, *541*, 920–927.

Ugurlu, A. (2020). An emission analysis study of hydrogen powered vehicles. *International Journal of Hydrogen Energy*, *45*(50), 26522–26535.

UNION, P., et al. (2008). Directive 2008/50/ec of the european parliament and of the council of 21 may 2008 on ambient air quality and cleaner air for europe. *Official Journal of the European Union*.

Vallero, D. A. (2014). *Fundamentals of air pollution*. Academic press.

Vardoulakis, S., Fisher, B. E., Pericleous, K., & Gonzalez-Flesca, N. (2003). Modelling air quality in street canyons: A review. *Atmospheric environment*, *37*(2), 155–182.

Vasudevan, M., Pilla, F., & McNabola, A. (2023). Enhancing ventilation in street canyons using adjustable roof-level wind flow deflectors. *Energy and Built Environment*.

Venkatram, A., Heist, D. K., Perry, S. G., & Brouwer, L. (2021). Dispersion at the edges of near road noise barriers. *Atmospheric pollution research*, *12*(2), 367–374.

Versteeg, H. K. (2007). *An introduction to computational fluid dynamics the finite volume method, 2/e*. Pearson Education India.

Walsh, M. P. (2001). Global trends in diesel emissions regulation–a 2001 update. *SAE Transactions*, 107–127.

Wang, S., & Wang, X. (2019). Modeling and analysis of the effects of noise barrier shape and inflow conditions on highway automobiles emission dispersion. *Fluids*, *4*(3), 151.

Waxman, H. A. (1991). An overview of the clean air act amendments of 1990. *Envtl. L.*, *21*, 1721.

Weaver, C., Liang, X.-Z., Zhu, J., Adams, P., Amar, P., Avise, J., Caughey, M., Chen, J., Cohen, R., Cooter, E., et al. (2009). A preliminary synthesis of modeled climate change impacts on us regional ozone concentrations. *Bulletin of the American Meteorological Society*, *90*(12), 1843–1864.

WHO. (2006). *Air quality guidelines: Global update 2005: Particulate matter, ozone, nitrogen dioxide, and sulfur dioxide*. World Health Organization.

WHO et al. (2010). *Who guidelines for indoor air quality: Selected pollutants*. Regional Office for Europe, WHO.

WHO et al. (2017). *Don't pollute my future! the impact of the environment on children's health* (tech. rep.). World Health Organization.

WHO et al. (2019). *Healthy environments for healthier populations: Why do they matter and what can we do?* (Tech. rep.). World Health Organization.

Xiaomin, X., Zhen, H., & Jiasong, W. (2006). The impact of urban street layout on local atmospheric environment. *Build. Environ.*, *41*(10), 1352–1363.

Yim, S. H. L., Fung, J. C. H., Lau, A. K. H., & Kot, S. C. (2009). Air ventilation impacts of the "wall effect" resulting from the alignment of high-rise buildings. *Atmospheric Environment*, *43*(32), 4982–4994.

You, W., Gao, Z., Chen, Z., & Ding, W. (2017b). Improving residential wind environments by understanding the relationship between building arrangements and outdoor regional ventilation. *Atmosphere*, *8*(6), 102.

You, W., Shen, J., & Ding, W. (2017a). Improving wind environment design based on assessing spatial distribution of ventilation efficiency in regional space. *Energy Procedia*, *142*, 2923–2929.

Zhai, M., & Wolff, H. (2021). Air pollution and urban road transport: Evidence from the world's largest low-emission zone in london. *Environmental Economics and Policy Studies*, 1–28.

Zhang, K., Chen, G., Wang, X., Liu, S., Mak, C. M., Fan, Y., & Hang, J. (2019). Numerical evaluations of urban design technique to reduce vehicular personal intake fraction in deep street canyons. *Science of the Total Environment*, *653*, 968–994.

Zhang, K., Chen, G., Zhang, Y., Liu, S., Wang, X., Wang, B., & Hang, J. (2020). Integrated impacts of turbulent mixing and nox-o3 photochemistry on reactive pollutant dispersion and intake fraction in shallow and deep street canyons. *Sci. Total Environ.*, *712*, 135553.

Zhang, Q., Qi, W., Yao, W., Wang, M., Chen, Y., & Zhou, Y. (2016). Ambient particulate matter (pm2. 5/pm10) exposure and emergency department visits for acute myocardial infarction in chaoyang district, beijing, china during 2014: A case-crossover study. *Journal of Epidemiology*, *26*(10), 538–545.

Zhang, Y., Ma, R., Ban, J., Lu, F., Guo, M., Zhong, Y., Jiang, N., Chen, C., Li, T., & Shi, X. (2021). Risk of cardiovascular hospital admission after exposure

to fine particulate pollution. *Journal of the American College of Cardiology*, *78*(10), 1015–1024.

Zhang, Y.-W., Gu, Z.-L., Lee, S.-C., Fu, T.-M., & Ho, K.-F. (2011). Numerical simulation and in situ investigation of fine particle dispersion in an actual deep street canyon in hong kong. *Indoor Built Environ.*, *20*(2), 206–216.

Zhi, H., Qiu, Z., Wang, W., Wang, G., Hao, Y., & Liu, Y. (2020). The influence of a viaduct on pm dispersion in a typical street: Field experiment and numerical simulations. *Atmospheric Pollution Research*, *11*(4), 815–824.